THE ROLE OF BLOOD VESSEL EPICARDIAL SUBSTANCE IN THE MAINTENANCE OF INTESTINAL EPITHELIAL INTEGRITY

By

Vishruth Keesara Reddy

Dissertation

Submitted to the Faculty of the

Graduate School of Vanderbilt University

in partial fulfillment of the requirements

for the degree of

DOCTOR OF PHILOSOPHY

in

Cancer Biology

May, 2016

Nashville, Tennessee

Approved:

Christopher S. Williams, M.D., Ph.D.

David M. Bader, Ph.D.

Barbara M. Fingleton, Ph.D.

M. Kay Washington, M.D., Ph.D.

Keith T. Wilson, M.D

To my grandparents Vuppunutula Purushotham and Pushpamala Reddy, whose example I strive to live by,

To my parents Ugender and Pradeepta Reddy, whose selflessness and sacrifices have made my education possible, and whose patience and love have molded me into the person that I am,

And

To my wife Opal for her constant love, patience, and support in this continuing academic journey.

ACKNOWLEDGEMENTS

My graduate school training would not have been such a fulfilling experience without the constant support of my mentors, colleagues, family, and friends. I am especially thankful to my mentor Dr. Christopher Williams. Throughout my time in the laboratory, Dr. Williams has encouraged me to innovate, helped me overcome challenges, and supported me as a constant advocate. He has a contagious enthusiasm for science, cares deeply about those whom he mentors, and is incredibly selfless with his time. I could not have asked for a better mentor and consider myself privileged to have trained under his guidance.

My fellow laboratory members, both past and present, have also enriched this journey by fostering a collaborative environment of camaraderie where I have had the honor of learning from their many talents. I would like to acknowledge Dr. Sarah Short, Dr. Mukul Mittal, Bobak Parang, Cody Keating, Anthony Bilotta, Amy Motley, Karie Ballard, and former laboratory members Dr. Yash Choksi, Dr. Caitlyn Barrett, Dr. Shenika Poindexter, Wei Ning, and Amber Bradley.

The progress made on these projects would not have been possible without the support and technical guidance of our collaborators: Dr. Keith Wilson, Dr. Kay Washington, Dr. Raymond Burk, Dr. Lori Coburn, and Dr. Richard Peek. I also wish to thank my thesis committee, Dr. Barbara Fingleton, Dr. David Bader, Dr. Kay Washington, and Dr. Keith Wilson for their scientific mentorship, advice, and support over these years.

Additionally, I wish to express my sincerest gratitude to Dr. Terence Dermody, Dr. Larry Swift, Dr. Michelle Grundy, Dr. Jim Bills, Melissa Krasnove, and the rest of the Medical Scientist Training Program at Vanderbilt University. The program has been incredibly supportive of every aspect of my training, and I am incredibly fortunate to have been a part of it.

I am also thankful for the training opportunities provided by the Department of Cancer Biology and the Cancer Biology Graduate Program. I also wish to acknowledge our sources of funding throughout this project which have supported my work and that of the laboratory: NIH F30 DK103498-01 (Reddy), NIGMS T32 GM07347 to the Vanderbilt Medical Scientist Training Program, NIH R01 DK099204 (Williams), and NIH K08 DK080221 (Williams).

Finally, I am immensely grateful for the support and love of my entire family. I am particularly thankful to my grandparents and my parents Ugender and Pradeepta Reddy, whose selflessness and sacrifices have made my education and goals possible. I am thankful to my sister Shruthi Reddy, who is the most caring, thoughtful, and supportive sister anyone could ask for. I am also grateful to my parents Peter and Alana Lin-Tsai for their encouragement and support throughout my training. Finally, I could not have completed these past few years without the incredible patience, love, and encouragement of my wife Opal.

TABLE OF CONTENTS

Page

LIST OF TABLES

Table

LIST OF FIGURES

Figure

CHAPTER I

INTRODUCTION TO INTESTINAL HOMEOSTASIS

The Intestinal Epithelium: The Luminal Interface of the Gastrointestinal Tract

The gastrointestinal (GI) tract is one of the most rapidly proliferating and constantly renewing tissues in the body (Barker 2014; Clevers 2013). The GI tract encompasses all anatomical structures from the mouth to the anus and is generally divided into upper and lower segments (Moore, Dalley, and Agur 2009). The upper GI tract includes the mouth, esophagus, and stomach, while the lower GI tract comprises the small and large intestines (Moore, Dalley, and Agur 2009). The liver, biliary tract, and pancreas are critical components of the digestive system in humans and play a supportive role to the GI tract in carrying out its physiological functions (Moore, Dalley, and Agur 2009).

The lower GI tract can be further subdivided into smaller functional segments. The small intestine consists of the duodenum, jejunum, and ileum, while the large intestine is divided into the cecum, colon, rectum, and anus (Moore, Dalley, and Agur 2009). Although regional differences exist throughout the lower GI tract, histological characterization reveals tissue organization that can be divided into 4 concentric layers: (1) mucosa, (2) submucosa, (3) *muscularis externa*, and (4) adventitia or serosa (Mills 2012; Young, O'Dowd, and Woodford 2013). The mucosa, or innermost layer, is in direct contact with the lumen and is comprised of an epithelium, a lamina propria, and a thin smooth muscle layer known as the muscularis mucosa, which facilitates peristalsis.

Beneath the mucosa lies the submucosa, a loose, paucicellular layer of connective tissue that houses blood vessels, lymphatics, and nerves that branch into the mucosa and the muscularis externae (Mills 2012; Moore, Dalley, and Agur 2009). The muscularis externa is a thick outer smooth muscle later comprised of an inner circular and outer longitudinally running layer of muscle that supports peristalsis and coordinates the movement of contents through the GI tract (Mills 2012; Moore, Dalley, and Agur 2009). Finally, the adventitia or serosa makes up the outermost layer of the GI tract and is comprised of multiple layers of connective tissue (Mills 2012; Moore, Dalley, and Agur 2009).

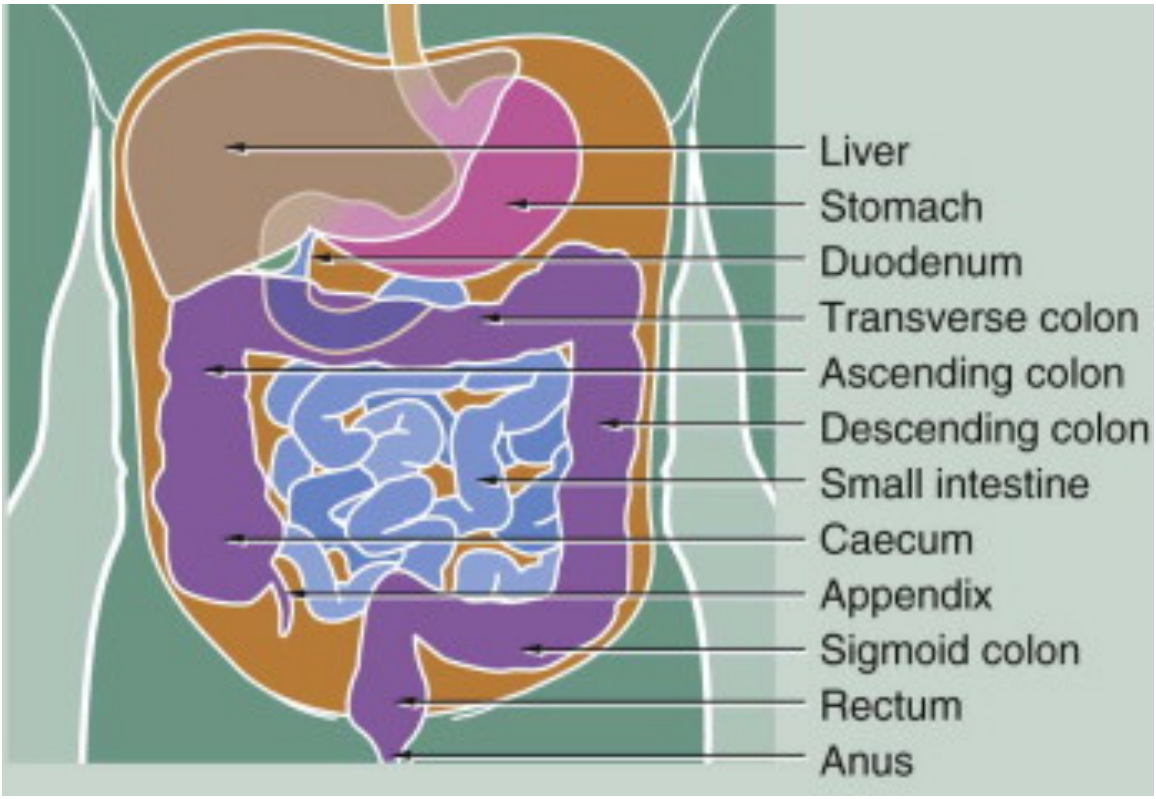

Figure 1. Components of the gastrointestinal tract. The lower GI tract comprises the small and large intestine. Figure from Young, O'Dowd, and Woodford 2013.

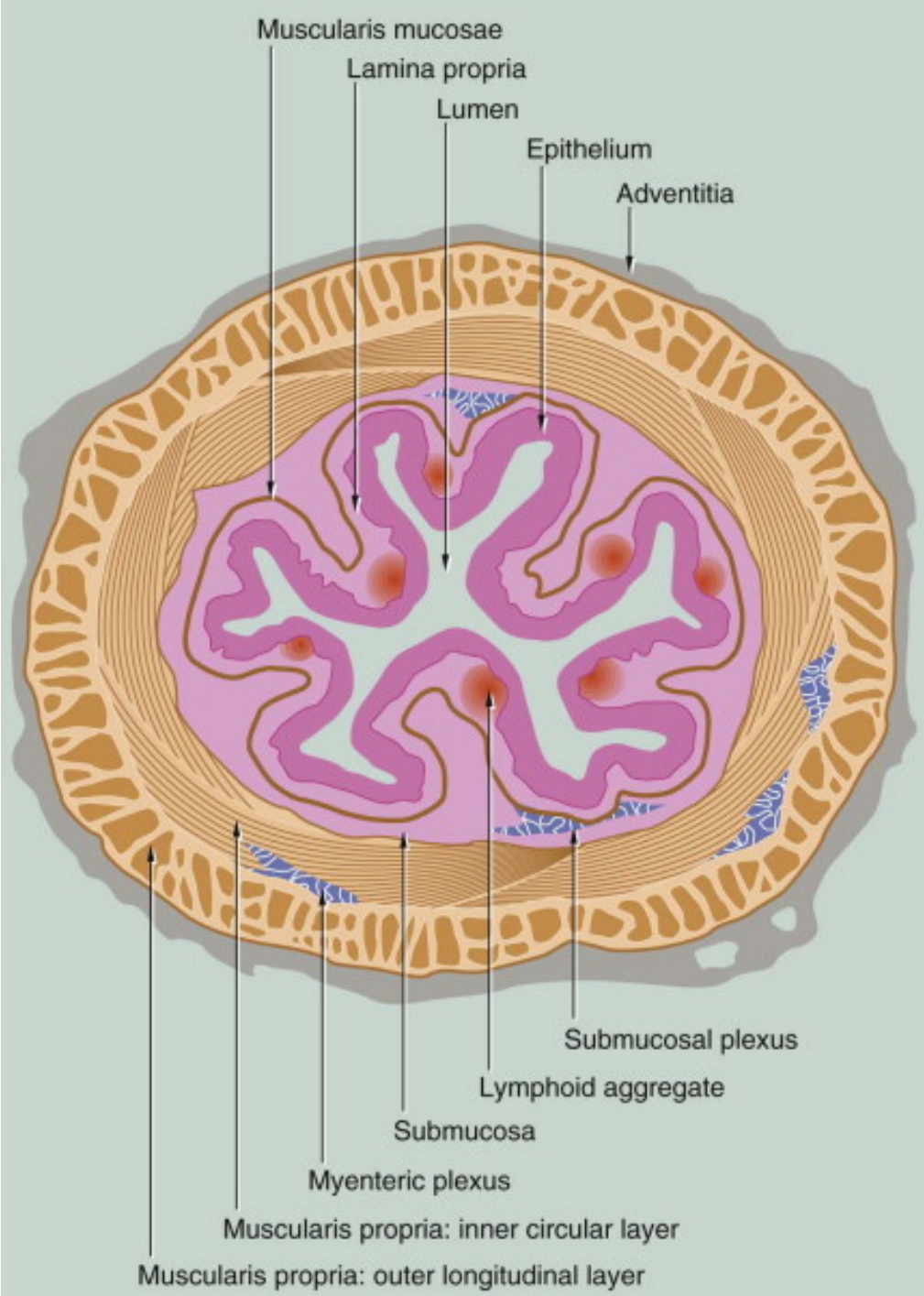

Figure 2. Concentric layers of the lower gastrointestinal tract. Histological characterization of the lower gastrointestinal tract reveals four concentric layers: a (1) mucosa, (2) submucosa, (3) *muscularis externa*, and (4) adventitia or serosa. Figure from Young, O'Dowd, and Woodford 2013.

The intestinal epithelium is the innermost component of the mucosa and the luminal interface of the GI tract which is responsible for carrying out many of its functions (Mills 2012). Intestinal homeostasis is maintained through constant proliferation, differentiation, and repair of this continuously renewing epithelium (Barker 2014; Maloy and Powrie 2011). The epithelium of the small intestine contains finger-like projections known as villi that maximize the absorptive surface area of the small intestine and are critical to carrying out its primary function of absorbing ingested nutrients (Barker 2014; Clevers 2013; Mills 2012). Adjacent to the villi are invaginations of the intestinal epithelium known as intestinal crypts which are responsible for epithelial cell renewal (Barker 2014; Clevers 2013; Mills 2012).

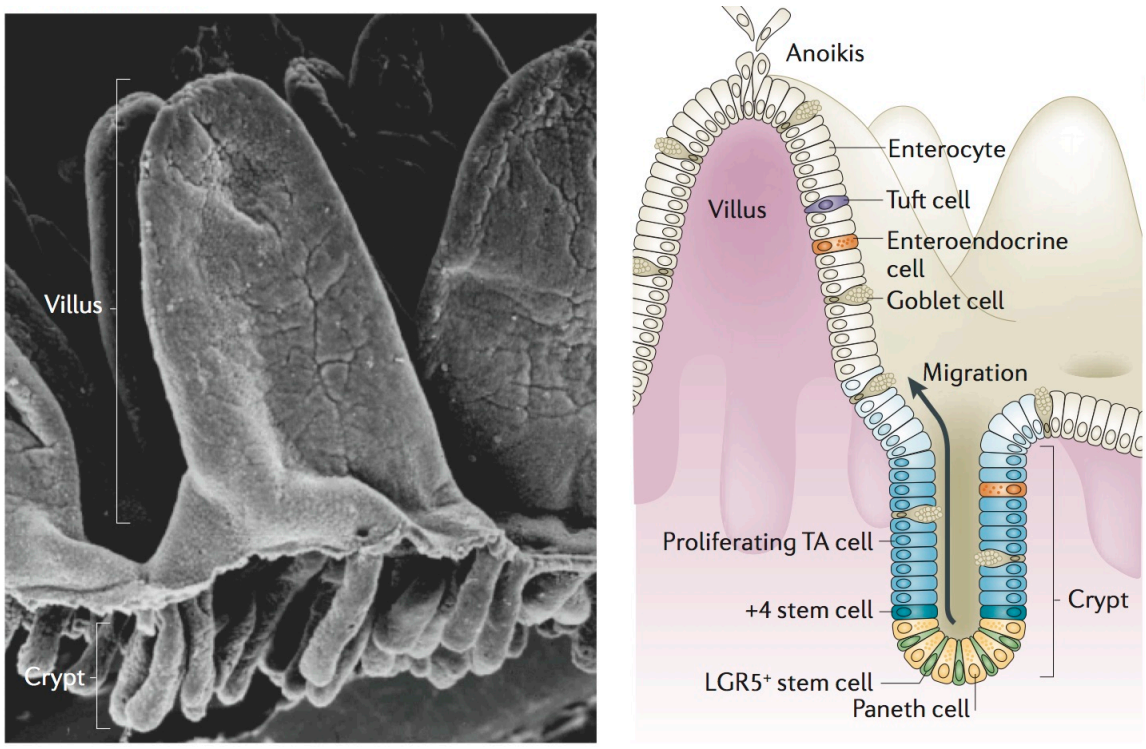

Figure 3. Small intestine structural organization. Scanning electron micrograph (left) and illustration (right). The epithelium of the small intestine contains finger-like projections known as villi, which project into the lumen. Adjacent to the villi are the intestinal crypts, which drive epithelial renewal. Figure from Barker 2014.

While the colon also houses these invaginations or crypts, it does not contain villi (Barker 2014; Clevers 2013).

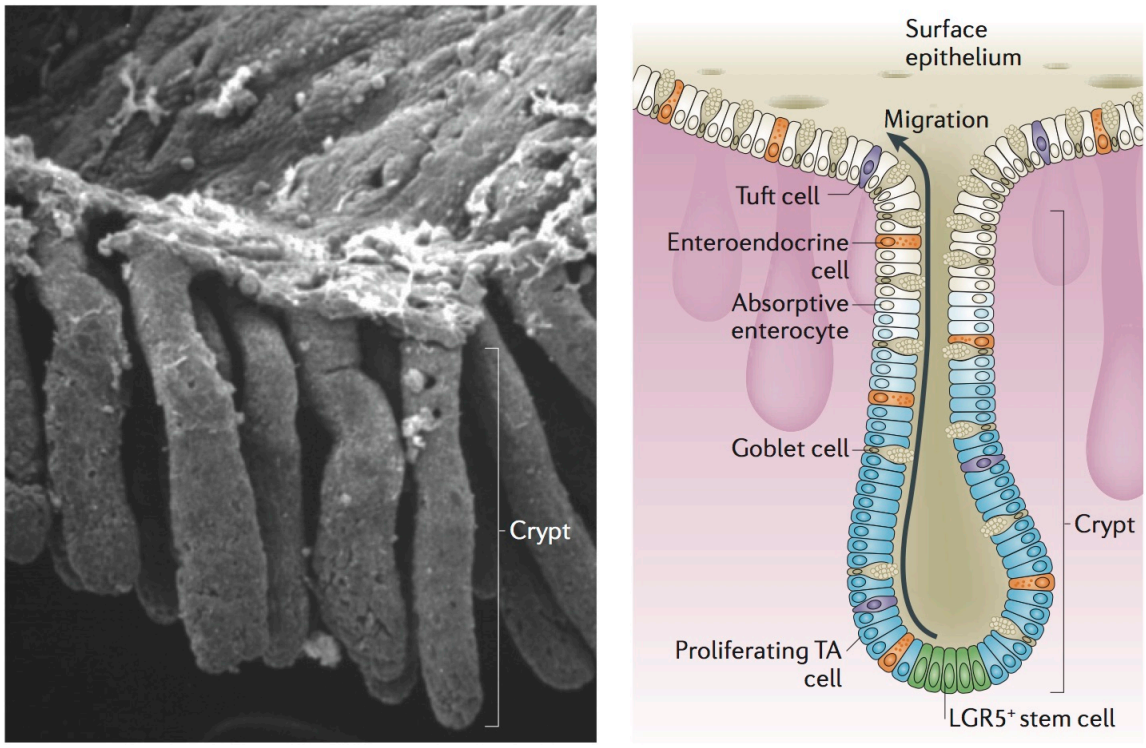

Figure 4. Colon structural organization. Scanning electron micrograph (left) and illustration (right). The colonic epithelium contains crypts but no villi. Figure from Barker 2014.

A number of differentiated cell types comprise the intestinal epithelium with several distinct functions (Clevers 2013; Mills 2012). The most abundant cell type is the absorptive enterocyte, which is a polarized columnar cell with an elaborate brush border (Clevers 2013; Mills 2012). Also present are goblet cells which secret mucus, a critical component in the regulation of epithelial barrier integrity, and enteroendocrine cells, which secrete a number of hormones involved in digestive processes (Clevers 2013; Mills 2012). Tuft cells are present throughout the crypt-villus axis and are thought to serve as sensors of luminal contents (Clevers 2013; Mills 2012). Paneth cells, which are exclusive

to the small intestine, are present towards the bases of the intestinal crypts, and are known to secrete bactericidal products and serve as sources of ligands critical to maintaining the intestinal stem cell niche (Clevers 2013; Mills 2012; Sato et al. 2009; Sato, van Es, et al. 2011). Finally, microfold (M) cells are present in specific areas of the epithelium that overlie lymphoid accumulations in the GI tract, such as Peyer's patches, and play a critical role in mediating mucosal immunity (Clevers 2013; Mills 2012).

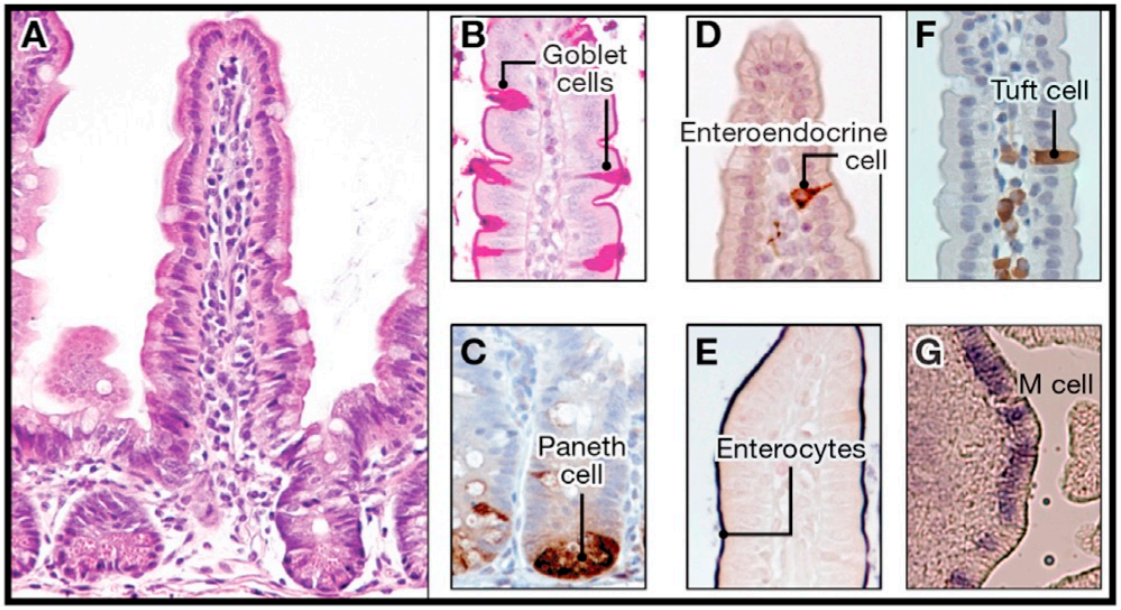

Figure 5. Small intestine epithelial cell types. (A) Hematoxylin and eosin staining of the small intestinal epithelium. (B) Periodic acid-Schiff staining for goblet cells. (C) Lysozyme staining for Paneth cells at the crypt base. (D) Chromogranin staining for enteroendocrine cells. (E) Alkaline phosphatase staining (blue, at luminal brush border) of villus enterocytes (F) DCAMKL-1 stained tuft cell (G) Spi-B expression in microfold (M) cells. Figure from Clevers 2013.

Intestinal Stem Cells: Drivers of Intestinal Epithelial Renewal

While differentiated epithelial cells are critical to the functioning of the intestinal epithelium, intestinal renewal is maintained by dynamic stem cell populations that reside

in the intestinal crypts (Barker, van de Wetering, and Clevers 2008; Barker 2014; Clevers 2013). The intestinal epithelium is thought to renew itself approximately every 5 days, with cells progressively differentiating and moving out of the crypts in conveyor belt-like fashion, with the notable exception of Paneth cells, which remain adjacent to stem cell populations at the crypt bases (Barker 2014; Sato and Clevers 2013). Until recently, thorough characterization of intestinal stem cell populations has remained challenging due to the absence of specific markers for their identification (Barker 2014; Potten et al. 2009). However, recently-discovered adult intestinal stem cell markers, and recently-developed lineage tracing technologies and *ex vivo* tissue cultures or "organoid" systems have greatly facilitated their identification and characterization (Barker 2014; Barker et al. 2007; Sato et al. 2009; Sato, van Es, et al. 2011).

Some of the first successful investigations of intestinal stem cell populations were conducted by Cheng, Leblond, and colleagues, who proposed the existence of continuously-cycling crypt base columnar (CBC) stem cells wedged between post-mitotic Paneth cells (Barker, van de Wetering, and Clevers 2008; Barker 2014; Cheng and Leblond 1974a, 1974b; Clevers 2013). Lineage tracing experiments identified that after ^{3}H-thymidine injection, surviving CBC cells phagocytosed dead CBC cells which produced radioactive, traceable "hot" phagosomes that at first appeared exclusive to the CBC cells but were later noted in differentiated cells (Cheng and Leblond 1974a, 1974b; Clevers 2013). This work was followed up by Bjerknes and Cheng who proposed a "stem cell zone" model in which CBC stem cells and Paneth cells, residing in the crypt base, occupy a niche that maintains stemness (Bjerknes and Cheng 1981a, 1981b; Clevers 2013). Stem cell daughter cells that divide and are no longer directly adjacent to Paneth

cells then differentiate and migrate along the crypt axis, with the exception of Paneth cell progenitors, which migrate downwards (Bjerknes and Cheng 1981a, 1981b; Clevers 2013).

Meanwhile, Potten and colleagues reported a cell type that resided in the "+4" position, or directly above the Paneth cells, that was rare and DNA-label-retaining and thus a "label-retaining cell" or LRC (Clevers 2013; Potten, Owen, and Booth 2002; Potten et al. 1978). While DNA label retention is a characteristic that is associated with mitotic quiescence and used as a surrogate marker of stem cells, it has since been suggested that this retention may not be due to quiescence but instead to a process of asymmetric segregation of labeled and unlabeled DNA strands between these putative stem cells and their daughter cells, respectively (Clevers 2013; Marshman, Booth, and Potten 2002; Potten, Owen, and Booth 2002).

Thus, the current model of the intestinal stem cell suggests the existence of ≥2 intestinal stem cell (ISC) populations: (1) a rapidly-cycling, crypt-based columnar (CBC) stem cell population at the base of the intestinal crypts, whose markers include Lgr5, a transmembrane receptor for R-spondin that amplifies Wnt tone, as well as Ascl2, Olfm4, Msi1, Smoc2, and Sox9; and (2) a more slowly-cycling, quiescent "+4" stem cell population that resides primarily at the +4 position from the base of the crypt and is marked by Bmi1, TERT, Lrig1, and Hopx (Barker 2014; Durand et al. 2012; Van Landeghem et al. 2012; Li and Clevers 2010; Potten et al. 2009). The contribution of each of these subsets to normal intestinal epithelial renewal and repair after injury is still under debate, but a number of studies have identified a role for each in restoring

epithelial integrity after injury (Buczacki et al. 2013; Hua et al. 2012; Metcalfe et al. 2014; Tian et al. 2011).

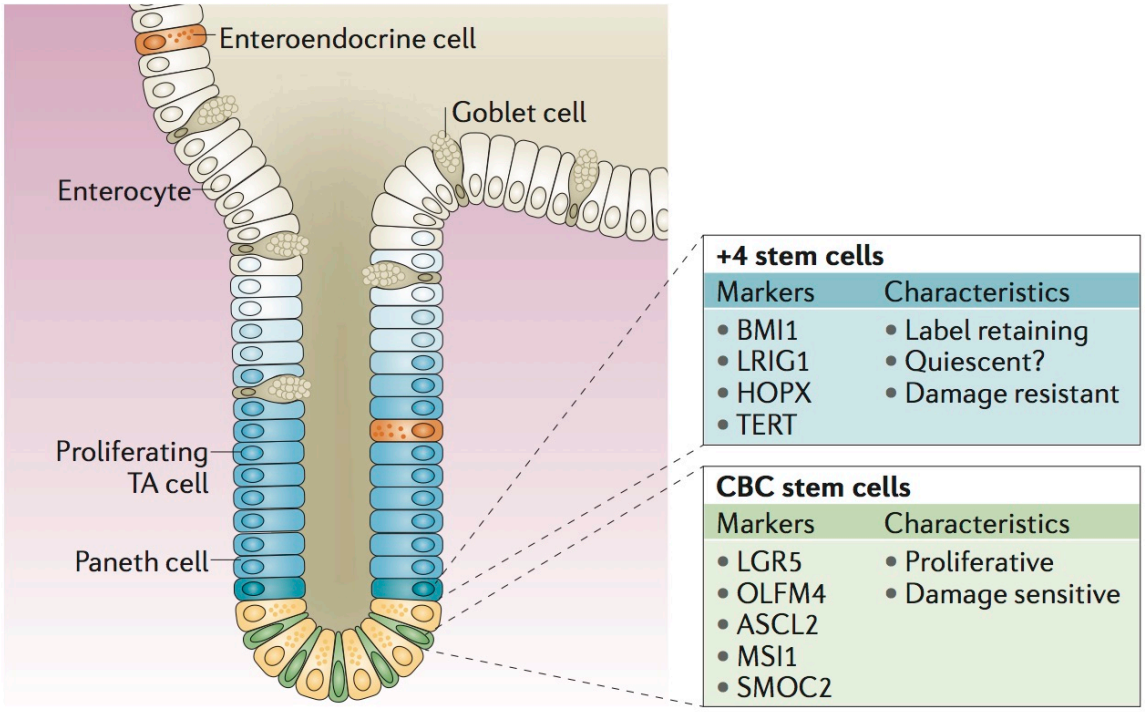

Figure 6. Putative stem cell populations of the intestinal crypt. The current model of the intestinal stem cell suggests the existence of ≥2 intestinal stem cell (ISC) populations: (1) a rapidly-cycling, crypt-based columnar (CBC) population and (2) a more slowly-cycling, quiescent "+4" stem cell population. Figure from Barker 2014.

The development of 3D *ex vivo* intestinal cultures by Dr. Hans Clevers's group in 2009 represented a remarkable advancement in our ability to model intestinal architecture, and to better understand intestinal homeostasis and the stem cell niche (Sato and Clevers 2013; Sato et al. 2009). These Matrigel-based systems have allowed for culturing and serial propagation of miniguts from small intestinal tissue ("enteroids") as well as colonic tissue ("colonoids") from both mice and humans *ex vivo* (Li and Clevers 2012; Sato and Clevers 2013; Sato et al. 2009; Sato, Stange, et al. 2011). Whole crypts

that contain CBC stem cells wedged between Paneth cells, or single Lgr5+ sorted stem cells are capable of generating these miniguts when supplemented with growth factors (Mahé et al. 2014; Sato and Clevers 2013; Sato et al. 2009).

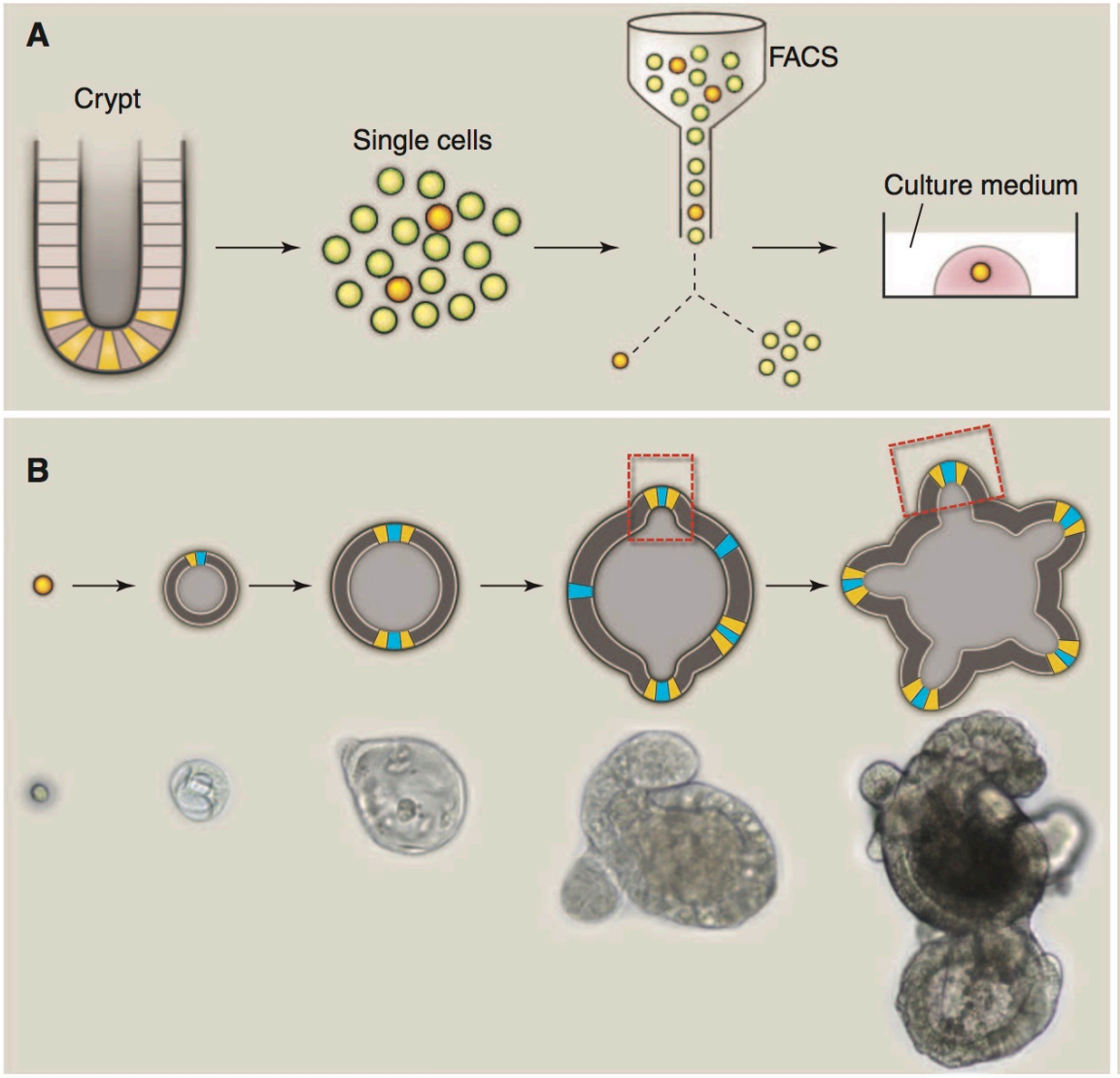

Figure 7. Minigut or "enteroid" culture systems. (A) Lgr5+ CBC cells can be sorted and embedded in Matrigel supplemented with growth factors to form enteroids. (B) Time course of growth of enteroids. Lgr5+ CBC stem cells are represented in yellow and Paneth cells in blue. Figure from Sato and Clevers 2013.

A critical growth factor for the enteroid systems includes Rspondin, a ligand which binds with its receptor Lgr5 to amplify Wnt tone (Sato and Clevers 2013). Other growth factors include the BMP inhibitor Noggin as well as EGF (Mahé et al. 2014; Sato and Clevers 2013; Sato et al. 2009).

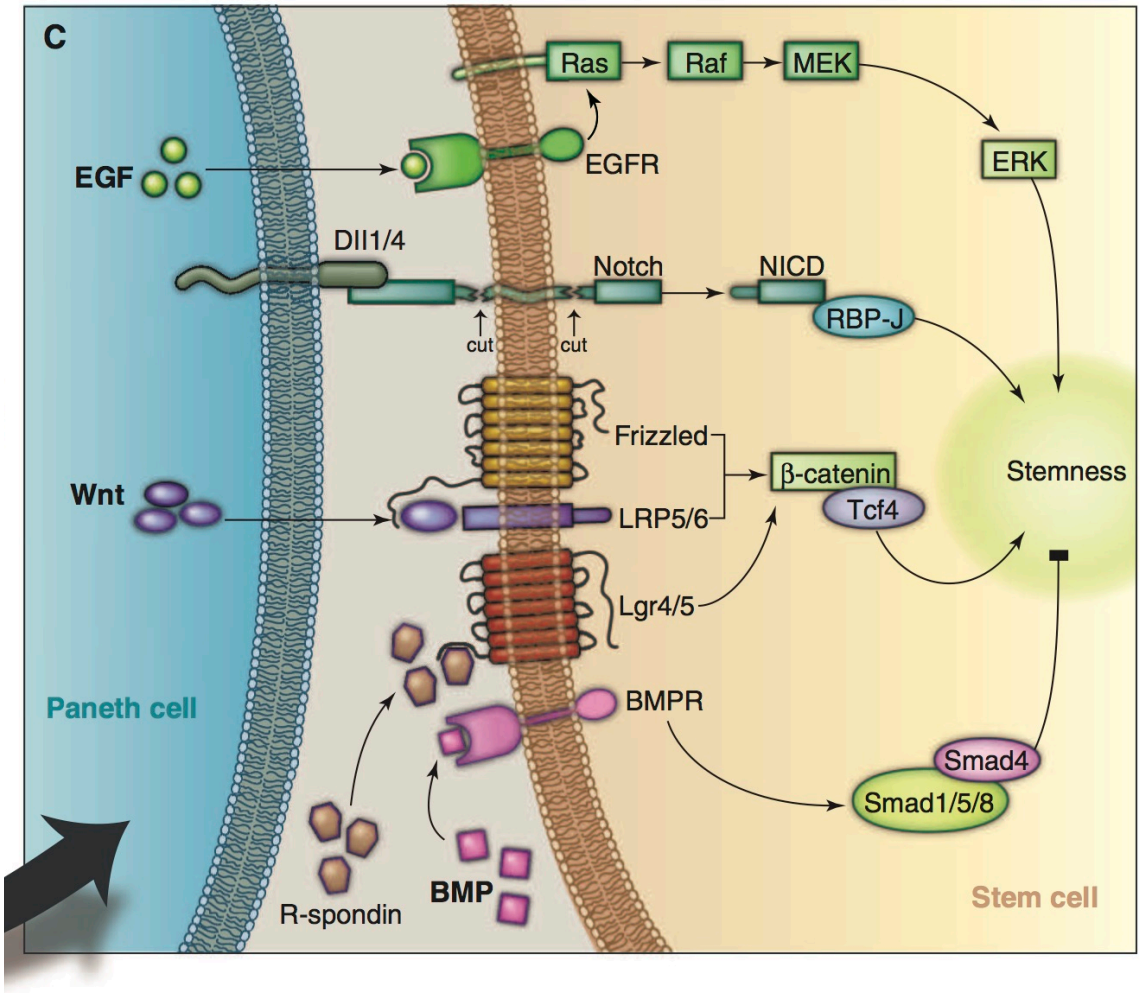

Figure 8. The intestinal stem cell niche. EGF, Notch, and Wnt pathway activation is essential for intestinal epithelial stemness, and BMP negatively regulates stemness. For full activation of Wnt, Rspondin-Lgr4/5 signal is required. Figure from Sato and Clevers 2013.

By many metrics, these *ex vivo* miniguts faithfully recapitulate characteristics of their *in vivo* counterparts (Li and Clevers 2012; Sato and Clevers 2013; Sato et al. 2009). They consist of a simple, polarized epithelium and develop into cysts containing a central lumen with multiple budding projections (Sato and Clevers 2013). The basal side of the miniguts is oriented towards the outside and in contact with the Matrigel, while the luminal sides form the central cystic structure into which cells of the miniguts are constantly shed (Sato and Clevers 2013). Intestinal organoids can be passaged, genetically manipulated, and maintained in culture for years without any apparent karyotypic alterations (Koo et al. 2012; Li and Clevers 2012; Sato and Clevers 2013). In addition to assisting with the study of intestinal crypt development, these novel modeling systems offer numerous therapeutic opportunities. A number of studies have shown that implantation of organoids in the intestines of injured mice results in successful engraftment as well as improvement of clinical parameters such as weight loss after colonic injury (Fordham et al. 2013; Li and Clevers 2012; Shaker and Rubin 2012; Yui et al. 2012).

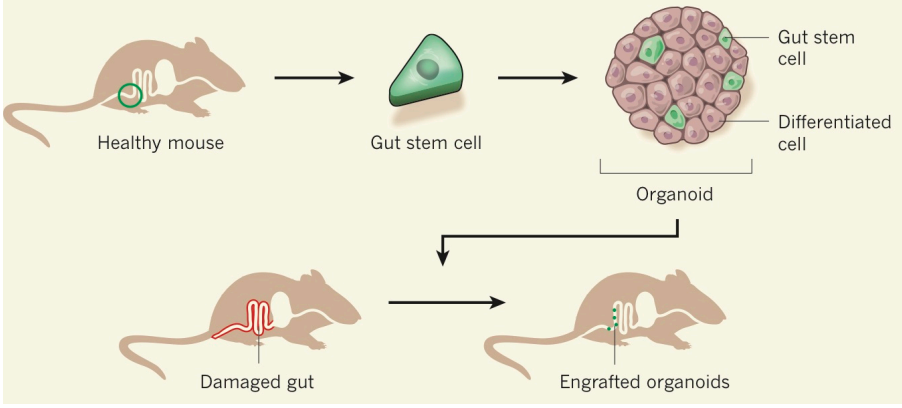

Figure 9. Epithelial repair with organoids. Organoids cultured *in vitro* can be successfully transplanted/engrafted into the colons of mice with superficial intestinal ulcerations. Figure from Shaker and Rubin 2012.

Moreover, development of intestinal organoid cultures for delivery of therapeutics, as well as high-throughput screening for drug sensitivity, remain avenues of great therapeutic potential (Hynds and Giangreco 2013; Sato and Clevers 2013).

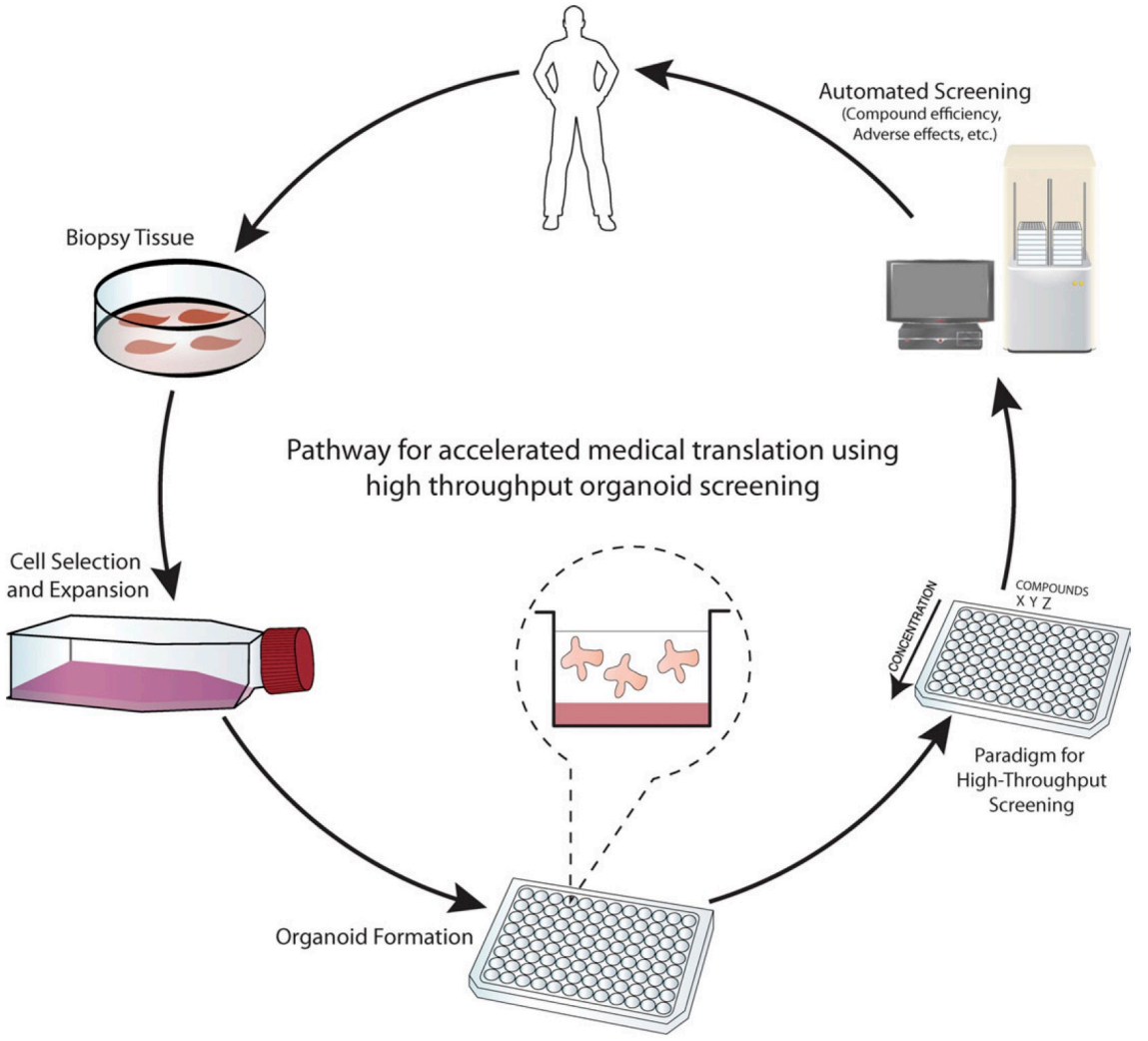

Figure 10. Paradigms for high-throughput screening utilizing organoids. Stem cells derived from patient biopsies can be cultured, expanded as organoids, and utilized for therapeutic screening. Organoids may predict responses to therapy given their resemblance to the *in vivo* tissues from which they are derived. Figure from Hynds and Giangreco 2013.

Of the many signaling pathways which govern intestinal homeostasis, the Wnt pathway, which regulates numerous biological processes ranging from development to malignancy, is critical to the maintenance of the intestinal stem cell niche and crypt proliferation (Clevers and Nusse 2012; Clevers 2013; J. H. van Es et al. 2012; Gregorieff and Clevers 2005; Pinto et al. 2003). Indeed, while dysregulated Wnt signaling is a central driver in the development of colon cancer, regulation of crypt dynamics and proliferation is mediated in large part by physiological Wnt signaling (Clevers and Nusse 2012; Clevers 2013; Gregorieff and Clevers 2005; Pinto et al. 2003). As a general overview, Wnt stimuli support a signaling pathway which regulates free cytoplasmic levels of β-catenin, which is otherwise rapidly degraded by the APC destruction complex (Clevers and Nusse 2012; Clevers 2013; Gregorieff and Clevers 2005; Pinto et al. 2003). The occupancy of Frizzled-Lrp5/6 receptors by Wnt proteins results in the stabilization and accumulation of β-catenin, which then travels to the nucleus to couple with Tcf transcription factors and activate the transcription of a number of Wnt/Tcf target genes (Clevers and Nusse 2012; Clevers 2013; Gregorieff and Clevers 2005; Pinto et al. 2003). The importance of this pathway in the maintenance of intestinal crypts is underscored by the fact that neonatal Tcf4 knockout mice lack proliferative crypts, suggesting that Wnt signaling is critical to the establishment of a proliferative stem cell compartment (Clevers 2013; Korinek et al. 1998). Moreover, multiple groups have demonstrated the persistent need for physiological Wnt signaling in adult intestinal crypts, through the transgenic expression of Wnt receptor antagonist Dkk1, as well as the conditional deletion of β-catenin or Tcf4 (Clevers 2013; V. Es et al. 2012; Fevr et al. 2007; Pinto et al. 2003).

Apical Junctional Complexes: Mediators of Intestinal Epithelial Barrier Integrity

The epithelial barrier comprises an almost $100m^2$ surface area which is lined by a simple columnar layer of intestinal epithelial cells that forms a surprisingly effective luminal barrier (Artis 2008; Maloy and Powrie 2011). Intestinal mucosal homeostasis requires competent epithelial barriers to withstand intestinal challenges, as it relies on the constant crosstalk between intestinal epithelial cells, immune cells, and the over 100 trillion microbes that are thought to inhabit the intestine (Artis 2008; Baumgart and Carding 2007; Hooper and Macpherson 2010; Maloy and Powrie 2011). Breakdown of this homeostasis is thought to be a primary component in the pathogenesis of a number of intestinal diseases such as inflammatory bowel disease (IBD) (Baumgart and Carding 2007; Maloy and Powrie 2011).

Critical to the maintenance of the intestinal barrier is the sealing of the paracellular space between adjacent epithelial cells (Balda and Matter 1998; Balda et al. 1992; Shen, Su, and Turner 2009; Shen 2012). This is accomplished by apical junctional complexes, which are primarily comprised of tight junctions, adherens junctions, and desmosomes (Shen, Su, and Turner 2009; Shen 2012). Most apically positioned between adjacent epithelial cells of the intestine are tight junctions, which form near-impermeable but nonetheless leaky paracellular connections that establish the division between the apical and basolateral plasma membrane domains (Henderson et al. 2011; Machen, Erlij, and Wooding 1972; Shen, Su, and Turner 2009). Below the tight junctions are adherens junctions, which are composed of a family of transmembrane proteins known as cadherins, which form strong homotypic interactions and play essential roles in the maintenance of cell polarity and differentiation (Henderson et al. 2011; Shen, Su, and

Turner 2009; Turner 2009). Below these complexes and at the basal side of the intestinal epithelial cells are desmosomes, which serve as anchors for keratin filaments and form complexes of intracellular proteins that connect the cytoskeleton to a number of adhesion proteins (Henderson et al. 2011; Turner 2009).

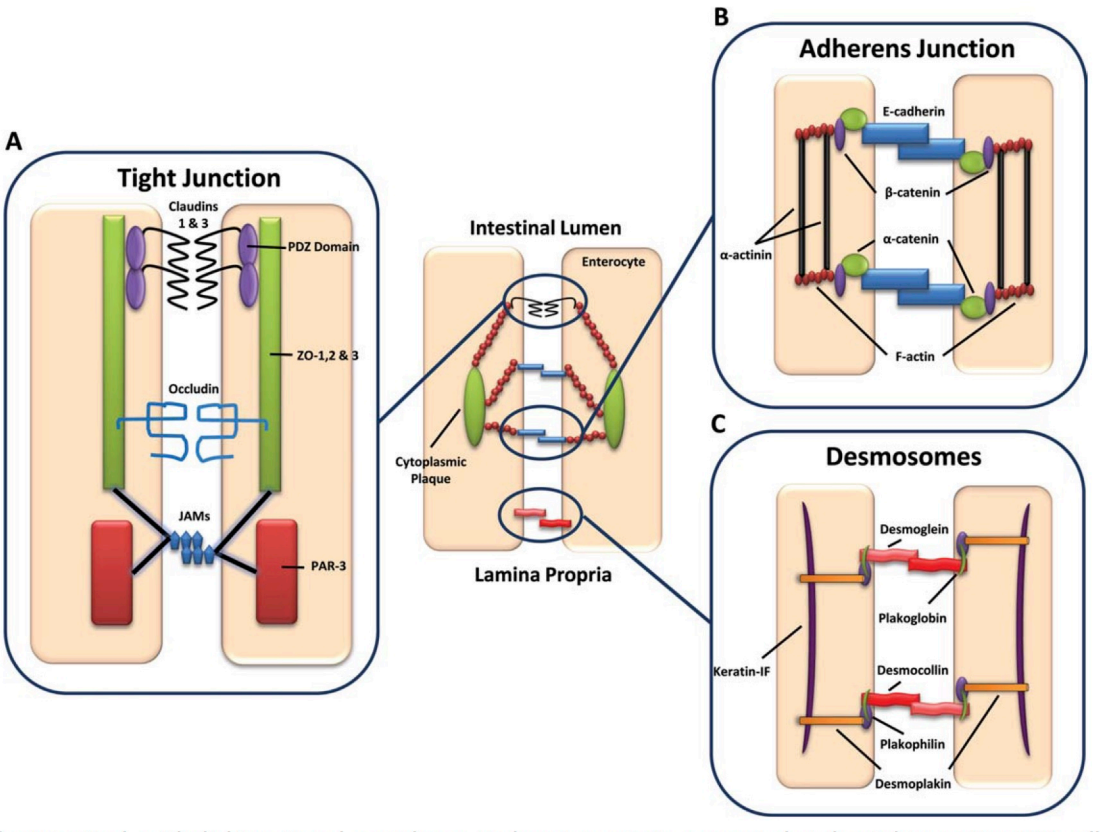

Figure 11. Components of apical junctional complexes. Adjacent intestinal epithelial cells are connected at the (A) tight junction, (B) adherens junction, and via (C) desmosomes from the luminal to lamina propria side, respectively. Figure from Henderson 2011.

Adherens junctions and desmosomes play critical supportive roles in providing adhesive force to maintain epithelial cell layer integrity and in regulating junctional signaling pathways critical to epithelial functions (Henderson et al. 2011; Hermiston and Gordon 1995; Shen, Su, and Turner 2009; Shen 2012). Yet, it is principally the tight

junctions of apical junction complexes that regulate paracellular barrier function and are critical to maintaining cell polarity and regulating the movement of substances such as water, electrolytes, lipids, and proteins across the epithelium (Henderson et al. 2011; Hermiston and Gordon 1995; Shen, Su, and Turner 2009; Shen 2012). Tight junctions are composed of complexes of transmembrane proteins, peripheral membrane or scaffolding proteins, and numerous regulatory proteins such as kinases (Shen, Su, and Turner 2009; Turner 2009). The principal transmembrane proteins of the tight junction are grouped intro three main families: claudins, occludin, and junctional adhesion molecules (JAMs) (Henderson et al. 2011; Hossain and Hirata 2008; Turner 2009). Peripheral membrane proteins ZO1 and ZO2 play supportive roles and are critical to tight junction assembly and maintenance (Turner 2009).

There is a clear pathological relevance for defects in intercellular junctions, as they can lead to increased epithelial barrier permeability (Baumgart and Carding 2007; Henderson et al. 2011; Shen, Su, and Turner 2009; Turner 2009). The epithelial barrier is known to be "leaky" in patients with IBD, with a number of studies demonstrating lower epithelial resistance and increased permeability of both inflamed and non-inflamed mucosa in Crohn's disease and ulcerative (Baumgart and Carding 2007; Pearson et al. 1982; Söderholm, Olaison, and Peterson 2002; Ukabam, Clamp, and Cooper 1983). Indeed, increased intestinal permeability has been shown to predict and possibly cause relapse of disease (Henderson et al. 2011; Porras et al. 2006; Wyatt et al. 1993). Moreover, disruption of tight-junctional integrity has been proposed as a key contributing factor to this epithelial barrier dysfunction (Heller et al. 2005; Ma et al. 2004; Shen, Su, and Turner 2009; Shen 2012; Söderholm, Olaison, and Peterson 2002; Turner 2009).

Studies have implicated altered expression of occludin, ZO1, and JAMs, and dysregulation of claudin as contributing factors to compromised barrier integrity present in IBD (Groschwitz and Hogan 2009; Henderson et al. 2011; Kucharzik et al. 2001; Ye, Ma, and Ma 2006; Zeissig et al. 2007; Zolotarevsky et al. 2002). Better understanding of tight junctional regulation, and its contribution to the maintenance of the intestinal epithelial barrier thus holds therapeutic potential for inflammatory bowel disease.

Modeling Intestinal Disease: Common Methods of Challenging Intestinal Epithelial Integrity

Mouse models remain among the most frequently-used models to interrogate intestinal disease processes given several considerations, both biological and practical (Eckmann 2006). Given their small size, short breeding timeline, and that over 99% of mouse genes possess a homolog in the human genome, they remain an excellent means of testing diseases possessed by their human counterparts (Eckmann 2006; Lander et al. 2001; Waterston et al. 2002). Over the years, multiple mouse models have been used to interrogate barrier dysfunction and immune dysregulation that often contribute to intestinal diseases, including spontaneous colitis models, inducible colitis models, genetically modified models, and adoptive transfer models (Eckmann 2006; Madsen et al. 1999; Neurath, Fuss, and Strober 2000; Perše and Cerar 2012; Wirtz and Neurath 2007; Wirtz et al. 2007).

Of the inducible models of murine colitis, one that has gained particular prominence over the years is the infectious colitis model using the epithelial-adherent pathogen *Citrobacter rodentium* (Eckmann 2006). Originally identified as the gram-

negative bacterium responsible for transmissible colonic hyperplasia in mouse breeding colonies, it was later understood to be a pathogen that infects and colonizes the cecal and colonic epithelium, causing superficial attaching-effacing (A/E) lesions (Barthold et al. 1976; Eckmann 2006; Luperchio and Schauer 2001; Schauer and Falkow 1993). These characteristic A/E lesions caused by *Citrobacter rodentium* resemble those formed by the human enteric pathogens enteropathogenic *Escherichia coli* (EPEC) and enterohemorrhagic *E. coli* (EHEC) (Eckmann 2006; Kaper, Nataro, and Mobley 2004; Welinder-Olsson and Kaijser 2005). Both pathogens remain major causes of morbidity and result in watery diarrhea (EPEC) or hemorrhagic colitis (EHEC) after consumption of undercooked meats (Eckmann 2006; Kaper, Nataro, and Mobley 2004; Welinder-Olsson and Kaijser 2005).

Citrobacter rodentium remains an excellent pathogen for testing the effects of mucosal inflammatory injury, as it typically does not cause systemic infection like other pathogens such as *Salmonella* (Bry and Brenner 2004; Eckmann 2006). Indeed, these bacteria attach to the host cell membrane and cause localized destruction of the brush border microvilli but do not invade deeper mucosal layers, making them primarily mucosal pathogens. Infection with *C. rodentium* results in a peak colonization of the cecal and colonic epithelium 1 week post-inoculation, with the majority of pathogens being cleared over the following 2-3 weeks (Eckmann 2006; Maaser et al. 2004). Weight loss and diarrhea are the primary consequences of infection, with minimal overall mortality (Barthold et al. 1978; Eckmann 2006).

In the colonic mucosa, infection with *C. rodentium* leads to a number of predictable features including hyperplasia of the intestinal crypts, goblet cell depletion,

and mucosal infiltration of lymphocytes, macrophages, neutrophils, and mast cells (Barthold et al. 1976; Eckmann 2006; Luperchio and Schauer 2001; Maaser et al. 2004). Lymphocytic responses are key mediators of *C. rodentium* infection and are characterized by mucosal infiltration of CD3+ T lymphocytes, particularly the CD4+ subset (Eckmann 2006; Higgins et al. 1999). These T cells are critical to the clearance of the bacteria, as studies have consistently demonstrated that mice with CD4+ T cell deficiency cannot effectively control the *C. rodentium* infection and experience high rates of mortality (Bry and Brenner 2004; Eckmann 2006; Simmons et al. 2003). More specifically, responses to *C. rodentium* are typically characterized by T helper cell-type 1 and 17 immune responses. Interleukin-12 (IL-12) and gamma-interferon (IFN-γ) are upregulated in the colons of infected mice, indicative of a polarization towards the Th1 immune response (Eckmann 2006; Higgins et al. 1999; Simmons et al. 2002). More recently, studies have identified a key role for Th17 type responses, as well (Harrington et al. 2005; Mangan et al. 2006). Along with T-cell driven adaptive immune responses, B cells have also been shown to be required for bacterial clearance, and colonized mice are known to develop IgA and IgG antibody responses to several *C. rodentium* bacterial proteins (Eckmann 2006; Maaser et al. 2004; Simmons et al. 2003).

Finally, innate immune responses are also known to play a role in mediating defenses against *C. rodentium*. Tumor necrosis factor (TNF)-α, an acute inflammatory cytokine that is induced on infection, has been shown to be required for clearance, and IL-6, a cytokine implicated in B cell function and acute-phase response, is upregulated after infection, with IL-6 deficiency leading to delayed clearance (Eckmann 2006; Kitamura et al. 2004; Yamamoto et al. 2000). Innate immune cells including mast cells

have been shown to play a role in defense against *C. rodentium*, with mast-cell deficiency resulting in more severe colonic inflammation, systemic infection, and mortality (Eckmann 2006; Wei et al. 2005).

While infectious colitis models such as *C. rodentium* can induce cecal injury, and genetic models such as the *Il-10*$^{-/-}$ model allow for the investigation of ileocecal inflammatory injury, small intestinal integrity is frequently challenged through alternate mechanisms (Eckmann 2006; Kühn et al. 1993). Given the rapidly proliferative nature of the small intestine, and the sensitivity of the various stem cell populations within the intestine to DNA damage induced by ionizing radiation, high dose whole body radiation (WBR) is frequently employed as a model to injure the small intestine and is considered the gold standard model to study intestinal stem cell-mediated crypt regeneration (Hua et al. 2012; Metcalfe et al. 2014; Potten and Hendry 1975; Potten 1977; Tian et al. 2011). The recent discovery of intestinal stem cell markers has allowed for investigation of the survival of various stem cell populations after radiation injury to the intestine (Barker 2014; Hua et al. 2012; Van Landeghem et al. 2012; Metcalfe et al. 2014; Tian et al. 2011). It is generally proposed that the two putative populations of intestinal stem cells have varying sensitivities to radiation, and studies have identified a role for each in repopulation of the intestinal epithelium after injury (Barker 2014; Hua et al. 2012; Tian et al. 2011).

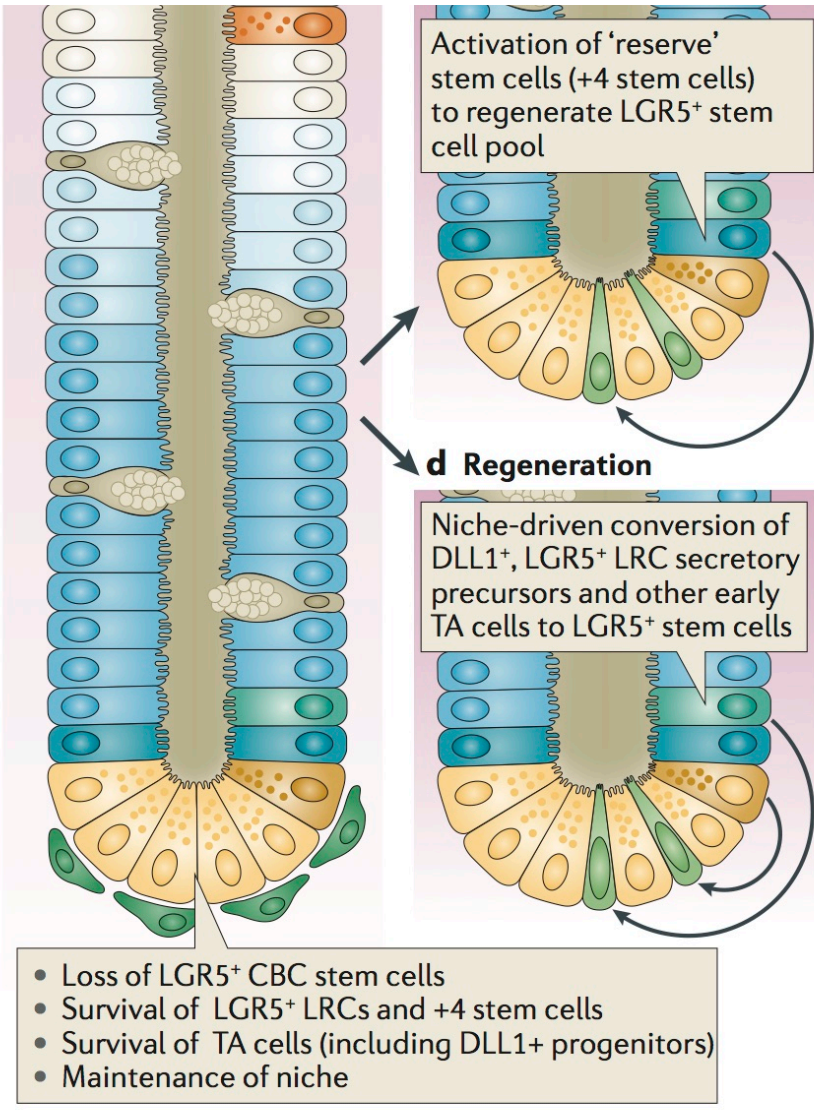

Figure 12. Epithelial regeneration in the small intestine. Loss of Lgr5+ stem cells after injury can activate reserve Lgr5+ cells as well as +4 cells to restore epithelial renewal. Figure from Barker 2014.

Gastrointestinal toxicity that occurs after ionizing radiation exposure results in diarrhea, dehydration, enterobacterial infection, as well as sepsis, circulatory shock, and death (Hauer-Jensen, Denham, and Andreyev 2014; Van Landeghem et al. 2012; Potten 1990). After exposure to high doses of whole body radiation, intestinal stem cell death and diminution results in denudation of the epithelium due to compromised intestinal

crypt regeneration (Booth and Potten 2000; Paris et al. 2001; Potten, Booth, and Pritchard 1997; Potten and Hendry 1975; Potten 1977; Potten et al. 2009). Between 8-12 Gray WBR, hematopoietic depletion and bone marrow failure are typically the causes of death in mice, while at higher doses, such as 14 Gy, GI toxicity precedes hematopoietic dysfunction and is the primary cause of death (Van Landeghem et al. 2012; Paris et al. 2001). Thus, most studies of crypt regeneration after high-dose WBR typically focus on early time points (day 1-9 after WBR) because of high animal mortality from complications of radiation (Van Landeghem et al. 2012).

INTRODUCTION TO BLOOD VESSEL EPICARDIAL SUBSTANCE (BVES)

BVES: Structure, Expression, and Proposed Functions

Blood Vessel Epicardial Substance or Popeye domain containing gene 1 (BVES/Popdc1) is a junctional-associated transmembrane protein originally discovered in a cDNA screen of the developing heart in the laboratories of Dr. David Bader and Dr. Thomas Brand (Andrée et al. 2000; Reese et al. 1999). BVES consists of 360 amino acid residues coding for three hydrophobic regions, two N-terminal glycosylation sites, and an intracellular domain of high intra-family homology termed the Popeye domain (Andrée et al. 2000; Knight, Bader, and Backstrom 2003; Osler, Chang, and Bader 2005). Popdc2 and Popdc3 are the other members of the Popdc family, and proteins which are 50 percent conserved with each other but with which BVES shares only 25 percent homology (Andrée et al. 2000; Hager and Bader 2009; Smith and Bader 2006).

As BVES shares little structural homology with other identified proteins, establishing its function from its structural sequence has not been possible (Reese et al. 1999). The N-terminus of BVES (amino acids 1-42) possesses two glycosylation sites, which are thought to facilitate recruitment of BVES to the cell membrane or prevent its degradation (Hager and Bader 2009; Knight, Bader, and Backstrom 2003). The intracellular C-terminus (amino acids 113-360) contains the Popeye domain and is highly conserved among the other family members (Brand 2005). BVES exists as a multimer through its intracellular C-terminus, which is thought to be essential for molecular regulation of cell-cell adhesion (Kawaguchi et al. 2008). In particular, amino acids K^{272}

and K^{273} in the intracellular domain are critical for BVES homodimerization (Kawaguchi et al. 2008).

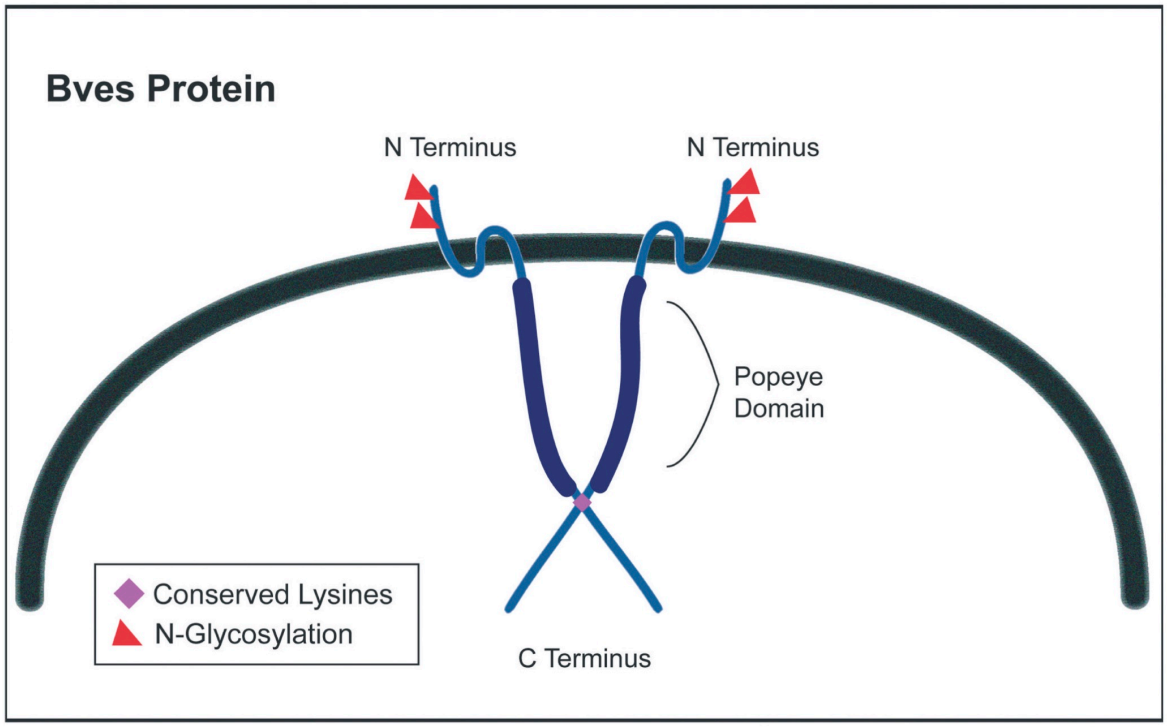

Figure 13. BVES protein. BVES is a transmembrane protein that homodimerizes. It possesses two N-glycosylation sites and a self-associating C-terminus, which contains the highly conserved Popeye domain. Figure from Hager and Bader 2009.

Bves is highly expressed in cells that are adherent, couple, or are interactive, such as those of the heart, skeletal and smooth muscle, brain, and various epithelia (Andrée et al. 2002; Hager and Bader 2009; Osler, Smith, and Bader 2006; Smith and Bader 2006; Torlopp et al. 2006; Vasavada, DiAngelo, and Duncan 2004). Within cells, BVES exhibits dynamic subcellular distribution: in cells that are subconfluent, BVES is visualized within the cell, but in cells that begin to adhere, BVES localizes to the membrane to points of cell-cell contact (Osler and Bader 2004; Smith and Bader 2006). Dr. Thomas Brand's group has generated mice null for the *Bves* gene (Andrée et al.

2002). These mice are fit and fertile and display a normal lifespan with no overt phenotypes, though they demonstrate impaired skeletal muscle regeneration after cardiotoxin injection (Andrée et al. 2002). As BVES has been shown to be important for many developmental processes, lack of embryonic lethality with its deletion may be due to functional compensation by other Popdc family members (Andrée et al. 2002; Ripley et al. 2006).

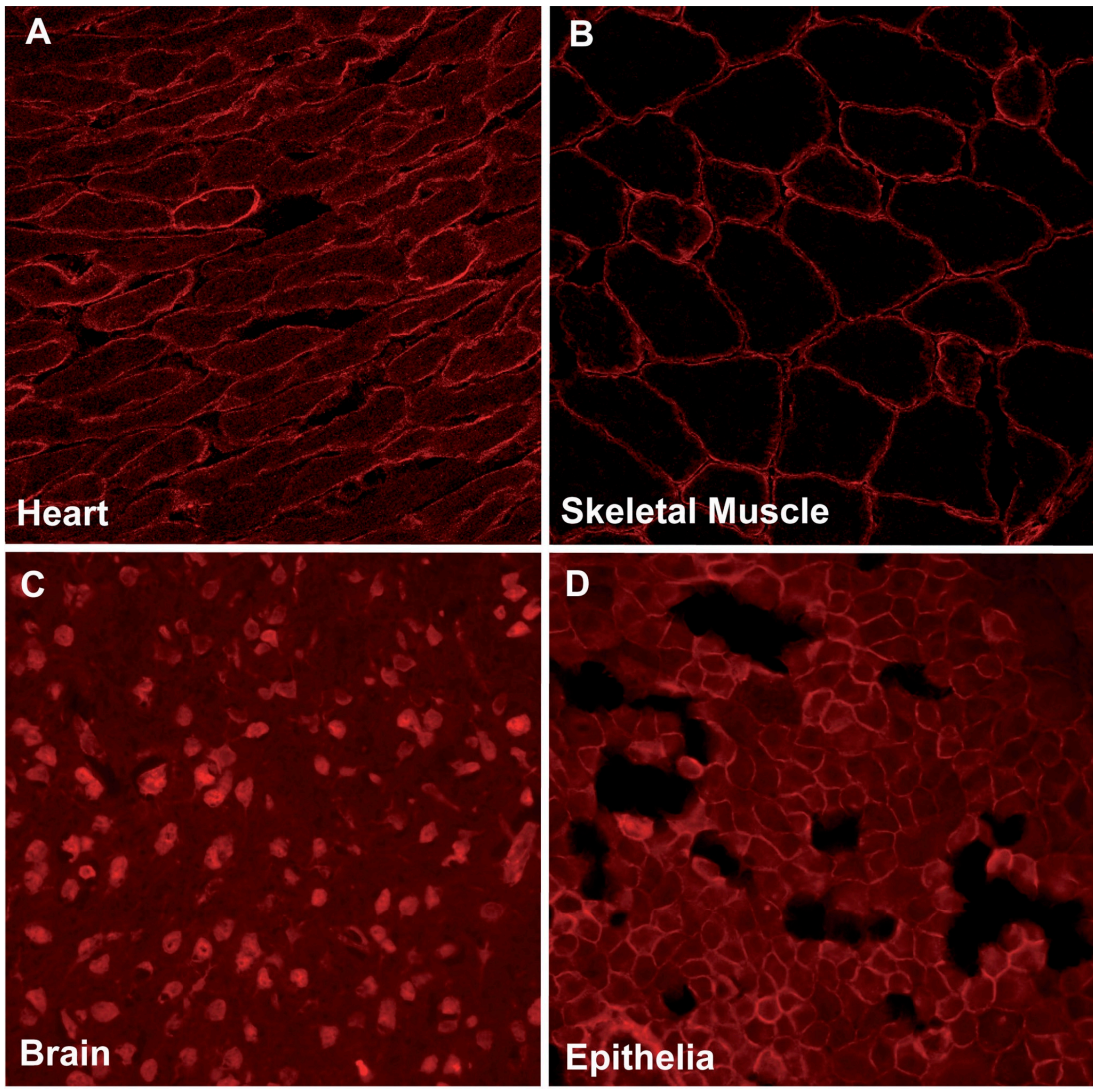

Figure 14. BVES expression in various tissues. Bves is highly expressed in cells that associate including the (A) heart, (B) skeletal muscle, (C) brain, and (D) various epithelia. Figure from Hager and Bader 2009.

Some of the proposed functions of BVES include the regulation of epithelial integrity through the maintenance of tight junctions, conference of adhesive properties, and regulation of cell motility (Osler, Chang, and Bader 2005; Smith et al. 2008; Williams et al. 2011). BVES traffics to points of cell–cell contact early in the process, suggesting a role for it in cell communication or cell-cell adhesion (Osler and Bader 2004; Osler, Chang, and Bader 2005; Wada, Reese, and Bader 2001). Transfection of wildtype Bves into normally non-adherent L-cells results in conspicuous formation of cell aggregates (Kawaguchi et al. 2008; Wada, Reese, and Bader 2001). However, transfection of Bves mutated or deleted at K^{272} and K^{273} results in L-cells that do not form continuous epithelial sheets, fail to maintain junctional proteins at the membrane, and demonstrate a dramatic reduction in transepithelial resistance, indicative of a loss of functional tight junctions (Kawaguchi et al. 2008). BVES is known to co-localize with ZO1 and Occludin, components of tight junctions, and GST pull-down experiments show an interaction between ZO1 and the intracellular C-terminal tail of BVES (Osler, Chang, and Bader 2005). In addition to co-localizing with junctional proteins, it has also been reported to co-localize with the adherens junction protein, E-cadherin (Osler, Chang, and Bader 2005; Smith and Bader 2006). It is possible that BVES serves as a dock or recruiting site for other junctional proteins which create cellular junctions (Hager and Bader 2009). While BVES may also regulate cellular interactions with other cells or the extracellular environment, as is typical of other transmembrane proteins, its extracellular N-terminus is thought to be too short to mediate an intercellular interaction; additionally, as it is not homologous across species like the highly conserved C-terminus, it is therefore most likely not essential (Hager and Bader 2009).

Moreover, BVES has been demonstrated to play a key role in regulating cell morphology and migration. Interfering with BVES function in human corneal epithelial (HCE) cells has been shown to induce mesenchymal morphology, increase proliferation and migration, expression of mesenchymal markers, and anchorage-independent growth (Kawaguchi et al. 2008; Williams et al. 2011). Conversely, restoring BVES expression in colorectal cancer (CRC) cells results in adoption of epithelial features, thus implicating BVES as a regulator of the balance between epithelial and mesenchymal phenotypes (Kawaguchi et al. 2008; Williams et al. 2011).

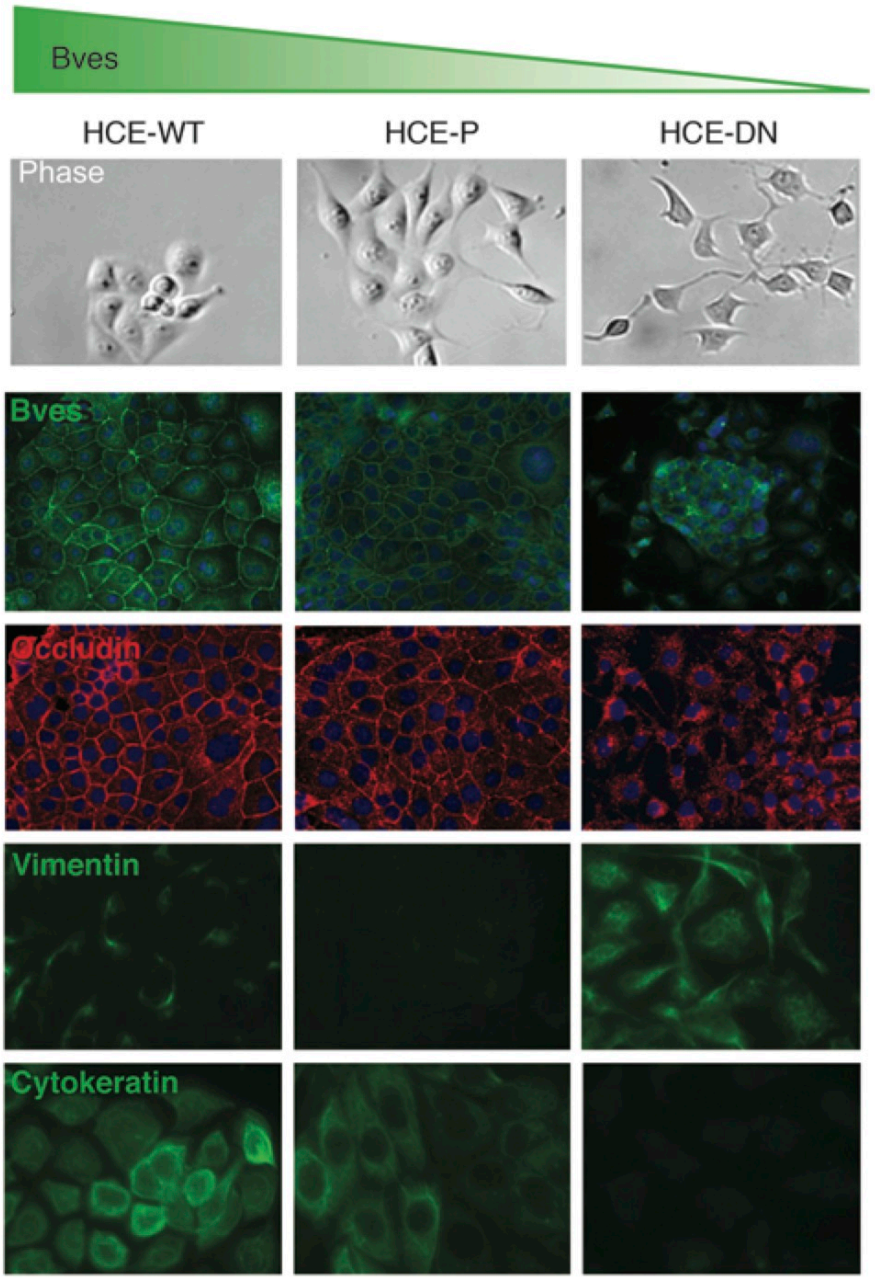

Figure 15. BVES regulates epithelial to mesenchymal transition in human corneal epithelial cells. Morphological changes in human corneal epithelial cells after BVES knockdown, and immunofluroescent localization of BVES, occludin, vimentin, and cytokeratin in confluent cultures. Figure from Williams et al. 2011.

Loss of BVES in HCE cells is associated with reduced E-cadherin levels, and both cytoplasmic and nuclear redistribution of β-catenin (Williams et al. 2011). Overexpression of BVES in human colon cancer cells is associated with increased E-cadherin, redistribution of β-catenin to the cell membrane, and decreased TCF4 activity, suggesting that BVES modulates canonical Wnt signaling (Williams et al. 2011). An inverse relationship between *BVES* and *ZEB1* expression has also been observed in colorectal cancer (Williams et al. 2011). ZEB1 promotes EMT via transcriptional repression of E-cadherin and other cell polarity genes (Aigner et al. 2007; Williams et al. 2011).

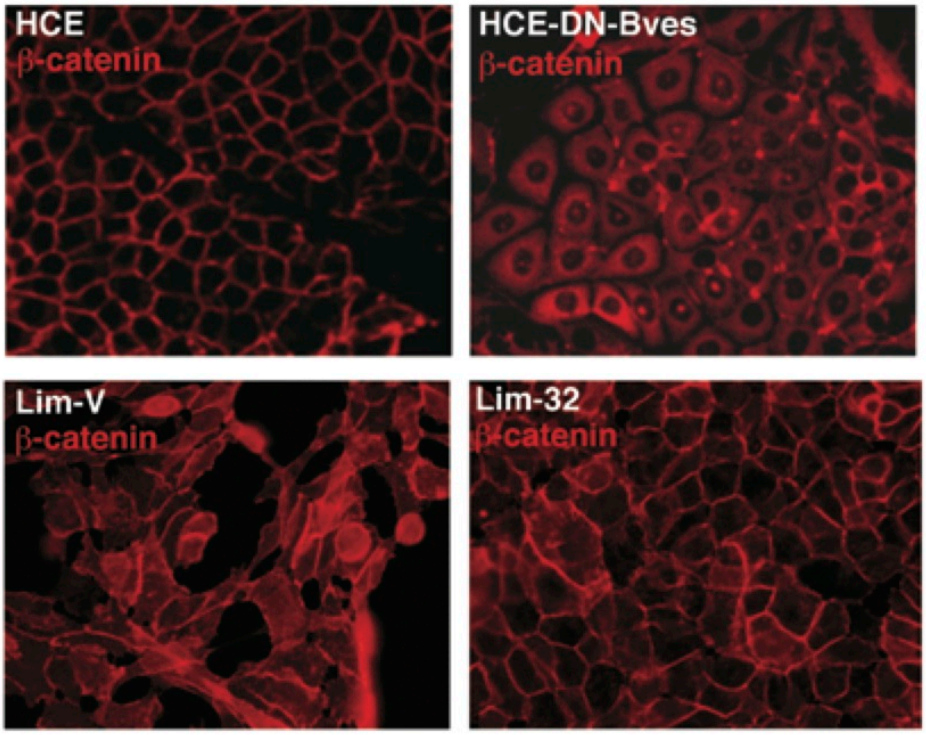

Figure 16. BVES modulates Wnt signaling. Immunofluorescence staining showing β-catenin cytoplasmic and nuclear redistribution after BVES knockdown in human corneal epithelial cells (Top) and membranous redistribution after BVES expression in LIM2405 colon cancer cell lines (Bottom). Figure from Williams et al. 2011.

BVES: Molecular Interactions

Studies have begun to uncover molecular interactions of BVES. A yeast-two-hybrid screen identified guanine nucleotide exchange factor T (GEFT) as a novel interacting protein (Smith et al. 2008). BVES and GEFT interact to modulate downstream effector proteins, Rac1 and Cdc42, Rho GTPases that induce lamellipodia and filopodia formation during cell migration (Guo et al. 2003; Hager and Bader 2009). However, the precise mechanism by which this occurs is yet to be established. Recently, BVES was shown to regulate RhoA signaling at least partially through its interaction with GEF-H1 and that this modulates EMT (Russ et al. 2011; Williams et al. 2011). Collectively, these data implicate BVES as a regulator of junctional signaling programs that are important in EMT and fundamental to intestinal epithelial restitution. Additionally, BVES was recently found to impact vesicular trafficking through its interaction with VAMP3, a SNARE protein that recycles transferrin and β1-integrin receptors (Hager et al. 2010). Moreover, as a protein originally discovered to play a role in cardiac development, BVES has been shown to regulate a number of processes relevant to cardiac physiology. For example, BVES binds cAMP with high affinity, interacts with the potassium channel TREK-1, and regulates cardiac pacemaking (Froese et al. 2012). Additionally, BVES interacts with the caveolin Cav3 to regulate the structural and functional integrity of caveolae in cardiac myocytes (Alcalay et al. 2013). Thus, BVES impacts a number of cellular processes with broad physiological implications. It is highly likely that other BVES interacting proteins exist, and their identification is critical to understanding the role of BVES in normal and pathological junctional biology.

BVES in Intestinal Diseases

BVES is a known regulator of epithelial and mesenchymal states and junctional-associated signaling. Epithelial-to-mesenchymal transition is a critical element in normal wound healing processes as well as the metastatic progression of many cancers (Kalluri and Weinberg 2009). Recently, it has been found that BVES is significantly underexpressed in all stages of human colorectal cancer and in adenomatous polyps, suggesting that its suppression may occur early in the transformation process (Williams et al. 2011). A number of colorectal cancer cell lines exhibit decreased BVES expression and promoter hypermethylation, which is associated with transcriptional silencing (Williams et al. 2011). Expression of BVES was discovered to be downregulated in gastric cancer cell lines and in gastric cancer tissues, with the BVES promoter regions hypermethylated in the cancer cell lines and tissues in which BVES was silenced (Kim et al. 2010). Moreover, BVES has also been implicated in hepatocellular carcinoma (HCC), and it has been found to be downregulated in human HCC tissues and HCC cell lines with high metastatic potential (Han et al. 2014). BVES inhibition in Huh7 hepatocellular carcinoma cells results in morphological changes including cytoskeleton rearrangement, junctional disruption, increased cell migration and invasion, and increased expression of epithelial-mesenchymal transition transcription factors Snail1 and Twist1 (Han et al. 2014).

As the regulation of EMT is critical to normal intestinal restitution processes, and the imbalance of epithelial and mesenchymal states contributes to many intestinal diseases and cancer metastases (Bataille and Rohrmeier 2008; Kalluri and Weinberg 2009), study of BVES may provide therapeutic opportunities. Additionally, considering

that disruption of tight-junctional integrity has been proposed as a key contributing factor to the increased intestinal permeability present in inflammatory bowel disease (Heller et al. 2005; Henderson et al. 2011; Ma et al. 2004; Porras et al. 2006; Shen, Su, and Turner 2009; Shen 2012; Söderholm, Olaison, and Peterson 2002; Turner 2009; Wyatt et al. 1993), better understanding of how BVES contributes to tight-junctional integrity may offer new insights into epithelial barrier dysfunction. Finally, given its role in the regulation of junctional signaling, particularly adherens junction-associated Wnt signaling, a pathway critical to intestinal stem cell signaling, crypt proliferation, and the development of colon cancer (Clevers and Nusse 2012; Clevers 2013; J. H. van Es et al. 2012), BVES may play a role in the regulation of intestinal homeostasis, response to injury, and the development of colon cancer.

Hypothesis

For my thesis work, it has been my hypothesis that BVES regulates intestinal homeostasis and response to injury. BVES is known to influence junctional-associated Wnt signaling, a critical regulator of intestinal stem cell signaling, crypt proliferation, and regeneration. Furthermore, as a tight junction-associated protein, it is possible that it plays a role in the regulation of intestinal epithelial barrier integrity and impacts responses to colonic injury. Thus, the primary objective of my work has been to contribute to our understanding of the role of BVES in basic intestinal biology and intestinal disease processes.

CHAPTER II

BVES REGULATES INTESTINAL STEM CELL PROGRAMS AND INTESTINAL CRYPT VIABILITY AFTER RADIATION

Abstract

Blood Vessel Epicardial Substance (BVES/Popdc1) is a junctional-associated transmembrane protein that is underexpressed in a number of malignancies and regulates epithelial-to-mesenchymal transition. We previously identified a role for BVES in regulation of the Wnt pathway, a modulator of intestinal stem cell programs, but its role in small intestinal (SI) biology remains unexplored. We hypothesized that BVES influences intestinal stem cell programs and is critical to SI homeostasis after radiation injury. At baseline, *Bves*$^{-/-}$ mice demonstrated increased crypt height, as well as elevated proliferation and expression of the stem cell marker *Lgr5* compared to wildtype (WT) mice. Intercross with Lgr5-EGFP reporter mice confirmed expansion of the stem cell compartment in *Bves*$^{-/-}$ mice. To examine stem cell function after BVES deletion, we employed *ex vivo* 3D-enteroid cultures. *Bves*$^{-/-}$ enteroids demonstrated increased stemness compared to WT, when examining parameters such as plating efficiency, stem spheroid formation, and retention of peripheral cystic structures. Furthermore, we observed increased proliferation, expression of crypt-base columnar "CBC" and "+4" stem cell markers, and amplified Wnt signaling in the *Bves*$^{-/-}$ enteroids. *Bves* expression was downregulated after radiation in WT mice. Moreover, after radiation, *Bves*$^{-/-}$ mice demonstrated significantly greater crypt viability, proliferation, and amplified Wnt

signaling in comparison to WT mice. *Bves*$^{-/-}$ mice also demonstrated elevation in *Lgr5* and *Ascl2* expression, and putative damage-responsive stem cell populations marked by *Bmi1* and *TERT*. Therefore, BVES is a key regulator of intestinal stem cell programs and mucosal homeostasis.

Introduction

The intestinal epithelium is a rapidly proliferating tissue that is thought to renew itself every 5 days (Barker 2014; Sato and Clevers 2013). Intestinal homeostasis is maintained by dynamic stem cell populations that reside in invaginations of the intestinal epithelium known as crypts (Barker, van de Wetering, and Clevers 2008; Barker 2014; Clevers 2013). Until recently, thorough characterization of these stem cell populations has remained challenging due to the absence of specific markers and suitable methodologies for their identification (Barker 2014; Potten et al. 2009). However, recently-discovered adult intestinal stem cell markers, and recently-developed lineage tracing technologies and innovative *ex vivo* 3D crypt cultures or "enteroid" systems have greatly facilitated their characterization (Barker 2014; Barker et al. 2007; Sato et al. 2009; Sato, van Es, et al. 2011).

Current evidence suggests the existence of ≥2 intestinal stem cell (ISC) populations: (1) a rapidly-cycling, crypt-based columnar (CBC) stem cell population at the base of the intestinal crypts, whose markers include Lgr5, a transmembrane receptor for R-spondin that amplifies Wnt tone, as well as Ascl2, Olfm4, Msi1, Smoc2, and Sox9; and (2) a more slowly-cycling, quiescent "+4" stem cell population that resides primarily at the +4 position from the base of the crypt and is marked by Bmi1, TERT, Lrig1, and

Hopx (Barker 2014; Durand et al. 2012; Van Landeghem et al. 2012; Li and Clevers 2010; Potten et al. 2009). Wnt signaling, which regulates numerous biological processes ranging from development to malignancy, is known to be one of the many signaling pathways that governs intestinal homeostasis and is critical to the maintenance of the intestinal stem cell niche (Clevers and Nusse 2012; Clevers 2013; J. H. van Es et al. 2012; Gregorieff and Clevers 2005; Pinto et al. 2003).

Small intestinal (SI) regenerative responses are often assessed via radiation injury modeling due to the sensitivity of intestinal stem cell populations to ionizing radiation (Booth and Potten 2000; Hua et al. 2012; Metcalfe et al. 2014; Ottewell et al. 2006; Potten, Booth, and Pritchard 1997). Successful intestinal tissue recovery and regeneration after radiation is mediated by the survival of a subset of stem cells which reconstitute the injured crypt-villus unit (Booth and Potten 2000; Potten, Booth, and Pritchard 1997). The contribution of $Lgr5^{+}$-CBC versus +4-ISC to normal intestinal epithelial renewal and repair after injury is still under debate, but a number of studies have identified a role for each in restoring epithelial integrity after injury (Buczacki et al. 2013; Hua et al. 2012; Metcalfe et al. 2014; Tian et al. 2011).

Blood Vessel Epicardial Substance (BVES/Popdc1) is a junctional-associated, three-pass transmembrane protein that was originally isolated from a cDNA screen of the developing heart (Andrée et al. 2000; Reese et al. 1999). BVES is highly expressed in epithelial tissues and regulates epithelial-to-mesenchymal transition (EMT) (Andrée et al. 2002; Han et al. 2014; Jayagopal et al. 2011; Kawaguchi et al. 2008; Reese et al. 1999; Vasavada, DiAngelo, and Duncan 2004; Williams et al. 2011). We have previously demonstrated that BVES regulates colonic epithelial phenotypes *in vitro* and is a

regulator of the Wnt pathway through stabilization of E-cadherin and alterations in β-catenin subcellular localization (Williams et al. 2011). As the Wnt pathway is a critical regulator of small intestinal stem cell programs (Clevers 2013; Pinto et al. 2003), we hypothesized that BVES influences intestinal stem cell signaling and is critical to SI homeostasis after radiation injury.

In the present study, we have identified BVES as a key modulator of intestinal epithelial stem cell programs and epithelial regeneration after radiation-induced injury. At baseline, *Bves*$^{-/-}$ mice exhibited higher proliferation, greater crypt depth, and an expanded crypt stem cell compartment. *Ex vivo* 3D-enteroid cultures of *Bves*$^{-/-}$ crypts demonstrated increased stemness, when examined by parameters such as plating efficiency, stem spheroid formation, and retention of peripheral cystic structures. This was accompanied by increased proliferation and expression of CBC rapidly-cycling stem cell markers, +4 stem cell markers, and amplified Wnt signaling. Furthermore, we found that *Bves* expression is downregulated in response to radiation in wildtype (WT) mice, and that this downregulation is biologically relevant, as *Bves*$^{-/-}$ mice are protected from radiation-induced injury and demonstrate greater crypt viability, more active stem cell populations, and amplified Wnt signaling after radiation. Finally, enteroids cultured from *Bves*$^{-/-}$ crypts after radiation demonstrated greater plating efficiency, indicating an epithelial tissue-autonomous role for BVES in modulating intestinal crypt viability. Results from these studies suggest that BVES regulates intestinal stem cell signaling and intestinal crypt viability after radiation and that it may serve as a predictive biomarker for patients undergoing radiotherapy.

Methods

Mouse Models

WT (C57BL/6 background) were obtained from the Jackson Laboratories. *Bves*$^{-/-}$ mice have been described in detail (Andrée et al. 2002). Lgr5-EGFP-ires-CreERT2 mice (Barker et al. 2007) (The Jackson Laboratory, Bar Harbor, ME) were obtained from R. Coffey (Vanderbilt University). All experiments were performed with 8 to 10 week old male and female mice on C57BL/6 background under guidelines approved by the Vanderbilt Institutional Animal Care and Use Committee (IACUC).

γ-Irradiation Protocol

WT and *Bves*$^{-/-}$ mice were placed in a plexiglass-partitioning device and onto a turntable delivery platform, ensuring uniform radiation dosing of all mice. WT and *Bves*$^{-/-}$ mice received 12 Gy whole-body radiation (WBR) from a Mark I ^{137}Cs source delivered at 1.58 Gy/min. Ninety-three hours after radiation, mice were injected with 0.02 mg/kg of vincristine sulfate (Sigma-Aldrich, St. Louis, MO) to arrest cells in metaphase and facilitate identification of regenerative crypts (Ottewell et al. 2006; Poindexter et al. 2015). Mice were euthanized three hours later at the ninety-six hour time point to examine crypt regeneration (Lund 2012; Poindexter et al. 2015). In a separate experiment, to assess *ex vivo* crypt viability after radiation, WT and *Bves*$^{-/-}$ mice were sacrificed four hours after 12 Gy radiation, with crypts harvested and plated for enteroid cultures (Poindexter et al. 2015).

Small Intestinal Organoid (Enteroid) Cultures

The crypt-enteroid culture method was modified from Sato et al (Mahe et al. 2013; Sato et al. 2009). Six centimeters of the proximal small intestine was dissected, flushed with ice cold phosphate buffered saline (PBS), dissected into 1 cm pieces, suspended in 5 mL ice cold PBS, and vortexed for 3 seconds. PBS was removed with a pipettor, and the wash was repeated. Tissue was transferred to 5 mL chelation buffer (1mM ethylenediaminetetraacetic acid (EDTA), made fresh in Dulbecco's phosphate buffered saline (DPBS) and rocked for 10 minutes at 4°C prior to washing twice with 10 mL PBS. 5 mL PBS was added, and the tissue was then shaken gently for 2 minutes. The supernatant was removed, 5 mL PBS was added, and the tissue was again gently shaken for 2 minutes. Supernatant was then decanted. 5 mL fresh chelation buffer was added and chelation was performed for 10 minutes at 4°C with gentle rocking. Crypts were filtered through a 70 μm filter into a pre-chilled 50 mL tube. The filter was rinsed with 5 mL cold shaking buffer (PBS with 43.3mM sucrose and 54.9mM Sorbitol). Complete crypts were counted and enough volume of shaking buffer was transferred for 1200 crypts to a pre-chilled 5 mL round-bottomed tube. Crypts were centrifuged at 150 x g for 10 minutes at 4°C. Shaking buffer was aspirated and crypts were resuspended in 50 μl of Matrigel (BD Bioscience, San Jose, CA, USA), per well, supplemented with 50 ng/mL EGF (R&D Systems, Minneapolis, MN, USA), 100 ng/mL Noggin (R&D Systems), 500 ng/mL R-Spondin (R&D Systems), and 50 μg/mL Wnt3a (Millipore, Billerica, MA, USA). Matrigel was overlayed with 500 μl Minigut culture media (Advanced DMEM/F12 (Invitrogen, Carlsbad, CA, USA)), L-Glutamine (Invitrogen), Penicillin-Streptomycin (Invitrogen), HEPES (Mediatech), N2 Supplement (R&D Systems), B27 Supplement

(Invitrogen) and growth factors. Every 4 days, media was replaced with fresh Minigut media. Plating efficiencies were calculated by dividing the total number of enterospheres formed by the original number of crypts plated at Day 0 and multiplying by 100. Enterospheres were visualized and counted at 24 and 48 hours after plating. Experiments were performed in triplicate and repeated two times.

Immunohistochemistry and Immunofluorescence Staining

At time of sacrifice, small intestines were removed, rinsed with phosphate-buffered saline (PBS), and Swiss-rolled for histological assessment. The tissues were fixed in 10% formalin overnight and transferred to 70% ethanol. Tissues were submitted to Vanderbilt Tissue Processing Shared Resource (TPSR) core for processing and paraffin embedding. For immunohistochemistry (IHC), five micrometer sections were cut, dewaxed, hydrated, and endogenous peroxidase activity quenched with 0.03% hydrogen peroxide in MeOH (Barrett et al. 2011, 2012, 2013; Williams et al. 2013). Antigen retrieval was conducted using Antigen Unmasking Reagent (Vector Laboratories, Burlingame, California, USA) according to manufacturer's instructions. After blocking, primary antibody was added overnight at 4°C. Isotype-matched antibodies were used as negative controls on serial sections. The Vectastain ABC Elite System (Vector Laboratories) was used to visualize staining for immunohistochemistry. Proliferation was measured using anti-phospho-Histone H3 (pH3) Ser10 antibody (Millipore) that labels cells in the mitotic (M) phase of the cell cycle at 1:150 dilution. Enteroendocrine cells were assessed by Chromogranin A (CgA) staining using anti-CgA at 1:1000 (ImmunoStar Inc., Hudson, WI). Anti-lysozyme antibody (Dako, Carpentaria,

CA) at 1:500 was utilized to identify Paneth cells. Goblet cells were identified by Periodic Acid Schiff (PAS) staining. Identification of apoptotic cells was conducted using the ApopTag Plus Peroxidase In Situ Apoptosis Kit (Millipore) according to the manufacturer's protocol. For GFP immunofluorescence (IF) staining, anti-GFP (Novus, Littleton, CO) at 1:500 was utilized, and slides were counterstained and mounted with ProLong Gold antifade including 4′,6-diamidino-2-phenylindole (Invitrogen). Crypt proliferation, Paneth cell quantification, and GFP+ cell counts was generated by counting cells in 40 sequential, well-aligned crypts from the proximal small intestine. This is presented as the mean number of positive cells per crypt. Crypt apoptosis, enteroendocrine cell counts, and goblet cell counts were obtained by counting cells in 40 sequential, well-aligned crypts and adjacent villi from the proximal small intestine. This is presented as the mean number of positive cells per crypt-villus unit.

qRT-PCR analysis

RNA from *Bves*$^{-/-}$ or WT proximal small intestine was isolated using the RNeasy Mini Kit (Qiagen, Valencia, Santa Clarita, California, USA). 20 µl of cDNA was synthesized using the iScript cDNA synthesis kit (Bio-rad, Hercules, California, USA) from 1 µg of total RNA. 1 µl of cDNA was used as a template in each subsequent PCR reaction. SYBR green qRT-PCR was performed using mouse Wnt signaling primer library I (Cat #: MWNT-I), as well as *Lgr5, Ascl2*, *Axin2*, and *PCNA* primers obtained from RealTimePrimers.com according to manufacturer's instructions. Sequences for validated primers for *Lrig1*, *Bmi1*, *Tert, Olfm4, Nanog, Muc2*, *and Bves* were obtained from Harvard Primer Bank (Cambridge, MA) and SYBR green qRT-PCR was performed

according to manufacturer's instructions (Invitrogen). Expression was analyzed using the delta-delta Ct method and normalized to Glyceraldehyde 3-phosphate dehydrogenase (*Gapdh*).

Statistical Methods

Analyses comparing two groups were analyzed using the Student's *t*-test. One-way ANOVA and Newman-Keuls post-test was used to compare multiple groups. Data is presented as the mean +/- the standard error of the mean (SEM) in bar graphs and a line identifying the mean is shown when all data points are plotted. All of these analyses were performed using GraphPad Prism®6.0c (San Diego, CA, USA). A $P<0.05$ was considered statistically significant.

Results

BVES regulates intestinal crypt homeostasis

Previous studies have demonstrated that BVES regulates colonic epithelial phenotypes *in vitro* and Wnt signaling through alterations in β-catenin subcellular localization (Williams et al. 2011). However, its role in small intestinal biology and the impact of its deletion *in vivo* on SI homeostasis was not previously examined. To determine if BVES deletion alters crypt morphology, proliferation, or differentiation in the small intestine, we performed histological characterization of *Bves*$^{-/-}$ mice and examined the proximal small intestine. While villus height was comparable to that of WT mice, *Bves*$^{-/-}$ mice demonstrated significantly greater crypt depth **(Figure 17A).** Analysis of crypt dynamics revealed no differences in apoptosis **(Figure 17B, 18)**; however

proliferation, as measured by phospho-histone H3 IHC, was increased in *Bves*$^{-/-}$ mice **(Figure 17C, 18)**. Additionally, the number of PAS-labeled goblet cells was increased compared to WT mice **(Figure 17D, 18),** although there were no differences in numbers of Paneth **(Figure 17E, 18)** or enteroendocrine cells **(Figure 17F, 18)**. These data demonstrate that BVES regulates proliferation, intestinal lineage allocation, and crypt morphology, indicating a previously unrecognized role for BVES in regulating intestinal homeostasis.

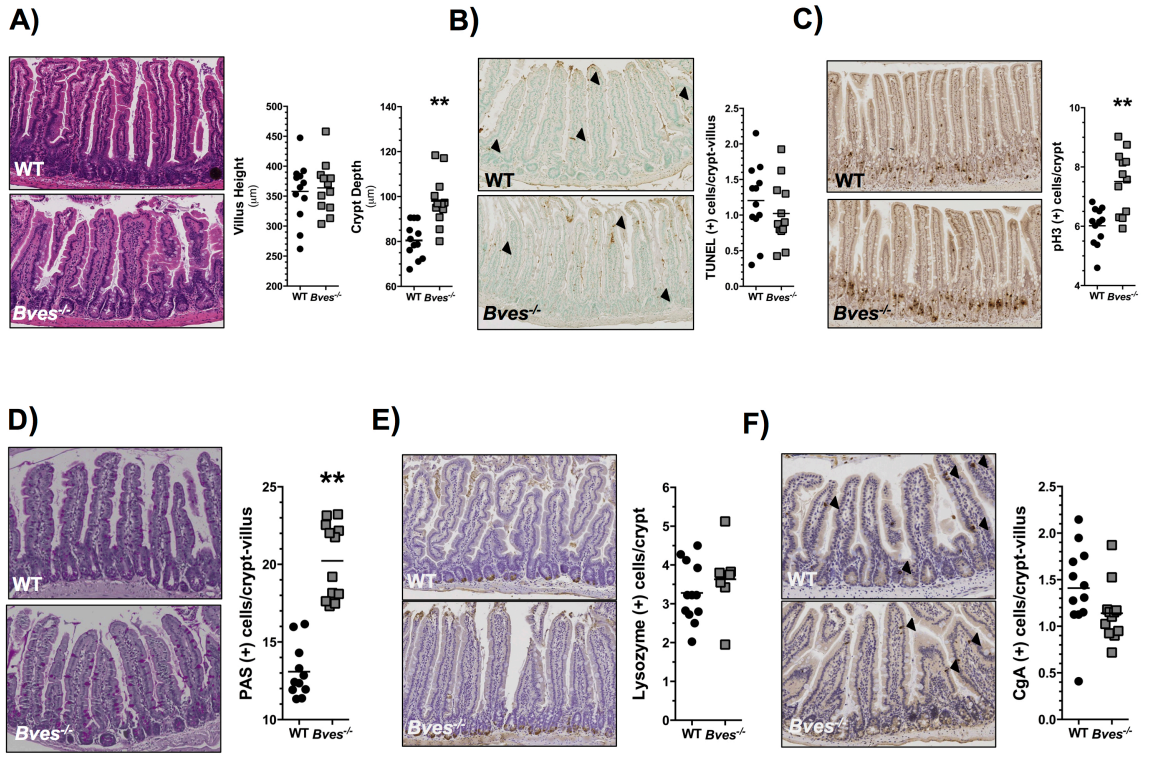

Figure 17. BVES regulates intestinal proliferation, lineage allocation, and crypt morphology. Small intestines were isolated and Swiss-rolled. (A) Representative H&E staining of sections of WT and *Bves*$^{-/-}$ small intestine. Images (left) and quantification (right) of WT and *Bves*$^{-/-}$ villus height (358 μm vs. 364 μm, P=0.76) and crypt depth (80.4 μm vs. 98.0 μm, **P<0.01, n=24). (B) Images (left) and quantification (right) of apoptotic cells per crypt/villus unit (1.2 vs. 1.0 TUNEL^{+} cells/crypt-villus unit, P=0.37, n=24). (C) Images (left) and quantification (right) of crypt proliferation (6.0 vs. 7.5 phospho-Histone H3^{+} cells/crypt, **P<0.01, n=24). (D) Images (left) and quantification (right) of goblet cells/crypt-villus unit (13.1 vs. 20.2 PAS^{+} cells/crypt, **P<0.01, n=23). (E) Images (left) and quantification (right) of Paneth cells/crypt-villus unit (3.3 vs. 3.6 Lysozyme^{+} cells/crypt, P=0.39, n=19). (F) Images (left) and quantification (right) of enteroendocrine cells/crypt-villus unit (1.4 vs. 1.1 CgA^{+} cells/crypt, P=0.10, n=24). All images were captured at 100x magnification. Black arrows indicate positively-stained cells.

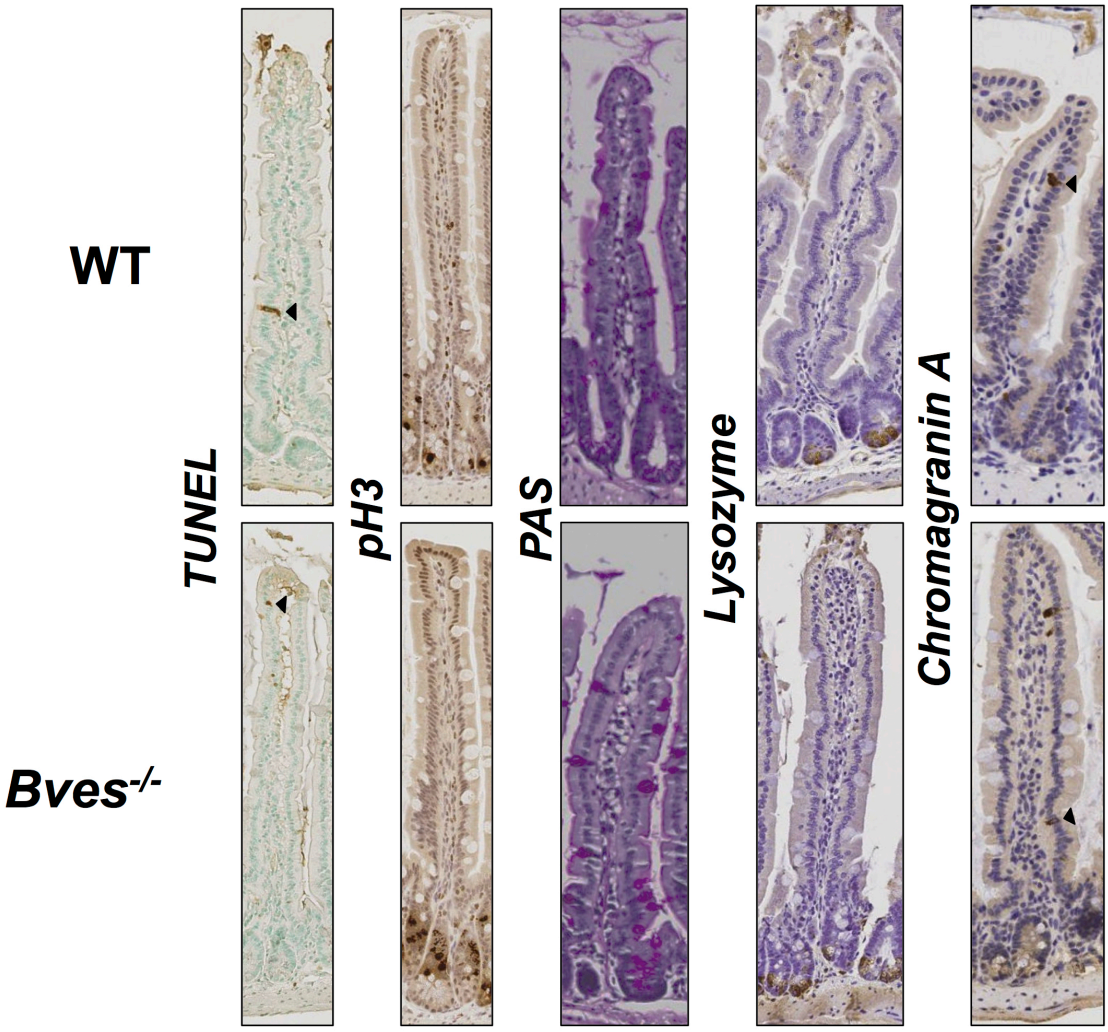

Figure 18. Magnification of WT and *Bves*$^{-/-}$ small intestine. Left to Right: TUNEL staining for apoptotic cells, pH3 staining for proliferating cells, PAS staining for goblet cells, lysozyme staining for Paneth cells, and CgA staining for enteroendocrine cells. Black arrows indicate positively-stained cells.

BVES modulates intestinal stem cell dynamics

As stem cell programs and Wnt pathway activation are critical in regulating intestinal homeostasis, we investigated expression of Wnt targets and intestinal stem cell markers in the *Bves*$^{-/-}$ intestine. Transcript levels of *Axin2* were significantly elevated at baseline in the *Bves*$^{-/-}$ SI **(Figure 19A)**. Additionally, we found significant elevation in

expression of *Lgr5,* a marker of CBC stem cells and another well-defined Wnt target in the *Bves*$^{-/-}$ SI **(Figure 19B)**. There were trending increases in expression of *Lrig1* and *Bmi1*, markers of +4 more slow-cycling stem cell populations **(Figure 19C)**. To confirm that BVES loss may be driving the expansion of crypt base columnar stem cell populations, we crossed WT and *Bves*$^{-/-}$ mice with a Lgr5-EGFP reporter line(Barker et al. 2007), which demonstrated an almost 2-fold increase in the number of GFP^{+} cells/$^{+}$crypt in the *Bves*$^{-/-}$ cohort compared to WT **(Figure 19D)**.

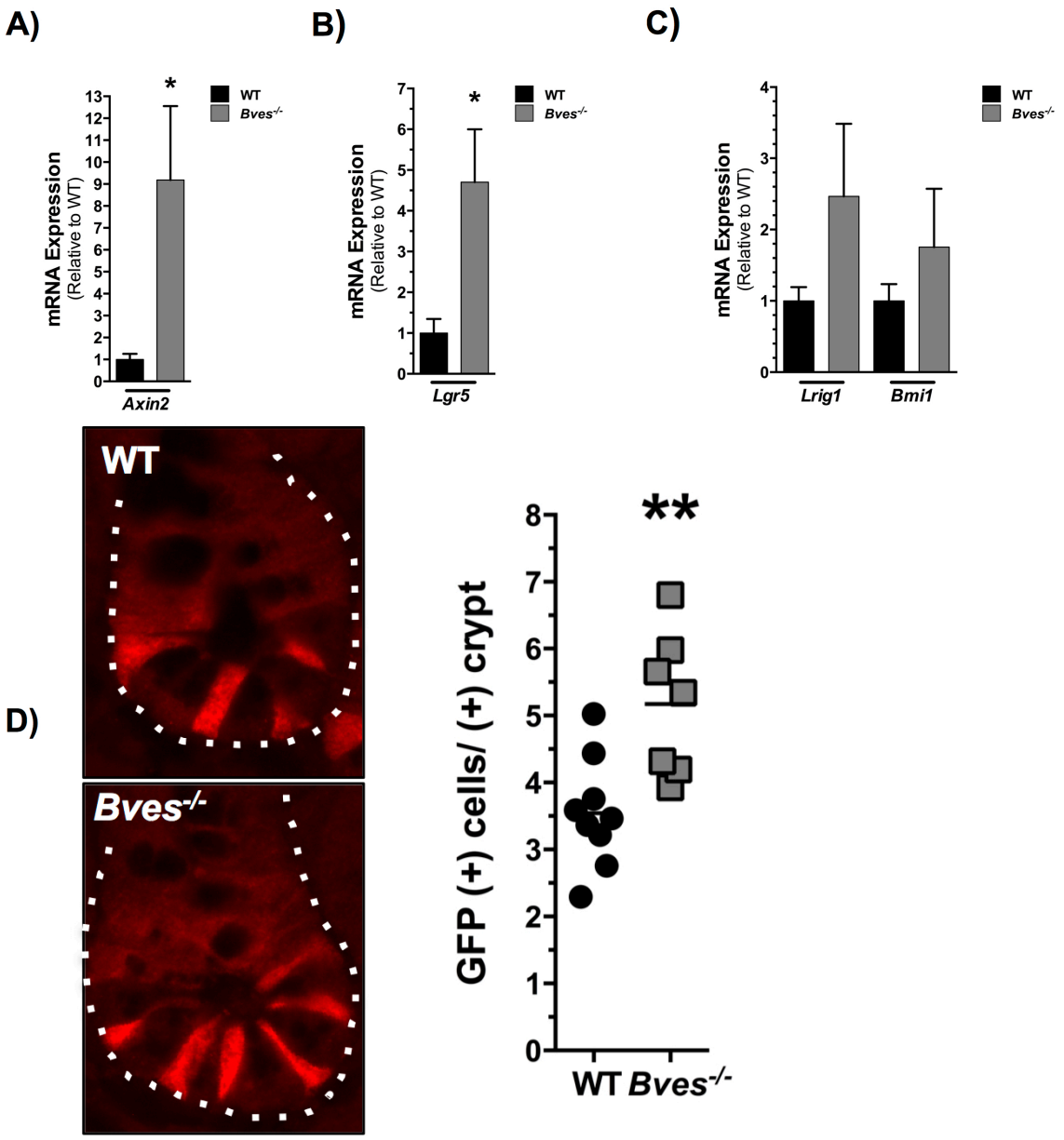

Figure 19. BVES regulates intestinal stem cell dynamics *in vivo*. (A) qRT-PCR analysis revealed increased expression of (A) *Axin2* (**P*<0.05, n=12) and (B) *Lgr5* (**P*<0.05, n=12) but no significant difference in mRNA levels of (C) *Lrig1* (*P*=0.21, n=12) and *Bmi1* (*P*=0.41, n=12) in *Bves*$^{-/-}$ proximal small intestine compared to WT. (D) Intercross of WT and *Bves*$^{-/-}$ mice with Lgr5-EGFP-ires-CreERT2 mice revealed increased number of GFP^{+} cells/$^{+}$crypt (3.5 vs. 5.2, ***P*<0.01, n=16) in the *Bves*$^{-/-}$ cohort. Images were captured at 400x magnification.

To further interrogate the role of BVES in SI stem cell behavior in an epithelial tissue-autonomous manner, we decided to employ the enteroid modeling system using *ex vivo* cultures of WT and BVES null crypts. Enteroids derived from *Bves*$^{-/-}$ mice demonstrated increased proliferation as determined by *PCNA* expression when harvested 5 days after plating **(Figure 20A)**. *Bves*$^{-/-}$ mice also demonstrated a 3-fold elevation in *Muc2* expression 96 hours after plating **(Figure 20B)**. Thus, the enteroid platform accurately recapitulated some of the phenotypes observed *in vivo*.

The enteroid platform is ideal for testing stem cell function (Durand et al. 2012; Farin, Van Es, and Clevers 2012; Sato et al. 2009). The "stemness" of an enteroid can be measured by several growth parameters. For instance, augmented stem cell survival can be measured by an increase in the number of crypts that survive plating when considering the total number of crypts plated and is represented as the plating efficiency. Additionally, percentages of cystic, stem-spheroid structures at specific time points can also serve as a marker for stemness. *Bves*$^{-/-}$ enteroids demonstrated higher plating efficiency **(Figure 20C)** and increased frequency of stem spheroids **(Figure 20D)** at 24 and 48 hours post-plating. After repassaging and maintenance in culture, *Bves*$^{-/-}$ enteroids consistently retained a significantly higher proportion of peripheral cystic structures in comparison to WT enteroids 5 days after passaging **(Figure 20E)**. Therefore, *Bves*$^{-/-}$ enteroids consistently demonstrated increased stemness when maintained in culture.

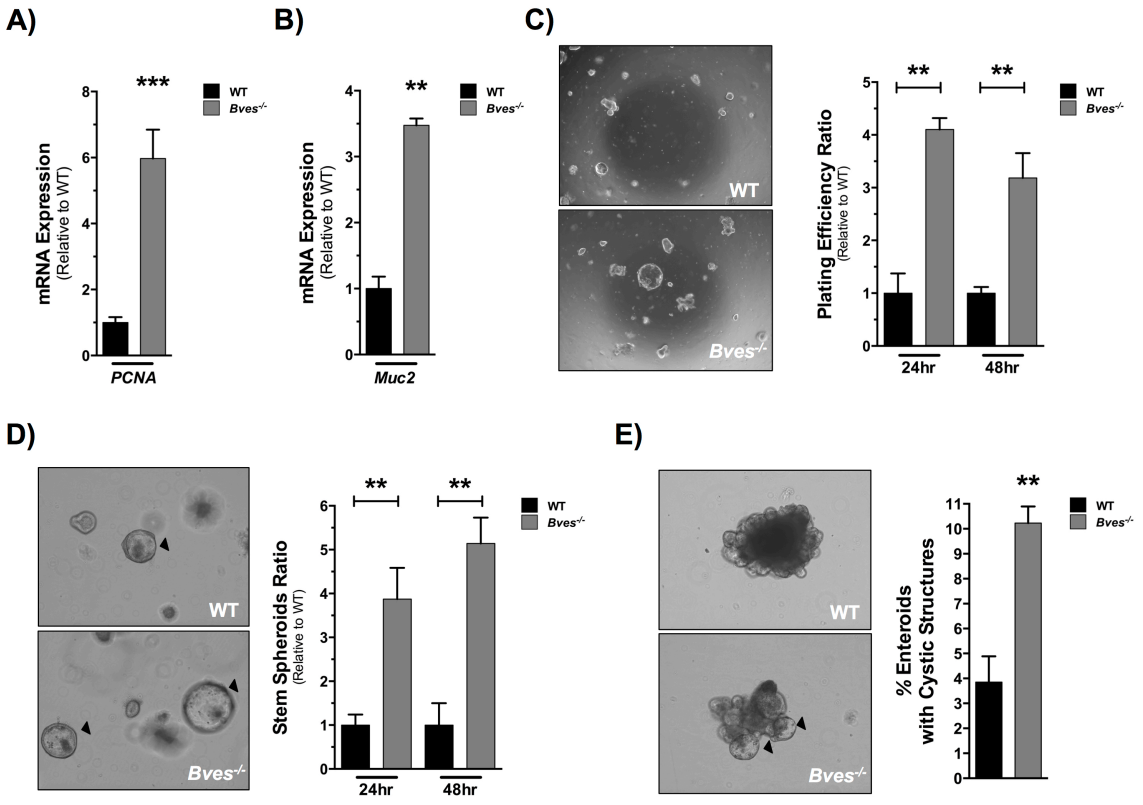

Figure 20. *Bves*$^{-/-}$ enteroids exhibit increased stemness *ex vivo*. Small intestinal crypts were isolated from WT or *Bves*$^{-/-}$ mice and embedded in Matrigel. (A) qRT-PCR analysis revealed increases in (A) *PCNA* (***P<0.001, n=6) and (B) *Muc2* (**P<0.01, n=6) mRNA levels in *Bves*$^{-/-}$ enteroids compared to WT. Enteroid stem cell properties determined based on (C) plating efficiency ratio, as measured by percentage of surviving enteroids 24 and 48 hours post-plating compared to total crypts plated (24 hours, **P<0.01; 48 hours, **P<0.01; n=6); (D) ratio of stem spheroid proportions counted 24 and 48 hours post-plating (24 hours, **P<0.01; 48 hours, **P<0.01; n=6) and (E) percentage of enteroids maintaining peripheral cystic structures 5 days after passaging (3.8 ± 1.0% vs. 10.2 ± 0.6%, **P<0.01, n=6). Images were captured at 40x magnification (20C) or 100x magnification (20D, 20E).

To investigate if these stemness phenotypes corresponded to expansion of stem cell populations, we surveyed for expression of stem cell markers. Both CBC **(Figure 21A)** and +4 stem cell populations **(Figure 21B)** were significantly elevated in the *Bves*$^{-/-}$

enteroids. Additionally, we observed a significant upregulation of Wnt ligands (*Wnt2*, *Wnt2b*, *Wnt3*, *Wnt7a*, *Wnt8B*), Frizzled receptors, which serve as cell-surface receptors of the Wnt pathway (*Fzd1*, *Fzd2*, *Fzd5*, *Fzd6*, *Fzd7*, *Fzd9*, *Fzd10*)**,** and Wnt targets (*Axin2*, *CCND1*, *CD44*, and *EGFR*) in *Bves*$^{-/-}$ enteroids **(Figure 21C-E)**, suggesting that amplified Wnt signaling may contribute to these stemness phenotypes. Collectively, these data identify a previously unrecognized role for BVES in regulating stem cell dynamics of the small intestine.

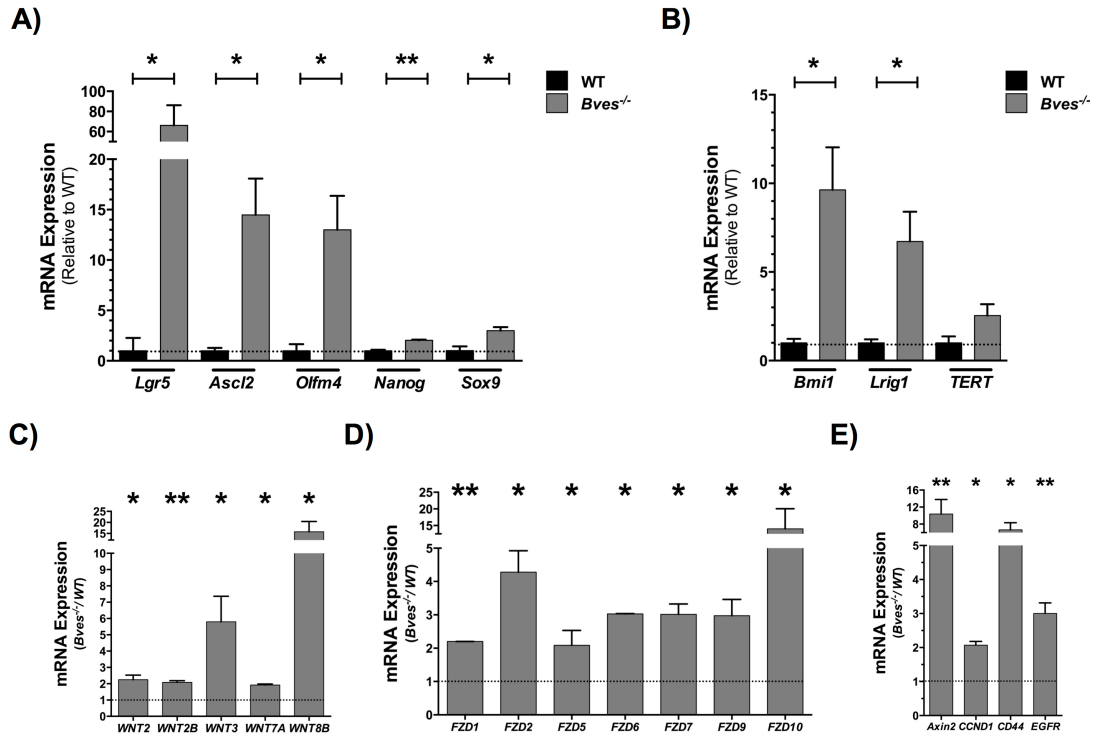

Figure 21. BVES regulates intestinal stem cell dynamics and Wnt signaling *ex vivo*. qRT-PCR analysis revealed increases in expression of **(**A) CBC stem cell markers in *Bves*$^{-/-}$ enteroids compared to WT. *Lgr5*, *Ascl2*, *Olfm4*, *Nanog*, and *Sox9* mRNA levels in *Bves*$^{-/-}$ enteroids compared to WT. qRT-PCR analysis also revealed increases in (B) +4 stem cell markers *Bmi1* and *Lrig1* mRNA levels in *Bves*$^{-/-}$ enteroids compared to WT with no significant differences in *TERT* expression (P=0.11). Expression of (C) Wnt ligands, (D) Wnt receptors, and (E) Wnt targets were significantly elevated in the *Bves*$^{-/-}$ enteroids. *P<0.05, **P<0.01 (n=6).

Intestinal Bves expression is downregulated after radiation and determines crypt viability

Stem cell populations are critical to repopulating the intestinal epithelium after radiation injury to the small intestine (Metcalfe et al. 2014; Tian et al. 2011). As we observed that BVES regulates stem cell programs, we postulated that BVES would impact crypt regenerative dynamics after ionizing radiation (Barker 2014; Ottewell et al. 2006). We first determined if *Bves* expression is altered in response to radiation, and observed that 96 hours after 12 Gy WBR that *Bves* messenger RNA was reduced more than 2.5-fold **(Figure 22A)**. This time point is known to be one of intestinal crypt regeneration (Van Landeghem et al. 2012; Lund 2012). We then took advantage of the availability of the $Bves^{-/-}$ mice to test if the observed difference in *Bves* expression was functionally relevant to intestinal injury responses. WT and $Bves^{-/-}$ cohorts were exposed to 12 Gy radiation and sacrificed after 96 hours. Mice were injected with vincristine, a mitotic inhibitor, three hours prior to sacrifice to facilitate identification of regenerative crypts. Examination of hematoxylin and eosin (H&E) stained sections revealed that $Bves^{-/-}$ mice exhibited significantly greater crypt viability in comparison to WT mice after radiation exposure **(Figure 22B)**. Crypts were considered viable if three or more mitotic bodies were observed per crypt (Ottewell et al. 2006; Poindexter et al. 2015). $Bves^{-/-}$ mice also exhibited significantly greater proliferation **(Figure 22C)** but no differences in apoptosis **(Figure 22D)**. Taken together, these data suggest that BVES modulates intestinal crypt viability after radiation and that its deletion promotes radioresistance.

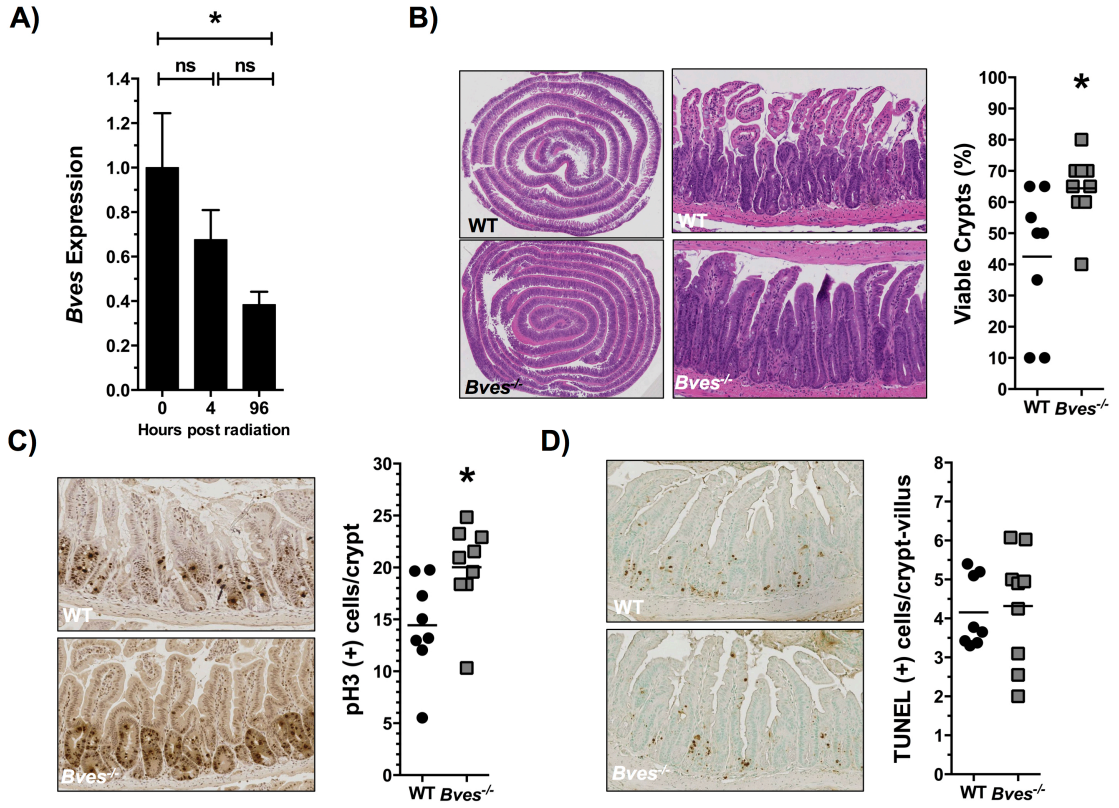

Figure 22. BVES regulates intestinal crypt viability after radiation. (A) qRT-PCR analysis comparing *Bves* mRNA expression in WT proximal small intestine prior to radiation vs. 4 hours (P=0.30, n=12), and 96 hours after 12 Gy radiation (*P=0.05, n=12). (B) Representative H&E stained sections and quantification of viable intestinal crypts in WT and *Bves*$^{-/-}$ mice. *Bves*$^{-/-}$ mice exhibited significantly greater crypt viability 96 hours after 12 Gy radiation (42.5 ± 7.8% vs. 64.4 ± 3.7% *P<0.05, n=17). Crypts were considered viable if 3 or more mitotic bodies were observed per crypt. 40 sequential, well-aligned crypts in the proximal one-third of the small intestine were counted per data point. The percent of surviving crypts was calculated using the following equation: (# of viable crypts/total # of crypts counted) x 100. (C) Images (left) and quantification (right) of crypt proliferation 96 hours after 12 Gy radiation (14.4 vs. 20.0 phospho-Histone H3^{+} cells/crypt, *P<0.05, n=17). (D) Images (left) and quantification (right) of apoptotic cells per crypt/villus unit (4.1 vs. 4.3 TUNEL^{+} cells/crypt-villus unit, P=0.79, n=17). Images were captured at 10x magnification (22B, left) or 100x magnification (22B, right, 22C, 22D).

BVES deletion results in amplified stem cell activity and Wnt signaling after radiation

Surviving stem cells are critical to the repopulation of intestinal crypts after radiation, and we observed an expanded stem cell population in the *Bves*$^{-/-}$ mice at baseline. Therefore, we investigated if alterations in surviving stem cell populations after radiation may be contributing to the increased crypt viability in these mice. qRT-PCR analysis revealed increases in *Bmi1* and *TERT* **(Figure 23A)** in *Bves*$^{-/-}$ mice, as well as *Lgr5* and *Ascl2* **(Figure 23B).** Therefore, unlike mice at baseline, we observed significant upregulation of markers of both +4 damage-responsive and CBC intestinal stem cell populations. Moreover, as Wnt signaling is a key signaling pathway that governs intestinal homeostasis and regeneration after injury, and given the amplified Wnt signaling present in the *Bves*$^{-/-}$ intestine at baseline and in *ex vivo* cultures, we assessed if alterations in the Wnt pathway were present after radiation. qRT-PCR analysis revealed significant upregulation of several Wnt ligands (*Wnt1*, *Wnt2*, *Wnt2b*, *Wnt3*, *Wnt3a*, *Wnt6, Wnt7b*, *Wnt8b*, *Wnt9a*, *Wnt10b*, and *Wnt16*)**,** Frizzled receptors (*Fzd3*, *Fzd8*, *Fzd9*, and *Fzd10*), and Wnt targets genes (*Lgr5*, *Ascl2*, *Sox2*, *VegfA*) in the *Bves*$^{-/-}$ mice compared to WT **(Figure 23C-E)**. Thus, amplified Wnt signaling may contribute to the increased proliferation and crypt viability observed in BVES knockout mice following radiation and supports stem cell survival and regeneration.

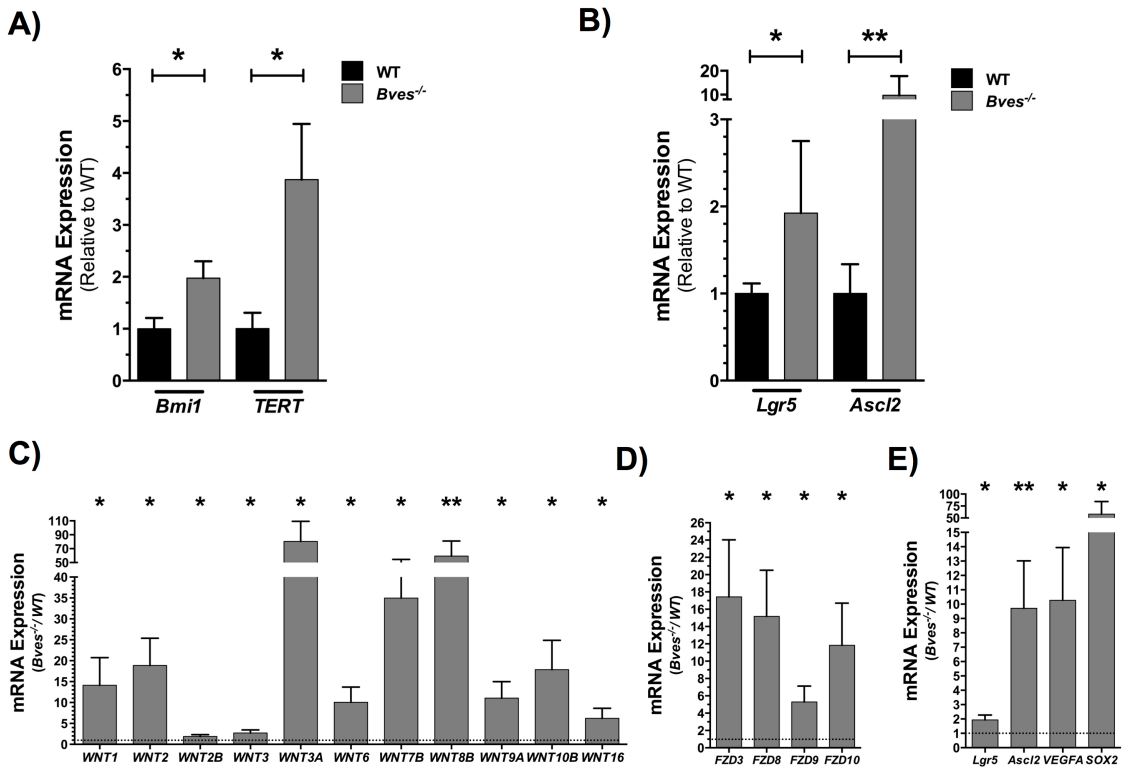

Figure 23. BVES modulates stem cell regenerative responses and Wnt signaling after radiation. Proximal small intestine was harvested from WT or *Bves*$^{-/-}$ mice after 12 Gy WBR. qRT-PCR analysis revealed increases in mRNA expression of (A) +4 stem cell markers *Bmi1* and *TERT* and (B) CBC stem cell markers *Lgr5* and *Ascl2* in *Bves*$^{-/-}$ proximal SI compared to WT. Expression of (C) Wnt ligands, (D) Wnt receptors, and (E) Wnt targets was significantly elevated in the *Bves*$^{-/-}$ proximal SI compared to WT. (**P*<0.05, ***P*<0.01, n=12)

Bves$^{-/-}$ *enteroids demonstrate radioresistance*

As we observed increased crypt viability *in vivo* after radiation of *Bves*$^{-/-}$ intestine, we hypothesized that *Bves*$^{-/-}$ enteroid plating efficiency, a surrogate marker for crypt viability, would be similarly impacted after radiation. We dosed mice with 12 Gy WBR, isolated SI tissue, and plated crypts 4 hours later. Consistent with our observations

at the 96 hour time point, we observed no differences in apoptosis between the cohorts **(Figure 24A)**. However, we observed a 2-fold increase in *Bves*$^{-/-}$ enteroid plating efficiency 24 hours after plating **(Figure 24B)**. These data suggest an epithelial tissue-autonomous role for BVES in regulating intestinal crypt viability after radiation.

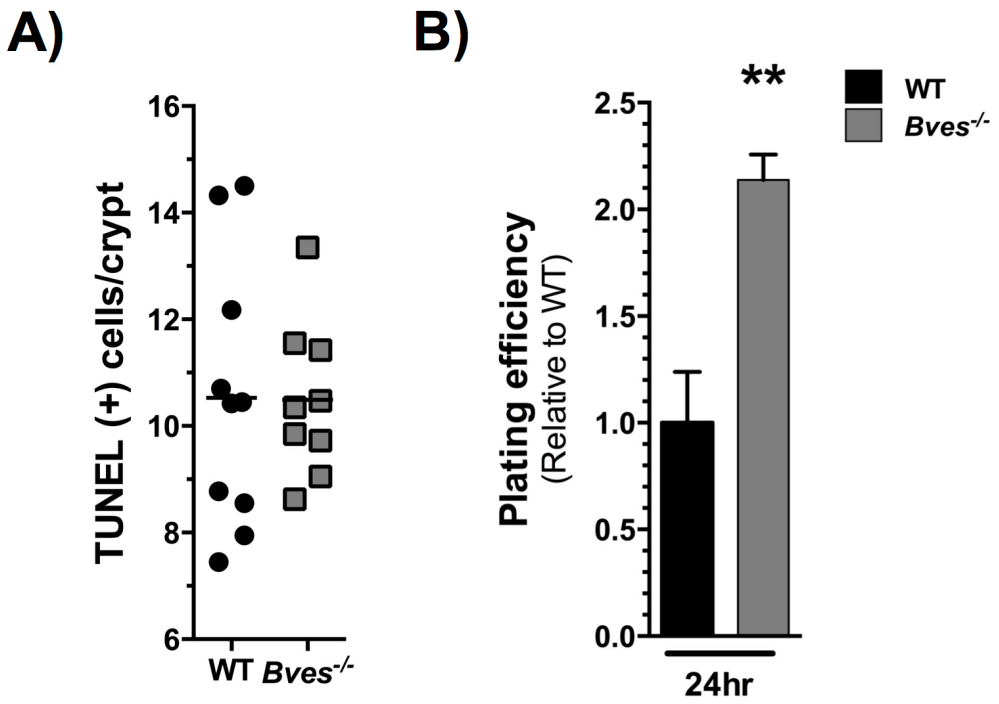

Figure 24. BVES deletion protects intestinal crypts after radiation. (A) Quantification of apoptotic cells per crypt/villus unit (10.5 vs. 10.5 TUNEL^{+} cells/crypt-villus unit, P=0.97, n=19) in WT and *Bves*$^{-/-}$ proximal SI 4 hours after 12 Gy radiation. (B) Enteroids harvested from *Bves*$^{-/-}$ mice after 12 Gy radiation demonstrated increased plating efficiency when compared to WT (**P<0.01).

Discussion

In this study, we investigated the role of BVES in intestinal homeostasis, stem cell function, and response to injury after ionizing radiation. At baseline, *Bves*$^{-/-}$ mice demonstrated altered lineage allocation, increased crypt size, and higher intestinal

proliferation with an expanded intestinal stem cell population. *Bves*$^{-/-}$ enteroids exhibited increased stemness with increased plating efficiency, proportion of stem spheroids, and retention of cystic structures, as well as increased expression of both CBC and +4 stem cell populations. These *ex vivo* studies suggest that the altered stem cell dynamics in the *Bves*$^{-/-}$ intestine do not require stromal-epithelial crosstalk, thus identifying a previously unrecognized role for BVES in stem cell biology that is epithelial cell-autonomous. Moreover, we found that *Bves* expression was downregulated in WT SI after radiation, and *Bves*$^{-/-}$ mice displayed significantly greater crypt viability after radiation. Additionally, the *Bves*$^{-/-}$ cohort demonstrated increased populations of both CBC and damage-responsive +4 stem cell populations after radiation, along with significantly amplified Wnt signaling. Lastly, *Bves*$^{-/-}$ crypts isolated from mice 4 hours after 12 Gy radiation displayed increased plating efficiency, thus demonstrating increased viability in an *ex vivo* setting, as well.

Peak apoptosis of the Lgr5^{+}-CBC stem cell population is thought to occur 4-6 hours after 12 Gy WBR (Hua et al. 2012; Lund 2012). After peak crypt loss between 48-72 hours after 12 Gy WBR, crypt regeneration actively occurs at 96 hours (Hua et al. 2012; Lund 2012). It is generally accepted that there are at least two subsets of stem cells: (1) a rapidly-cycling, CBC stem cell population at the base of the intestinal crypts, whose marker is Lgr5, a transmembrane receptor for R-spondin that amplifies Wnt tone, as well as Ascl2, Olfm4, Msi1, Smoc2, and Sox9**;** and (2) a damage-responsive, reserve stem cell population that is capable of repopulating the crypt and replacing Lgr5^{+}-CBC stem cells in case of injury to the small intestinal epithelium (Barker 2014; Durand et al. 2012; Li and Clevers 2010; Potten et al. 2009; Tian et al. 2011). Markers for the latter subset of

stem cells include Bmi1, TERT, as well as Lrig1 and Hopx (Barker 2014; Van Landeghem et al. 2012). While the role of $Lgr5^{+}$-CBC and +4 stem cell populations in repopulating intestinal crypts is under debate, studies have demonstrated that there is a role for each population in crypt regeneration (Hua et al. 2012; Metcalfe et al. 2014; Tian et al. 2011). While the +4 stem cell population is thought to be a more damage-responsive population that is capable of repopulating the crypt after injury (Tian et al. 2011), recent studies have shown that $Lgr5^{+}$-CBC stem cell populations are radioresistant and are critical to crypt regeneration after injury (Hua et al. 2012; Metcalfe et al. 2014). Interestingly, markers for both the CBC and the putative +4 damage-responsive populations were elevated in the BVES knockout mice, suggestive of either higher proportions in survival of an already expanded stem cell population, or a more robust reparative mechanism driven by surviving stem cell populations.

The Wnt signaling pathway is known to play a key role in the regulation of intestinal epithelial homeostasis as Wnt activation drives stem cell activity and maintains the intestinal stem cell niche (Fevr et al. 2007; Gregorieff and Clevers 2005; Pinto et al. 2003). Multiple studies have demonstrated that Wnt signaling is essential to mediating the survival of stem/progenitor cell populations after radiation (Fevr et al. 2007; Kim et al. 2012; Woodward et al. 2007). We have previously demonstrated that BVES regulates Wnt signaling through E-cadherin stabilization and alterations in β-catenin distribution (Williams et al. 2011), but this is the first study to directly link BVES to intestinal stem cell regulation *in vivo* and *ex vivo*. In support of BVES deletion altering intestinal stem cell function, baseline characterization of $Bves^{-/-}$ mice demonstrated elevated expression of *Lgr5* as well as an expanded stem cell compartment when crossed with the Lgr5-EGFP

reporter line. *Bves*$^{-/-}$ crypts in the enteroid culture system demonstrated increased plating efficiency, proportions of stem spheroids, and enteroids with peripheral cystic structures, along with elevations in stem cell markers and Wnt ligands, receptors, and targets. Correspondingly, amplified Wnt signaling was also present in the *Bves*$^{-/-}$ intestine after radiation-induced injury, and may contribute to the increased crypt proliferation and viability observed after BVES deletion.

While we observed alterations in the Wnt pathway after BVES deletion, with impacts on intestinal stem cell dynamics and response to radiation injury, it is also possible that the observed phenotypes are being influenced by other signaling pathways that are known to be modulated by BVES. Indeed, studies have identified BVES as a regulator of a diverse group of pathways and cellular processes. We have previously shown that BVES alters cellular motility and cytoskeletal arrangement through its regulation of RhoA signaling (Russ et al. 2011; Williams et al. 2011). Additionally, BVES was recently found to impact vesicular trafficking through its interaction with VAMP3, a SNARE protein that recycles transferrin and β1-integrin receptors (Hager et al. 2010). Moreover, as a protein originally discovered to play a role in cardiac development, BVES has been shown to regulate a number of processes relevant to cardiac physiology. For example, BVES binds cAMP with high affinity, interacts with the potassium channel TREK-1, and regulates cardiac pacemaking (Froese et al. 2012). Additionally, BVES interacts with the caveolin Cav3 to regulate the structural and functional integrity of caveolae in cardiac myocytes (Alcalay et al. 2013). Thus, BVES impacts a number of cellular processes with broad physiological implications. Given the known prominent role of Wnt signaling in stem cell biology, however, we postulate that

the phenotype of radioresistance described in this report is due to loss of BVES repression of Wnt signaling.

In conclusion, our findings demonstrate that BVES is critical for multiple aspects of small intestinal homeostasis and response to injury. Specifically, BVES regulates intestinal stem cell programs and is important in radiation-induced injury responses. This is the first study to identify that *Bves* is regulated in response to radiation, and that its underexpression has a clear biological impact on crypt regeneration, as the $Bves^{-/-}$ intestine is protected from radiation injury. This study offers promise in understanding the molecular mechanisms that regulate response to radiation therapy and a potentially attractive target for predicting radiation response in patients undergoing radiotherapy.

CHAPTER III

BVES IS REQUIRED FOR MAINTENANCE OF COLONIC EPITHELIAL INTEGRITY IN EXPERIMENTAL COLITIS

Abstract

Blood Vessel Epicardial Substance (BVES/Popdc1) is a tight junction-associated transmembrane protein that regulates epithelial-to-mesenchymal transition (EMT) and is underexpressed in a number of malignancies, including colon cancer. We have previously identified that impaired BVES function promotes EMT, leads to abnormal junctional signaling, and increases epithelial permeability *in vitro*, all of which have been implicated in inflammatory bowel disease (IBD). However, there have been no *in vivo* studies investigating the role of BVES in intestinal biology. We hypothesized that BVES regulates colonic homeostasis and is critical to maintaining epithelial integrity after injury. At baseline, *Bves*$^{-/-}$ mice demonstrated increased proliferation, decreased apoptosis, altered intestinal lineage allocation, and increased permeability *ex vivo*. We employed the *Citrobacter rodentium* infectious colitis model to test if impaired permeability in the *Bves*$^{-/-}$ mice would impact severity of colitis. *Bves*$^{-/-}$ mice inoculated with *C. rodentium* exhibited significantly more edematous colons, with greater injury and colonic hyperplasia when assessed histologically. *Bves*$^{-/-}$ mice also demonstrated increased bacterial colonization and amplified immune responses after *C. rodentium* inoculation, both of which may be contributing to this worsened injury. Finally, *BVES*

mRNA levels were underexpressed in human ulcerative colitis biopsy specimens, suggesting relevance to human disease. These studies identify BVES as a key regulator of colonic mucosal integrity and suggest that it may play a protective role in IBD.

Introduction

Inflammatory bowel disease (IBD) affects over 1.4 million people in the United States, causing numerous and debilitating complications such as malnutrition, infection, severe pain, and an elevated risk of colorectal cancer (Baumgart and Carding 2007; Baumgart and Sandborn 2007). Despite concerted research efforts, the fundamental pathophysiology of IBD remains poorly understood. Intestinal mucosal homeostasis relies on continuous proliferation, differentiation, and repair of the epithelium in response to injury (Iizuka and Konno 2011; Maloy and Powrie 2011; Sturm and Dignass 2008). Maintenance of intestinal integrity requires competent epithelial barriers as well as intact repair programs to respond to intestinal challenges (Iizuka and Konno 2011; Maloy and Powrie 2011; Sturm and Dignass 2008). The epithelial barrier is known to be "leaky" in patients with IBD, with a number of studies demonstrating lower epithelial resistance and increased permeability of both inflamed and non-inflamed mucosa in Crohn's disease and ulcerative colitis (Baumgart and Carding 2007; Shen, Su, and Turner 2009; Söderholm, Olaison, and Peterson 2002). Tight junctions are principal components of apical junctional complexes that are critical to the maintenance of epithelial barriers (Balda and Matter 1998; Balda et al. 1992). Disruption of tight-junctional integrity has been proposed as a contributing factor to epithelial barrier dysfunction present in IBD (Heller

et al. 2005; Ma et al. 2004; Shen, Su, and Turner 2009; Shen 2012; Söderholm, Olaison, and Peterson 2002; Turner 2009).

Blood Vessel Epicardial Substance (BVES/Popdc1) is tight junction-associated, three-pass transmembrane protein originally discovered from a cDNA screen of the developing heart (Andrée et al. 2000; Reese et al. 1999). BVES is highly expressed in epithelial tissues, including the intestinal epithelium, and regulates epithelial-to-mesenchymal transition (EMT) (Andrée et al. 2002; Han et al. 2014; Jayagopal et al. 2011; Kawaguchi et al. 2008; Reese et al. 1999; Vasavada, DiAngelo, and Duncan 2004; Williams et al. 2011). We have previously demonstrated that BVES regulates colonic epithelial phenotypes *in vitro* (Williams et al. 2011) but its *in vivo* role in the maintenance of intestinal homeostasis remains unexplored. We hypothesized that BVES influences colonic homeostasis and is critical to maintaining colonic epithelial integrity after injury.

In the present study, we have identified BVES as a key regulator of colonic mucosal integrity. At baseline, *Bves*$^{-/-}$ mice exhibit defects in intestinal secretory lineage allocation, along with higher cellular proliferation and decreased apoptosis. *Ex vivo* studies showed that *Bves*$^{-/-}$ colons have increased mucosal permeability. After inoculation with *C. rodentium*, *Bves*$^{-/-}$ mice demonstrated exacerbated colitis in comparison to their wildtype (WT) counterparts, along with significantly increased bacterial colonization and amplified immune responses. Lastly, analysis of human ulcerative colitis samples showed decreased *BVES* expression in comparison to normal biopsy specimens, suggesting relevance to human disease. Collectively, these findings indicate that BVES regulates colonic homeostasis, potentially protecting against intestinal epithelial injury, and may play a protective role in inflammatory bowel disease.

Methods

Mouse Models

Wildtype (C57BL/6 background) were obtained from the Jackson Laboratories. *Bves*$^{-/-}$ mice have been described in detail (Andrée et al. 2002). All experiments were performed with 8 to 10 week old male and female mice on C57BL/6 background under guidelines approved by the Vanderbilt Institutional Animal Care and Use Committee (IACUC).

Permeability Analysis

In order to compare the permeability of colons of WT mice with those of *Bves*$^{-/-}$ mice, we employed Ussing Chambers to measure the movement of FITC-Dextran across the mouse intestine. Sections of distal colons were placed in Ussing Chambers, and 100 microliters of 80 mg/ml FITC-dextran solution used to measure movement of FITC-dextran across tissues.

Induction of Citrobacter rodentium colitis

Mice were orally inoculated with *C. rodentium* as done previously (Coburn et al. 2013; Gobert et al. 2004; Singh et al. 2011; Williams et al. 2013). Bacteria were grown overnight in Luria broth and mice were infected by oral gavage with 0.1 ml of broth containing $1x10^8$ CFU of *C. rodentium*. Control mice received sterile broth. At 14 days post inoculation, the animals were sacrificed, and the colons were removed, cleaned, and Swiss-rolled for histology. Distal colon pieces were taken for colonization studies. For colonization, tissues were homogenized, serially diluted in Luria broth and plated on

MacConkey Agar plates. Colonies were counted after 24 hours and CFU/g of colon tissues were calculated. M. B. P. reviewed and scored the *C. rodentium* slides in a blinded fashion. Both acute (neutrophilic) and chronic (lymphocytic) inflammation, extent of inflammation, and epithelial damage were each scored on 0–3 scale (Gobert et al. 2004; Williams et al. 2013). The aggregate histological injury score was the sum of acute and chronic inflammation multiplied by the extent of inflammation, plus the epithelial injury (0 –21) (Gobert et al. 2004; Williams et al. 2013).

Immunohistochemistry

At time of sacrifice, colons were removed, rinsed with phosphate-buffered saline (PBS), and Swiss-rolled for histological assessment. The tissues were fixed in 10% formalin overnight and transferred to 70% ethanol. Tissues were submitted to Vanderbilt Tissue Processing Shared Resource (TPSR) core for processing and paraffin embedding. For immunohistochemistry (IHC), five micrometer sections were cut, dewaxed, hydrated, and endogenous peroxidase activity quenched with 0.03% hydrogen peroxide in MeOH (Barrett et al. 2011, 2012, 2013; Poindexter et al. 2015; Williams et al. 2013). Antigen retrieval was conducted using Antigen Unmasking Reagent (Vector Laboratories, Burlingame, California, USA) according to manufacturer's instructions. After blocking, primary antibody was added overnight at 4°C. Isotype-matched antibodies were used as negative controls on serial sections. The Vectastain ABC Elite System (Vector Laboratories) was used to visualize staining for immunohistochemistry. Proliferation was measured using anti-phospho-Histone H3 (pH3) Ser10 antibody (Millipore) that labels cells in the mitotic (M) phase of the cell cycle at 1:150 dilution. Enteroendocrine cells

were assessed by Chromogranin A (CgA) staining using anti-CgA at 1:1000 (ImmunoStar Inc., Hudson, WI). Goblet cells were identified by Periodic Acid Schiff (PAS) staining. Identification of apoptotic cells was conducted using the ApopTag Plus Peroxidase In Situ Apoptosis Kit (Millipore) according to the manufacturer's protocol. Counts were generated by counting cells in 100 sequential, well-aligned crypts from the distal colon. This is presented as the mean number of positive cells per crypt.

qRT-PCR analysis

RNA from *Bves*$^{-/-}$ or WT colons was isolated using the RNeasy Mini Kit (Qiagen, Valencia, Santa Clarita, California, USA). 20 µl of cDNA was synthesized using the iScript cDNA synthesis kit (Bio-rad, Hercules, California, USA) from 1 µg of total RNA. 1 µl of cDNA was used as a template in each subsequent PCR reaction. SYBR green qRT-PCR was performed using mouse cytokine array libraries I (Cat #: MCA-I) and II (Cat #: MCA-II) purchased from RealTimePrimers.com (Elkins Park, Pennsylvania, USA) according to manufacturer's instructions. Individual cytokines were analyzed using the delta-delta Ct method and normalized to Hypoxanthine-Guanine Phosphoribosyltransferase *(Hprt)*. For analysis of *BVES* expression in human samples, BVES and GAPDH TaqMan probes were purchased from Applied Biosystems (Foster City, California, USA). Expression was normalized to *GAPDH*.

Human Subjects

Tissues were obtained during colonoscopies at the Vanderbilt University Medical Center, following a protocol approved by the Vanderbilt Institutional Review Board.

Statistical Methods

Analyses comparing two groups were analyzed using the Student's *t*-test. One-way ANOVA and Newman-Keuls post-test was used to compare multiple groups. Data is presented as the mean +/- the standard error of the mean (SEM) in bar graphs and a line identifying the mean is shown when all data points are plotted. All of these analyses were performed using GraphPad Prism®6.0c (San Diego, CA, USA). A $P<0.05$ was considered statistically significant.

Results

BVES regulates colonic crypt homeostasis and contributes to epithelial barrier function

Previous studies have demonstrated that BVES regulates colonic epithelial phenotypes *in vitro* (Williams et al. 2011). However, its role in intestinal biology and the impact of its deletion *in vivo* on colonic homeostasis were not previously examined. To determine if BVES deletion alters colonic proliferation, apoptosis, or lineage allocation, we performed histological characterization of *Bves*$^{-/-}$ mice and examined the distal colon. Proliferation, as measured by phospho-histone H3 IHC, was increased in *Bves*$^{-/-}$ mice **(Figure 25A)**. Colons of *Bves*$^{-/-}$ mice demonstrated decreased apoptosis **(Figure 25B)**. Additionally, the numbers of PAS-labeled goblet cells **(Figure 25C)** and enteroendocrine cells **(Figure 25D)** were increased compared to WT mice. Moreover, as we have previously identified that impaired BVES function leads to epithelial junctional compromise *in vitro* (Williams et al. 2011), we hypothesized that the *Bves*$^{-/-}$ intestine would be more permeable. We employed Ussing Chambers, an *ex vivo* physiologic system to measure the movement of FITC-Dextran across WT and *Bves*$^{-/-}$ colons and

found that the *Bves*$^{-/-}$ intestine was significantly more permeable **(Figure 25E)**. These data demonstrate that BVES regulates intestinal proliferation, apoptosis, lineage allocation, and mucosal permeability, indicating a previously unrecognized role for BVES in regulating intestinal homeostasis.

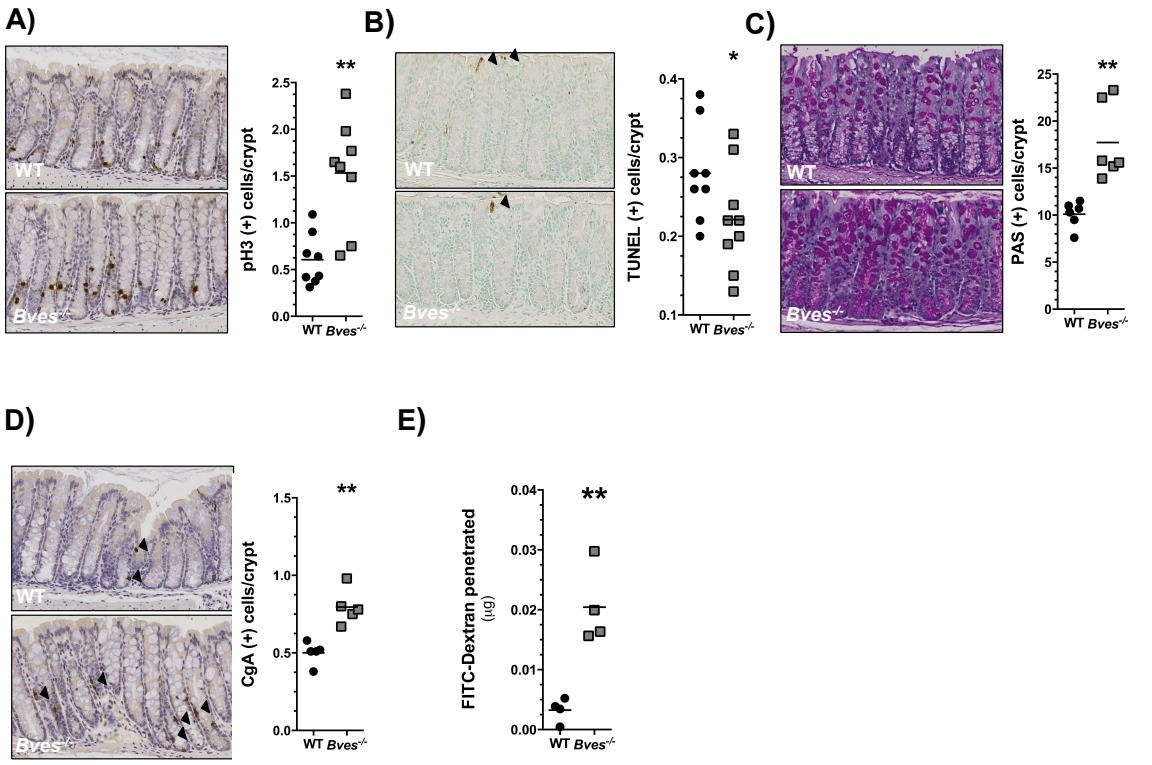

Figure 25. BVES regulates colonic proliferation, apoptosis, lineage allocation, and permeability. Colons were isolated and Swiss-rolled. (A) Images (left) and quantification (right) of crypt proliferation (0.6 vs. 1.5 phospho-Histone H3^{+} cells/crypt, ***P*<0.01, n=16). (B) Images (left) and quantification (right) of apoptotic cells per crypt/villus unit (0.3 vs. 0.2 TUNEL^{+} cells/crypt, **P*=0.05, n=17). (C) Images (left) and quantification (right) of goblet cells/crypt (10.1 vs. 17.7 PAS^{+} cells/crypt, ***P*<0.01, n=12). (D) Images (left) and quantification (right) of enteroendocrine cells/crypt-villus unit (0.5 vs. 0.8 CgA^{+} cells/crypt, ***P*<0.01, n=10). (E) Ussing chamber *ex vivo* permeability studies revealed increased permeability of *Bves*$^{-/-}$ colons compared to WT (***P*<0.01, n=8). All images were captured at 200x magnification. Black arrows indicate positively-stained cells.

BVES maintains colonic epithelial integrity after C. rodentium colitis

Tight junction integrity has been proposed to be a key mediator of epithelial barrier integrity and is thought to be disrupted in IBD (Heller et al. 2005; Ma et al. 2004; Shen, Su, and Turner 2009; Shen 2012; Söderholm, Olaison, and Peterson 2002; Turner 2009). Given the increased permeability at baseline of the *Bves*$^{-/-}$ intestine, we hypothesized that it would result in more severe colitis after inoculation with *Citrobacter rodentium* **(Figure 26A)**. Both WT and *Bves*$^{-/-}$ mice lost weight after *C. rodentium* inoculation; however, by day 3 *Bves*$^{-/-}$ mice exhibited accelerated weight loss, and from day 4 to day 14, delayed recovery **(Figure 26B).** At necropsy, both genotypes had edematous appearing colons. However, the ratio of colon weight (% of body weight) as well as colon weight/colon length was significantly greater in the *Bves*$^{-/-}$ mice **(Figure 26C-D).**

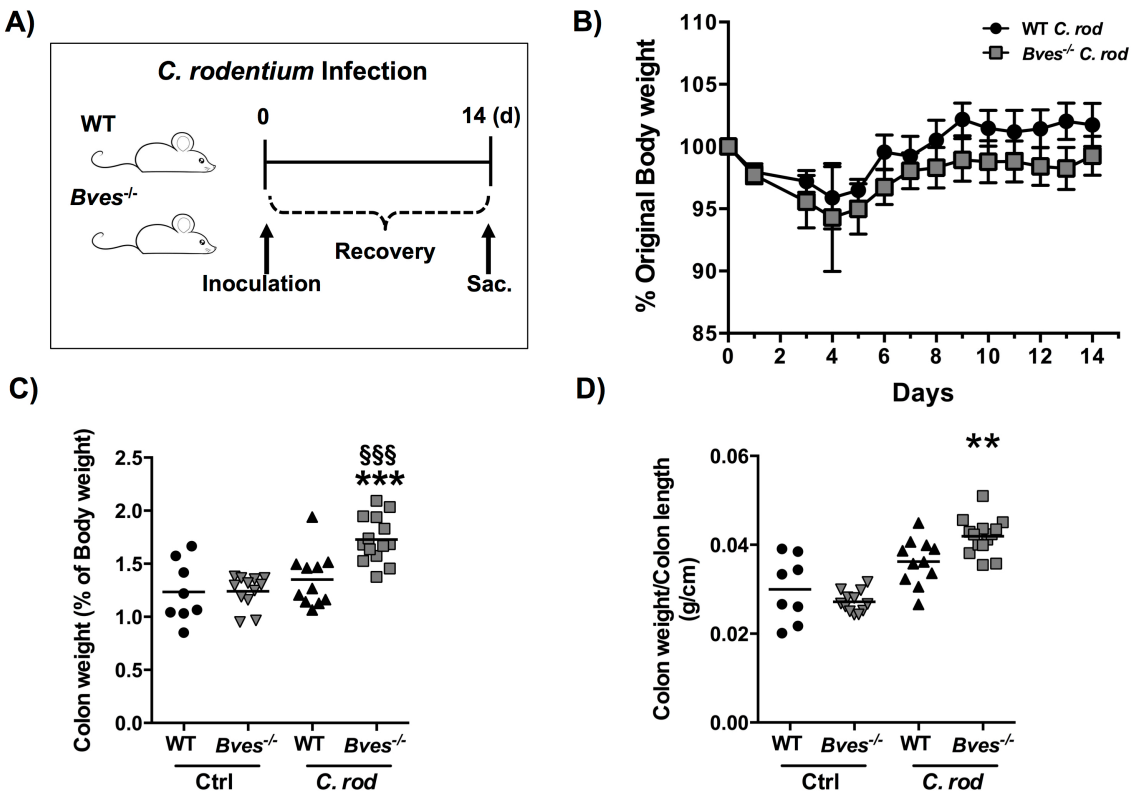

Figure 26. *Bves*$^{-/-}$ mice have more edematous colons after *C. rodentium* infection. (A) Schematic of *C. rodentium* inoculation protocol. WT and *Bves*$^{-/-}$ mice were sacrificed 14 days after inoculation. (B) *Bves*$^{-/-}$ mice exhibited trending but not significant increases in weight loss but significantly more edematous colons after C. *rodentium* inoculation compared to WT when measured as (C) ratio of colon weight (% of body weight) as well as (D) colon weight/colon length.

Histological review of H&E-stained Swiss-rolled colons **(Figure 27A)** by an expert gastrointestinal pathologist examining metrics such as epithelial ulceration, inflammatory infiltrate, submucosal edema, and impaired regeneration revealed significantly greater injury in *Bves*$^{-/-}$ mice **(Figure 27B).** These observations indicate that BVES contributes to the maintenance of epithelial integrity after colonic injury.

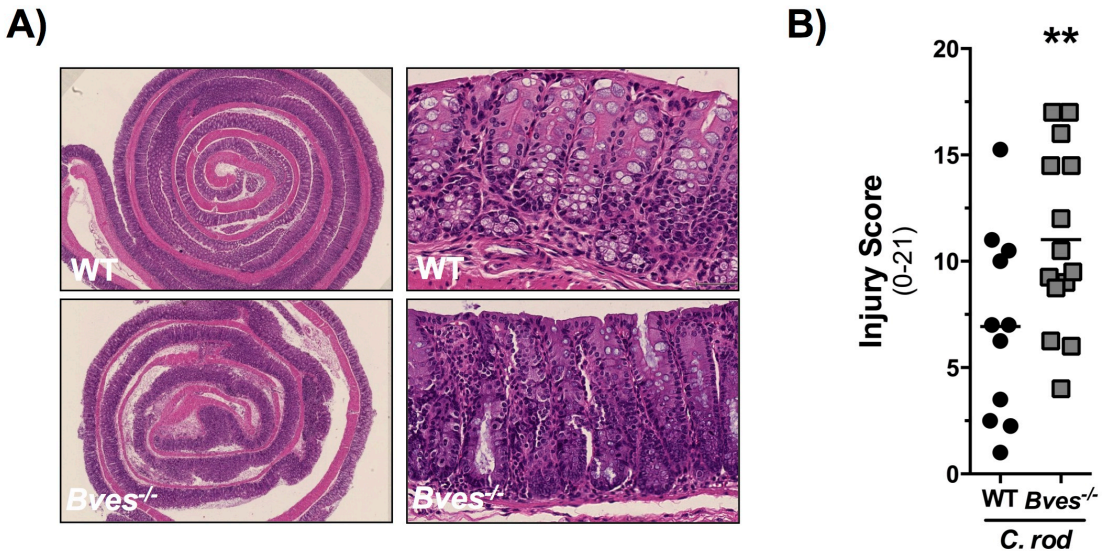

Figure 27. *Bves*$^{-/-}$ mice demonstrate exacerbated colitis after *C. rodentium* infection. (A) Representative H&E stained sections of WT and *Bves*$^{-/-}$ mice. (B) *Bves*$^{-/-}$ mice exhibited significantly greater injury after *C. rodentium* infection (Injury Score: 6.9 vs. 11.0 $^{**}P<0.01$, n=25). Histological injury score using a multi-point scale as described in the Methods section. Images were captured at 10x magnification (27A, left) or 100x magnification (27A, right).

Bves$^{-/-}$ *mice demonstrate increased bacterial colonization and amplified immune responses after C. rodentium infection*

As the BVES knockout mice demonstrated increased epithelial barrier permeability at baseline and worsened colitis, we hypothesized that they might sustain an increased bacterial load. Culturing of colonic mucosa indicated increased bacterial colonization in the *Bves*$^{-/-}$ cohort **(Figure 28A)**. Moreover, cytokine profiling suggested increased expression of cytokines involved in Th1 and Th17 immune responses in the *Bves*$^{-/-}$ colon after *C. rodentium*-induced injury/inflammation **(Figure 28B)**.

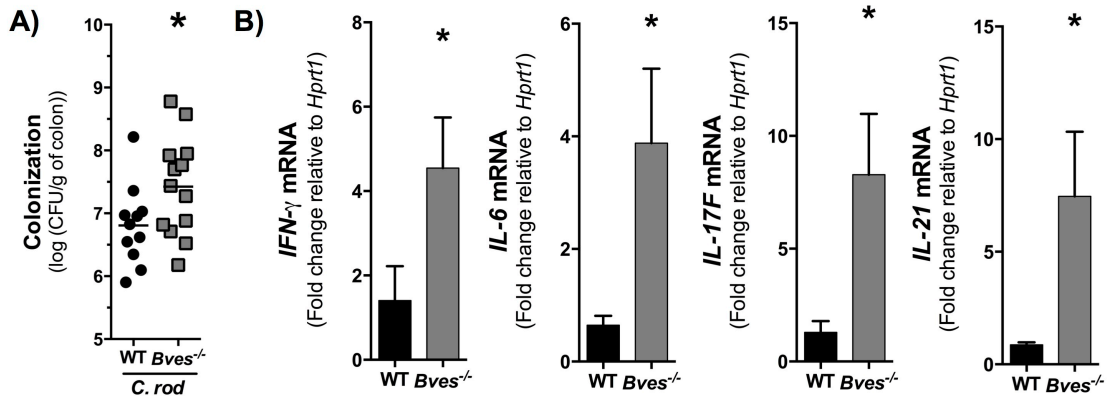

Figure 28. *Bves*$^{-/-}$ *mice* demonstrate increased bacterial colonization and amplified immune responses after *C. rodentium* infection. (A) Colonic bacterial colonization in WT and *Bves*$^{-/-}$ colons. (B) qRT-PCR analysis revealed increased mRNA expression of *IFN-γ* (**P*<0.05, n=12), *IL-6* (**P*<0.05, n=12), *IL-17F* (**P*<0.05, n=12), and *IL-21* (**P*<0.05, n=12), in *Bves*$^{-/-}$ colons compared to WT.

BVES is underexpressed in ulcerative colitis

Based on our above observations, we hypothesized that patients with ulcerative colitis would have decreased *BVES* expression. We extracted RNA from colonic biopsies collected prospectively from normal controls or ulcerative colitis patients with varying degrees of disease activity based on histological analysis. There were no differences in use of 5-ASA, corticosteroids, immunomodulators or biologics between the colitis groups (data not shown). qRT-PCR was performed, and ddCt calculations between normal and disease samples revealed a 2.3-fold reduction of *BVES* mRNA levels in samples from patients with moderate/severe disease in comparison to normal controls **(Figure 29)**. These data suggest that decreased *BVES* expression may be correlated with disease severity in IBD.

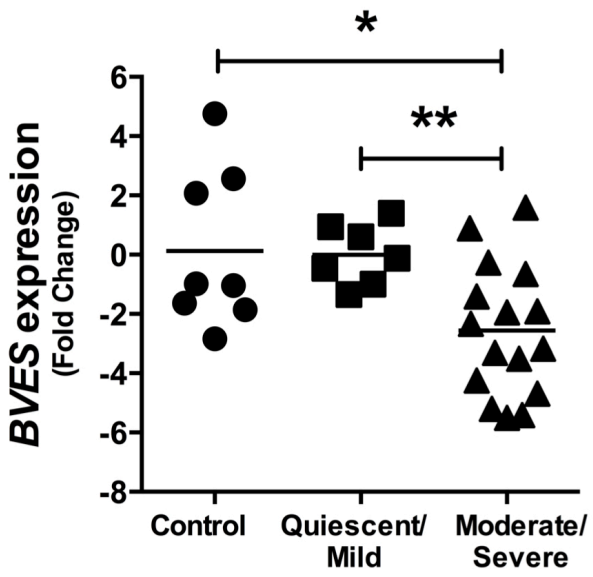

Figure 29. *BVES* is underexpressed in moderate to severe ulcerative colitis. *BVES* mRNA levels were determined using qRT-PCR on UC biopsy specimens. (A) *BVES* mRNA levels expressed as negative ddCt in normal (n=8), quiescent/mild UC (n=7), and moderate/severe UC (n=16). This represents a 2.3-fold decrease in expression in moderate/severe UC.

Discussion

In this study, we investigated the role of BVES in intestinal homeostasis and response to injury after experimental colitis. At baseline, *Bves*$^{-/-}$ mice demonstrated altered lineage allocation, higher intestinal proliferation, and decreased apoptosis. Additionally, *Bves*$^{-/-}$ colons exhibited increased permeability *ex vivo*, corresponding to prior findings that impairing BVES function alters transepithelilal resistance and junctional integrity *in vitro*. Moreover, we found that after *C. rodentium*-inoculation *Bves*$^{-/-}$ mice demonstrated exacerbated colitis. This was accompanied by an increased bacterial load in the *Bves*$^{-/-}$ colons. Lastly, we found that *BVES* expression was significantly downregulated in human biopsy specimens of patients with ulcerative

colitis, suggesting relevance to human disease and a potentially protective role for BVES in IBD.

A number of studies have identified increased epithelial barrier permeability as a key factor in driving the pathogenesis of inflammatory bowel disease (Baumgart and Carding 2007; Henderson et al. 2011; Shen, Su, and Turner 2009; Turner 2009). This epithelial barrier dysfunction is thought to be at least in part due to compromised tight-junctional integrity (Heller et al. 2005; Ma et al. 2004; Shen, Su, and Turner 2009; Shen 2012; Söderholm, Olaison, and Peterson 2002; Turner 2009). Prior studies have demonstrated that impairing BVES function leads to alteration in tight junctional composition and failure to maintain tight junctional proteins such as ZO1 at the membrane (Osler, Chang, and Bader 2005; Russ et al. 2011; Williams et al. 2011). This study is the first to identify that BVES deletion increases epithelial permeability *ex vivo* and there is a biological significance to this epithelial barrier alteration as *Bves*$^{-/-}$ mice demonstrate increased colonization and worsened colitis after *C. rodentium*-inoculation.

Citrobacter rodentium is an ideal pathogen for testing mucosal inflammation in the colon (Borenshtein, McBee, and Schauer 2008; Eckmann 2006). It induces superficial attaching/effacing lesions in the cecum and colon, with systemic infection much less likely when compared to other models of infectious colitis (Borenshtein, McBee, and Schauer 2008; Eckmann 2006). While *C. rodentium* infection has been known to induce Th1 adaptive immune responses, recent studies have identified a role for Th17 immune responses, as well (Chung et al. 2009; Harrington et al. 2005; Higgins et al. 1999; Maloy and Kullberg 2008; Mangan et al. 2006). Interferon gamma (*IFN-γ*) was significantly upregulated in the colons of *Bves*$^{-/-}$ mice relative to WT, suggestive of a polarization

towards Th1 immune responses (Eckmann 2006; Higgins et al. 1999; Simmons et al. 2002). Moreover, we observed that the *Bves*$^{-/-}$ mice had increased transcript levels of *IL-17F* and *IL-21*, cytokines produced by Th17 cells and known to have pro-inflammatory effects, as well as *IL-6*, a key driver of murine Th17 cell differentiation from naïve CD4+ T cells (Bettelli et al. 2006; Chung et al. 2009; Maloy and Kullberg 2008; Maloy and Powrie 2011). Thus, it is possible that amplified immune responses, potentially in response to the increased bacterial burden in the *Bves*$^{-/-}$ mice after *C. rodentium* infection, may be contributing to the worsened injury in this cohort.

In conclusion, our findings demonstrate that BVES is critical for multiple aspects of intestinal homeostasis and response to injury. Specifically, BVES regulates colonic proliferation, apoptosis, lineage allocation, permeability, and is important to the maintenance of colonic epithelial integrity after colitis induction. This is the first study to identify that *BVES* is underexpressed in patients with inflammatory bowel disease and offers promise in better understanding mechanisms that underlie epithelial barrier dysfunction in IBD.

CHAPTER IV

SUMMARY AND CONCLUSIONS

Our findings from these studies have identified a previously-unrecognized role for BVES in maintaining intestinal epithelial integrity. While the directed aims of these studies have been to uncover the role of BVES in the maintenance of intestinal homeostasis and response to injury, these studies have broad implications beyond intestinal biology and specifically for the field of cancer biology. Upon initial survey, these findings appear to identify a differing role for BVES in the small intestine and colon: 1) While radiation injury modeling has uncovered a protective role for BVES deletion in the small intestine after radiation injury, given an expanded stem cell compartment at baseline and increased survival of stem cell populations supported by amplified Wnt signaling, 2) The deletion of BVES in the colon increases epithelial barrier permeability, as well as colonization and injury after inoculation with the pathogen *Citrobacter rodentium*. Nonetheless, a unifying principle of these underlying findings is their implications for the field of cancer biology.

While our previous studies have identified a role for BVES in regulating Wnt signaling *in vitro,* our studies presented here demonstrate that BVES deletion in mice amplifies Wnt signaling *in vivo* at baseline and in response to injury in the small intestine, as well as in *ex vivo* cultures of intestinal crypts. While physiological Wnt signaling has been shown to play a critical role in the maintenance of crypt proliferation and stem cell maintenance, aberrant Wnt signaling is a prominent driver of a number of cancers,

including colorectal cancer (Clevers and Nusse 2012; Clevers 2013; J. H. van Es et al. 2012; Pinto et al. 2003). Indeed, many studies identifying the mechanisms by which Wnt signaling regulates intestinal epithelial homeostasis were conducted in parallel with those that uncovered its role in driving colorectal carcinogenesis (Clevers and Nusse 2012; Clevers 2013). Additionally, given that BVES knockout mice demonstrate increased proliferation at baseline throughout the span of the lower gastrointestinal tract, the alterations in Wnt signaling may be a prominent contributor to this phenotype. Further investigation of how this altered Wnt signaling and increased proliferation may impact tumorigenesis in the intestine is certainly warranted given the known roles of each in driving intestinal cancers.

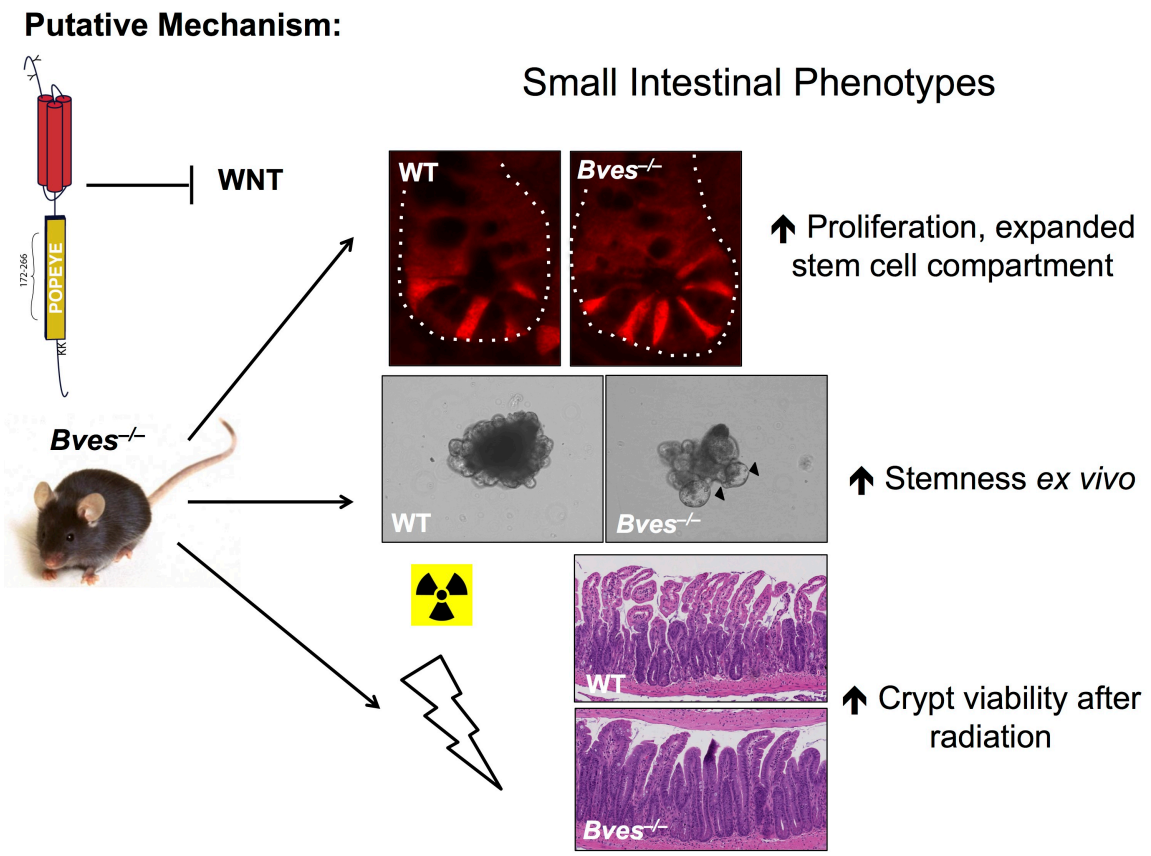

Figure 30. Putative mechanisms by which BVES regulates small intestinal integrity. BVES may participate in a repression circuit that attenuates Wnt signaling. *Bves* null crypts possess an expanded intestinal stem cell compartment *in vivo* and demonstrate increased stemness when cultured as miniguts *ex vivo*. *Bves*$^{-/-}$ mice demonstrate increased intestinal crypt viability after radiation injury.

Additionally, our finding that BVES deletion results in an expansion of the stem cell compartment in the small intestine remains a potent observation. The role of stem cells in tumorigenesis and the existence of putative cancer cells functioning in a stem cell-like manner have been an intriguing and central aspect of cancer research for decades. Some of the earliest studies identifying the functional heterogeneity of cancer cells suggested the existence of a subset of cancer cells that exhibit a stem-like nature (Bruce and Van Der Gaag 1963; Hamburger and Salmon 1977). Recently, studies have

attempted to merge two competing ideas about the identity of cancer populations (Greaves and Maley 2012). Moreover, given the recent identification of intestinal stem cell markers such as *Lgr5*, significant advances have been made in our understanding of the contribution of various populations of intestinal stem cells to tumorigenesis. Specifically, studies have identified that $Lgr5^{+}$ cells fuel the growth of established adenomas (Schepers et al. 2012). Identifying whether the expansion of the intestinal stem cell compartment is also present in the colon after BVES deletion and how such an expansion may affect intestinal tumorigenesis remain promising avenues of future investigation with concrete implications for the field of cancer biology.

Moreover, our findings that BVES deletion protects the small intestine after radiation injury, given the increased crypt viability and surviving stem cell populations after ionizing radiation, also offers clear translational implications for cancer treatment. While ionizing radiation is commonly utilized to treat a number of malignancies of different origin and stage, it frequently presents serious side effects for rapidly proliferating tissues such as those of the gastrointestinal tract (Gudkov and Komarova 2003; Shadad et al. 2013). With approximately seventy percent of patients with cancer receiving some form of radiation therapy, better understanding of the impact of radiation injury on normal tissues is an important aspect of cancer research. Radiation enteropathy, an intestinal injury process resulting from exposure to ionizing radiation, remains a major health concern in patients receiving radiation therapy for treatment of malignancies (Harb, Abou Fadel, and Sharara 2014). The incidence of radiation enteropathy is expected to continue to rise due to the unprecedented use of ionizing radiation for cancer treatment (Harb, Abou Fadel, and Sharara 2014; Shadad et al. 2013). The sensitivity of

various stem cell populations to damage from ionizing radiation is thought to have evolutionarily served as a protective mechanism to prevent initiation of tumorigenesis (Barker, van de Wetering, and Clevers 2008; Barker 2014). Studying radiation effects to the intestine is critical to develop better predictive biomarkers and therapeutics that address this radiation-related morbidity, and particularly because collateral damage to normal tissues frequently drives radiation dose limitations and thus represents a potential hurdle to effective cancer treatment (Harb, Abou Fadel, and Sharara 2014). Results from these studies suggest that BVES impacts intestinal crypt viability after radiation and could serve as a predictive biomarker of radiation response or as a potential therapeutic target.

BVES was originally discovered to be a junctional-associated protein with a critical role in the regulation of tight and adherens junction integrity. Indeed, a number of studies have shown that manipulating BVES results in improper localization of a number of tight junction proteins such as ZO1, with other studies showing that its deletion results in failure to maintain adherens junction proteins such as E-cadherin at the membrane (Osler, Chang, and Bader 2005; Williams et al. 2011). Perturbations in junctional molecules, particularly adherens junction components such as E-cadherin and p120, have been shown by many groups to be associated with increased tumor invasiveness (Thoreson and Reynolds 2002; Yap 1998). Conversely, cancer cell lines that express E-cadherin have been shown to demonstrate decreased invasiveness (Van Aken et al. 1993). Additionally, though less is known about tight junction regulation and cancer development, tight junction dysfunction has also been implicated in the development and progression of a number of carcinomas. A number of studies have identified that

overexpression of claudin-1, -3, -4, and -7 is present in ovarian, colorectal, and gastric cancers (Dhawan et al. 2005; Hewitt, Agarwal, and Morin 2006), though other studies have suggested that claudin-1 functions as a tumor suppressor in gastric cancer (T. L. Chang et al. 2010). A common pathway by which each of these junctional proteins may influence tumorigenesis is through regulation of intracellular signaling pathways that contribute to or attenuate a protumorigenic phenotype. For example, while adherens junctions are known to regulate the WNT pathway, specifically through E-cadherin-sequestration of β-catenin, tight junctions are known to regulate cytoskeletal networks (Rho/Rac) that are fundamental to modulation of migratory processes (Debruyne et al. 2006; Williams et al. 2011). Moreover, both tight junctions and adherens junctions have been implicated in the regulation and modulation of epithelial-to-mesenchymal transition, a fundamental process in the metastatic progression of many cancers (Acloque et al. 2009; Debruyne et al. 2006; Kalluri and Weinberg 2009; Williams et al. 2011; Zeisberg and Neilson 2009).

Our studies have demonstrated that BVES regulates not only junctional integrity and epithelial permeability, but also wound healing processes and epithelial restitution in the intestine, which are key processes regulated by EMT. Indeed, while EMT is a critical feature in normal wound healing programs, there is considerable overlap between programs that regulate normal wound healing and those that underlie carcinogenesis and the metastatic progression of a number of cancers—basic processes such as proliferation, apoptosis, and cellular migration (Acloque et al. 2009; Kalluri and Weinberg 2009; Zeisberg and Neilson 2009). Some of the earliest parallels observed between wound healing programs and cancer programs resulted in the description of cancer as an

overhealing wound (Dvorak 2009; Kalluri and Weinberg 2009; Schäfer and Werner 2008). Further investigation of the role of BVES in regulating epithelial-to-mesenchymal transition remains a promising avenue of research with important implications for both intestinal and cancer biology.

Finally, given that BVES knockout mice have altered cytokine production at baseline, heightened susceptibility to inflammatory injury after *C. rodentium* inoculation, and that *BVES* is underexpressed in human ulcerative colitis biopsy specimens, our studies also carry broad implications for diseases that contribute to human cancers. Inflammatory injury is a key driver of many cancers, including colitis-associated carcinoma, with ulcerative colitis being a prominent risk factor for its development (Baumgart and Carding 2007; Clevers 2004; Itzkowitz and Yio 2004; Loftus and Sandborn 2002; Maloy and Powrie 2011).

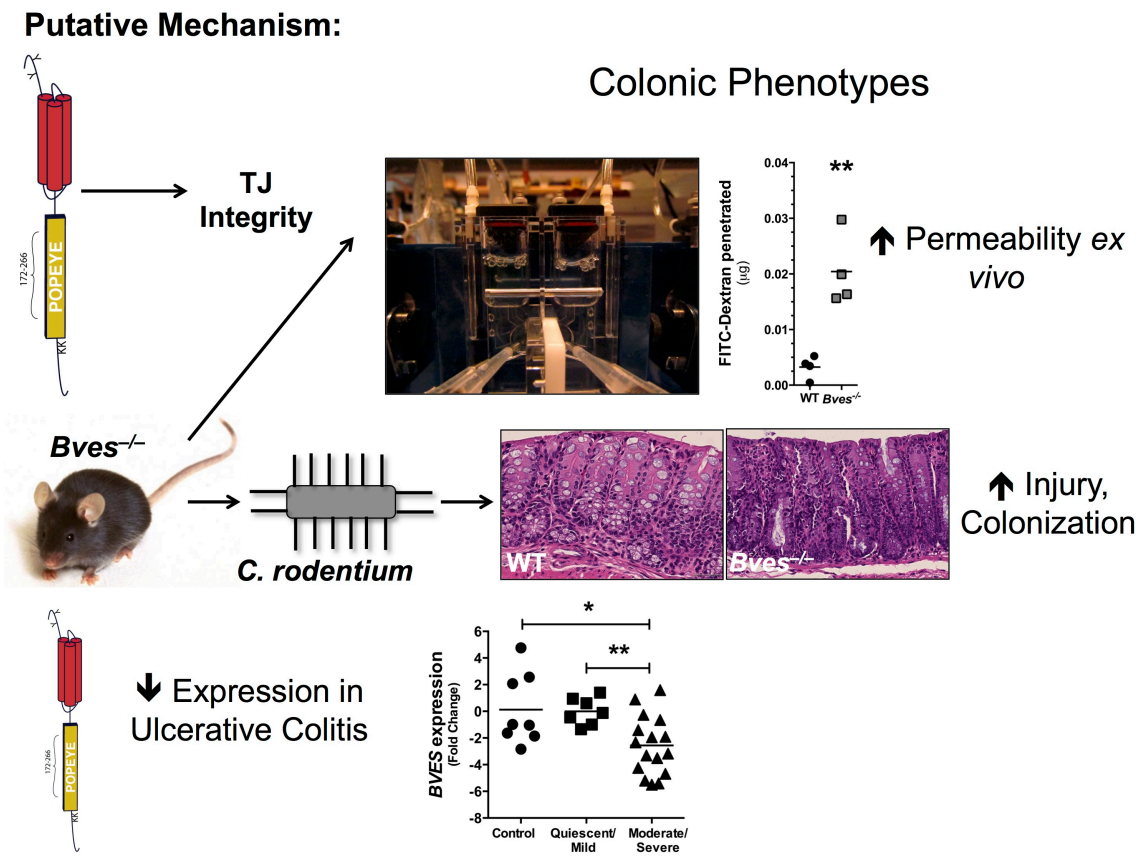

Figure 31. Putative mechanisms by which BVES impacts colonic integrity. BVES contributes to junctional integrity in the colon. *Bves*$^{-/-}$ colons demonstrate increased permeability *ex vivo*, with increased injury and colonization after inoculation with the pathogen *C. rodentium*. Moreover, *BVES* is underexpressed in human ulcerative colitis biopsy specimens, suggesting relevance to human disease.

Ultimately, these studies, which have identified a seemingly divergent role for BVES in regulating small intestinal and colonic integrity, are unifying in their implications for the field of cancer biology. As a junctional-associated protein that modulates Wnt signaling, small intestinal integrity after radiation injury, colonic inflammatory injury, as well as epithelial restitution processes and epithelial-to-

mesenchymal transition, its continued study will have direct implications for our understanding of carcinogenesis and the field of cancer biology.

CHAPTER V

FUTURE DIRECTIONS

Since the discovery of BVES in 1999, much progress has been made in contributing to our understanding of its structure, function, and role in basic cellular processes. It has been shown to play a critical role in the maintenance of tight junctions and regulation of junctional signaling programs. Here, we demonstrate that BVES is a key regulator of intestinal epithelial integrity *in vivo*. We show that BVES regulates intestinal proliferation and stem cell programs, epithelial barrier integrity, and response to injury. However, much remains uninvestigated, and future studies of BVES and its contribution to intestinal homeostasis may expand our understanding of its role in basic intestinal biology and provide therapeutic advances for intestinal diseases. Future directions for these current projects can broadly be grouped into two categories: (1) further interrogation of the role of BVES in maintaining intestinal integrity utilizing complementary models of colitis, and (2) further investigation of the mechanisms by which BVES regulates junctional signaling.

Utilization of Complementary Models of Colitis and Colonic Injury

While our current studies tested the role of BVES in the maintenance of colonic integrity using *C. rodentium*, it is one of many models that can be used to induce colitis. *C. rodentium* is a pathogen that infects and colonizes the murine colonic epithelium in the same fashion that enteropathogenic *Escherichia coli* infects humans, and under histological examination, it mimics characteristics of Crohn's disease: namely, thickening of the colon and transmural inflammation (Eckmann 2006). Another frequently-employed model of colitis is the dextran sodium sulfate (DSS) model, which induces colonic mucosal injury (Okayasu et al. 1990; Perše and Cerar 2012). DSS is a heparin-like polysaccharide that is thought to cause epithelial cytotoxicity and epithelial barrier disruption, resulting in weight loss, diarrhea, rectal bleeding, ulceration, and loss of epithelium, as well as leukocytic infiltration, and increased mucosal permeability (Dieleman et al. 1998; Okayasu et al. 1990; Perše and Cerar 2012). Interestingly, these changes are often accompanied by alterations in tight junctional components, including the loss or redistribution of occludin, ZO1, and various claudins (Mennigen et al. 2009; Poritz et al. 2007).

Our preliminary data indicate that BVES knockout mice are more sensitive to DSS-induced colitis in multiple models of injury: an acute injury model in which mice are maintained on 4% DSS for 5 days prior to sacrifice and an injury-repair model in which mice are maintained on 4% DSS for 5 days and then water for 5 days prior to sacrifice **(Figure 32).** As the BVES knockout mice demonstrate increased permeability at baseline and worsened colitis in response to *C. rodentium* infection, the DSS model would be a complementary model with which to interrogate the role of BVES in

maintaining intestinal integrity after injury. Subsequent experiments would include employing DSS chronically, characterizing immune responses after DSS–injury, and determining the impact of BVES deletion on tight junction composition at baseline and after DSS injury.

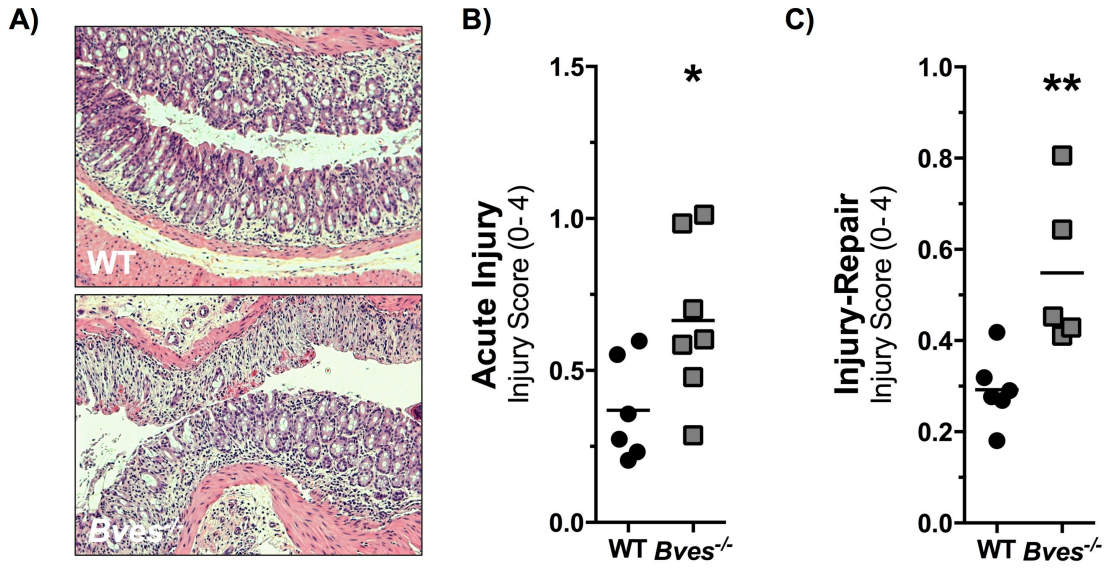

Figure 32. *Bves*$^{-/-}$ mice are more sensitive to DSS-induced colitis. (A) Hematoxylin and eosin (H&E) stained sections of WT and *Bves*$^{-/-}$ mice after DSS injury. (B) Acute injury trial with mice maintained on 4% DSS for 5 days prior to sacrifice. (C) Injury-Repair trial with mice maintained on 4% DSS for 5 days and water for 5 days prior to sacrifice. *$P < 0.05$, **$P < 0.01$

To understand why *Bves*$^{-/-}$ mice have increased permeability and are more susceptible to epithelial injury/damage in the *C. rodentium* model, we evaluated baseline chemokine/cytokine changes in *Bves*$^{-/-}$ colons as chemokines/cytokines can alter intestinal epithelial barrier function (Abraham and Medzhitov 2011; Matricon, Barnich, and Ardid 2010; Nishimura et al. 2009; Papadakis and Targan 2000; Strober and Fuss 2011). Using RNA-seq, we identified a number of dysregulated cytokines in *Bves*$^{-/-}$ colons. Particularly interesting was a downregulation of *IL-10ra*, which has been

identified to have a critical, protective role in IBD (Amre et al. 2009; Glocker et al. 2009). This finding is interesting as it has previously been shown that permeability deficits can exacerbate *IL-10*-mediated colitis (Arrieta et al. 2009; Madsen et al. 1999; Wang, Fang, and Hasselgren 2001). Utilization of the *IL-10*$^{-/-}$ model of enterocolitis would be ideal to further define the *in vivo* effects of BVES loss in immune-mediated intestinal inflammatory disease and allow for probing of epithelial-immune crosstalk which is heavily implicated in IBD etiology (Amre et al. 2009; Franke et al. 2008; Madsen et al. 1999).

Moreover, while we show that after *C. rodentium* infection *Bves*$^{-/-}$ mice demonstrate worsened colitis, possibly in large part due to increased epithelial permeability, the contribution of adaptive and innate immune responses in driving this phenotype remains unexplored. *Bves*$^{-/-}$ mice displayed significantly elevated expression of *IL-6* and as well as trending elevations in *TNF-a,* mediators of innate immunity (Eckmann 2006; Papadakis and Targan 2000). *Bves*$^{-/-}$ mice also demonstrated significantly elevated expression of *IFN-γ*, *IL-21*, and *IL-17F* compared to WT, suggestive of amplified adaptive immune responses of the Th1 and Th17 subtypes, which have been implicated in *C. rodentium* colitis (Chung et al. 2009; Maloy and Powrie 2011; Siegmund 2010). Multiple studies have demonstrated a key role for each in mediating protection from *C. rodentium*: innate immune responses mediate mucosal damage in *C. rodentium* infections while adaptive immunity develops to elicit bacterial clearance (Borenshtein, McBee, and Schauer 2008; Eckmann 2006; Khan, Ma, and Knodler 2006; Lebeis et al. 2007). Collectively, these data suggest that BVES loss dysregulates cytokine production and that BVES may modulate epithelial-immune crosstalk after *C. rodentium*-

induced colitis. To further investigate the role of BVES in innate versus adaptive immunologic responses in inflammatory injury, utilization of a *Rag2*$^{-/-}$ mouse would be an ideal model and has previously been employed to interrogate the role of innate immunity specifically in *C. rodentium*-induced colitis (Satoh-Takayama et al. 2009) and other models of infectious colitis (Sun et al. 2013). As RAG2 deletion results in compromised adaptive immunity due to impaired lymphocyte development at the progenitor stage, the *Rag2*$^{-/-}$ model would allow us to investigate the role of BVES in innate immune responses during colitis (Akamatsu et al. 2003; Shinkai et al. 1992).

Finally, given that BVES is known to regulate EMT, a critical mediator of physiological wound healing processes (Kalluri and Weinberg 2009; Williams et al. 2011), investigation of the role of BVES in wound healing/epithelial restitution after intestinal injury would offer further insight into its role in maintaining intestinal homeostasis. Models of mechanical injury in which superficial biopsies are induced and monitored by endoscopy have been employed for probing intestinal wound healing processes (Seno et al. 2009). Our preliminary data indicates that the BVES knockout mice have impaired wound healing when compared to their WT counterparts **(Figure 33)**. When examining wound areas at multiple time points after injury, as well as parameters of morbidity, such as the presence of blood and exudate, *Bves*$^{-/-}$ mice suffer worse injury. Optimization of this injury model and histological assessment of colons post-biopsy remain future directions for this project.

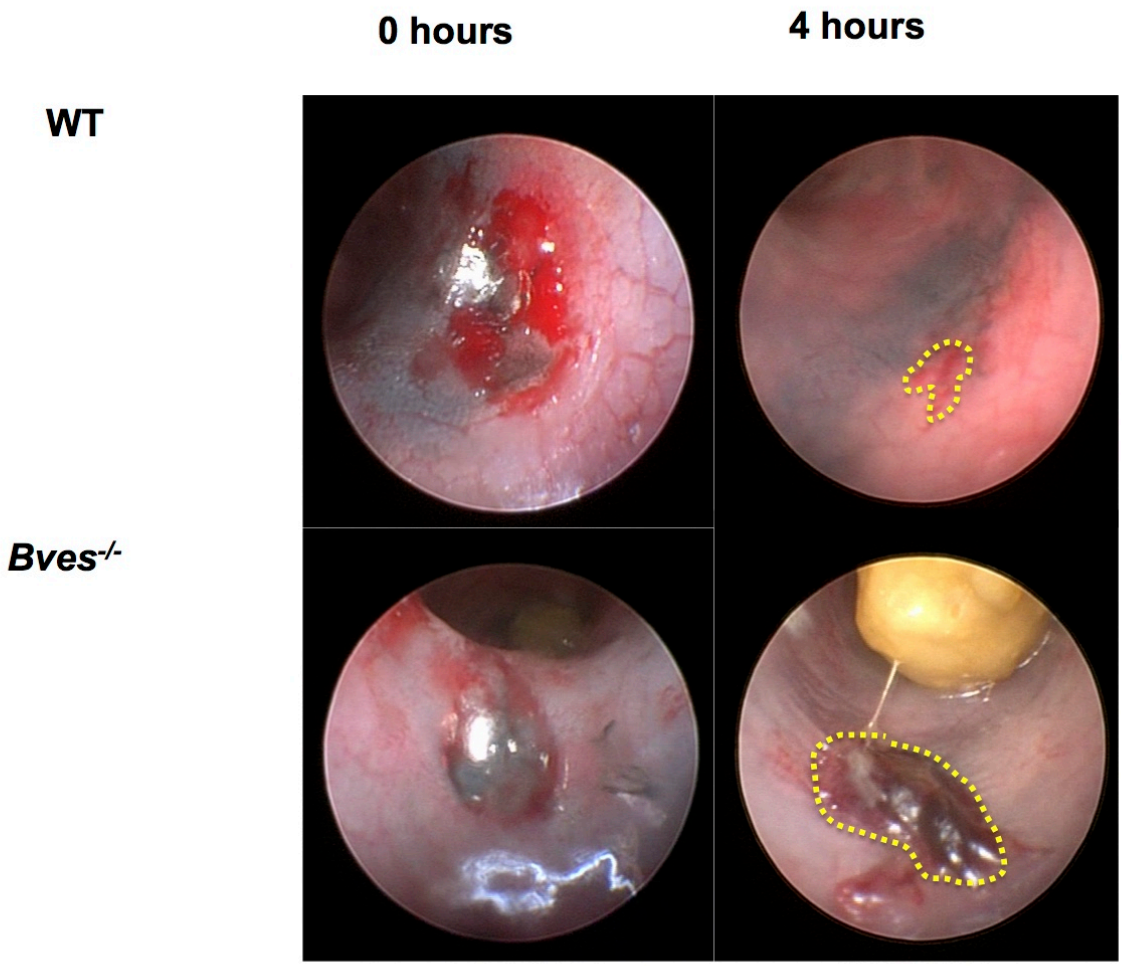

Figure 33. *Bves*$^{-/-}$ mice demonstrate impaired wound healing. Endoscopic images of WT and *Bves*$^{-/-}$ colons immediately after and 4 hours following mechanical injury.

Identification of Mechanisms by which BVES Regulates Junctional Signaling

While a number of interacting proteins have been identified for BVES, the known interactions do not explain all of the BVES-dependent phenotypes observed. Osler et al. demonstrated that BVES could interact with ZO1, a tight junction protein (Osler, Chang, and Bader 2005). More recently, we demonstrated that BVES regulates RhoA signaling at least partially through its interaction with GEF-H1 and that this modulates EMT (Williams et al. 2011). Collectively, these data implicate BVES as a regulator of

junctional signaling programs that are fundamental to intestinal epithelial homeostasis and restitution after injury. It should be noted that these novel functions of BVES would not have been realized without using an unbiased approach such as the yeast-two-hybrid method, as examination of its primary structure reveals little information (Andrée et al. 2000; Reese et al. 1999). It is highly likely that other BVES interacting proteins exist, and their identification is critical to understanding the role of BVES in normal and pathologic junctional biology. Because we have identified numerous BVES-dependent phenotypes that are not completely explained by known BVES-interacting proteins and pathways (i.e. WNT and RhoA signaling), we sought to identify other BVES binding partners via a yeast-two-hybrid (Y2H) screen. Twenty-six high probability BVES interactors were identified **(Figure 34)**, including RSK1, a member of the RSK family of serine/threonine kinases that lie downstream of the Ras-MAPK cascade.

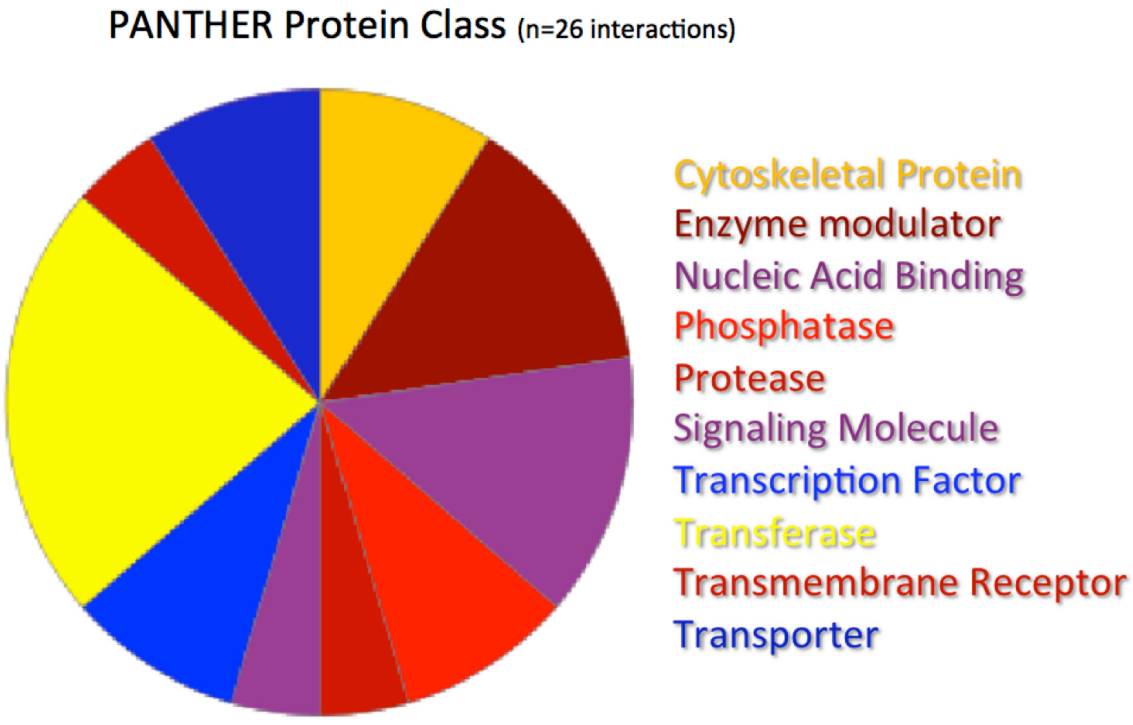

Figure 34. PANTHER assignment of the BVES interactome.

RSK1 has been shown to regulate cellular proliferation, survival, and motility (Anjum and Blenis 2008; Larrea and Hong 2009; Romeo, Zhang, and Roux 2012), all cellular processes that are critical to epithelial injury recovery and influenced by BVES (Williams et al. 2011). This is particularly exciting as RSK1 specifically regulates RhoA activity (Larrea and Hong 2009), a BVES-regulated process (Smith et al. 2008; Williams et al. 2011), and has been identified as a key effector of Ras/ERK-mediated EMT (Doehn et al. 2009). Accumulating evidence indicates that Rho signaling is essential in restoring mucosal integrity (Cetin et al. 2004; Santos et al. 1997). We have confirmed the BVES:RSK1 interaction by directed Y2H. Refinement of this mapping, identification of the structural requirements for the BVES:RSK1 interaction, and testing the functional significance of this interaction would be next steps in determining if this interaction carries significance.

Appendix A

SELENOPROTEIN P LOSS PROMOTES STEMNESS, OXIDATIVE DAMAGE AND INFLAMMATORY TUMORIGENESIS[1]

Abstract

Patients with Inflammatory Bowel Disease are at increased risk for colon cancer due to augmented oxidative stress and also have compromised antioxidant defenses secondary to nutritional deficiencies. Selenium, a micronutrient essential to selenoprotein production, is transported from the liver to target tissues via Selenoprotein P (SEPP1). Target tissues also produce SEPP1 where it is thought to possess an endogenous antioxidant function. We show that *Sepp1* haploinsufficiency or mutation of either the selenium transport or enzymatic domain increases colitis-associated carcinogenesis with resulting increased genomic instability and promotion of a pro-tumorigenic microenvironment. This includes a marked increase in M2-polarized macrophages, indicating a role for SEPP1 in macrophage polarization and immune function. Furthermore, complete SEPP1 loss results in significantly fewer tumors, in part due to increased apoptosis. *Sepp1*-null "mini-gut" cultures, in comparison to WT cultures, display increased stem cell characteristics coupled with increased ROS production, DNA damage, proliferation, decreased cell

[1] Published in *The Journal of Clinical Investigation*. *Caitlyn W. Barrett, *Vishruth K. Reddy, Amy K. Motley, Mary K. Lintel, Amber M. Bradley, Tanner Freeman, Jefferson Vallance, Wei Ning, Bobak Parang, Shenika V. Poindexter, Barbara Fingleton, Xi Chen, Mary K. Washington, Keith T. Wilson, Noah F. Shroyer, Kristina E. Hill, Raymond F. Burk, Christopher S. Williams. 2015. *Selenoprotein P loss promotes stemness, oxidative damage and inflammatory tumorigenesis*. *Co-first Authorship.

survival, and modulation of WNT signaling in response to H_2O_2-mediated oxidative stress. These data demonstrate that SEPP1 influences inflammatory tumorigenesis by impacting genomic stability, the inflammatory microenvironment, and epithelial stem cell functions.

Introduction

Inflammatory Bowel Disease (IBD) primarily comprises two types of chronic inflammatory disorders of the intestine: Crohn's disease (CD) and ulcerative colitis (UC). IBD affects approximately 1.4 million Americans, with typical onset occurring between 15 and 30 years of age (Loftus and Sandborn 2002). While the etiology of IBD is incompletely understood, prevailing thought presents a model in which the interplay of 1) intestinal microbiota or other undefined environmental exposures; 2) genetic susceptibility; and 3) inappropriately sustained and severe autoimmune inflammatory responses leads to repetitive injury of the GI tract, resulting in a pro-tumorigenic microenvironment rich in reactive oxygen and nitrogen species that predisposes to colon cancer (Abraham and Cho 2009; Roessner et al. 2008). Colitis-associated cancer (CAC) risk in IBD is influenced by several factors including age of diagnosis, disease extent, and severity of inflammation (Herrinton et al. 2012; Jess et al. 2012; Neumann et al. 2011; Nguyen and Bressler 2012; Rubin et al. 2008). Importantly, as increased disease activity is associated with increased cancer risk, understanding modifiers of IBD severity and CAC risk factors are of paramount importance.

Selenium is a trace element that is specifically incorporated into selenoproteins as selenocysteine through a specialized UGA codon encoded in the mRNA. Selenium

deficiency results in stimulation of the Wnt and Nrf2 pathways (Brigelius-Flohé and Kipp 2013; Burk et al. 2008; Kipp et al. 2009), both heavily implicated in the pathogenesis of colon cancer (L.-C. Chang et al. 2013; Kim et al. 2011; Reya and Clevers 2005). Selenoproteins are enzymes that participate in oxidative defense and are thought to protect against colon cancer, especially in settings of high oxidant stress, such as chronic inflammatory states. Several epidemiological studies have inversely correlated nutritional selenium status and cancer risk, particularly in colon cancer (Shamberger and Willis 1971). Recently, our laboratory has demonstrated that selenium deficiency in mice exacerbates intestinal injury in response to chemical models of colitis and increases tumorigenesis in CAC modeling (Barrett et al. 2013).

SEPP1 is a major selenoprotein and is thought to serve two main roles: supplying tissues with selenium and acting in an antioxidant defense capacity. The transport role is carried out by the C-terminal domain of SEPP1, which contains nine selenocysteine residues (Hill et al. 2003; Schomburg et al. 2003). The antioxidant role is carried out by a single selenocysteine within a UxxC redox motif at amino terminal residues 40-43 (Burk and Hill 2005), a domain that has recently been shown to have peroxidase activity (Kurokawa et al. 2014). As selenoproteins are produced in a hierarchical manner based on selenium availability, the importance of SEPP1 is underscored by the fact that even under conditions of severe selenium deficiency, its production perseveres (Burk and Hill 2005). Previous studies have shown that *SEPP1* is downregulated in colorectal cancers (Al-Taie et al. 2004), and single nucleotide polymorphisms (SNPs) within the gene are associated with advanced adenoma risk (Peters et al. 2008). Because SEPP1 serves as the major selenium transport protein, the known effects of selenium on Wnt and Nrf2

signaling in target tissues may partially depend on SEPP1. The antioxidant function of SEPP1 also suggests that it could play a role in cancer prevention, particularly in the context of inflammatory cancers characterized by increased oxidative stress, such as CAC (Dincer et al. 2007). Indeed, the gastrointestinal tract is susceptible to oxidative damage resulting from direct contact of the colonic epithelium with microbial and food-derived reactive oxygen species (ROS), and the loss of SEPP1 might result in increased oxidative damage-induced tumor initiation in the colonic mucosa. This potential damage is augmented in the context of IBD, during which oxidative stress plays a major role (Dincer et al. 2007). Thus, SEPP1 may regulate stem cell pathways and protect from CAC.

In the present study, we investigated the role of SEPP1 in colonic epithelial biology and how its loss impacts colitis-associated carcinoma. We demonstrate that SEPP1 loss contributes to increases in colonic epithelial stem cell properties, decreased cell survival and increased oxidative DNA damage in response to oxidative stress, and modulation of Wnt tone in intestinal organoids. These SEPP1-dependent phenotypes ultimately contribute to an increase in inflammatory tumorigenesis in its complete absence or upon loss of either the redox active site or the selenium transport domain of SEPP1. SEPP1 manipulation was found to alter the tumor microenvironment and genomic integrity. Our findings establish a critical role for SEPP1 in intestinal biology, homeostasis, injury response, preservation of genomic integrity, and inflammatory carcinogenesis.

Methods

Ethics Statement

This study was performed in strict accordance with the recommendations in the Guide for the Care and Use of Laboratory Animals of the National Institutes of Health. The protocol was approved by the Institute of Animal Care and Use Committee at Vanderbilt University (protocol number: M/10-355).

Murine Carcinogenesis Protocols

Sepp1$^{-/-}$ mice exhibit decreased survival on standard chow (Hill et al. 2004) and require selenium supplementation. Therefore, these mice were fed Torula yeast-based diets supplemented with 1.0 mg selenium as sodium selenite per kg. Accordingly, to properly control the experiment, WT and *Sepp1*$^{+/-}$ mice were also maintained on an identical diet. In a separate experiment, WT and *Sepp1*$^{+/-}$ mice were maintained on a normal selenium Torula yeast-based diet (0.25 mg per kg selenium as sodium selenite per kg). These diets were prepared and pelleted to our specifications (Hill et al. 2004) by Harlan-Teklad (Madison, WI, USA). For AOM only experiments **(Figure 36A)**, eight- to twelve-week old C57Bl/6 wild type (WT) (n=4), *Sepp1*$^{+/-}$ (n=4), or *Sepp1*$^{-/-}$ (n=4) mice (Hill et al. 2003; Schomburg et al. 2003) were injected with 12.5 mg/kg of AOM (Sigma-Aldrich, St. Louis, MO, USA) intraperitoneally. Mice were monitored for tumor burden by endoscopy once per month for 6 months and sacrificed 180 days post-AOM injection. For chronic DSS experiments, eight- to twelve-week old C57Bl/6 wild type (WT) (n=7), *Sepp1*$^{+/-}$ (n=10), or *Sepp1*$^{-/-}$ (n=10) mice (Hill et al. 2003; Schomburg et al. 2003) were subjected to three 5-day cycles of 3% DSS *ad libitum* with each cycle being followed by

a 16-day recovery period **(Figure 36B)**. Mice were monitored for colonic injury by endoscopy 4 days into the recovery period after each DSS administration. Injury was evaluated based on the murine endoscopic index of colitis severity (MEICS) which grades mucosal thickening, vasculature pattern, granularity, exudate, and stool consistency (Becker, Fantini, and Neurath 2007). For AOM/DSS protocols, eight- to twelve-week old C57Bl/6 wild type (WT) (n=13), *Sepp1*$^{+/-}$ (n=9), or *Sepp1*$^{-/-}$ (n=11) mice (Hill et al. 2003; Schomburg et al. 2003) (constitutional knockout experiment with mice fed 1.0 mg selenium per kg diet), WT (n=16) or *Sepp1*$^{+/-}$ (n=17) (constitutional knockout experiment with mice fed 0.25 mg selenium per kg diet), WT (n=16) or *Sepp1*$^{\Delta 240\text{-}361/\Delta 240\text{-}361}$ (n=14) mice (Hill et al. 2007) (truncation experiments), WT (n=12) or *Sepp1*$^{U40S/U40S}$ (n=15) (Kurokawa et al. 2014) (redox motif mutant experiments) (Table 1) were injected with 12.5 mg/kg of AOM (Sigma-Aldrich, St. Louis, MO, USA) intraperitoneally. Three days post-injection, the animals were started on the first of three cycles of 3% DSS *ad libitum*. Each cycle lasted 5 days and was followed by a 16-day recovery period. During each cycle of recovery, colonoscopy was performed to assess injury, tumor multiplicity, and grade (Becker, Fantini, and Neurath 2007). All mice were sacrificed on day 70, with the exception of cohorts maintained on 0.25 mg selenium per kg diet, which were sacrificed on day 52 due to increased mortality following the third cycle of DSS. All tumor counts and measurements were performed in a blinded fashion under stereo-dissecting microscopy. Histologic analysis was performed in a blinded fashion for severity of inflammation (Dieleman et al. 1998) and dysplasia on hematoxylin and eosin (H&E) stained "Swiss rolled" colons by a gastrointestinal pathologist (MKW).

Immunohistochemistry and immunofluorescence staining

For SEPP1 and phalloidin staining, colons and small intestines were embedded in OCT media and flash frozen in liquid nitrogen. Five-micrometer sections were cut and SEPP1 staining was performed as described previously (Olson et al. 2008). For all other staining, standardized protocols were followed to ensure the integrity of the samples for IHC/IF applications. In brief, immediately upon sacrifice the colons were harvested, flushed with ice cold PBS, "Swiss rolled" without delay, and fixed in fresh neutral buffered 10% formalin, subsequently exchanged for 70% EtOH. Processing was performed at the Vanderbilt University Translational Pathology Shared Resource. Five-micrometer sections of paraffin-embedded colons were cut and haematoxylin and eosin (H&E) staining was performed. For IHC cut sections were dewaxed, hydrated, and quenched of endogenous peroxidase activity with 0.03% hydrogen peroxide in methanol. Antigen retrieval was conducted using Antigen Unmasking Reagent (Vector Laboratories, Inc., Burlingame, California, USA) according to manufacturer's instructions. After blocking, primary antibody was added [α-Ki67 (NeoMarkers), 1:1,000; α-arginase I (ARG1, Santa Cruz), 1:500; α-IL-1β (R&D Systems), 1:40; α-F4/80 (ABd Serotec) 1:1000; α-8-OHdG (Santa Cruz), 1:500] and incubated overnight at 4°C. Isotype-matched antibodies were included as negative controls. Identification of intratumoral apoptotic cells was conducted using the ApopTag Plus Peroxidase In Situ Apoptosis Kit (Chemicon, Temecula, California, USA) according to the manufacturer's protocol. Control slides were obtained by omitting the terminal transferase (TnT) enzyme. For immunofluorescence staining of proliferation, macrophages, and DNA damage, slides were counterstained and mounted with ProLong Gold antifade including

4′,6-diamidino-2-phenylindole (DAPI, Invitrogen, Grand Island, New York, USA). Apoptosis, proliferation, DNA damage, and M1 and M2 macrophage indices were generated by counting either the number of positive cells per high-powered field (HPF; 40x objective) within each tumor or the number of positive cells per crypt in 20 crypts per mouse by a blinded observer. The average score was then calculated for each Swiss-rolled colon.

Colonic selenium measurements

The determination of colonic selenium was carried out using a modification of the fluorometric assay of Koh and Benson (Koh and Benson 1983) developed by Sheehan and Gao (Sheehan and Gao 1990). Briefly, tissue was digested in nitric and perchloric acids and, after adjustment of pH, selenium (as selenite) was complexed with diaminonaphthalene. Selenium-diaminonaphthalene was extracted into cyclohexane and fluorescence was measured in a Perkin-Elmer LS 55 fluorometer as described previously (Burk et al. 2006).

Western blot analysis of apoptosis and WNT pathway proteins

Flash-frozen sections of colon (n=6 for each genotype) were lysed in RIPA buffer including 1x protease inhibitor cocktail (Sigma) using a rotor homogenizer (Janke & Kunkel IKA-Labortechnik Ultra-Turrax T25). Protein quantification was performed using a Pierce BCA Protein Assay Kit (Thermo) according to manufacturer's instructions. Samples were suspended in loading buffer, boiled, and 40 μg was run on an SDS-PAGE gel for immunoblotting. The Apoptosis Antibody Sampler (mouse preferred,

#9930) and WNT signaling Antibody Sampler (#2915) kits (Cell Signaling Technology, Danvers, MA, USA) were used according to manufacturers' protocol. Quantification was performed using Odyssey Imaging Software and normalized either to total caspase or β-actin.

Bone marrow macrophage polarization and analysis.

Bone marrow macrophages were isolated and activated as has been previously published (Mosser and Zhang 2008; X. Zhang, Goncalves, and Mosser 2008). For the production of classically activated M1 macrophages, bone marrow macrophages were primed with 150 U/ml IFNγ for 6 hours and subsequently stimulated with 10 ng/ml LPS. For the production of alternatively activated M2 macrophages, bone marrow macrophages were treated with 20 U/ml IL13 for 12 hours. RNA was isolated using the RNEasy MiniKit (Qiagen, Valencia, CA, USA). 1 μg RNA was utilized to perform reverse transcription PCR using the iScript cDNA synthesis kit (Bio-Rad, Hercules, CA, USA). 1 μl of cDNA was used for qRT-PCR analysis of iNOS, IL-1β, and Ym1 using primers purchased from RealTimePrimers.com.

Plasma SEPP1 protein determination

Plasma SEPP1 was measured by ELISA (Hill et al. 2007). Plasma samples were diluted in PBST (PBS with 0.05% Tween-20) containing 2% rat plasma cleared of SEPP1 by monoclonal antibody 8F11 as described in (Read et al. 1990).

Small intestinal organoid culturing

Six centimeters of the distal small intestine were dissected, flushed with ice cold PBS, dissected into 1cm pieces, suspended in 5ml ice cold PBS and vortexed for 3 seconds. PBS was removed with a pipettor and the wash repeated. Tissue was transferred to 5ml chelation buffer (1mM EDTA, made fresh in DPBS) and rocked for 10 minutes at 4°C prior to washing twice with 10 ml PBS. 5 ml PBS was added and shaken gently for 2 minutes. The supernatant from the first shake was poured off. 5 ml PBS was added and the shake was repeated for 2 minutes then supernatant was poured off. 5 ml fresh chelation buffer was added and chelation was performed for 10 minutes at 4°C with rocking. Crypts were filtered through a 70 μm filter into a pre-chilled 50 ml tube. The filter was rinsed with 5 ml cold shaking buffer (PBS with 43.3mM sucrose and 54.9mM Sorbitol). Complete crypts were counted and enough volume was transferred for 1200 crypts to a pre-chilled 5 ml round-bottomed tube. Crypts were centrifuged at 150 x g for 10 minutes at 4°C. Shaking buffer was aspirated and crypts were resuspended in 50 μl of Matrigel (BD Bioscience #356237, San Jose, CA, USA), per well, containing 50 ng/ml EGF (R&D Systems #2028-EG-200, Minneapolis, MN, USA), 100 ng/ml Noggin (R&D Systems #1967-NG-025/CF), 500 ng/ml R-Spondin (R&D Systems #3474-RS-050), and 200 ng/ml Wnt3a (Millipore #GF-160, Billerica, MA, USA). Matrigel was overlayed with 500 μl Minigut culture media (Advanced DMEM/F12 (Invitrogen #12634-010, Carlsbad, CA, USA), L-Glutamine (Invitrogen #25030), Pen-Strep (Invitrogen #15140-148), Hepes (Mediatech #25-060-CI), N2 Supplement (R&D Systems #390155), B27 Supplement (Invitrogen #17504044). Every 4 days, media was replaced with fresh Minigut media plus growth factors.

Whole-mount 6-carboxy-2',7'-dichlorodihydrofluorescein diacetate (Carboxy-H_2DCFDA) enteroid staining

Enteroids were grown for 4 days post-plating. The morning of hydrogen peroxide treatment, enteroid media was replaced with fresh Minigut media. Either 0 μM, 400 μM, or 800 μM hydrogen peroxide was added directly to media. Two hours post-hydrogen peroxide treatment, growth media was removed from cells. Cells were treated with pre-warmed DPBS containing either the probe carboxy-H_2DCFDA (Invitrogen #mp-36103) or, as a negative control, carboxy-DCFDA to provide a final working concentration of 5 mM. Enteroids were incubated at 37°C in a cell culture incubator for 1 hour. Loading buffer was removed and cells were returned to pre-warmed Minigut media. Cells were incubated at 37°C for 15 minutes. Media was removed and enteroids were fixed overnight at 4°C in 2% formaldehyde with gentle rocking. Fixative was removed and enteroids were washed twice with DPBS. Enteroids were imaged with a LSM 510 Confocal microscope using the same specifications for imaging of all enteroids. ROS were quantified as staining intensity using ImageJ Image Analysis software. The graph represents the fold change intensity relative to *WT* enteroids treated with 0 μM hydrogen peroxide. Error bars represent the standard error of the mean for three separate experiments performed in duplicate.

Whole-mount enteroid proliferation staining

Proliferation was determined using the Click-iT EdU cell proliferation assay (Invitrogen #C-10337) according to manufacturers' instructions. Enteroids were grown to 4 days post-plating. Enteroid media was replaced with fresh Minigut media and either 0

μM or 800 μM hydrogen peroxide was added directly to media. Two hours post-hydrogen peroxide treatment, media was replaced with fresh Minigut media and a 10 μM working solution of EdU was added to each well of the plate. Enteroids were incubated for 15 minutes under normal growth conditions. After incubation, media was removed and 1 ml of 2% formaldehyde in PBS was added to each well and incubated overnight at 4°C. The fixative was removed and enteroids were washed twice with 1 ml 3% BSA in PBS. Wash buffer was removed and 1 ml of 0.5% Triton X-100 in PBS was added to each well and incubated at room temperature for 20 minutes. Click-iT reaction cocktail was prepared and 0.5 ml was added to each well. The wash solution was removed and enteroids were stained with TO-PRO-3 (1:500 in PBS for 15 minutes at room temperature). Enteroids were imaged with a LSM 510 Confocal microscope using the same specifications for imaging of all enteroids. Proliferation was quantified as EdU^+ cells/crypt area where crypt area was determined using ImageJ Image Analysis software. The graph represents the fold change intensity relative to *WT* enteroids treated with 0 μM hydrogen peroxide. Error bars represent the standard error of the mean for three separate experiments performed in duplicate.

RNAseq assay and analysis

Tumors were dissected from WT and *Sepp1*$^{-/-}$ mice andRNA was isolated using the RNEasy MiniKit (Qiagen, Valencia, CA, USA). RNA integrity was determined using Experion RNA StdSens Analysis Kit (Bio-Rad, Hercules, CA, USA). All RNA samples had RNA integrity numbers (RINs) >8 and were deemed suitable for analysis. Initial raw sequencing data were aligned to reference mouse genome (mm10) using TopHat (version

2.0.8) software with default parameters (Trapnell, Pachter, and Salzberg 2009). The *Cuffdiff* software (version 2.1.1) was used to estimate read count for expression of each gene and to detect differentially expressed (DE) genes. For count based gene expression data, *Cuffdiff* uses the beta negative binomial model for each gene in each condition in order to estimate the null distribution of its log fold change under the null hypothesis (Trapnell et al. 2013). The p-values from *Cuffdiff* were adjusted by Benjamini and Hochberg's method to control false discovery rate (FDR) (Benjamini et al. 2001).

Statistical Methods

Analyses comparing two groups were analyzed using the Student's t-test, two-tailed. One-way ANOVA and Newman-Keuls post-test was used to compare multiple groups. Data is presented as the mean +/- the standard error of the mean (SEM) in bar graphs and a line identifying the mean is shown when all data points are plotted. Percentages of mice displaying altered dysplasia grade were determined using Chi-square contingency analysis for each grade. All of these analyses were performed using GraphPad Prism®5.0c (San Diego, CA, USA).

Results

Loss of SEPP1 enhances both tumor promotion and initiation

Because *SEPP1* mRNA expression is decreased as early as the adenoma stage in colorectal cancer **(Figures 35A)** (Smith et al. 2010) and in tumors of mice subjected to an inflammatory carcinogenesis protocol **(Figures 35B)**, we predicted that SEPP1 loss would enhance tumorigenesis.

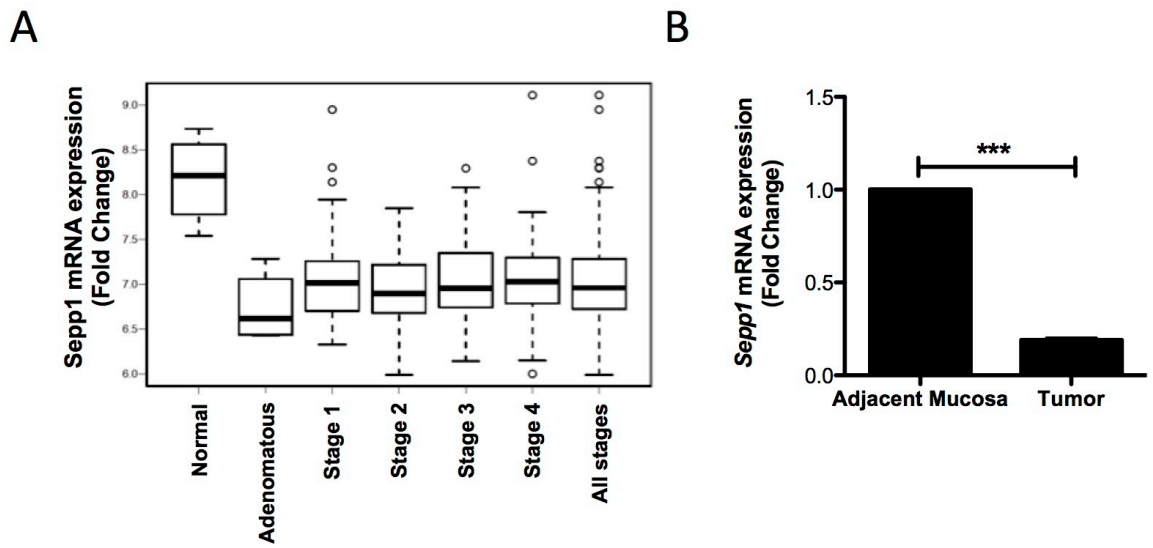

Figure 35. *Sepp1* message is decreased in human cancer and tumors from mice subjected to the AOM/DSS protocol. (A) Human *SEPP1* mRNA expression at various stages of colon tumorigenesis (10-normals, 6-adenomas, 33-Stage I, 76-Stage 2, 82-Stage 3, 59-Stage 4 for combined total of 250 CRC samples, GSE17538). (B) Mouse *Sepp1* mRNA expression in tumors (n = 5) isolated from AOM/DSS mice relative to adjacent non-malignant mucosa (n = 5), normalized to GAPDH. ***$P < 0.001$, 2-tailed unpaired t test.

In order to test the impact of SEPP1 loss on tumor initiation and promotion, respectively, we used both a six-month azoxymethane (AOM) protocol **(Figure 36A)** and a chronic dextran sodium sulfate (DSS) administration protocol **(Figure 36B)**. AOM is a procarcinogen that is metabolically activated to a potent alkylating agent forming O^6-methyl-guanine (Pegg 1984). DSS serves as a tumor-promoting agent, and repeated DSS administration produces chronic colonic inflammation (Okayasu et al. 1996). To determine if SEPP1 deletion influences colonic tumorigenesis, we utilized *Sepp1*$^{-/-}$ mice. These mice are globally null for SEPP1, and a lack of expression can be seen in both the colon and small intestine as compared to WT mice **(Figure 36C)**. Methylene blue

staining of colons 6 months post-AOM administration revealed an increase in aberrant crypt foci (ACF) in *Sepp1*$^{-/-}$ mice compared to WT mice (6.0 ± 0.6 vs 2.5 ± 0.3 ACF/colon, $P<0.001$, **Figure 36D**), indicating a role for SEPP1 loss in tumor initiation. Endoscopic injury analysis of mice subjected to chronic DSS administration using the MEICS scoring system (Becker et al. 2005) revealed increased injury in response to DSS after three cycles (8.1 ± 0.4 vs 4.1 ± 0.5 MEICS score, $P<0.0001$, **Figure 36E**, left). Furthermore, chronic DSS treatment led to increased ACF formation in *Sepp1*$^{-/-}$ mice compared to both WT and *Sepp1*$^{+/-}$ mice (*Sepp1*$^{-/-}$: 3.2 ± 0.4 vs *Sepp1*$^{+/-}$: 2.1 ± 0.3 and WT: 1.9 ± 0.3 tumors/colon, $P<0.05$, **Figure 36E**, right), suggesting that complete SEPP1 loss exacerbates injury and tumorigenesis in response to DSS. *Sepp1*$^{-/-}$ mice also demonstrated decreased proliferation after chronic DSS treatment in comparison to *Sepp1*$^{+/-}$ and WT mice (**Figure 36E**, bottom) with no differences in apoptosis (data not shown) amongst the cohorts.

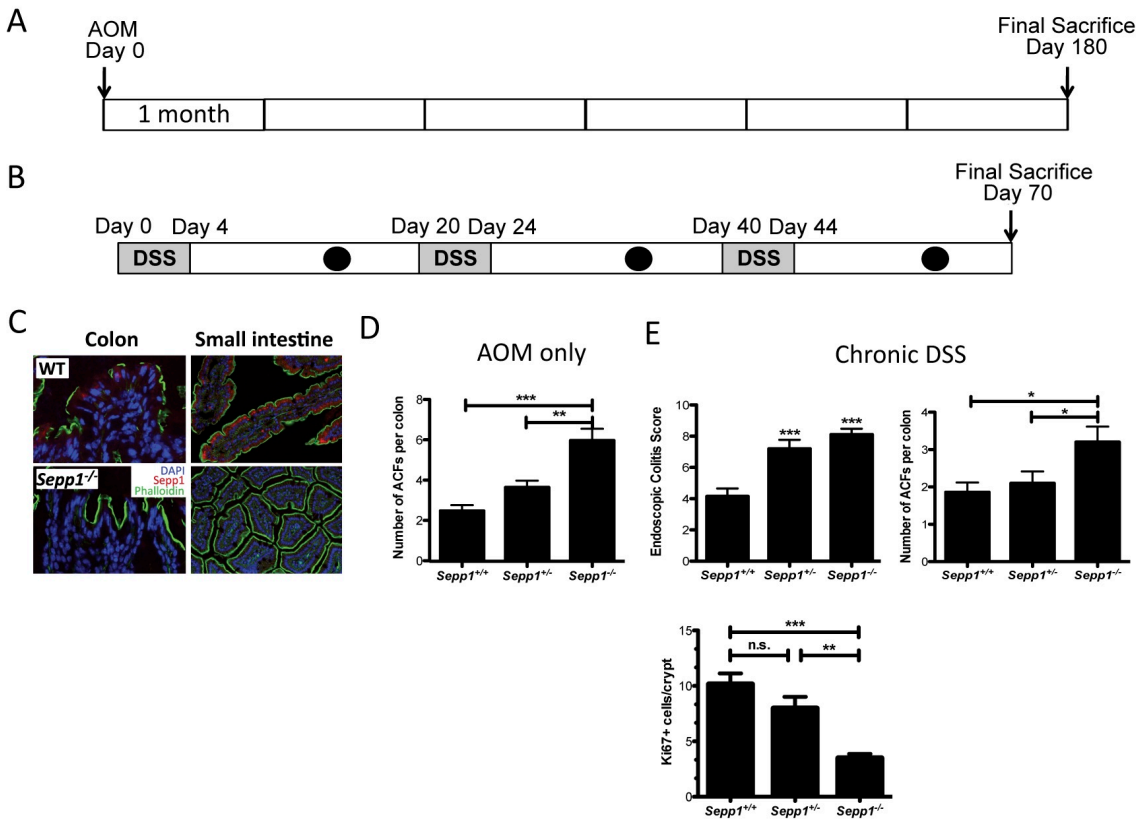

Figure 36: Absence of SEPP1 exacerbates tumorigenesis in response to AOM and injury after chronic DSS treatment. (A) Schematic of the AOM protocol utilized. Mice are injected with AOM and aged for 6 months before being sacrificed on day 180 post-AOM treatment. (B) Schematic of the chronic DSS protocol utilized. Mice are subjected to three five-day cycles of 3% DSS *ad libitum*. There are 16 days of recovery between each DSS administration and mice are monitored for injury by endoscopy four days after each DSS cycle (black circles). (C) Immunofluorescent staining of SEPP1 (red) within the colon and small intestine of WT and *Sepp1*$^{-/-}$ mice (100x magnification). (D) Aberrant crypt foci counts (ACF/mouse) in WT ($n = 4$), *Sepp1*$^{+/-}$ ($n = 4$), and *Sepp1*$^{-/-}$ ($n = 3$) mice subjected to the AOM protocol. (E) Endoscopic colitis score (left), ACF counts (ACF/mouse, right), and Ki67 staining (bottom) in mice subjected to the chronic DSS protocol (7, WT; 10, *Sepp1*$^{+/-}$; 10, *Sepp1*$^{-/-}$). *$P < 0.05$, **$P < 0.01$, ***$P < 0.001$, 1-way ANOVA, Newman-Keuls Multiple Comparison Test.

Table 1: The genotypes of mice subjected to the AOM/DSS protocol and the symbols used for each genotype.

Nomenclature	Mouse Description
WT	Wild-type N10 C57Bl/6
Sepp1$^{+/-}$	Heterozygous selenoprotein P knockout (C57Bl/6)
Sepp1$^{-/-}$	Homozygous selenoprotein P knockout (C57Bl/6)
Sepp1$^{\Delta 240\text{-}361/\Delta 240\text{-}361}$	Homozygous deletion of Sepp1 amino acids 240-361 (C57Bl/6)
Sepp1$^{U40S/U40S}$	Homozygous point mutation of position 40 selenocysteine to serine in Sepp1 (C57Bl/6)

SEPP1 is a haploinsufficient tumor suppressor in inflammatory carcinogenesis

Based on the impact of SEPP1 loss on initiation in response to AOM and DSS as single modalities, we predicted that SEPP1 would play a critical role in ensuring tumor cell survival after inflammatory injury. We used the azoxymethane, repeated-dose dextran sodium sulfate (AOM/DSS) CAC model in WT, *Sepp1*$^{+/-}$, and *Sepp1*$^{-/-}$ mice. As expected, complete loss of SEPP1 decreased colonic selenium content **(Figure 37A)**, though we note that this decrease was modest, indicating that SEPP1 is not the only mechanism of selenium supply in the colon. Complete loss of SEPP1 led to a decrease in tumor multiplicity (2.7 ± 0.7 vs 5.2 ± 0.8 tumors/mouse, *P*=0.02, **Figure 37B** and **Figure 37C**) and alteration in tumor size in *Sepp1*$^{-/-}$ mice compared to *Sepp1*$^{+/-}$ mice, but not WT mice (2.5 ± 0.4 vs 4.2 ± 0.5 mm^2, *P*=0.01, **Figure 35B** and **Figure 37D**), suggesting that complete loss of SEPP1 impaired survival or proliferation of initiated epithelial cells. In contrast, partial loss of SEPP1 led to increased tumor multiplicity (8.3 ± 1.2 vs 5.2 ± 0.8 tumors/mouse, *P*=0.03, **Figure 37B**, and **Figure 37C**) but no change in tumor size. However, histopathological examination suggested more advanced dysplasia in the *Sepp1*$^{+/-}$ mice **(Figure 37E)**.

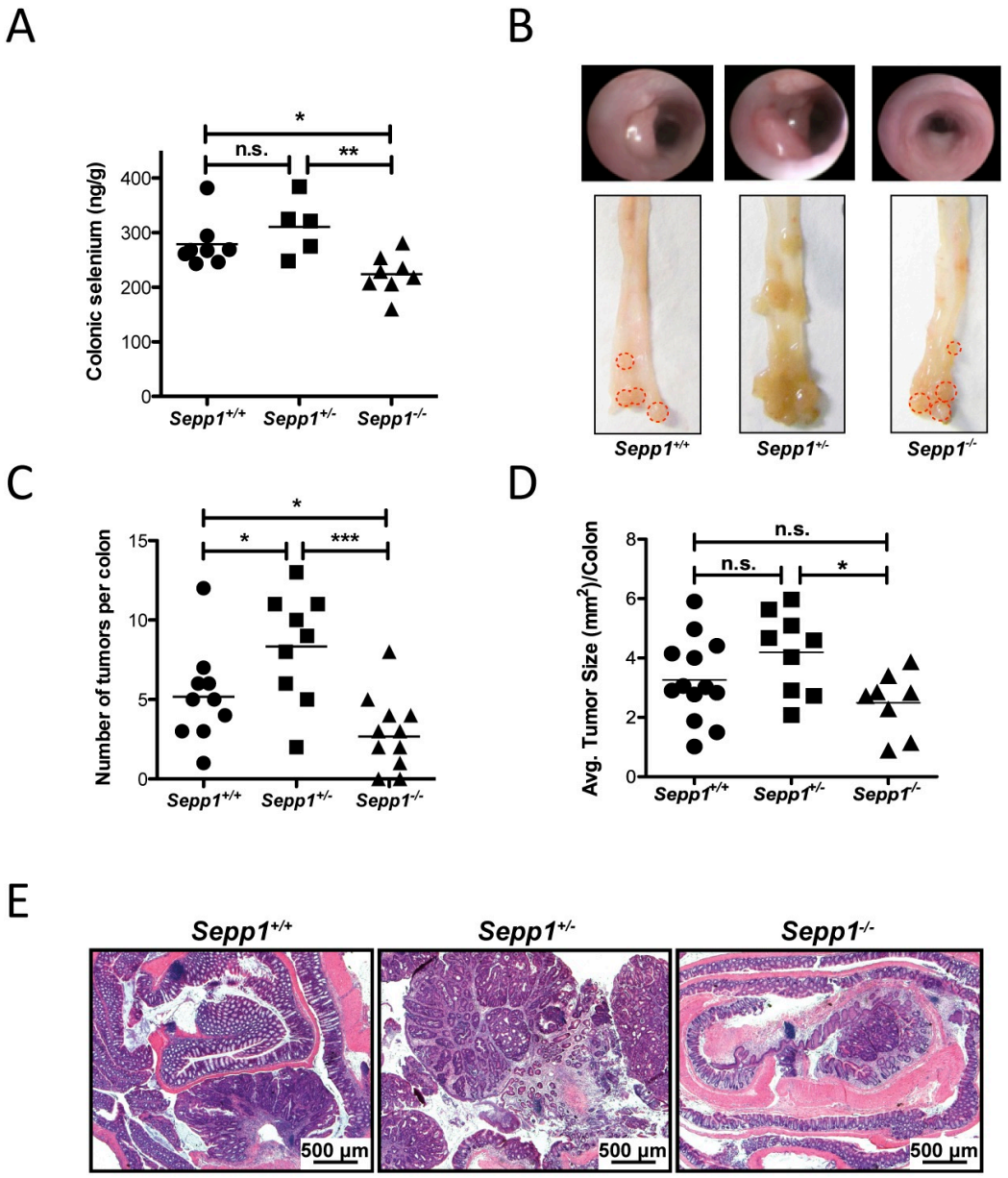

Figure 37: *Sepp1* haploinsufficiency augments inflammatory carcinogenesis. (A) Quantification of colonic selenium in WT (n = 8), *Sepp1*$^{+/-}$ (n = 5), and *Sepp1*$^{-/-}$ (n = 8) mice fed a selenium-supplemented (1.0 PPM) diet. (B) Representative gross colon images. (C) Tumor number (tumors/mouse, left) and (D) average tumor size (mm^2, right) per mouse (17, WT; 15, *Sepp1*$^{+/-}$; 20, *Sepp1*$^{-/-}$). *P < 0.05, **P < 0.01, ***P < 0.001, 1-way ANOVA, Newman-Keuls Multiple Comparison Test. (E) Representative images of Swiss rolled colons from each genotype (25x magnification).

The decrease in tumorigenesis in the *Sepp1*$^{-/-}$ mice was concomitant with increased apoptosis as measured by TUNEL staining (74.4 ± 10.9 vs 34.3 ± 3.1 TUNEL^{+} cells/tumor high-powered field (HPF) in WT, P<0.01, **Figure 38A**, left & **Figures 39A & B**, top) and western blotting for markers within the intrinsic apoptosis pathway (**Figure 38A**, right & **Figure 39B**, bottom). Therefore, we hypothesized that decreased tumor multiplicity might be caused, in part, by clearance of initiated cells due to oxidative injury beyond that which total SEPP1 loss can compensate. This phenomenon has been hypothesized to play a role in the initiation process of many cancers and was recently demonstrated in the process of ferroptosis, a mechanism of cell death triggered via the production of iron-dependent ROS (Szatrowski and Nathan 1991; Yang et al. 2014). Moreover, proliferation was increased in *Sepp1*$^{+/-}$ tumors (85.9 ± 2.9 vs 55.6 ± 2.8 Ki67^{+} cells/tumor HPF in WT, P<0.0001, **Figure 38B** and **Figure 39D**) and decreased in *Sepp1*$^{-/-}$ tumors (19.0 ± 6.9 vs 55.6 ± 2.8 Ki67^{+} cells/tumor HPF, P<0.0001, **Figure 38B** and **Figure 39D**) and crypts (1.6 ± 0.2 vs 4.6 ± 0.2 Ki67^{+} cells/crypt, P<0.0001, **Figure 39C**). These data support a role for clearance of initiated cells in *Sepp1*$^{-/-}$ tumors.

Intratumoral DNA damage increases in a dose-dependent manner with decreased SEPP1 levels

Selenium has been identified as a potential contributor to the maintenance of genomic stability (Bera et al. 2013; Ferguson et al. 2012). However, the role of SEPP1 in DNA damage repair is unknown. We wanted to test the impact of SEPP1 deficiency on crypt and intratumoral DNA damage. 8-hydroxyguanine staining, a measure of oxidative DNA damage, demonstrated that intratumoral DNA damage increases with decreased

Sepp1 expression (WT: 8.1 ± 0.8, *Sepp1*$^{+/-}$: 15.3 ± 1.5, *P*=0.002, *Sepp1*$^{-/-}$: 23.3 ± 3.4 8-hydroxyguanine^{+} cells/tumor HPF, *P*=0.0007, **Figure 38C** & **Figure 39F**), though crypt DNA damage was not altered when compared to WT mice in response to SEPP1 deficiency **(Figure 39E)**. These data suggest that, within the tumor microenvironment, decreasing *Sepp1* expression leads to an increase in oxidative DNA damage.

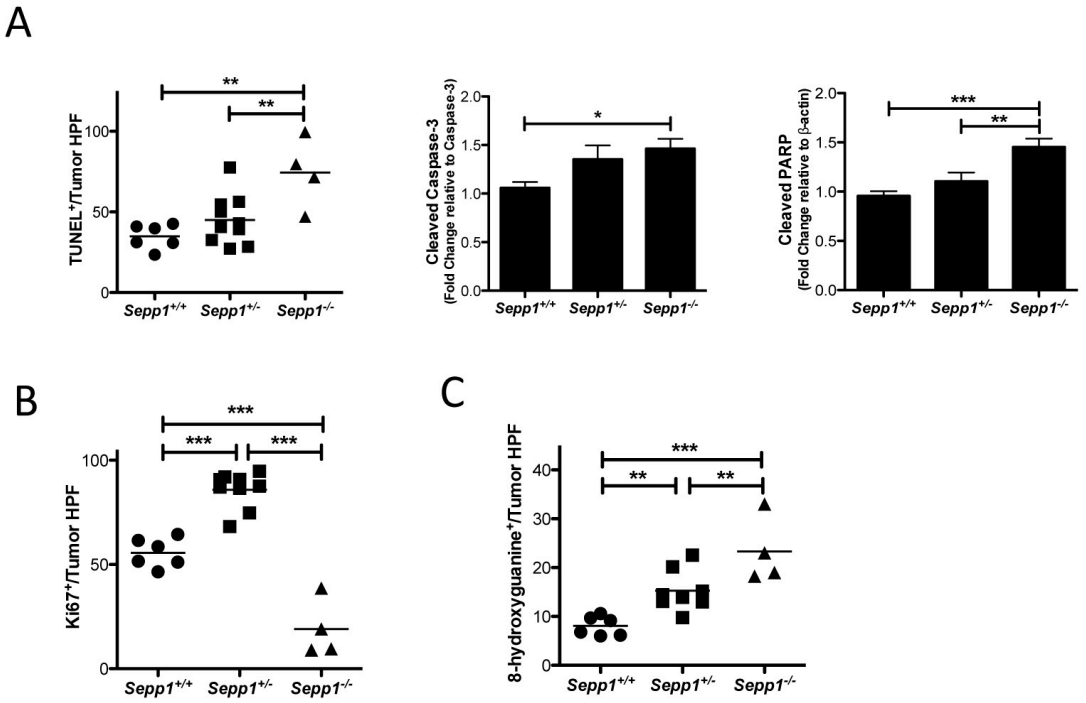

Figure 38: Intratumoral apoptosis and DNA damage are increased in response to complete *Sepp1* knockout and proliferation is increased in *Sepp1*$^{+/-}$ tumors. (A) Quantification of intratumoral apoptosis as determined by TUNEL+ cells/tumor high-powered field (left, HPF: 40x magnification; 6, WT; 10, *Sepp1*$^{+/-}$; 4 *Sepp1*$^{-/-}$). Quantification of cleaved caspase-3 protein normalized to caspase-3 (middle) and cleaved PARP protein normalized to β-actin (right). Quantification is shown as fold change relative to WT (*n* = 6 per group). (B) Quantification of intratumoral proliferation as determined by Ki67+ cells/tumor HPF (6, WT; 10, *Sepp1*$^{+/-}$; 4 *Sepp1*$^{-/-}$). (C) Quantification of intratumoral DNA damage as measured by 8-hydroxyguanine+ cells/tumor HPF (6, WT; 10, *Sepp1*$^{+/-}$; 4 *Sepp1*$^{-/-}$). *$P < 0.05$, **$P < 0.01$, ***$P < 0.001$, 1-way ANOVA, Newman-Keuls Multiple Comparison Test.

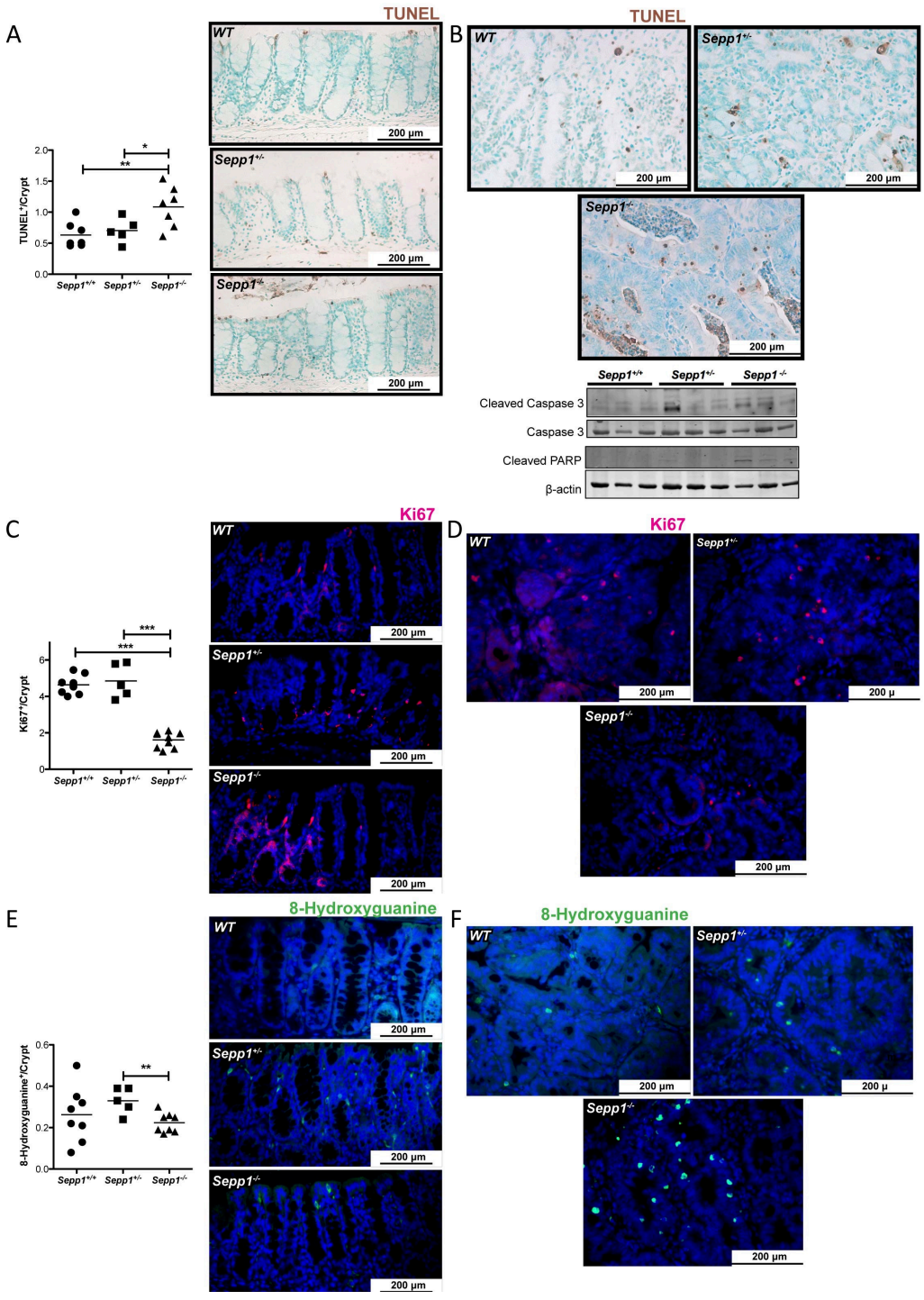

Figure 39: Crypt apoptosis is increased and crypt proliferation is decreased in *Sepp1*$^{-/-}$ AOM/DSS-treated colons. (A) Quantification (left) and images (right) of crypt apoptosis (average TUNEL^{+}/crypt; WT, 7; *Sepp1*$^{+/-}$, 6; *Sepp1*$^{-/-}$, 7). Intratumoral protein expression of cleaved caspase-3, caspase-3, cleaved PARP, and β-actin as a loading

control with three replicates within each genotype (bottom right). (B) Representative images of TUNEL staining within the tumor high-powered field. (C) Quantification (left) and representative images (right) of crypt proliferation (average ki67^{+}/crypt; WT, 8; *Sepp1*$^{+/-}$, 5; *Sepp1*$^{-/-}$, 8). (D) Representative images of ki67 staining within the tumor high-powered field. (E) Quantification (left) and representative images (right) of DNA damage (average 8-OHdG^{+}/crypt; WT, 8; *Sepp1*$^{+/-}$, 5; *Sepp1*$^{-/-}$, 8). (F) Representative image of 8-hydroxyguanine staining within the tumor high-powered field. All images were taken at 40x magnification. **P* < 0.05, ***P* < 0.01, ****P* < 0.001, 1-way ANOVA, Newman-Keuls Multiple Comparison Test.

Pro-tumorigenic M2 macrophage polarization is increased in Sepp1$^{+/-}$ *tumors*

The most significantly-induced gene after polarization of macrophages to the M2 phenotype is *SEPP1* (Bosschaerts et al. 2008; Ghassabeh et al. 2006; Solinas et al. 2010). Moreover, proinflammatory cytokines induce iNOS, which results in down-regulation of *SEPP1* (Speckmann et al. 2010). To determine if SEPP1 influences macrophage phenotypes and inflammation, we analyzed tumors from WT, *Sepp1*$^{+/-}$ and *Sepp1*$^{-/-}$ mice post-AOM/DSS for macrophage polarization. Immunohistochemistry of tumors for the pan-macrophage marker F4/80 and either the M1 macrophage marker IL-1β or the M2 macrophage marker Arginase I (Arg1) revealed an increase of total macrophages in *Sepp1*$^{+/-}$ tumors (WT: 13.1 ± 1.3, *Sepp1*$^{+/-}$: 23.2 ± 3.0, *P*<0.01, *Sepp1*$^{-/-}$: 13.1 ± 0.8 F4/80^{+} cells/tumor HPF, **Figure 40A**), apparently resulting from an increased M2 macrophage presence (WT: 8.4 ± 0.8, *Sepp1*$^{+/-}$: 18.0 ± 3.9, *Sepp1*$^{-/-}$: 8.3 ± 1.1 F4/80^{+}/ArgI^{+} cells/tumor HPF, **Figure 40C**) as M1 macrophage numbers remain unaltered **(Figure 40B)**. Interestingly, *Sepp1*$^{-/-}$ tumors did not demonstrate increased M2 polarized macrophage infiltration. In order to determine whether this effect was due to recruitment or polarization, we isolated bone marrow macrophages from WT, *Sepp1*$^{+/-}$, and *Sepp1*$^{-/-}$

mice and treated with IFNγ and LPS to polarize to the M1 and IL-13 to polarize to the M2 phenotype. Analysis of M1 markers *iNOS* and *IL-1β* demonstrated decreased M1 polarization in *Sepp1*$^{+/-}$ macrophages (iNOS: 19,494 ± 593.8 vs 14,961 ± 782.3 fold change, P<0.001, IL-1β: 337.6 ± 0.78 vs 225.1 ± 20.66 fold change, P<0.001, **Figure 40D**), while the M2 marker *Ym1* indicated increased polarization to M2 (13.1 ± 3.3 vs 26.6 ± 0.3, P<0.001, **Figure 40E**). These data indicate that *Sepp1* haploinsufficiency leads to altered macrophage polarization upon directed stimulation, a phenotype observed *in vivo* in the inflammatory infiltrates in *Sepp1*$^{+/-}$ tumors. Therefore, it is possible that altered immune responses may contribute to a pro-tumorigenic microenvironment in these mice.

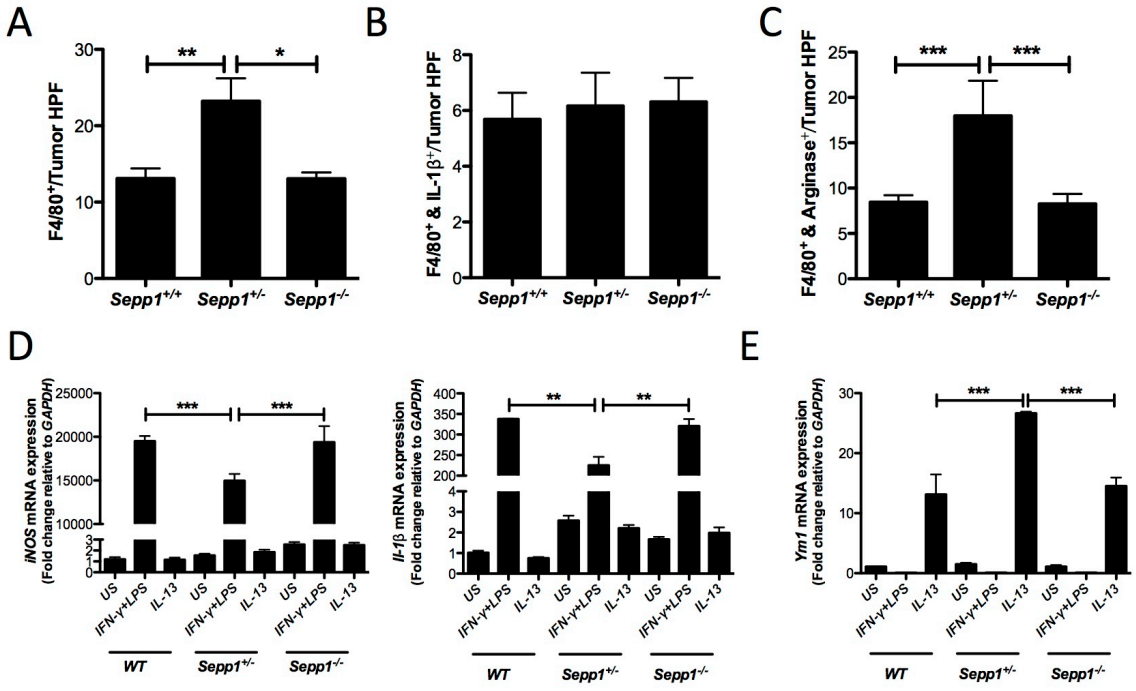

Figure 40: SEPP1 regulates pro-tumorigenic M2 macrophage polarization. Quantification of (A) intratumoral total macrophage staining as determined by F4/80+ cells/tumor HPF. (B) M1 macrophage staining as determined by F4/80+/IL-1β+ cells/tumor HPF. (C) M2 macrophage staining as determined by F4/80+/ArgI+

cells/tumor HPF (8, WT; 12, *Sepp1*$^{+/-}$; 8, *Sepp1*$^{-/-}$). (D) *iNOS* (left, n = 5 per genotype) and *IL-1β* (right, n = 6 per genotype). (E) *Ym1* mRNA expression (n = 6 per group) in WT, *Sepp1*$^{+/-}$, and *Sepp1*$^{-/-}$ *in vitro*-activated bone marrow macrophages. Graphs demonstrate fold change in expression relative to unstimulated (US) WT macrophages normalized to *Gapdh*. *P < 0.05, **P < 0.01, ***P < 0.001, 1-way ANOVA, Newman-Keuls Multiple Comparison Test.

Loss of the selenium-rich C-terminal domain of SEPP1 promotes inflammatory tumorigenesis

SEPP1 is considered to be a selenium transport protein, and deletion of the selenium-rich C-terminal domain (*Sepp1*$^{\Delta 240\text{-}361/\Delta 240\text{-}361}$) results in severe selenium deficiency in the brain and testes of mice (Hill et al. 2007). Colonic selenium levels were also decreased in *Sepp1*$^{\Delta 240\text{-}361/\Delta 240\text{-}361}$ mice (394.5 ± 19.6 vs 260.2 ± 10.6 ng selenium/g colon, P=0.0001, **Figure 41A**), yet the presence of selenium suggests that while SEPP1 contributes to selenium delivery to the colon, it is not the sole source. Because selenium has been implicated in DNA damage repair via regulation of p53 (Seo, Kelley, and Smith 2002), WNT and Nrf2 signaling, and modification of several cancer types including colorectal, lung, laryngeal, hepatic, and prostate (Connelly-Frost et al. 2009; Jaworska et al. 2013; Kasaikina et al. 2013; Steinbrecher et al. 2010), we determined whether the loss of the selenium-rich domain of SEPP1 would contribute to tumorigenesis. We subjected WT and *Sepp1*$^{\Delta 240\text{-}361/\Delta 240\text{-}361}$ mice to the AOM/DSS protocol and analyzed them for tumor burden. We found that SEPP1 truncation resulted in an increase in tumor number (7.9 ± 1.4 vs 3.9 ± 0.7 tumors/mouse, P=0.02, **Figure 41B**). We have previously determined that selenium deficiency results in increased dysplasia grade in this model

(Barrett et al. 2013). Similarly, tumor grade was more advanced in *Sepp1*$^{\Delta 240\text{-}361/\Delta 240\text{-}361}$ (P<0.05, **Figure 41C**) mice.

Along with an increase in tumor number, we also observed an increase in intratumoral proliferation (20.3 ± 2.2 vs 13.4 ± 1.7 Ki67^{+} cells/tumor HPF, P=0.04, **Figure 41D** & **Figure 42**), but no change in crypt proliferation **(Figure 44A)** or crypt or tumor apoptosis **(Figures 43B & C)**. Consistent with a role of selenium in DNA damage, there was an increase in crypt (1.0 ± 0.08 vs 0.7 ± 0.04 8-OHdG^{+} cells/crypt, P=0.02, **Figure 41E** & **Figure 42B**) and intratumoral (29.8 ± 2.8 vs 17.1 ± 2.7 8-OHdG^{+} cells/tumor HPF, P=0.01, **Figure 41F** & **Figure 42C**) DNA damage indices in mice lacking the selenium-rich C-terminal domain. These data suggest that the selenium-rich domain of SEPP1 may protect from tumor initiation by preserving genomic integrity.

Mutation of the redox active selenocysteine in SEPP1 promotes inflammatory tumorigenesis

Residues 40-43 of the N-terminal domain of SEPP1 comprise a UXXC redox motif that acts as a peroxidase (Burk and Hill 2005; Kurokawa et al. 2014). As such, SEPP1 may contribute to antioxidant activity independent of its roles in selenium transport. In order to test whether loss of this antioxidant domain would modify tumorigenesis, we subjected mice in which the selenocysteine (U) at amino acid 40 was mutated to an enzymatically dead serine (S) (*Sepp1*$^{U40S/U40S}$) to the AOM/DSS protocol. SEPP1-mutated mice displayed increased tumor number (7.3 ± 1.1 vs 3.8 ± 0.7 tumors/mouse, P=0.02, **Figure 41G**) and tumor size (3.1 ± 0.3 vs 1.6 ± 0.2 mm^2, P=0.002, **Figure 41H**). This increase in tumorigenesis was likely at least partially

dependent upon an increase in crypt proliferation (0.5 ± 0.04 vs 0.3 ± 0.02 $Ki67^+$ cells/crypt, *P*=0.0009, **Figure 41I** & **Figure 44A**) and intratumoral proliferation (33.5 ± 2.6 vs 15.2 ± 1.6 $Ki67^+$ cells/tumor HPF, *P*<0.0001, **Figure 41J** & **Figure 44B**), despite no changes in apoptosis **(Figure 45A & B)**. We did note an increase in crypt DNA damage (0.6 ± 0.02 vs 0.3 ± 0.03 8-$OHdG^+$ cells/crypt, *P*<0.0001, **Figure 41K** & **Figure 44C**) and intratumoral DNA damage (28.7 ± 2.6 vs 10.8 ± 1.2 8-$OHdG^+$ cells/tumor HPF, *P*<0.0001, **Figure 41L** & **Figure 44D**) in the SEPP1-mutated mice, suggesting that the redox site of SEPP1 contributes to protection from DNA damage.

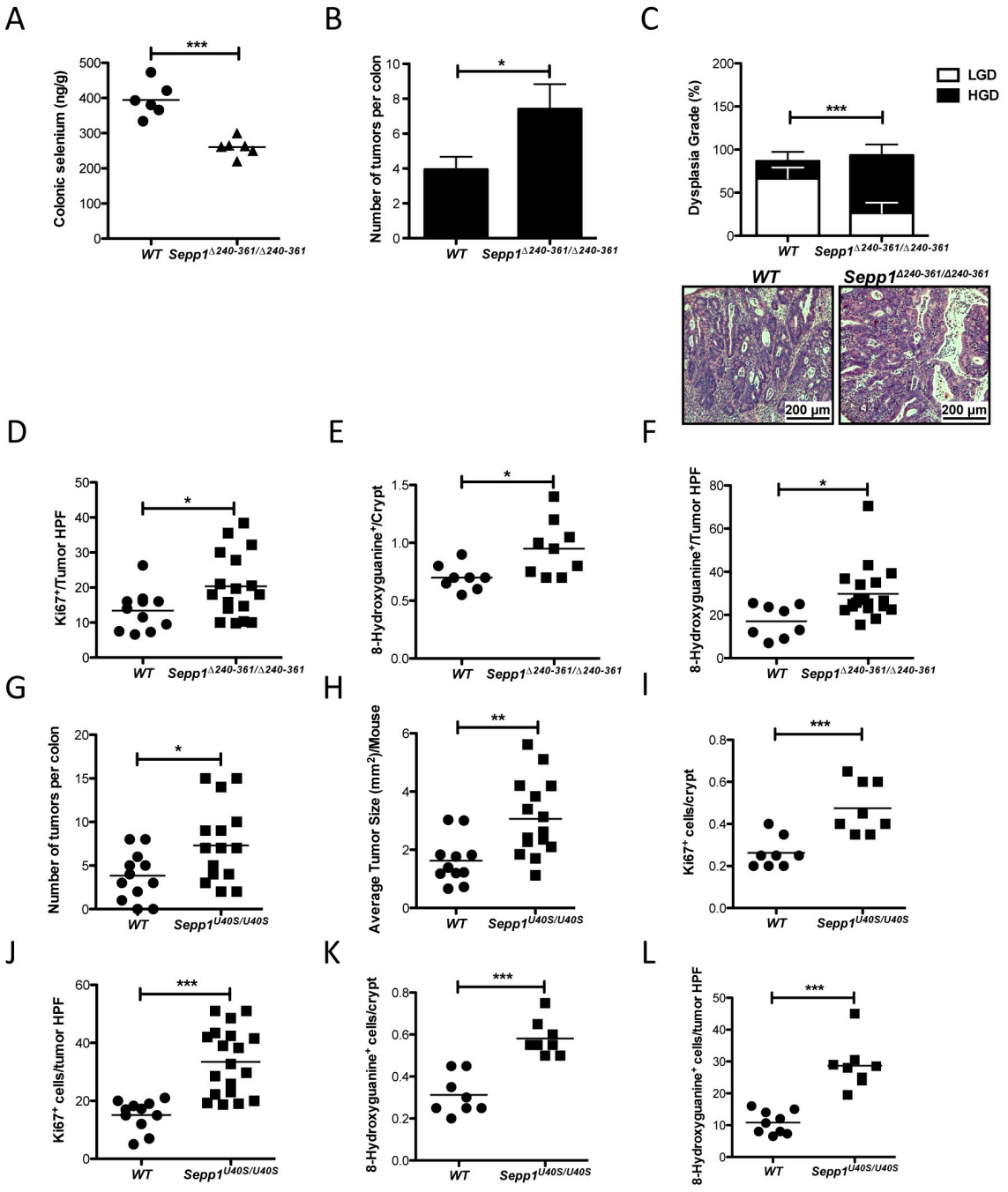

Figure 41: Both the selenium-rich region and putative antioxidant domain of SEPP1 protect from inflammatory tumorigenesis. (A) Quantification of colonic selenium in WT (n = 6) and *Sepp1*$^{\Delta 240\text{-}361/\Delta 240\text{-}361}$ (n = 6) mice. (B) Number of tumors per mouse (16, WT; 15, *Sepp1*$^{\Delta 240\text{-}361/\Delta 240\text{-}361}$). *$P$ < 0.05, ***P < 0.001, 2-tailed unpaired t test. (C) Percentage of total tumors per genotype with either high grade dysplasia (HGD, black) or low grade dysplasia (LGD, white) (top) (n = 15 per group, ***P < 0.001, Chi-square

contingency analysis) and representative images from tumors of the given genotypes (40x magnification, bottom). (D) Quantification of intratumoral proliferation as measured by Ki67+ cells/tumor HPF (12, WT; 17, *Sepp1*$^{\Delta 240\text{-}361/\Delta 240\text{-}361}$). (E) Crypt DNA damage as measured by 8-hydroxyguanine+ cells/crypt averaged from 20 crypts within each mouse (8, WT; 9, *Sepp1*$^{\Delta 240\text{-}361/\Delta 240\text{-}361}$). (F) Intratumoral DNA damage as measured by 8-hydroxyguanine+ cells/tumor HPF (8, WT; 17, *Sepp1*$^{\Delta 240\text{-}361/\Delta 240\text{-}361}$). (G) Number of tumors and (H) average tumor size within either WT (n = 12) or *Sepp1*$^{U40S/U40S}$ (n = 16) mice. (I) Quantification of crypt proliferation as measured by Ki67+ cells/crypt averaged from 20 crypts within each mouse (8, WT; 8, *Sepp1*$^{U40S/U40S}$) (J) intratumoral proliferation as measured by Ki67+ cells/tumor HPF (11, WT; 19 , *Sepp1*$^{U40S/U40S}$), (K) crypt DNA damage as measured by 8-hydroxyguanine+ cells/crypt averaged from 20 crypts within each mouse (8, WT; 8, *Sepp1*$^{U40S/U40S}$), and (L) intratumoral DNA damage as measured by 8-hydroxyguanine+ cells/tumor HPF (9, WT; 8, *Sepp1*$^{U40S/U40S}$). *$P < 0.05$, **$P <$ 0.01, ***$P < 0.001$, 2-tailed unpaired t test.

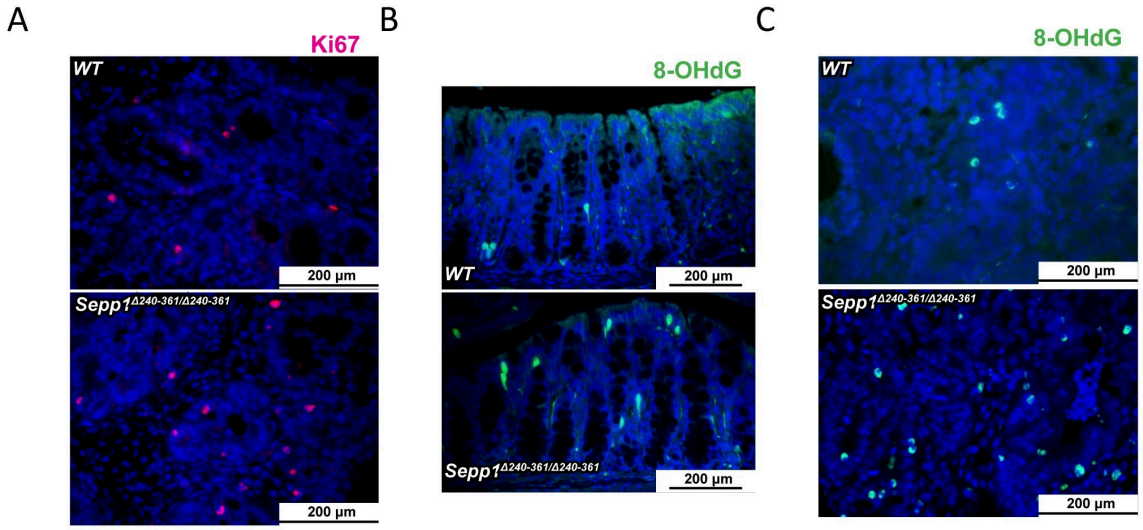

Figure 42: Proliferation and DNA damage are increased in *Sepp1*$^{\Delta 240\text{-}361/\Delta 240\text{-}361}$ colons post-AOM/DSS administration. (A) Representative intratumoral proliferation staining as determined by ki67 positivity. (B) Crypt and (C) intratumoral DNA damage as measured by 8-hydroxyguanine staining. Images taken at 40x magnification.

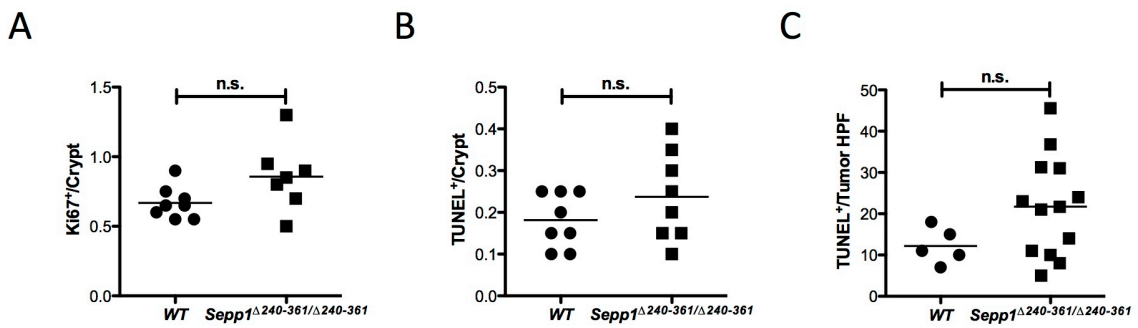

Figure 43: Crypt proliferation and crypt and tumor apoptosis are unaltered in *Sepp1*$^{\Delta 240\text{-}361/\Delta 240\text{-}361}$ colons. (A) Quantification of crypt proliferation (ki67^{+} cells/crypt; WT, 8; *Sepp1*$^{\Delta 240\text{-}361/\Delta 240\text{-}361}$, 7). (B) Quantification of crypt (TUNEL^{+} cells/crypt; WT, 8; *Sepp1*$^{\Delta 240\text{-}361/\Delta 240\text{-}361}$, 8) and (C) intratumoral (TUNEL^{+} cells/tumor HPF; WT, 5; *Sepp1*$^{\Delta 240\text{-}361/\Delta 240\text{-}361}$, 13) apoptosis.

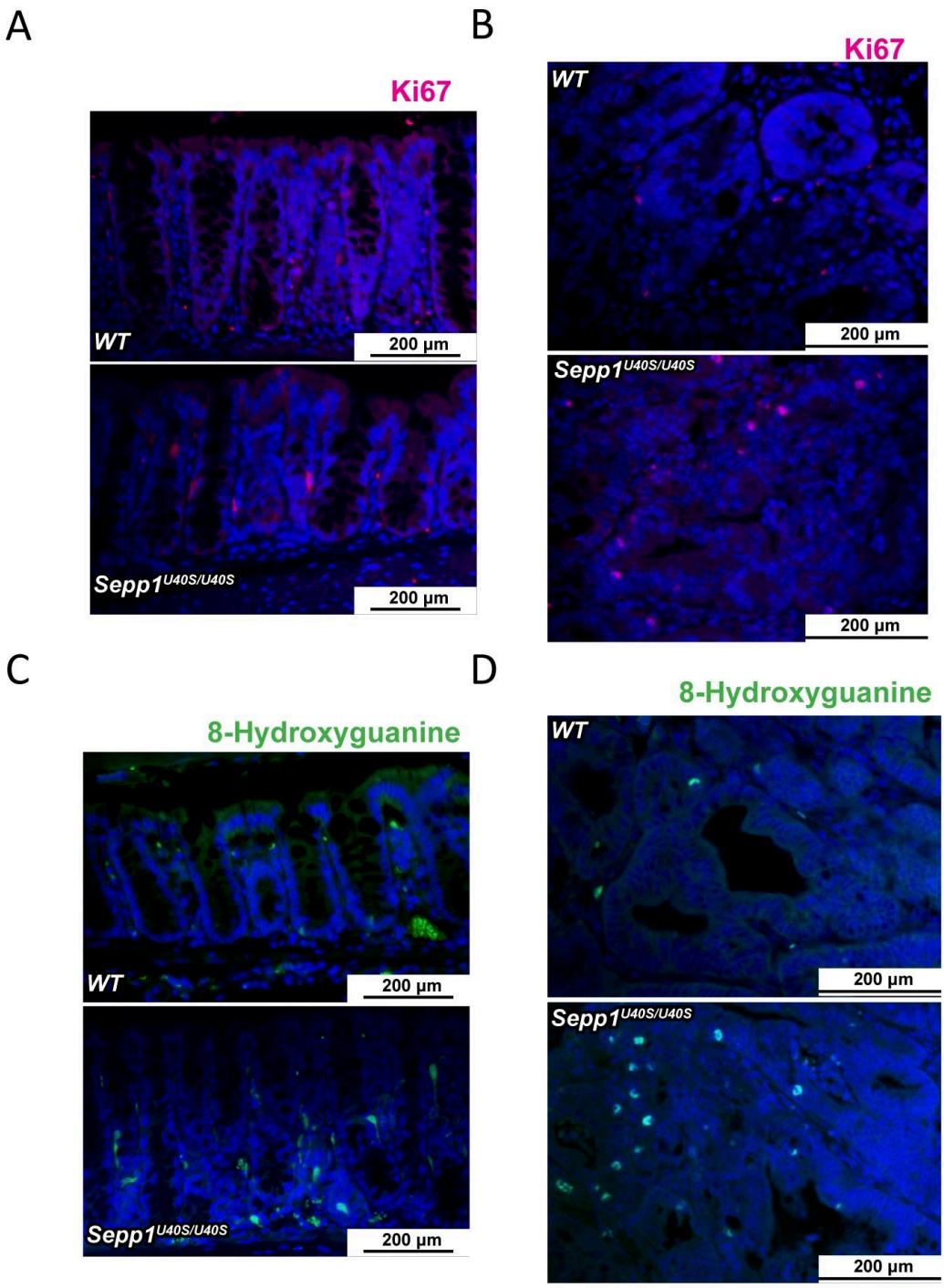

Figure 44: Proliferation and DNA damage are increased in colons of *Sepp1*$^{U40S/U40S}$ mice. (A) Representative images of proliferation in crypts (ki67^{+} cells/crypt) and (B) tumors (ki67^{+} cells/tumor HPF). (C) Representative images of DNA damage in crypts (8-OHdG^{+} cells/crypt) and (D) tumors (8-OHdG^{+} cells/tumor HPF). HPF is 40x magnification.

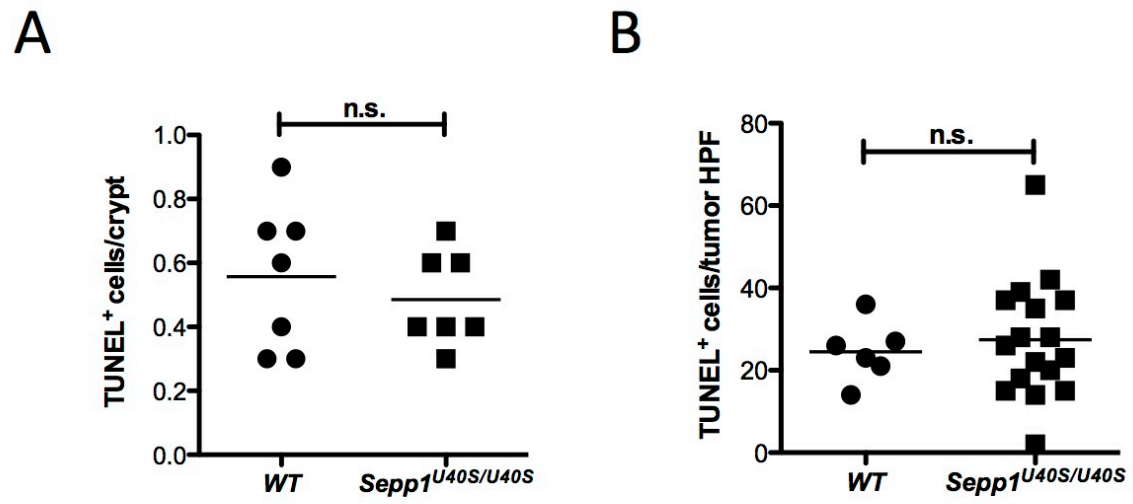

Figure 45: Apoptosis is unaltered in colons of *Sepp1*$^{U40S/U40S}$ mice post-AOM/DSS protocol. (A) Quantification of crypt (TUNEL^{+} cells/crypt; WT, 7; *Sepp1*$^{U40S/U40S}$, 7) and (B) intratumoral (TUNEL^{+} cells/tumor HPF; WT, 6; *Sepp1*$^{U40S/U40S}$, 17) apoptosis in colons of mice treated with the AOM/DSS protocol.

Sepp1 haploinsufficiency-driven CAC persists in mice fed normal selenium diets

Sepp1$^{-/-}$ mice require selenium supplementation to survive (Hill et al. 2004); therefore all of the above experiments were conducted in the setting of supranutritional selenium levels. Our results indicate that *Sepp1* haploinsufficiency augments tumorigenesis. We next determined whether *Sepp1* heterozygosity would also augment tumorigenesis if mice were maintained on a normal selenium diet (0.25 PPM selenium). *Sepp1*$^{+/-}$ mice demonstrated an increase in tumor number when determined by both endoscopy (9.8 ± 1.2 vs 4.6 ± 0.8 tumors/mouse, $P<0.01$, **Figure 46A**, **B**) and analysis of tumor burden at sacrifice (11.6 ± 1.0 vs 5.5 ± 0.9 tumors/mouse, $P<0.001$, **Figure 46C**, D), and in general, these tumors were also larger than those observed in WT colons ($P<0.05$, **Figure 46E**). When comparing overall survival of cohorts maintained on a normal selenium diet (0.25 PPM selenium) versus selenium supplemented diet (1.0 PPM

selenium), cohorts maintained on selenium-supplemented diet demonstrated a significant survival benefit (P<0.001, **Figure 46F**). These results may have potential translational implications, as the 0.25 PPM diet more closely approximates selenium levels in the typical Western diet.

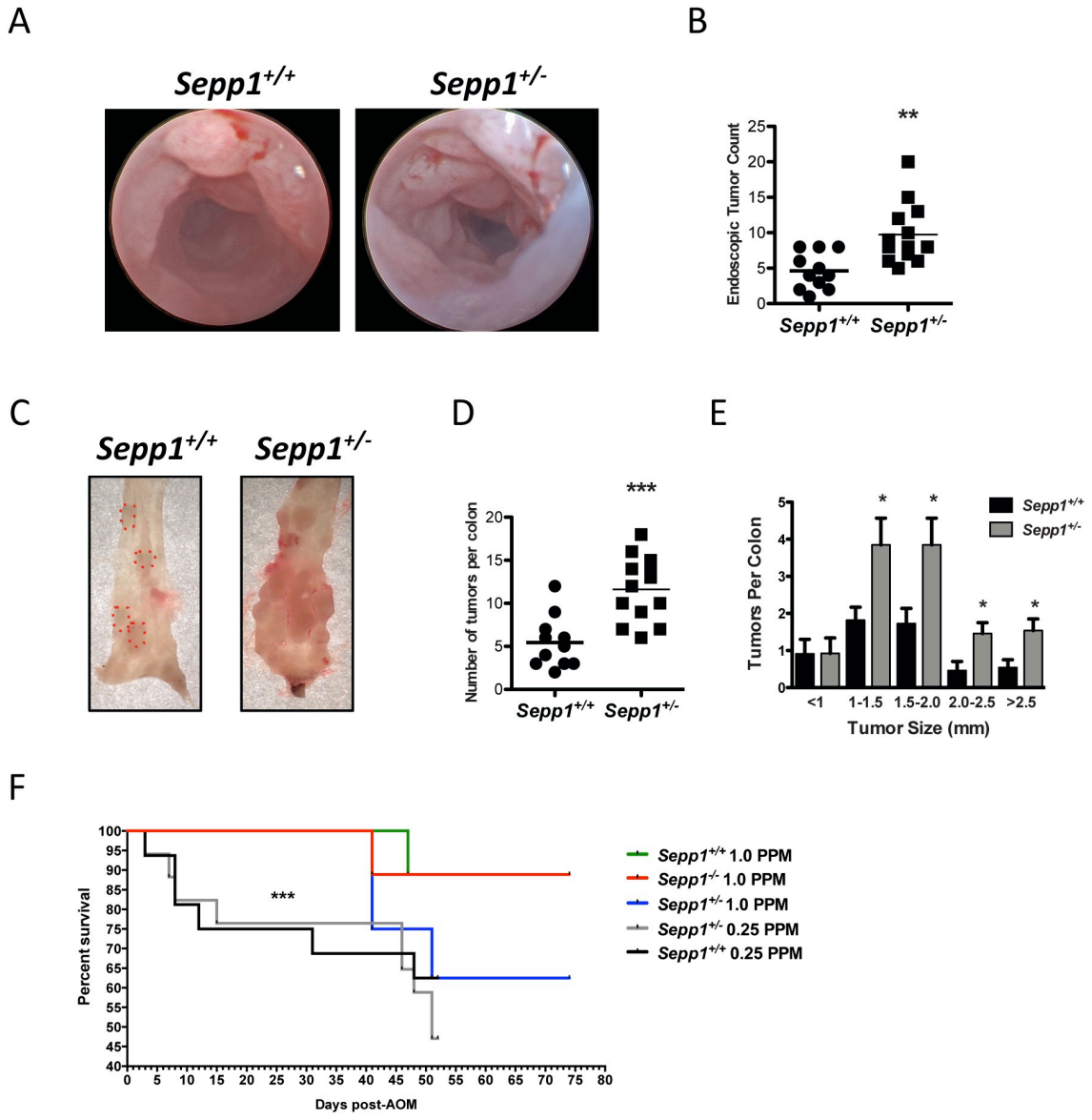

Figure 46: *Sepp1* haploinsufficiency-driven CAC persists in mice maintained on normal selenium diets. (A) Endoscopic images of WT and *Sepp1*$^{+/-}$ colons after the second cycle of DSS administration. (B) Endoscopic tumor burden quantitative assessment (11, WT; 13, *Sepp1*$^{+/-}$). (C) Gross representative images of tumors (D) and

tumor counts at necropsy (11, WT; 13, *Sepp1*$^{+/-}$). 2-tailed unpaired *t* test. (E) Tumor size distribution. Unpaired *t* test with Welch's correction. **P* < 0.05, ***P* < 0.01, ****P* < 0.001. (F) Survival analysis of AOM/DSS-treated mice maintained on the indicated diets. Unpaired *t* test with Welch's correction, **P*<0.05, ***P*<0.01, ****P*<0.001.

Absence of SEPP1 augments stem cell properties and reduces the ability of enteroids to survive in response to hydrogen peroxide

SEPP1 regulates oxidative stress and toxicity (Arteel et al.; Xiao et al. 2013), and consistent with a function in WNT signaling, has been shown to play a role in differentiation and stem cell properties (Sampson et al. 2011; Y. Zhang and Chen 2011). Recently, a model for epithelial crypt growth has been established based on the isolation of stem cells from the small intestinal crypt. From single crypts, complex structures can be grown *in vitro* that closely resemble their *ex vivo* counterparts (enteroids) (Sato and Clevers 2013). Using this model system, we sought to determine how SEPP1 influences intestinal epithelial biology. Importantly, *Sepp1* expression in intestinal organoids was similar to expression in both the colon and the brain, a tissue known to produce high levels of SEPP1 (Steinbrenner and Sies 2013), indicating these cultures would accurately recapitulate an *in vivo* setting **(Figure 47A)**.

Enteroids can be grown from a single stem cell or complete crypts (Fuller et al. 2012), and the "stemness" of enteroids have been measured by several growth parameters (Durand et al. 2012; Farin, Van Es, and Clevers 2012; Sato, van Es, et al. 2011). For instance, augmented stem cell survival can be measured by an increase in the number of crypts that survive plating versus the total number of crypts plated (plating efficiency). Furthermore, the percentage of branching enteroids or stem spheroids present at certain time points can establish the differentiation capacity of the stem cells and the extent of

stem cell signaling, respectively. Finally, the number of branches within each enteroid indicates the ability of the stem cells to self-propagate and establish new crypts. To determine if *Sepp1* contributes to epithelial cell growth and stem cell function at baseline, we analyzed *Sepp1*$^{-/-}$ enteroids for each of these properties (plating efficiency: 96.5 ± 2.4 % enteroids of total crypts plated, branching enteroids: 61.5 ± 1.8 % branching enteroids, stem spheroids: 14.5 ± 0.2 % stem spheroids, number of branches: 3.2 ± 0.2 number of branches per branching enteroid, **Figure 47B**) and observed increased stem cell fitness and growth abilities compared to WT enteroids (plating efficiency: 65.5 ± 2.0 % enteroids of total crypts plated, $P<0.0001$, branching enteroids: 42.1 ± 2.4 % branching enteroids, $P=0.02$, stem spheroids: 7.6 ± 0.9 % stem spheroids, $P=0.002$, number of branches: 1.9 ± 0.1, $P=0.003$, **Figure 47B**).

Because SEPP1 serves as a peroxidase *in vitro* (Kurokawa et al. 2014), we next determined the response of *Sepp1*$^{-/-}$ enteroids to hydrogen peroxide treatment. Analysis of ROS produced after treatment with hydrogen peroxide revealed a decreased ability of *Sepp1*$^{-/-}$ small intestine to respond to oxidative stress, as demonstrated by increased carboxy-H_2DCFDA staining intensity (800 μM H_2O_2: 1.6 ± 0.4 vs 3.3 ± 0.4 fold-change intensity relative to 0 μM H_2O_2 WT, $P=0.04$, **Figure 47C**); however, there was no change in staining intensity of the oxidative-insensitive analogue carboxy-DCFDA. Moreover, baseline proliferation was increased in *Sepp1*$^{-/-}$ enteroids (1.0 ± 0.06 vs 1.4 ± 0.1 fold-change EdU^+ cells/crypt area relative to 0 μM H_2O_2 WT, $P<0.05$, **Figure 47D**) and while treatment with hydrogen peroxide resulted in decreased *Sepp1*$^{-/-}$ proliferation compared to untreated null enteroids (1.4 ± 0.1 vs 0.9 ± 0.09 fold-change EdU^+ cells/crypt area relative to 0 μM H_2O_2 *Sepp1*$^{-/-}$, $P<0.01$, **Figure 47D**), *Sepp1*$^{-/-}$ enteroids retained

increased proliferation compared to WT enteroids (0.4 ± 0.09 vs 0.9 ± 0.09 fold-change EdU^+ cells/crypt area relative to 0 μM H_2O_2 *WT*, $P<0.05$, **Figure 47D**). Finally, *Sepp1*$^{-/-}$ enteroids demonstrated decreased survival in response to multiple daily administrations of hydrogen peroxide ($P=0.005$, **Figure 47E**). These data indicate that absence of SEPP1 increases baseline stem phenotypes and proliferation and compromises the antioxidant potential of enteroids. These data are particularly compelling because they indicate an epithelial cell-autonomous role for SEPP1 in processes that would likely contribute to tumorigenesis in CAC, a cancer characterized by increased microenviromental oxidative stress.

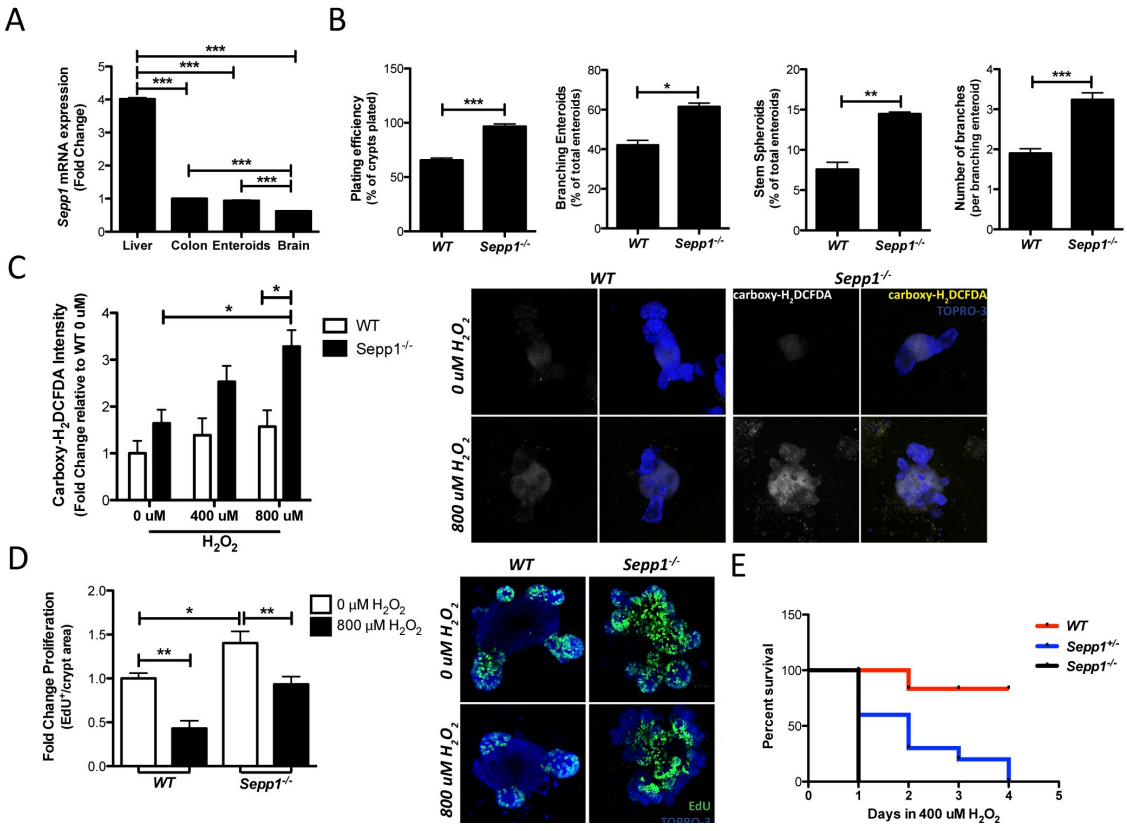

Figure 47: *Sepp1*$^{-/-}$ enteroids display increased stem cell characteristics and ROS production, proliferation, and decreased survival after oxidative stress. (A) *Sepp1*

mRNA expression in tissue isolated from WT mice (n = 3/group). Fold change expression normalized to *Gapdh* and relative to colonic *Sepp1* expression. 1-way ANOVA, Newman-Keuls Multiple Comparison Test. (B) Percentage of surviving enteroids one day post-plating, percent of branching enteroids and stem spheroids counted three days post-plating, and average number of branches per branching enteroid at four days post-plating (n = 4/group /experiment). 2-tailed unpaired t test. (C) ROS quantification by carboxy-H_2DCFDA staining intensity measured 2 hours post-treatment with H_2O_2. Fold change in intensity relative to WT enteroids treated with 0 μM H_2O_2 (left, n = 4/group). Representative images of the single carboxy-H_2DCFDA channel and merged carboxy-H_2DCFDA and TO-PRO3 channels in WT and *Sepp1*$^{-/-}$ enteroids treated with either 0 μM or 800 μM H_2O_2 (100x magnification, right). (D) Proliferation as determined by EdU+ cells/crypt area within WT and *Sepp1*$^{-/-}$ enteroids after two hours of treatment with either 0 μM or 800 μM H_2O_2 (left, n = 4/group with analysis of 10 enteroids/genotype) and representative images of EdU staining in WT and *Sepp1*$^{-/-}$ enteroids post-treatment with either 0 μM or 800 μM H_2O_2 (100x magnification, right). 1-way ANOVA, Newman-Keuls Multiple Comparison Test. (E) Survival curves for WT (red), *Sepp1*$^{+/-}$ (blue), and *Sepp1*$^{-/-}$ (black) enteroids after daily treatment with 400 μM H_2O_2. *$P < 0.05$, **$P < 0.01$, ***$P < 0.001$.

Wnt signaling and oxidative stress gene signatures are altered in Sepp1$^{-/-}$ *epithelium*

Enteroids rely on the addition of growth factors EGF, Noggin, and R-spondin for growth and differentiation (Sato and Clevers 2013). As *Sepp1*$^{-/-}$ enteroids demonstrate increased stem cell properties and fitness, we next determined growth factor dependency of *Sepp1*$^{-/-}$ enteroids. Depletion of EGF, Noggin, and R-spondin resulted in similar decreases in survival in all three genotypes, indicating that all three pathways are important for enteroid persistence **(Figure 48A)**.

In order to acquire an unbiased understanding of transcriptome changes within tumors of *Sepp1*$^{-/-}$ mice, we performed RNAseq analysis of tumors isolated from WT and

Sepp1$^{-/-}$ mice subjected to the AOM/DSS protocol. Ingenuity pathway analysis indicated that the Wnt pathway was among the most significantly-altered canonical pathways **(Figure 49)**, as *Sepp1*$^{-/-}$ tumors demonstrated increases in TGFβR3, APPL2, SFRP-4 and -5, and Cdh2 expression, among other abnormalities (Table 2, **Figure 50**). As further validation of altered Wnt signaling in these tumors, protein analysis demonstrated increased expression of the Wnt targets LEF-1, Cyclin D1, and MMP-7 upon loss of *Sepp1* expression **(Figure 48B)**. We next determined whether SEPP1 loss influenced production of other oxidative defense genes. First, we tested for compensation by other selenoproteins at the RNA level and did not observe differences in their message between WT and *Sepp1*$^{-/-}$ tumors. We did, however, note significant alterations in several cytochrome P450 gene family members as well as beta-hydroxysteroid dehydrogenase genes **(Figure 51)**, suggesting that other antioxidant genes are upregulated in an attempt to compensate for SEPP1 loss.

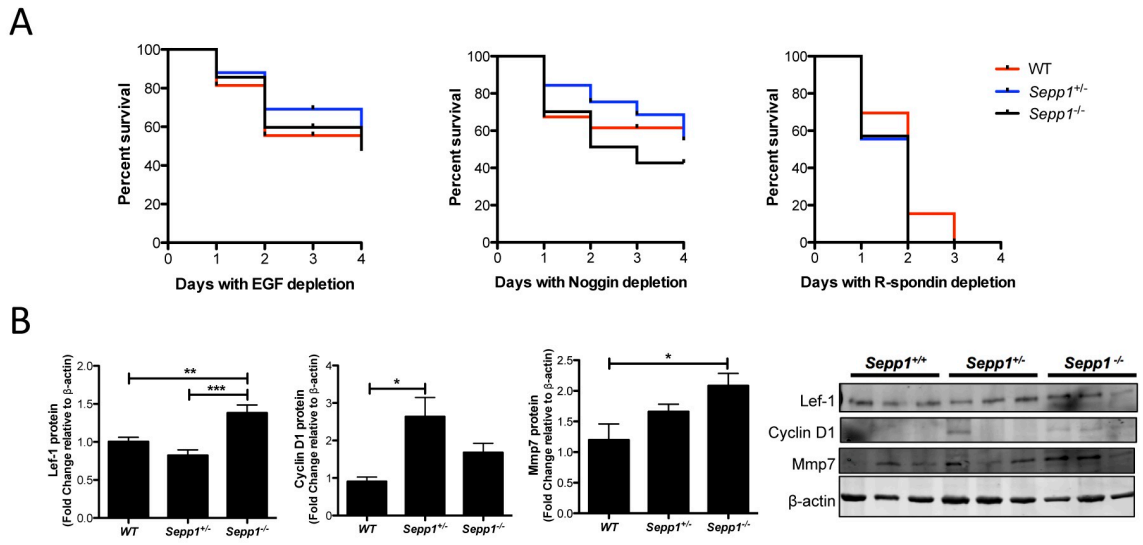

Figure 48: WNT signaling plays a pivotal role in the *Sepp1*$^{-/-}$ phenotype. (A) Survival curves in response to growth factor depletion in WT, *Sepp1*$^{+/-}$, and *Sepp1*$^{-/-}$ enteroids. (B) Quantification of WNT proteins LEF-1, Cyclin D1, and MMP-7 normalized to β-actin.

Quantification is shown as fold change relative to WT (left) and representative images of blots from three individual tumors from each genotype (right).

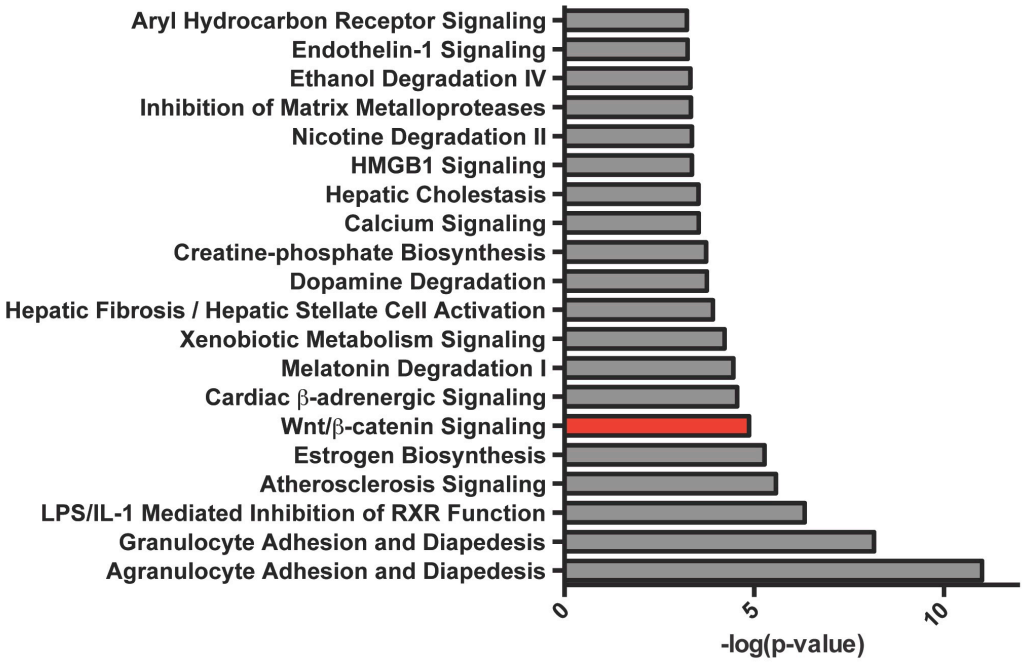

Figure 49: Ingenuity pathway analysis of alterations in Canonical Signaling in *Sepp1*$^{-/-}$ tumor RNAseq data relative to WT data. The Wnt pathway was one of the most significantly altered pathways (highlighted in red).

Gene Symbol	Gene Name	Fold Change	P-value
TGFbR3	Transforming growth factor b-3	3.4	5.00E-05
APPL2	Adapter protein containing PH domain, PTB domain and leucine zipper motif 2	2.4	0.0015
SFRP4	Secreted frizzled-related protein 4	2.7	0.00015
SFRP5	Secreted frizzled-related protein 5	2.9	5.00E-05
Cdh-2	Cadherin-2	2.1	0.00035

Table 2: Ingenuity Pathway Analysis of *Sepp1*$^{-/-}$ tumor RNAseq data relative to WT data. Select genes from the WNT signaling pathway that are overexpressed in *Sepp1*$^{-/-}$ tumors.

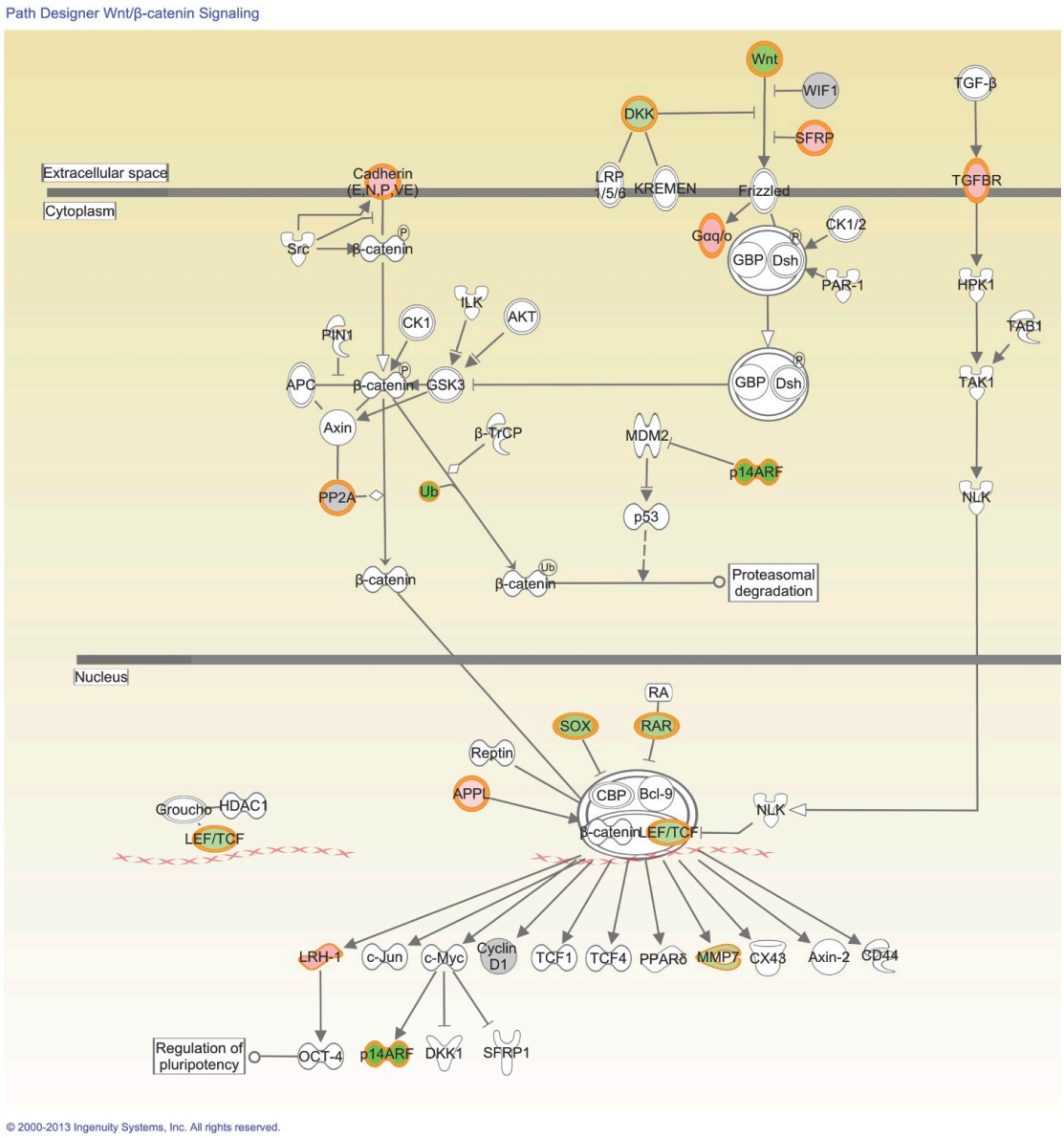

Figure 50: Ingenuity pathway analysis of *Sepp1*$^{-/-}$ tumor RNAseq data relative to WT data. WNT pathway alterations demonstrated in a pathway map. Genes highlighted with red are overexpressed and genes highlighted with green are suppressed. Intensity of color indicates extent of expression where darker color indicates a greater expression change.

A

Gene Symbol	Gene Name	Enzymatic Activity	Fold Change	P-value
Cyp2b10	Cytochrome P450 2B10	oxidoreductase activity	-2.1	0.0001
Aldh1a1	Retinal dehydrogenase 1	oxidoreductase activity	2	5.00E-05
Hpd	4-hydroxyphenylpyruvate dioxygenase	oxidoreductase activity	2.1	5.00E-05
Hsd3b2	3 beta-hydroxysteroid dehydrogenase/Delta 5-->4-isomerase type 2	oxidoreductase activity	2.2	5.00E-05
Cyp2d9	Cytochrome P450 2D9	oxidoreductase activity	2.2	5.00E-05
Fmo2	Dimethylaniline monooxygenase [N-oxide-forming] 2	oxidoreductase activity	2.2	5.00E-05
Hsd17b13	17-beta-hydroxysteroid dehydrogenase 13	oxidoreductase activity	2.2	5.00E-05
Nos1	Nitric oxide synthase, brain	oxidoreductase activity	2.2	5.00E-05
Cyp2c65	Cytochrome P450, family 2, subfamily c, polypeptide 65	oxidoreductase activity	2.3	5.00E-05
Cyp4b1	Cytochrome P450 4B1	oxidoreductase activity	2.3	0.00065
Cyp4f14	Leukotriene-B4 omega-hydroxylase 3	oxidoreductase activity	2.34	5.00E-05
Hao2	Hydroxyacid oxidase 2	oxidoreductase activity	2.4	5.00E-05
Nrxn2	Protein Nrxn2	oxidoreductase activity	2.5	0.00025
Ddo	D-aspartate oxidase	oxidoreductase activity	2.5	0.00035
Dpyd	Dihydropyrimidine dehydrogenase [NADP(+)]	oxidoreductase activity	2.6	5.00E-05
Hsd3b3	3 beta-hydroxysteroid dehydrogenase/Delta 5-->4-isomerase type 3	oxidoreductase activity	2.6	5.00E-05
Cyp2c55	Cytochrome P450 2C55	oxidoreductase activity	2.7	5.00E-05
Cd163	Scavenger receptor cysteine-rich type 1 protein M130	oxidoreductase activity	3.2	5.00E-05
Cyp2d12	Cytochrome P450, family 2, subfamily d, polypeptide 12	oxidoreductase activity	3.7	5.00E-05
Clvs2	Clavesin-2	oxidoreductase activity	3.8	0.0011
Cyp2e1	Cytochrome P450 2E1	oxidoreductase activity	4.1	5.00E-05

Figure 51: Oxidoreductase proteins are alternatively regulated at the mRNA level in *Sepp1*$^{-/-}$ tumors, but expression of other selenoproteins is unaltered. (A) RNAseq analysis of significantly-altered antioxidant genes.

Discussion

The efficacy of antioxidants as chemopreventive agents of malignancy in the general population has been disappointing. However, most studies have been conducted in the setting of relatively normal selenium levels, which ensures sufficient production of the majority of selenoproteins. Patients with inflammatory bowel disease are reported to be selenium deficient, potentially skewing selenoprotein production. Our findings suggest that modifying production of selenoproteins (i.e. SEPP1) in IBD patients may impact cancer risk. Here we show that reduced levels of a major selenoprotein, SEPP1, results in increased colonic epithelial stem cell properties, increased oxidative DNA damage, and increased Wnt signaling. These SEPP1-dependent phenotypes ultimately contribute to an increase in inflammatory tumorigenesis upon loss of either the redox active site or the selenium transport domain of SEPP1, via its effects on the tumor microenvironment and preservation of genomic integrity. These data establish a critical role for SEPP1 in

intestinal biology, homeostasis, injury response, preservation of genomic integrity, and inflammatory carcinogenesis.

Induction of several signaling pathways have been linked to selenium depletion, including Nrf2 (Burk et al. 2008) and Wnt (Brigelius-Flohé and Kipp 2013), and there is little known about the contribution of SEPP1 to the observed alterations in these pathways. We therefore performed an unbiased RNAseq analysis of tumors from WT and *Sepp1*$^{-/-}$ mice post-AOM/DSS protocol. Amongst the most severely-altered pathways in response to SEPP1 loss was the Wnt pathway. While genes were both up- and down-regulated in this pathway, some of particular importance included modulators of Wnt signaling (SFRP4 & SFRP5), the transcriptional effector LEF/TCF, and the Wnt target MMP-7, which we also validated at the protein level. Genes that demonstrated increased expression included those coding for the TGF-β receptor, N-cadherin, and the liver receptor homologue-1 (LRH-1), which is important for maintaining stem cell pluripotence during development (Gu et al. 2005). Importantly, Ingenuity Pathway Analysis (IPA) identified the Wnt/β-catenin signaling pathway as being stimulated in *Sepp1*$^{-/-}$ tumors. This is of particular importance because SEPP1 is a selenium transporter, and selenium deficiency leads to an increase in Wnt signaling, suggesting that the selenium transport function of SEPP1 may contribute to Wnt modulation.

An extensive literature has implicated selenium in the modulation of immune processes, particularly in relation to macrophage activity (Carlson et al. 2009, 2010; Vunta et al. 2008). We noted an increase in M2 polarized macrophages in tumors of AOM/DSS treated *Sepp1*$^{+/-}$ mice and hypothesized that this was due to an effect of SEPP1 on macrophage polarization. Isolation of bone marrow macrophages from

Sepp1$^{+/-}$ mice and subsequent polarization with either IFNγ and LPS (M1) or IL-13 (M2) resulted in deficits in expression of the M1 markers *iNOS* and *IL-1β* and increased expression of the M2 marker *Ym1*. This altered polarization may contribute to tumorigenesis by altering the tumor microenvironment in *Sepp1*$^{+/-}$ mice. As such, SEPP1 may reduce inflammatory tumorigenesis by attenuating pro-inflammatory immune cell activation. This is especially important to note when considering the potential positive impact of selenium supplementation on patients with nutritional deficiencies due to diseases such as IBD.

The influence of plasma SEPP1 on delivery of selenium to target tissues has been extensively studied (Burk et al. 2006; Hill et al. 2007). Our enteroid studies demonstrate a role for tissue-produced SEPP1 in intestinal biology, as loss of intestinal epithelial cell-autonomous *Sepp1* impacts cellular growth, differentiation, and response to ROS. Because it is a secreted protein, we hypothesize that SEPP1 provides localized antioxidant benefit to the proximate epithelial microenvironment. It was recently shown that SEPP1 antioxidant capacity is due, at least in part, to its ability to act as a substrate for thioredoxin reductase-1, which catalyzes NADPH oxidation (Kurokawa et al. 2014). From these studies, we postulate that extracellular SEPP1 within the near-cell environment may be cooperating with intracellular selenoproteins such as thioredoxin reductase-1, Gpx2, and Gpx4 to protect the epithelium from oxidative damage.

Whether selenium supplementation is of potential value in reducing cancer risk has been studied. The U.S. case-control SELECT study did not demonstrate any clear association between serum selenium levels and the risk of recurrent CRC (Lippman et al. 2009), and a meta-analysis of intervention trials concluded that oral administration of

antioxidants including selenium were not effective in preventing colorectal neoplasia in the general population (Papaioannou et al. 2011). A major limitation of these studies, however, was patient selection, as patients in both studies had near-normal selenium levels. Our data suggest that targeted supplementation in populations known to be selenium deficient might be an effective prevention strategy. IBD patients are selenium deficient as measured by both plasma selenium and SEPP1 levels (Ojuawo and Keith 2002). Furthermore, the plasma concentration of SEPP1 is reduced 53% in patients with CD compared to healthy controls (Andoh et al. 2005). This suggests that patients with IBD are selenium deficient to such an extent that selenium supplementation might increase SEPP1 levels and subsequently reduce risk of CAC arising from IBD. Indeed, in line with the idea of a protective role for selenium supplementation, our study demonstrated a significant survival benefit in cohorts of mice that were on high selenium diet in comparison to those on normal selenium diet when subjected to an AOM/DSS inflammatory carcinogenesis protocol.

Importantly, several SNPs have been identified in *SEPP1* that might contribute to decreased expression in tumors. For instance, SNPs in *SEPP1* are associated with decreased plasma SEPP1 in men and increased prostate cancer risk (Cooper et al. 2008; Steinbrecher et al. 2010). Furthermore, four *SEPP1* variants have been significantly associated with advanced colorectal adenoma risk including the variant *SEPP1 -4166G* which exists within the promoter region, two loci in the 3' region of *SEPP1*, and a third locus in the 3' region of *SEPP1* which is inversely associated with risk of colorectal adenoma (Peters et al. 2008). Additionally, genetic instability has been observed within the $(T)_{17}$ repeat motif within the *SEPP1* promoter in CRC to the mutator phenotype.

Thus, this *SEPP1* repeat structure may be of functional relevance to *SEPP1* gene expression and thus modify tumorigenesis (Al-Taie et al. 2002). A mechanism by which some of these polymorphisms may alter SEPP1 status is by either altering expression or proportions of SEPP1 isoforms. Several functional polymorphisms in the *SEPP1* gene have been shown to influence isoform expression, and it is thought that increased expression of the 60 kDa isoform of SEPP1 may increase selenoprotein synthesis and decrease CRC risk (Méplan et al. 2009). Thus, genotyping of *SEPP1* in patients with CAC may indicate increased responsiveness to selenium supplementation.

In conclusion, we demonstrate a cell-autonomous role for SEPP1 in the intestinal epithelium and that its reduction, *in vivo*, augments inflammatory carcinogenesis. These *in vivo* effects occur via independent enzymatic and transport activities. Our studies establish a critical role for SEPP1 in intestinal biology, homeostasis, injury response, preservation of genomic integrity, and inflammatory carcinogenesis and suggest that SEPP1 could serve as a therapeutic target in the prevention of CAC.

Appendix B

TRANSCRIPTIONAL CO-REPRESSOR MTG16 REGULATES SMALL INTESTINAL CRYPT PROLIFERATION AND CRYPT REGENERATION AFTER RADIATION-INDUCED INJURY[2]

Abstract

Myeloid translocation genes (MTGs) are transcriptional co-repressors implicated in development, malignancy, differentiation, and stem cell function. While MTG16 loss renders mice sensitive to chemical colitis, the role of MTG16 in the small intestine is unknown. Histological examination revealed that *Mtg16*$^{-/-}$ mice have increased enterocyte proliferation and goblet cell deficiency. After exposure to radiation, *Mtg16*$^{-/-}$ mice exhibited increased crypt viability and decreased apoptosis in comparison to WT mice. Flow cytometric and immunofluorescence analysis of intestinal epithelial cells for phospho-Histone H2A.X also indicated decreased DNA damage and apoptosis in *Mtg16*$^{-/-}$ intestines. To determine if *Mtg16* deletion affected epithelial cells in a cell-autonomous fashion, intestinal crypts were isolated from *Mtg16*$^{-/-}$ mice. *Mtg16*$^{-/-}$ and WT intestinal crypts showed similar enterosphere forming efficiencies when cultured in the presence of EGF, Noggin, and R-spondin. However, when *Mtg16*$^{-/-}$ crypts were cultured in the presence of Wnt3a, they demonstrated higher enterosphere forming efficiencies and

[2] Published in the *American Journal of Physiology: Gastrointestestinal and Liver Physiology*. *Shenika V. Poindexter, *Vishruth K. Reddy, Mukul K. Mittal, Amanda M. Williams, M. Kay Washington, Elizabeth Harris, Amanda Mah, Scott W. Hiebert, Kshipra Singh, Rupesh Chaturvedi, Keith T. Wilson, P. Kay Lund, Christopher S. Williams. *Transcriptional co-repressor MTG16 regulates small intestinal crypt proliferation and crypt regeneration after radiation-induced injury*, 308: G562-G571, Copyright (2015). *Co-first Authorship.

delayed progression to mature enteroids. *Mtg16*$^{-/-}$ intestinal crypts isolated from irradiated mice exhibited increased survival in comparison to WT intestinal crypts. Interestingly, *Mtg16* expression was reduced in a stem cell-enriched population at the time of crypt regeneration. This is consistent with MTG16 negatively regulating regeneration *in vivo*. Taken together, our data demonstrates that MTG16 loss promotes radioresistance and impacts intestinal stem cell function, possibly due to shifting cellular response away from DNA damage-induced apoptosis and towards DNA repair after injury.

Introduction

Radiation enteritis is a pathological condition in which the small intestine is injured following exposure to ionizing radiation (Harb, Abou Fadel, and Sharara 2014). Risk factors associated with radiation enteritis include mutations in DNA repair genes such as *BRCA1* and *BRCA2* (Ernestos et al. 2010; Nieuwenhuis 2002) or in DNA damage response genes such as *Tp53* (Mazzatti et al. 2005) and B-Cell Lymphoma 6 Protein (*BCL6*) (Margalit et al. 2006). Sensitivity to intestinal radiation-induced injury may be further influenced by changes in cell cycle kinetics, synchronization of replicating cell populations, or inhibition of effective DNA repair (Brown and Rzucidlo 2011; Shadad et al. 2013). Typically, DNA repair of radiation-induced DNA double-strand breaks depends on the activation of DNA damage response programs that induce phosphorylation of histone H2A.X and activation of a number of mediators that phosphorylate *Tp53*. Together, the actions of these proteins ultimately lead to DNA repair or apoptosis if DNA repair is insufficient (Sulli, Micco, and Fagagna 2012).

Myeloid translocation genes (MTGs) were discovered in acute myeloid leukemia (AML) (Miyoshi et al. 1993). The MTGs—MTG8, MTGR1, and MTG16—serve as scaffold proteins and facilitate the formation of transcriptional repression complexes containing histone deacetylases (HDACs), nuclear receptor co-repressor 1 (NcoR), and mammalian switch-independent 3A (mSin3A) (Amann et al. 2001; Davis, McGhee, and Meyers 2003; Lutterbach et al. 1998; Wang et al. 1998). Because MTGs are unable to bind DNA directly, association with transcription factors such as B-Cell Lymphoma 6 (BCL6), promyelocytic leukemia zinc finger (PLZF), and T-cell factor 4 (TCF4) dictate target specificity (Moore et al. 2008). We have recently shown that MTGs compete with β-catenin for TCF4 occupancy, and MTG binding attenuates TCF4-mediated transcriptional activation (Moore et al. 2008). Given that TCF4 is critical for stem cell renewal in the adult intestine (V. Es et al. 2012), MTGs may regulate key stem cell signaling pathways necessary for homeostasis and injury repair (Davis, McGhee, and Meyers 2003; Moore et al. 2008). In support of this concept, *Mtg16*$^{-/-}$ mice have stress-induced hematopoietic stem cell defects (Chyla et al. 2008), as well as abnormal crypt regeneration in the colon after injury-induced inflammation (Williams et al. 2013). However, the effect of *Mtg16* deletion on small intestine injury responses has yet to be determined.

Given that MTG16 impacts colonic responses to chemically-induced colitis, we hypothesized that MTG16 may alter radiation-induced small intestinal regenerative responses. In the present study, we link MTG16 to epithelial regeneration after radiation-induced injury. At baseline, *Mtg16*$^{-/-}$ mice exhibited decreased goblet cell numbers and higher proliferation. Furthermore, after 12 Gy whole-body radiation, *Mtg16*$^{-/-}$ mice

showed protection from radiation-induced DNA damage and p53 activation. *Ex vivo* culturing of *Mtg16*$^{-/-}$ enteroids revealed increased Wnt responsiveness and delayed maturation. Complementary to *in vivo* findings, *Mtg16*$^{-/-}$ enteroids were more radioresistant than WT counterparts, indicating an epithelial cell-autonomous role for *Mtg16* in radiation-induced epithelial responses. Lastly, examination of a post-irradiation gene expression array dataset indicated that during the proliferative recovery phase, *Mtg16* expression was reduced in stem cell populations.

Methods

Mouse Models

WT (C57BL/6 background) mice were obtained from the Jackson Laboratories. *Mtg16*$^{-/-}$ mice were obtained from S.W. Hiebert (Vanderbilt University) and have been described in detail (Chyla et al. 2008). All experiments were performed with 8 to 12 week old WT and *Mtg16*$^{-/-}$ male and female mice on C57BL/6 background. All *in vivo* experimental procedures were performed under guidelines approved by the Vanderbilt Institutional Animal Care and Use Committee (IACUC).

Gamma Irradiation

WT and *Mtg16*$^{-/-}$ mice were placed in a plexiglass-partitioning device and onto a turntable delivery platform, ensuring uniform radiation dosing of all mice. Mice received 12 Gy whole-body radiation from a Mark I ^{137}Cs source delivered at 1.58 Gy/min. To assess early injury responses, mice were sacrificed four hours after irradiation, a time

known in WT mice to be associated with maximal induction of p53-mediated apoptosis (Leibowitz et al. 2011).

To assess regenerative response, WT and *Mtg16*$^{-/-}$ mice were dosed with 12 Gy irradiation as described above. Ninety-three hours after irradiation, mice were injected with 0.02 mg/kg of vincristine sulfate (Sigma-Aldrich, St. Louis, MO) to arrest cells in metaphase, facilitating identification of crypt cells entering mitosis over the three-hour period between administration and tissue harvest (Alferez and Goodlad 2007; Ottewell et al. 2006). Mice were euthanized three hours later **(Figure 55A)** at the ninety-six hour time point. The ninety-six hour post-irradiation time point was chosen as it is a time point of crypt regeneration (Lund 2012; Potten et al. 1995; Tian et al. 2011).

Immunohistochemistry and Immunofluorescence

Baseline Characterization

Following sacrifice, small intestines were removed, rinsed with Phosphate Buffered Saline (PBS), and Swiss-rolled for histological examination. The tissues were fixed in 10% formalin overnight and transferred to 70% ethanol. Tissues were submitted to the Vanderbilt University Translational Pathology Shared Resource (TPSR) core for processing and paraffin-embedding. Five micron sections were cut for histology. The distal one-third of small intestinal sections from WT and *Mtg16*$^{-/-}$ mice was evaluated for crypt morphology, crypt depth, villus height, and biomarkers of proliferation and secretory lineages. Goblet cells were identified by Periodic Acid-Schiff (PAS) staining. Enteroendocrine cells (EECs) were assessed by Chromogranin A (CgA) staining using anti-CgA (ImmunoStar Inc., Hudson, WI) at 1:1000 dilution. Paneth cells were identified

using anti-lysozyme antibody (Dako, Carpentaria, CA) at 1:500 dilution. Proliferation was measured using anti-phospho-Histone H3 (pH3) Ser10 antibody (Millipore/Upstate Bedford, MA) that labels cells in the mitotic (M) phase of the cell cycle at 1:150 dilution. Vectastain Elite ABC Kit (Vector Laboratories, Burlingame, CA) was used for secondary antibody and visualization.

Four Hours Post-Irradiation Analyses

Small intestines were harvested 4 hours post-irradiation and ~3-4 cm segments of the distal small intestine were excised and further dissected prior to snap freezing in liquid nitrogen for use in subsequent flow cytometric analysis (Chaturvedi et al. 2011, 2014). The remaining section of the distal small intestine was Swiss-rolled, fixed and submitted to the Vanderbilt TPSR core for processing and sectioning. For phospho-Histone H2A.X immunofluorescence, antigen retrieval was performed by using 500mL of 1M sodium citrate buffer (pH=6.0). Slides were placed in a pressure cooker and heated for 15 minutes on high pressure. Slides were then rinsed with deionized H_2O to remove excess citrate buffer. Tissue sections were permeabilized by adding 50μL of 0.1% Tween 20 to each section and allowed to incubate for 30 minutes in a covered chamber. Slides were washed twice to remove permeabilization buffer. Tissue sections were blocked in 5% goat serum in Tris-Buffered Saline (TBS). Anti-phospho-Histone H2A.X (Ser139) from Millipore (EMD Millipore, Billerica, MA) was used at 1:100 dilution and slides incubated overnight at 4°C. Isotype-matched antibodies were included as negative controls. Sections were then washed in 1X PBS and incubated for one hour at room temperature in Alexa Fluor 488 goat anti-mouse-IgG (Invitrogen, Grand Island, NY) at

1:100 dilution. Slides were counterstained and mounted with ProLong Gold Antifade with 4′,6-diamidino-2-phenylindole (DAPI, Invitrogen, Grand Island, NY).

Ninety-Six Hours Post-Irradiation Analyses

At 96 hours post-irradiation, small intestines were harvested and Swiss-rolled as described above. Crypt regeneration was assessed by examination of H&E stained sections for the number of mitotic figures present per crypt in the distal one-third of the small intestine.

Flow Cytometric Analysis of Epithelial Cell Isolates

Flow cytometric analysis of epithelial cell isolates including both crypt and villus populations was performed as previously described (Chaturvedi et al. 2011). Frozen tissue segments were thawed in calcium and magnesium free 1X Dulbecco's Phosphate Buffered Saline (DPBS). DPBS was decanted and samples were resuspended in cold Hanks' Balanced Salt Solution (HBSS) containing 3mM ethylenediaminetetraacetic acid (EDTA) and dithiothreitol (DTT) for 1 hour with gentle shaking every 15 minutes. HBSS/EDTA/DTT solution was decanted and epithelial cells from crypts and villi were resuspended three times in 25mL of 1X DPBS. After each resuspension, conical tubes were shaken vigorously for a minimum of 30 seconds. The cell suspension was passed through a 70-µm cell strainer to remove clumps. Epithelial cells were pelleted, centrifuged at 1500 rpm for 10 min, and resuspended in 1 mL of 1X DPBS. Cells were manually counted using a hemocytometer. $1x10^6$ cells were resuspended in 1 mL of 37% formaldehyde (Ted Pella Inc., Redding, CA) diluted to a final concentration of 4% and

incubated at room temperature for 10 minutes. Epithelial cell isolates were stained according to manufacturer's instructions for expression of the following antibodies: Biotinylated E-cadherin (ABCAM, Cambridge, MA) and Streptavidin-Peridinin chlorophyll protein (PerCP)-Cy5.5 tagged antibody (BD Bioscience, San Jose, CA) were used to identify epithelial cells. Phospho-Histone H2A.X (Ser139) PE conjugated antibody (Cell Signaling, USA, MA) was used to identify DNA damage in epithelial cells. p53 antibody conjugated to Alexa Fluor 488 (Cell Signaling, Danvers, MA) was used as a marker to detect p53 induction since this is a critical mediator of radiation-induced apoptosis or DNA repair. All cells were analyzed by flow cytometry on a Becton Dickinson LSR II and first gated for E-cadherin expression. At least 10,000 events were collected. The percentage of epithelial cells positive for phospho-Histone H2A.X or p53 was calculated using FlowJo software (TreeStar Inc., Ashland, OR).

Apoptosis Assays

Apoptosis in epithelial cell isolates was quantified using the Cell Death Detection ELISA^{PLUS} kit (Roche Applied Sciences, Indianapolis, IN) following the manufacturer's protocol. TUNEL staining on tissue sections was conducted with ApopTag Plus Peroxidase *In Situ* Apoptosis Detection Kit (EMD Millipore, Billerica, MA) according to the manufacturer's protocol. Control stains were obtained by omitting the terminal deoxynucleotide transferase (TdT) enzyme. Crypt apoptotic indices were generated by averaging the number of apoptotic cells in 40 sequential, well-aligned crypts per mouse in the distal one-third of the small intestine. This is presented as the mean number of TUNEL^{+} cells per crypt in each animal.

Enteroid Cultures

The crypt-enteroid culture method was modified from Sato et al (Mahe et al. 2013; Sato et al. 2009). Briefly, mouse proximal small intestine (~10 cm) was excised, opened longitudinally, and washed with ice-cold 1X DPBS. The intestine was cut into small pieces and incubated in ice-cold 1X DPBS containing 1mM EDTA on a rocking platform for 30 minutes. After being rinsed once with ice-cold PBS to remove EDTA, the intestinal fragments were resuspended 3 times by gentle shaking in 5mL of ice-cold 1X DPBS. After each resuspension, supernatant was collected and passed through a 70-μm cell strainer (Fisher Scientific, USA, MA) to remove villus fragments. The cell strainer was cleared using 5mL of dissociation buffer. 400 crypts were resuspended in Matrigel (BD Bioscience) containing growth factors all obtained from R&D Systems (R&D Systems, Minneapolis, MN): 50ng/mL EGF, 100ng/mL Noggin, and 500ng/mL R-spondin (ENR media) or 100ng/mL Wnt3A+ENR (WENR media). Neither media nor growth factors were replaced throughout the course of the experiment. Plating efficiencies were calculated by dividing the total number of enterospheres formed by the original number of crypts plated at Day 0 and multiplying by 100. Enterospheres were visualized and counted at 24, 48, and 72 hours after plating. Experiments were performed in duplicate and repeated three times.

Statistical Analysis

Statistical analysis and graphs were generated using GraphPad Prism 6.0. All data are represented as the standard deviation, unless stated otherwise. Student *t*-test was performed to compare two groups. One-way analysis of variance with Tukey's multiple

comparison tests was performed to compare more than two groups. A $P<0.05$ was considered statistically significant.

Results

MTG16 regulates crypt proliferation and goblet cell numbers in vivo

Previous studies have demonstrated that MTGs regulate lineage specification and proliferation in a number of tissues (Chyla et al. 2008; Lindberg et al. 2005) hematopoiesis; (Williams et al. 2013) colon). In the small intestine, *Mtgr1* knockout mice exhibited defects in secretory lineage allocation (Amann et al. 2005), while loss of *Mtg16* has been reported to promote colonocyte proliferation and exacerbate colonic response to injury (Williams et al. 2013). The role of MTG16 in small intestinal biology is unknown. To define whether MTG16 deletion alters morphology, proliferation, or secretory cell lineage allocation in the small intestine, we performed a histological characterization of *Mtg16*$^{-/-}$ mice. *Mtg16*$^{-/-}$ mice had normal crypt architecture with both villus height and crypt depth being comparable to WT mice **(Figure 52A)**. In contrast, pH3^{+} cells/crypt-villus unit were increased in *Mtg16*$^{-/-}$ intestine **(Figure 52B)**, indicating increased enterocyte proliferation. There were no significant differences in numbers of enteroendocrine or Paneth cells **(Figure 52C)**. However, PAS-labeled goblet cells per crypt villus unit were significantly reduced in *Mtg16*$^{-/-}$ mice **(Figure 52C)**. Thus, MTG16 regulates proliferation in the small intestinal crypts and is required for efficient goblet cell production.

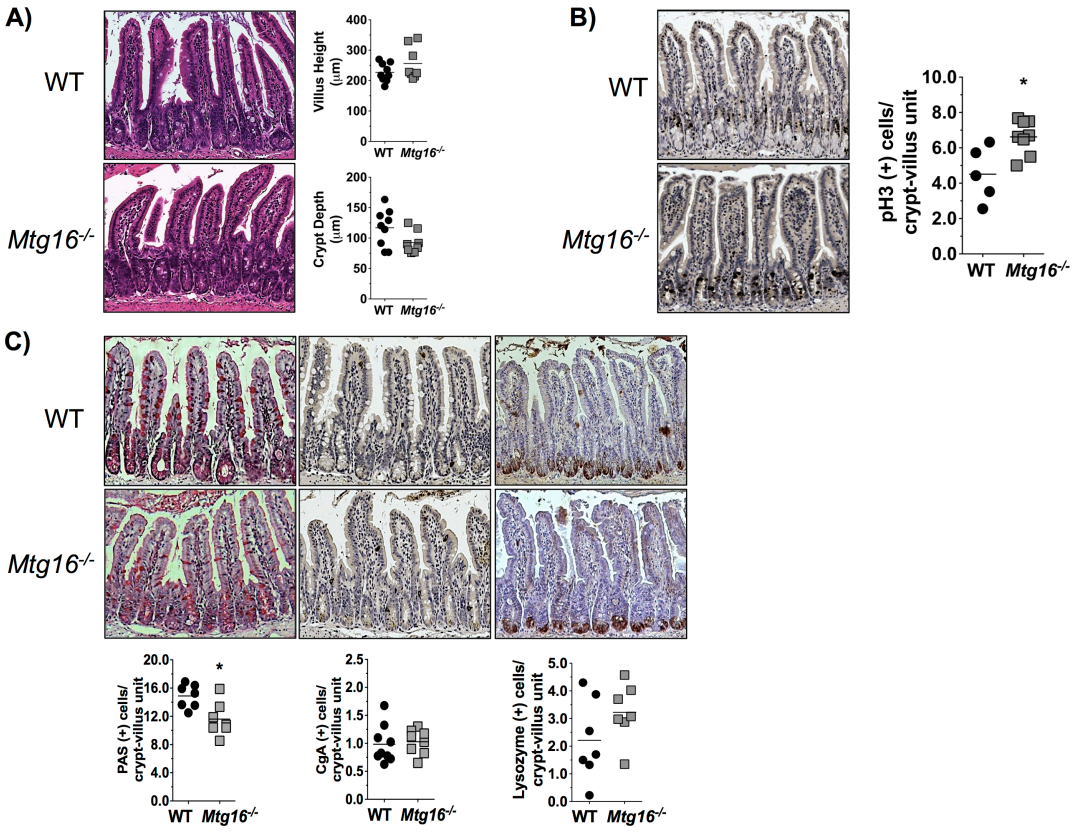

Figure 52. MTG16 regulates epithelial progenitor cell lineage allocation and proliferation. Small intestines were isolated and Swiss-rolled. (A) Representative H&E demonstrating normal crypt morphology in WT and *Mtg16*$^{-/-}$ small intestine. Measurement of villus height and crypt depth of 100 crypts from the distal small intestine demonstrating no differences between *Mtg16*$^{-/-}$ and WT mice (n=17 mice). (B) pH3^{+} cells demonstrate increased proliferation in *Mtg16*$^{-/-}$ small intestine (n=5) when compared to WT (n=8, **P*=0.01). (C) (i) Period Acid Schiff (PAS) stain demonstrated reduced number of goblet cells in *Mtg16*$^{-/-}$ small intestine when compared to WT (n=7 each, **P*<0.05). (ii) Chromogranin A (CgA) staining demonstrated no difference in the number of enteroendocrine cells between *Mtg16*$^{-/-}$ (n=8) and WT (n=9, *P*=0.75). (iii) Lysozyme staining demonstrated no differences in number of Paneth cells between WT and *Mtg16*$^{-/-}$ mice (n=7 in each group, *P*=0.16). All images were captured at 10x magnification.

MTG16 is critical for radiation-induced DNA damage response

To assess intestinal injury responses, WT and *Mtg16*$^{-/-}$ mice were exposed to 12 Gy of ionizing radiation. DNA damage and apoptosis were quantified 4 hours post-irradiation **(Figure 53A)**, the peak time for detection of p53-induced apoptosis in the small intestine in response to irradiation (Leibowitz et al. 2011). Flow cytometric analysis for phospho-histone H2A.X on epithelial isolates from irradiated WT and *Mtg16*$^{-/-}$ mice revealed significantly decreased levels in *Mtg16*$^{-/-}$ intestine when compared to WT **(Figure 53B)**. This was confirmed by immunofluorescence staining of WT and *Mtg16*$^{-/-}$ intestine for phospho-Histone H2A.X **(Figure 53C)**.

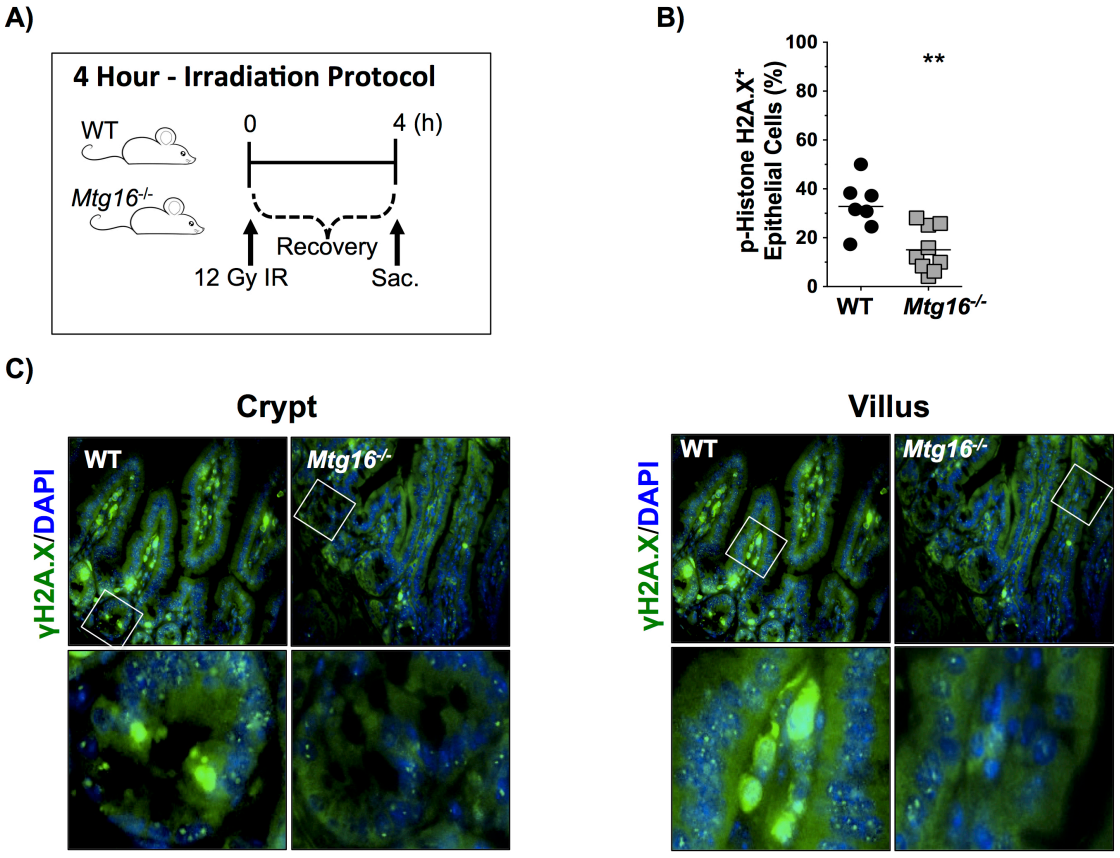

Figure 53. MTG16 is required for proper response to radiation-induced DNA damage. (A) Schematic of 4-hour irradiation protocol. (B) Detection of phospho-Histone H2A.X by flow cytometry in epithelial cells isolated from WT (n=7) and *Mtg16*$^{-/-}$ (n=9)

mice (**P=0.003). (C) Top panels: Representative immunofluorescent staining of WT and *Mtg16*$^{-/-}$ small intestine for phospho-γH2A.X with DAPI 4 hours after 12 Gy irradiation (10x magnification). The areas in white boxes are shown at higher magnification (40x magnification) in the bottom panels.

In addition, while analysis of p53 positive epithelial cells by flow cytometry revealed no significant differences between the cohorts **(Figure 54A)**, analysis of phospho-Histone H2A.X/p53 double positive epithelial cells indicated a significant reduction in the percentage of double positive cells in epithelial isolates from *Mtg16*$^{-/-}$ mice at 4 hours post-irradiation **(Figure 54B)**. Further, apoptosis assessed by cell death ELISA was also reduced in *Mtg16*$^{-/-}$ intestine **(Figure 54C)**. Taken together, these data suggest that *Mtg16* deletion protects from injury via decreased triggering of apoptosis after radiation-induced injury.

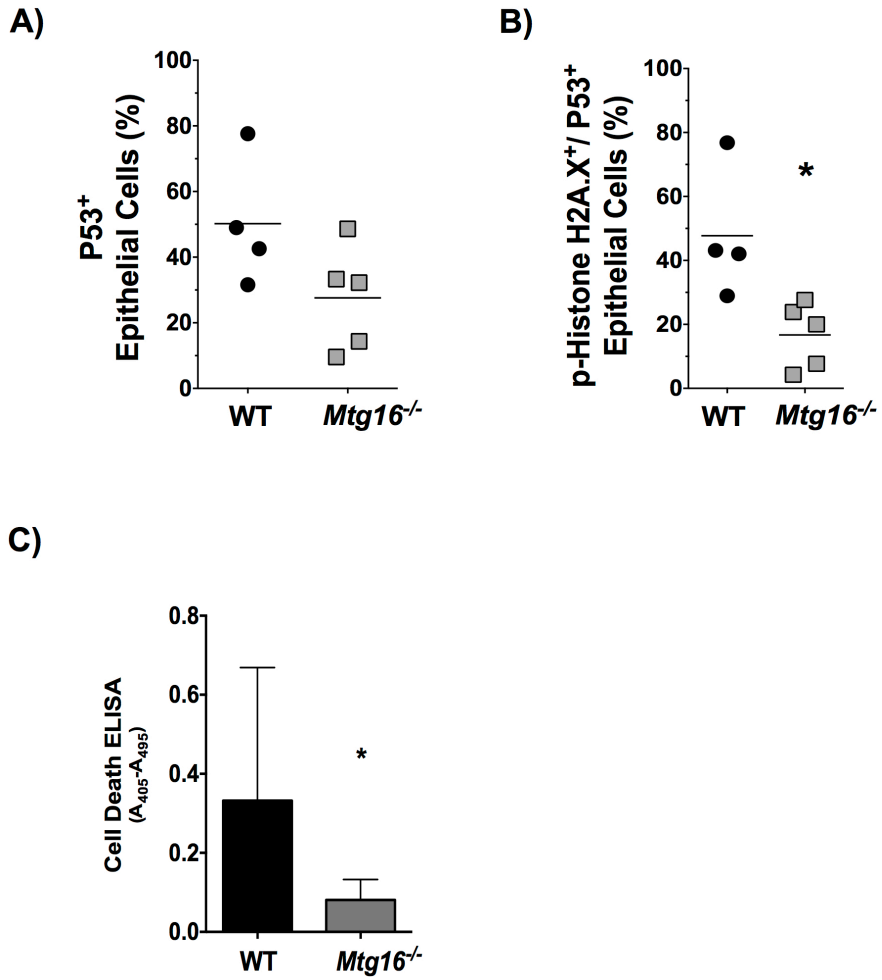

Figure 54. **MTG16 is critical for p53-mediated apoptosis.** (A) Flow cytometry detection of P53 in epithelial isolates from irradiated WT (n=4) and *Mtg16*$^{-/-}$ (n=5) mice (B) Flow cytometry detection of phospho-Histone H2A.X and P53 in epithelial isolates from irradiated WT (n=4) and *Mtg16*$^{-/-}$ (n=5) mice (**P*=0.02). (C) Apoptosis was measured by Cell Death ELISA (**P*=0.03, n=10 in each group).

MTG16 loss promotes crypt regeneration

Since we observed decreases in DNA damage and apoptosis, we postulated that MTG16 would impact crypt regenerative dynamics in response to ionizing radiation (Barker, van de Wetering, and Clevers 2008; Leibowitz et al. 2011; Martin et al. 1998; Ottewell et al. 2006). Therefore, we exposed WT and *Mtg16*$^{-/-}$ mice to 12 Gy irradiation

followed by a 93-hour recovery period **(Figure 55A)**. Three hours prior to sacrifice, mice were injected with vincristine, a mitotic inhibitor, facilitating identification of regenerative crypts. At the 96-hour time point, proliferation of stem cells leads to crypt regeneration (Van Landeghem et al. 2012; Martin et al. 1998; Potten and Chadwick 1994; Potten et al. 1995). *Mtg16*$^{-/-}$ mice had 20% increased crypt viability in comparison to WT mice **(Figure 55B)** with a concurrent reduction in TUNEL positive intestinal epithelial cells **(Figure 55C)**. Taken together, these data indicate that the absence of MTG16 protects the epithelium from radiation-induced apoptosis during the regenerative phase, as well.

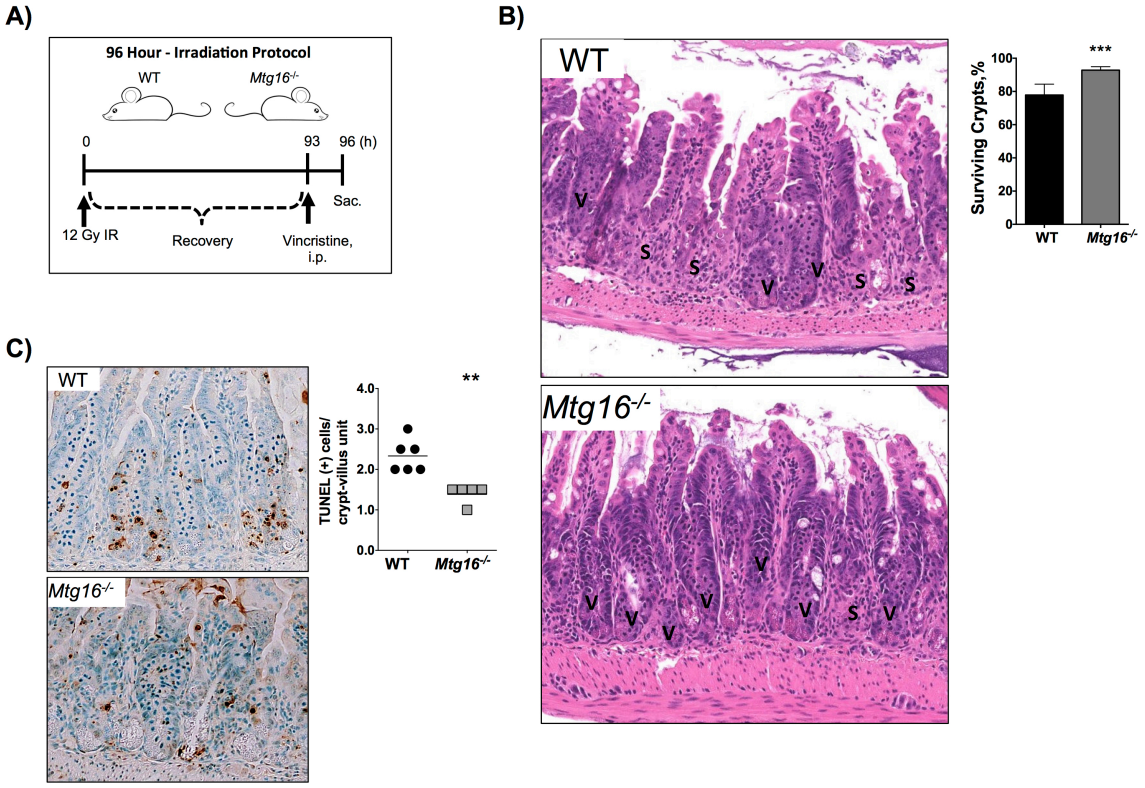

Figure 55. *Mtg16*$^{-/-}$ mice are protected from radiation-induced injury. (A) Schematic diagram of 96-hour irradiation protocol. (B) Representative H&E demonstrating small intestinal crypt survival in WT and *Mtg16*$^{-/-}$ mice. The letter "**V**" denotes viable crypts and the letter "**S**" denotes sterile crypts. *Mtg16*$^{-/-}$ (n=8) mice have a higher percentage of

surviving crypts than WT (n=6) (***P=0.0002). Crypts were considered viable if 3 or more mitotic bodies were observed per crypt. 40 sequential, well-aligned crypts in the distal one-third of the small intestine were counted per data point. The percent of surviving crypts was calculated using the following equation: (# of viable crypts/total # of crypts counted) x 100. (C) TUNEL staining demonstrated a reduction in the number of TUNEL$^+$ cells in *Mtg16*$^{-/-}$ (n=6) vs. WT (n=5) (**P=0.001). All images were captured at 10x magnification.

MTG16 impacts stem cell growth, maturation and Wnt3A response

To investigate the mechanisms by which MTG16 might contribute to stem cell survival we examined growth patterns of three-dimensional enteroid cultures of crypts isolated from WT and *Mtg16*$^{-/-}$ mice. Specifically, we calculated the enterosphere forming efficiency. We considered enterospheres to be "spherical structures composed of several small intestinal epithelial cells that appear as a rounded-off epithelial cysts" when evaluated 24 hours post-plating (Stelzner et al. 2012). There were no differences in plating efficiencies between the two groups when cultured in Matrigel containing EGF, Noggin, and R-spondin (ENR) **(Figure 56A)**. Because MTG16 is a negative regulator of Wnt signaling, as it can competitively bind to TCF4 and oppose β-catenin-dependent transcriptional activation (Moore et al. 2008), we postulated that *Mtg16*$^{-/-}$ enteroids may be hyper-responsive to Wnt activation. Therefore we added Wnt3A+ENR (WENR) to the Matrigel and plated freshly isolated crypts. In WENR supplemented crypt cultures, there was a 50% higher plating efficiency of *Mtg16*$^{-/-}$ crypts **(Figure 56B)**. Interestingly, *Mtg16*$^{-/-}$ enteroids also showed reduced progression to budding enteroids compared to WT enteroids at 72 hours post-plating **(Figure 56C)**. These observations suggest that

MTG16 affects stem cell growth and maturation in a Wnt-dependent manner, such that loss of *Mtg16* promotes increases in Wnt responsiveness.

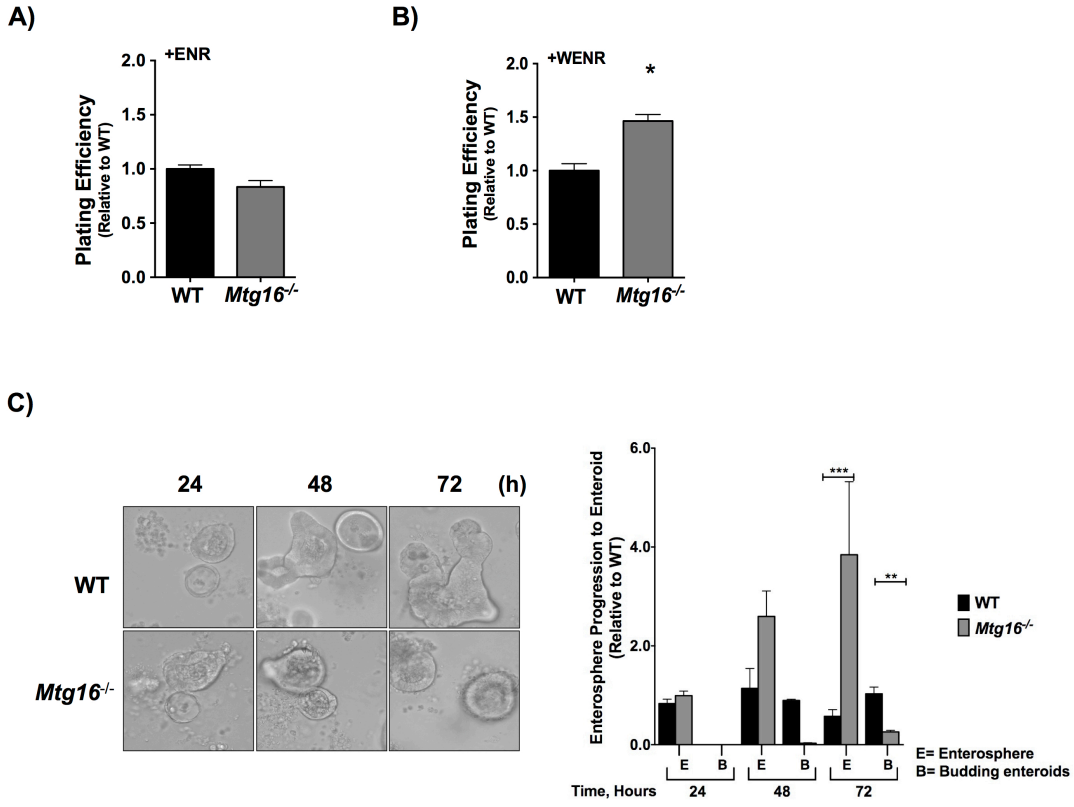

Figure 56. MTG16 regulates enteroid growth and Wnt3A response. Small intestinal crypts were isolated from WT or *Mtg16*$^{-/-}$ mice and plated at 400 crypts/well for all experiments. **(**A) Plating efficiency was calculated for crypts embedded in Matrigel containing EGF, Noggin and R-spondin (ENR). There was no significant difference in plating efficiency between *Mtg16*$^{-/-}$ and WT intestinal crypts (*P*=0.14). Plating efficiency was calculated using the following equation: (Total # of crypts that formed enterospheres at 24 hours /total # of crypts plated at 0 hours). (B) Plating efficiency was calculated for crypts embedded in Matrigel containing Wnt3A+ENR (WENR). *Mtg16*$^{-/-}$ enteroids exhibited higher plating efficiency than WT Enteroids (**P*=0.03) (C) (i) Enteroid morphology at 24, 48, and 72 hours (10x magnification). (ii) *Mtg16*$^{-/-}$ enteroids exhibited delayed enterosphere progression to budding enteroids at 72 hours (Enterosphere: ****P*<0.0001; Budding Enteroids: ***P*<0.001) E= enterosphere and B= budding enteroid. Experiments were performed in duplicate and repeated three times.

MTG16 modulates intestinal stem cell regenerative response after irradiation

Because increased crypt regeneration was observed *in vivo* after irradiation of *Mtg16*$^{-/-}$ mice, we hypothesized that *Mtg16*$^{-/-}$ enteroid plating efficiency, a surrogate marker for stem cell survival or growth, would be similarly impacted. To test this, mice were dosed with 12 Gy radiation and crypts were isolated and plated in Matrigel containing ENR 4 hours later. We observed a 70% increase plating efficiency in *Mtg16*$^{-/-}$ enteroids 24 hours after plating **(Figure 57A)**.

Given that specific gene expression programs are modified after intestinal injury and during regenerative phases, we sought to determine if *Mtg16* was regulated in response to radiation-induced injury. Using a well-characterized *Sox9* transgenic model (Gracz, Ramalingam, and Magness 2010; Van Landeghem et al. 2012), we assessed *Mtg16* RNA levels in different populations of Sox9-EGFP sorted cells. Prior studies have demonstrated that *Sox9*, a Wnt target gene, is a marker for self-renewing small intestinal epithelial stem cells (Formeister et al. 2009; Furuyama et al. 2011; Gracz, Ramalingam, and Magness 2010). Studies using Sox9-EGFP reporter mice have demonstrated that FACS for different levels of Sox9-EGFP expression yields Sox9-EGFP^{Negative} cells enriched for enterocyte markers, Sox9-EGFP^{Sublow} cells enriched for progenitors, Sox9-EGFP^{Low} cells enriched for Lgr5^{+} and other intestinal stem cell markers, and Sox9-EGFP^{High} cells enriched for enteroendocrine cells (Van Landeghem et al. 2012). In the present study, qRT-PCR on these populations for *Mtg16* indicated no significant difference in *Mtg16* levels across populations; however, after irradiation, *Mtg16* was specifically downregulated in the Sox9-EGFP^{Low} stem cell-enriched compartment and

increased in the Sox9-EGFP^{Negative} cells **(Figure 57B)**. Thus, these data suggest that MTG16 levels are regulated during the regenerative phase after radiation-induced injury.

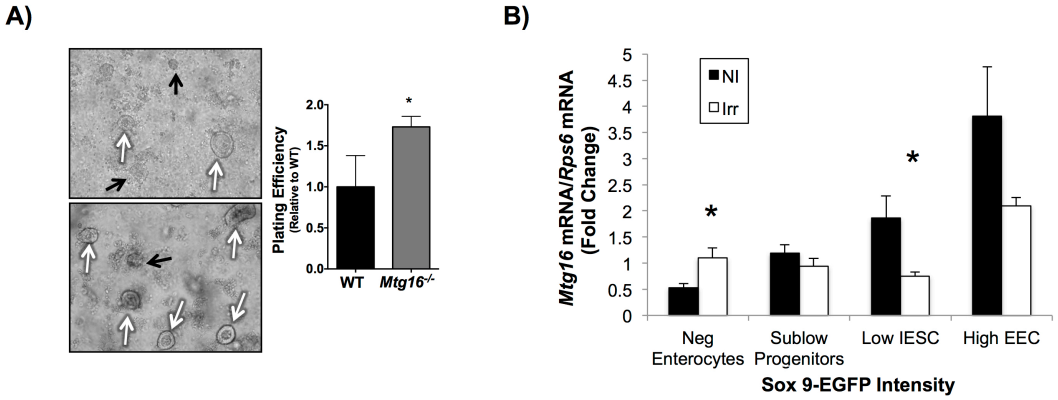

Figure 57. MTG16 decreases stem cell regenerative response after radiation-induced injury. (A) Plating efficiency of intestinal crypts isolated from WT and *Mtg16*$^{-/-}$ mice dosed with 12 Gy irradiation. Higher plating efficiencies were observed in crypts isolated from *Mtg16*$^{-/-}$ mice when compared to crypt isolation from WT mice (**P*=0.01) (White arrows indicate live and black arrows indicate dead enterospheres, 10x magnification). Experiments were performed in duplicate and repeated three times. (B) Quantitative PCR of *Mtg16* expression in Sox9-EGFP^{Negative}, Sox9-EGFP^{Sublow}, Sox9-EGFP^{Low}, and Sox9-EGFP^{High} cells from the intestines of both nonirradiated and irradiated mice. No significant differences were observed in *Mtg16* mRNA levels across populations. *Mtg16* mRNA expression is lower in intestinal epithelial stem cell (IESC) enriched Sox9-EGFP^{Low} and higher in terminally differentiated Sox9-EGFP^{Negative} cells 5 days post-irradiation (IESCs: **P*<0.05 and Enterocytes: **P*<0.05, n=5 per group). Black bars represent non-irradiated (NI) and white bars represents irradiated (Irr).

Discussion

The goal of the present study was to investigate the role of MTG16 in the small intestine by examining the effect of *Mtg16* deletion on baseline mucosal homeostasis and response to injury after ionizing radiation. At baseline, *Mtg16*$^{-/-}$ mice demonstrate higher

intestinal proliferation and altered lineage allocation. *Mtg16*$^{-/-}$ enteroids were hyper-responsive to Wnt activation and exhibited delayed progression to mature enteroids, suggesting altered stem cell activity in the *Mtg16*$^{-/-}$ intestine. After irradiation, *Mtg16*$^{-/-}$ mice were protected from DNA damage and had decreased p53 activation. Additionally, *Mtg16*$^{-/-}$ crypts isolated from mice at 4 hours after 12 Gy radiation had increased plating efficiency, indicating an epithelial cell-autonomous role for MTG16 in protecting crypt stem cells. Lastly, examination of *Mtg16* expression in isolated stem cells at the time of crypt regeneration demonstrated that *Mtg16* expression was reduced in stem cell populations.

Despite an increase in proliferation in the *Mtg16*$^{-/-}$ mice, we did not observe a difference in gross morphology or morphometry. There are multiple factors that influence crypt morphometry, with apoptosis and proliferation each partially contributing to overall crypt depth or villus height. We suspect that the rather subtle, but significant increase in proliferation may be insufficient to influence mucosal morphometry in the *Mtg16*$^{-/-}$ mice. *Mtg16*$^{-/-}$ mice exhibit hematopoietic lineage allocation defects with skewing of early myeloid progenitor cells toward granulocytic/macrophage lineages and a reduction in megakaryocyte-erythroid progenitor cells (Chyla et al. 2008). We report that these lineage allocation differences are not limited to hematopoiesis, as *Mtg16*$^{-/-}$ small intestine also has decreased goblet cell numbers. While the functional role of goblet cells in radiation injury is unclear (Becciolini and Fabbrica 1985; van Dongen, Kooyman, and Visser 1976; Kanter and Akpolat 2008), it is possible that decreased goblet cells in *Mtg16*$^{-/-}$ mice might impact crypt viability after radiation injury.

While we report higher crypt viability after radiation than what others have previously reported (Ottewell et al. 2006), we believe that differences in technique may account for this apparent discrepancy. With a Swiss-rolling technique and examination of 40 sequential, well-aligned crypts in the distal one-third of the small intestine at this time point and radiation dose, we reproducibly observe crypt viability in the 60-80% range in WT mice. We observed significantly higher crypt viability in the *Mtg16*$^{-/-}$ mice, suggesting either greater viability and survival post-irradiation or faster crypt regeneration. Other methods of assessment, such as evaluating cross-sections of small intestine often score lower indices of viability (Ottewell et al. 2006). Given our experimental design, we may also have higher crypt viability indices because regeneration occurs at 96 hours post-radiation, and it is possible that dead crypts may have already been cleared by this point and thus, would not be factored into our assessment.

While decreased phosphorylation of H2A.X in the *Mtg16*$^{-/-}$ mice suggests accelerated repair and decreased DNA damage in this cohort, an alternative consideration is that MTG16 regulates the phosphorylation of H2A.X in response to irradiation and triggers activation of DNA repair machinery. Thus *Mtg16* deletion may result in a failure to recognize damage after radiation due to compromised phosphorylation of H2A.X, and *Mtg16*$^{-/-}$ mice may suffer DNA damage and have defective initiation of repair mechanisms. Another important consideration for these studies is that while *Mtg16*$^{-/-}$ mice exhibit decreased apoptosis after radiation compared to WT mice, there is a possibility that intestinal cells that escape apoptosis may later undergo mitotic catastrophe, an indication of failed DNA repair. This phenomenon has been observed in *p53*$^{-/-}$ mice

(Gudkov and Komarova 2003). We did not test this as *Mtg16*$^{-/-}$ mice do not survive, secondary to marrow failure, even at lower doses of radiation. This experiment may be performed when *Mtg16* floxed mice become available.

After irradiation, and at time of crypt regeneration, *Mtg16* expression is reduced in Sox9-EGFP^{Low} stem cell-enriched compartments. Microarray analysis of Sox9-EGFP^{Low} stem cell has shown that genes involved in differentiation, crypt repair, and radiation-induced apoptosis are repressed in Sox9-EGFP^{Low} cells (Van Landeghem et al. 2012). Given this evidence, we postulate that lower MTG16 levels may permit activation of stem cell programs promoting epithelial reconstitution. We also observed that *Mtg16* expression is increased in Sox9-EGFP^{Negative} populations. As previously reported by Landeghem et al, Sox9-EGFP^{Negative} cells are enriched for differentiated lineages. Thus, MTG16 might repress stem cell programs and allow differentiation to progress after injury in this population of cells.

The Wnt signaling pathway plays an important role in regulating intestinal epithelial stem cell function (Fevr et al. 2007; Gregorieff and Clevers 2005; Pinto et al. 2003). We have previously shown that MTG16 competes with β-catenin for TCF4 occupancy and that the absence of MTG16 results in increased epithelial proliferation (Davis, McGhee, and Meyers 2003; Moore et al. 2008). In support of enhanced TCF4 activity in response to Wnt, baseline characterization of *Mtg16*$^{-/-}$ crypts in the enteroid culture system showed increased plating efficiency and delayed maturation in the presence of Wnt3A. Furthermore, several lines of evidence support a role for WNT/β-catenin signaling in survival of stem/progenitor cell populations after radiation (Kim et al. 2012; Woodward et al. 2007). *Ex vivo* studies presented here show that enteroids

isolated from irradiated *Mtg16*$^{-/-}$ mice have increased survival in comparison to WT enteroids. Together, these data suggest that MTG16 may be important in modifying survival programs in stem cell populations after radiation.

Our findings indicate that MTG16 is critical for multiple aspects of small intestinal homeostasis and response to injury. Specifically, MTG16 controls goblet cell allocation, enterocyte proliferation, and is important in radiation-induced injury responses. Importantly, because current treatment modalities are aimed at targeting the symptoms of radiation enteritis (Carr and Holden 1986; Schembri, Azzopardi, and Ellul 2014), this study offers promise in understanding the underlying molecular mechanisms that regulate responses to radiation therapy.

REFERENCES

Abraham, Clara, and Judy H Cho. 2009. "Inflammatory Bowel Disease." *The New England Journal of Medicine* 361(21): 2066–78.

Abraham, Clara, and Ruslan Medzhitov. 2011. "Interactions between the Host Innate Immune System and Microbes in Inflammatory Bowel Disease." *Gastroenterology* 140(6): 1729–37.

Acloque, Hervé et al. 2009. "Epithelial-Mesenchymal Transitions : The Importance of Changing Cell State in Development and Disease." *The Journal of Clinical Investigation* 119(6): 1438–49.

Aigner, K et al. 2007. "The Transcription Factor ZEB1 (deltaEF1) Promotes Tumour Cell Dedifferentiation by Repressing Master Regulators of Epithelial Polarity." *Oncogene* 26(49): 6979–88.

Akamatsu, Yoshiko et al. 2003. "Deletion of the RAG2 C Terminus Leads to Impaired Lymphoid Development in Mice." *Proceedings of the National Academy of Sciences of the United States of America* 100(3): 1209–14.

Van Aken, J et al. 1993. "Immunohistochemical Analysis of E-Cadherin Expression in Human Colorectal Tumours." *Pathology, research and practice* 189(9): 975–78.

Al-Taie OH, Uceyler N, Eubner U, Jakob F, Mörk H, Scheurlen M, Brigelius-Flohe R, Schöttker K, Abel J, Thalheimer A, Katzenberger T, Illert B, Melcher R, Köhrle J. 2004. "Expression Profiling and Genetic Alterations of the Selenoproteins GI-GPx and SePP in Colorectal Carcinogenesis." *Nutr Cancer* 48(August 2013): 37–41.

Al-Taie, Oliver H et al. 2002. "A Complex DNA-Repeat Structure within the Selenoprotein P Promoter Contains a Functionally Relevant Polymorphism and Is Genetically Unstable under Conditions of Mismatch Repair Deficiency." *European journal of human genetics : EJHG* 10(9): 499–504.

Alcalay, Yifat et al. 2013. "Popeye Domain Containing 1 (Popdc1/Bves) Is a Caveolae-Associated Protein Involved in Ischemia Tolerance." *PLoS ONE* 8(9): e71100.

Alferez, D, and R A Goodlad. 2007. "To Best Measure Cell Proliferation in Samples from the Intestine." *Cell Proliferation* 40(2): 231–40.

Amann, Joseph M et al. 2001. "ETO , a Target of T (8;21) in Acute Leukemia , Makes Distinct Contacts with Multiple Histone Deacetylases and Binds mSin3A through Its Oligomerization Domain." *Molecular and cellular biology* 21(19): 6470–83.

Amann, Joseph M et al. 2005. "Mtgr1 Is a Transcriptional Corepressor That Is Required for Maintenance of the Secretory Cell Lineage in the Small Intestine." *Molecular and cellular biology*.

Amre, D K et al. 2009. "Interleukin 10 (IL-10) Gene Variants and Susceptibility for Paediatric Onset Crohn's Disease." *Alimentary pharmacology & therapeutics* 29(9): 1025–31.

Andoh, Akira et al. 2005. "Serum Selenoprotein-P Levels in Patients with Inflammatory Bowel Disease." *Nutrition* 21(5): 574–79.

Andrée, B et al. 2000. "Isolation and Characterization of the Novel Popeye Gene Family Expressed in Skeletal Muscle and Heart." *Developmental biology* 223(2): 371–82.

Andrée, Anne Fleige, Hans-henning Arnold, and Thomas Brand. 2002. "Mouse Pop1 Is Required for Muscle Regeneration in Adult Skeletal Muscle." *Molecular and cellular biology* 22(5): 1504–12.

Anjum, Rana, and John Blenis. 2008. "The RSK Family of Kinases: Emerging Roles in Cellular Signalling." *Nature reviews. Molecular cell biology* 9(10): 747–58.

Arrieta, M C, K Madsen, J Doyle, and J Meddings. 2009. "Reducing Small Intestinal Permeability Attenuates Colitis in the IL10 Gene-Deficient Mouse." *Gut* 58(1): 41–48.

Arteel, G E et al. "Protection by Selenoprotein P in Human Plasma against Peroxynitrite-Mediated Oxidation and Nitration." *Biological chemistry* 379(8-9): 1201–5.

Artis, David. 2008. "Epithelial-Cell Recognition of Commensal Bacteria and Maintenance of Immune Homeostasis in the Gut." *Nature reviews. Immunology* 8(6): 411–20.

Balda, M. B. Fallon, C. M. Van Itallie, and J. M. Anderson. 1992. "Structure, Regulation, and Pathophysiology of Tight Junctions in the Gastrointestinal Tract." *Yale Journal of Biology and Medicine* 65(6): 725–35.

Balda, and K Matter. 1998. "Tight Junctions." *Journal of cell science* 111 (Pt 5: 541–47.

Barker, Nick et al. 2007. "Identification of Stem Cells in Small Intestine and Colon by Marker Gene Lgr5." *Nature* 449(7165): 1003–7.

Barker, Nick et al. 2014. "Adult Intestinal Stem Cells: Critical Drivers of Epithelial Homeostasis and Regeneration." *Nature reviews. Molecular cell biology* 15(1): 19–33.

Barker, Nick, Marc van de Wetering, and Hans Clevers. 2008. “The Intestinal Stem Cell.” *Genes & development* 22(14): 1856–64.

Barrett et al. 2011. “MTGR1 Is Required for Tumorigenesis in the Murine AOM/DSS Colitis-Associated Carcinoma Model.” *Cancer research* 71(4): 1302–12.

Barrett et al. 2012. “Tumor Suppressor Function of the Plasma Glutathione Peroxidase Gpx3 in Colitis-Associated Carcinoma.” *Cancer Research* 73(3): 1245–55.

Barrett, Caitlyn W et al. 2013. “Dietary Selenium Deficiency Exacerbates DSS-Induced Epithelial Injury and AOM/DSS-Induced Tumorigenesis.” *PloS one* 8(7): e67845.

Barthold, S W et al. 1976. “The Etiology of Transmissible Murine Colonic Hyperplasia.” *Laboratory animal science* 26(6 Pt 1): 889–94.

Barthold, S W et al. 1978. “Transmissible Murine Colonic Hyperplasia.” *Veterinary pathology* 15(2): 223–36.

Bataille, Frauke, and Christian Rohrmeier. 2008. “Evidence for a Role of Epithelial Mesenchymal Transition during Pathogenesis of Fistulae in Crohn’s Disease.” *Inflammatory bowel diseases* 14(11): 1514–27.

Baumgart, and Simon R Carding. 2007. “Inflammatory Bowel Disease: Cause and Immunobiology.” *The Lancet* 369: 1627–40.

Baumgart, and WJ Sandborn. 2007. “Inflammatory Bowel Disease: Clinical Aspects and Established and Evolving Therapies.” *The Lancet* 369(9573): 1641–57.

Beachy, P, S S Karhadkar, and D M Berman. 2004. “Tissue Repair and Stem Cell Renewal in Carcinogenesis.” *Nature* 432(7015): 324–31.

Becciolini, A, and D Fabbrica. 1985. “Quantitative Changes in the Goblet Cells of the Rat Small Intestine after Irradiation.” *Acta radiologica. Oncology* 24(October 1984).

Becker, C et al. 2005. “In Vivo Imaging of Colitis and Colon Cancer Development in Mice Using High Resolution Chromoendoscopy.” *Gut* 54(7): 950–54.

Becker, C, M C Fantini, and M F Neurath. 2007. “High Resolution Colonoscopy in Live Mice.” *Nature Protocols* 1(6): 2900–2904.

Benjamini, Y et al. 2001. “Controlling the False Discovery Rate in Behavior Genetics Research.” *Behavioural brain research* 125(1-2): 279–84.

Bera, Soumen, Viviana De Rosa, Walid Rachidi, and Alan M. Diamond. 2013. “Does a Role for Selenium in DNA Damage Repair Explain Apparent Controversies in Its Use in Chemoprevention?” *Mutagenesis* 28(2): 127–34.

Bettelli, Estelle et al. 2006. “Reciprocal Developmental Pathways for the Generation of Pathogenic Effector TH17 and Regulatory T Cells.” *Nature* 441(7090): 235–38.

Bjerknes, M, and H Cheng. 1981a. “The Stem-Cell Zone of the Small Intestinal Epithelium. I. Evidence from Paneth Cells in the Adult Mouse.” *The American journal of anatomy* 160(1): 51–63.

Bjerknes, M, and H Cheng. 1981b. “The Stem-Cell Zone of the Small Intestinal Epithelium. III. Evidence from Columnar, Enteroendocrine, and Mucous Cells in the Adult Mouse.” *The American journal of anatomy* 160(1): 77–91.

Booth, C, and C S Potten. 2000. “Gut Instincts: Thoughts on Intestinal Epithelial Stem Cells.” *The Journal of clinical investigation* 105(11): 1493–99.

Borenshtein, Diana, Megan E McBee, and David B Schauer. 2008. “Utility of the Citrobacter Rodentium Infection Model in Laboratory Mice.” *Current opinion in gastroenterology* 24(1): 32–37.

Bosschaerts, Tom et al. 2008. “Associated with African Trypanosomiasis through the IL-10.” *The Journal of Immunology* 180(7): 6168–75.

Brand, Thomas. 2005. “The Popeye Domain-Containing Gene Family.” *Cell biochemistry and biophysics* 43(1): 95–103.

Brigelius-Flohé, Regina, and Anna Patricia Kipp. 2013. 527 Methods in Enzymology *Selenium in the Redox Regulation of the Nrf2 and the Wnt Pathway*. 1st ed. Elsevier Inc.

Brown, Kellie R, and Eva Rzucidlo. 2011. “Acute and Chronic Radiation Injury.” *Journal of Vascular Surgery*: 15–21.

Bruce, W R, and H Van Der Gaag. 1963. “A Quantitative Assay For the Number of Murine Lymphoma Cells Capable of Proliferation in Vivo.” *Nature* 199: 79–80.

Bry, Lynn, and Michael B Brenner. 2004. “Critical Role of T Cell-Dependent Serum Antibody, but Not the Gut-Associated Lymphoid Tissue, for Surviving Acute Mucosal Infection with Citrobacter Rodentium, an Attaching and Effacing Pathogen.” *Journal of immunology (Baltimore, Md. : 1950)* 172(1): 433–41.

Buczacki, Simon J a et al. 2013. “Intestinal Label-Retaining Cells Are Secretory Precursors Expressing Lgr5.” *Nature* 495(7439): 65–69.

Burk, Raymond F, and Kristina E Hill. 2005. “Selenoprotein P: An Extracellular Protein with Unique Physical Characteristics and a Role in Selenium Homeostasis.” *Annual review of nutrition* 25: 215–35.

Burk, Raymond F. et al. 2006. “Deletion of Selenoprotein P Upregulates Urinary Selenium Excretion and Depresses Whole-Body Selenium Content.” *Biochimica et Biophysica Acta - General Subjects* 1760(12): 1789–93.

Burk, Raymond F. et al. 2008. “Selenium Deficiency Activates Mouse Liver Nrf2-ARE but Vitamin E Deficiency Does Not.” *Free Radical Biology and Medicine* 44(8): 1617–23.

Carlson, Bradley a et al. 2009. “Selenoproteins Regulate Macrophage Invasiveness and Extracellular Matrix-Related Gene Expression.” *BMC immunology* 10: 57.

Carlson, Bradley a et al. 2010. “Role of Selenium-Containing Proteins in T-Cell and Macrophage Function.” *The Proceedings of the Nutrition Society* 69(3): 300–310.

Carr, N D, and D Holden. 1986. “Pathogenesis and Treatment of Radiation Bowel Disease: Discussion Paper.” *Journal of the Royal Society of Medicine*: 1–4.

Cetin, Selma et al. 2004. “Endotoxin Inhibits Intestinal Epithelial Restitution through Activation of Rho-GTPase and Increased Focal Adhesions.” *The Journal of biological chemistry* 279(23): 24592–600.

Chang, Liang-Che et al. 2013. “Immunohistochemical Study of the Nrf2 Pathway in Colorectal Cancer: Nrf2 Expression Is Closely Correlated to Keap1 in the Tumor and Bach1 in the Normal Tissue.” *Applied immunohistochemistry & molecular morphology : AIMM / official publication of the Society for Applied Immunohistochemistry* 21(6): 511–17.

Chang, Ti Ling et al. 2010. “Claudin-1 Has Tumor Suppressive Activity and Is a Direct Target of RUNX3 in Gastric Epithelial Cells.” *Gastroenterology* 138(1): 255–65.

Chaturvedi, Rupesh et al. 2011. “Spermine Oxidase Mediates the Gastric Cancer Risk Associated with Helicobacter Pylori CagA.” *Gastroenterology* 141(5): 1696–1708.

Chaturvedi, Rupesh et al. 2014. “Activation of EGFR and ERBB2 by Helicobacter Pylori Results in Survival of Gastric Epithelial Cells with DNA Damage.” *Gastroenterology* 146(7): 1739–51.e14.

Cheng, H, and C P Leblond. 1974a. “Origin, Differentiation and Renewal of the Four Main Epithelial Cell Types in the Mouse Small Intestine. I. Columnar Cell.” *The American journal of anatomy* 141(4): 461–79.

Cheng, H, and C P Leblond. 1974b. “Origin, Differentiation and Renewal of the Four Main Epithelial Cell Types in the Mouse Small Intestine. V. Unitarian Theory of the Origin of the Four Epithelial Cell Types.” *The American journal of anatomy* 141(4): 537–61.

Chung, Yeonseok et al. 2009. “Critical Regulation of Early Th17 Cell Differentiation by Interleukin-1 Signaling.” *Immunity* 30(4): 576–87.

Chyla, Brenda J et al. 2008. “Deletion of Mtg16, a Target of t(16;21), Alters Hematopoietic Progenitor Cell Proliferation and Lineage Allocation.” *Molecular and cellular biology* 28(20): 6234–47.

Clevers, Hans. 2004. “At the Crossroads of Inflammation and Cancer.” *Cell* 118(6): 671–74.

Clevers, Hans. 2013. “The Intestinal Crypt, a Prototype Stem Cell Compartment.” *Cell* 154(2): 274–84.

Clevers, Hans, and Roel Nusse. 2012. “Wnt/β-Catenin Signaling and Disease.” *Cell* 149(6): 1192–1205.

Coburn, Lori a. et al. 2013. “High-Throughput Multi-Analyte Luminex Profiling Implicates Eotaxin-1 in Ulcerative Colitis.” *PLoS ONE* 8(12).

Connelly-Frost, Alexandra et al. 2009. “Selenium, Folate, and Colon Cancer.” *Nutrition and cancer* 61(2): 165–78.

Cooper, Matthew L et al. 2008. “Interaction between Single Nucleotide Polymorphisms in Selenoprotein P and Mitochondrial Superoxide Dismutase Determines Prostate Cancer Risk.” *Cancer research* 68(24): 10171–77.

Davis, J.Nathan, Laura McGhee, and Shari Meyers. 2003. “The ETO (MTG8) Gene Family.” *Gene* 303: 1–10.

Debruyne, Delphine et al. 2006. “Colon Cancer Cells: Pro-Invasive Signalling.” *The International Journal of Biochemistry & Cell Biology* 38(8): 1231–36.

Dhawan, Punita et al. 2005. “Claudin-1 Regulates Cellular Transformation and Metastatic Behavior in Colon Cancer.” *The Journal of Clinical Investigation* 115(7): 1765–76.

Dieleman, L a et al. 1998. “Chronic Experimental Colitis Induced by Dextran Sulphate Sodium (DSS) Is Characterized by Th1 and Th2 Cytokines.” *Clinical and experimental immunology* 114(3): 385–91.

Dincer, Yildiz et al. 2007. “Oxidative DNA Damage and Antioxidant Activity in Patients with Inflammatory Bowel Disease.” *Digestive Diseases and Sciences* 52(7): 1636–41.

Doehn, Ulrik et al. 2009. “RSK Is a Principal Effector of the RAS-ERK Pathway for Eliciting a Coordinate Promotile/invasive Gene Program and Phenotype in Epithelial Cells.” *Molecular cell* 35(4): 511–22.

Van Dongen, J M, J Kooyman, and W J Visser. 1976. “The Influence of 400 R X-Irradiation on the Number and the Localization of Mature and Immature Goblet Cells and Paneth Cells in Intestinal Crypt and Villus.” *Cell and tissue kinetics* 9: 65–75.

Durand, A. et al. 2012. “Functional Intestinal Stem Cells after Paneth Cell Ablation Induced by the Loss of Transcription Factor Math1 (Atoh1).” *Proceedings of the National Academy of Sciences* 109(23): 8965–70.

Dvorak, Harold. 2009. “Tumors: Wounds That Do Not Heal. Similarities between Tumor Stroma Generation and Wound Healing.” *The New England Journal of Medicine* 315(26): 1650–59.

Eckmann, Lars. 2006. “Animal Models of Inflammatory Bowel Disease: Lessons from Enteric Infections.” *Annals of the New York Academy of Sciences* 1072: 28–38.

Ernestos, Beroukas et al. 2010. “Increased Chromosomal Radiosensitivity in Women Carrying BRCA1/BRCA2 Mutations Assessed with the G2 Assay.” *International journal of radiation oncology, biology, physics* 76(4): 1199–1205.

Van Es, Johan H et al. 2012. “A Critical Role for the Wnt Effector Tcf4 in Adult Intestinal Homeostatic Self-Renewal.” *Molecular and cellular biology* 32(10): 1918–27.

Es, Van et al. 2012. “A Critical Role for the Wnt Effector Tcf4 in Adult Intestinal Homeostatic Self-Renewal.” *Molecular and Cellular Biology* 32(10): 1918–27.

Farin, Henner F., Johan H. Van Es, and Hans Clevers. 2012. “Redundant Sources of Wnt Regulate Intestinal Stem Cells and Promote Formation of Paneth Cells.” *Gastroenterology* 143(6): 1518–29.e7.

Ferguson, Lynnette R., Nishi Karunasinghe, Shuotun Zhu, and Alice H. Wang. 2012. “Selenium and Its’ Role in the Maintenance of Genomic Stability.” *Mutation Research - Fundamental and Molecular Mechanisms of Mutagenesis* 733(1-2): 100–110.

Fevr, Tea, Sylvie Robine, Daniel Louvard, and Joerg Huelsken. 2007. “Wnt/beta-Catenin Is Essential for Intestinal Homeostasis and Maintenance of Intestinal Stem Cells.” *Molecular and cellular biology* 27(21): 7551–59.

Fordham, Robert P. et al. 2013. “Transplantation of Expanded Fetal Intestinal Progenitors Contributes to Colon Regeneration after Injury.” *Cell Stem Cell* 13(6): 734–44.

Formeister, Eric J et al. 2009. "Distinct SOX9 Levels Differentially Mark Stem/progenitor Populations and Enteroendocrine Cells of the Small Intestine Epithelium." *American journal of physiology. Gastrointestinal and liver physiology* 296(5): G1108–18.

Franke, Andre et al. 2008. "Sequence Variants in IL10, ARPC2 and Multiple Other Loci Contribute to Ulcerative Colitis Susceptibility." *Nature genetics* 40(11): 1319–23.

Froese, Alexander et al. 2012. "Popeye Domain Containing Proteins Are Essential for Stress-Mediated Modulation of Cardiac Pacemaking in Mice." *Journal of Clinical Investigation* 122(3): 1119–30.

Fuller, Megan K. et al. 2012. "Intestinal Crypts Reproducibly Expand in Culture." *Journal of Surgical Research* 178(1): 48–54.

Furuyama, Kenichiro et al. 2011. "Continuous Cell Supply from a Sox9-Expressing Progenitor Zone in Adult Liver, Exocrine Pancreas and Intestine." *Nature genetics* 43(1): 34–41.

Ghassabeh, Gholamreza Hassanzadeh et al. 2006. "Identification of a Common Gene Signature for Type II Cytokine – Associated Myeloid Cells Elicited in Vivo in Different Pathologic Conditions." *In Vivo* 108(2): 575–83.

Glocker, Erik-Oliver et al. 2009. "Inflammatory Bowel Disease and Mutations Affecting the Interleukin-10 Receptor." *The New England journal of medicine* 361(21): 2033–45.

Gobert, Alain P et al. 2004. "Protective Role of Arginase in a Mouse Model of Colitis." *Journal of immunology (Baltimore, Md. : 1950)* 173(3): 2109–17.

Gracz, Adam D, Sendhilnathan Ramalingam, and Scott T Magness. 2010. "Sox9 Expression Marks a Subset of CD24-Expressing Small Intestine Epithelial Stem Cells That Form Organoids in Vitro." *American journal of physiology. Gastrointestinal and liver physiology* 298(5): G590–600.

Greaves, Mel, and Carlo C. Maley. 2012. "Clonal Evolution in Cancer." *Nature* 481(7381): 306–13.

Gregorieff, Alex, and Hans Clevers. 2005. "Wnt Signaling in the Intestinal Epithelium: From Endoderm to Cancer." *Genes & development* 19(8): 877–90.

Groschwitz, Katherine R., and Simon P. Hogan. 2009. "Intestinal Barrier Function: Molecular Regulation and Disease Pathogenesis." *Journal of Allergy and Clinical Immunology* 124(1): 3–20.

Gu, Peili et al. 2005. "Orphan Nuclear Receptor LRH-1 Is Required To Maintain Oct4 Expression at the Epiblast Stage of Embryonic Development Orphan Nuclear Receptor LRH-1 Is Required To Maintain Oct4 Expression at the Epiblast Stage of Embryonic Development." *Molecular and cellular biology* 25(9): 3492–3505.

Gudkov, Andrei V, and Elena a Komarova. 2003. "The Role of p53 in Determining Sensitivity to Radiotherapy." *Nature reviews. Cancer* 3(2): 117–29.

Guo, Xiangrong et al. 2003. "A Rac/Cdc42-Specific Exchange Factor, GEFT, Induces Cell Proliferation, Transformation, and Migration." *The Journal of biological chemistry* 278(15): 13207–15.

Hager, and D M Bader. 2009. "Bves: Ten Years After." *Histology and Histopathology* 24(6): 777–87.

Hager, Hillary et al. 2010. "Identification of a Novel Bves Function: Regulation of Vesicular Transport." *The EMBO journal* 29(3): 532–45.

Hamburger, A, and S E Salmon. 1977. "Primary Bioassay of Human Myeloma Stem Cells." *The Journal of Clinical Investigation* 60(4): 846–54.

Han, Ping et al. 2014. "BVES Inhibition Triggers Epithelial-Mesenchymal Transition in Human Hepatocellular Carcinoma." *Digestive diseases and sciences* 59(5): 992–1000.

Harb, Ali H, Carla Abou Fadel, and Ala I Sharara. 2014. "Radiation Enteritis." *Current gastroenterology reports* 16(5): 383.

Harrington, Laurie E et al. 2005. "Interleukin 17-Producing CD4+ Effector T Cells Develop via a Lineage Distinct from the T Helper Type 1 and 2 Lineages." *Nature immunology* 6(11): 1123–32.

Hauer-Jensen, Martin, James W. Denham, and H. Jervoise N. Andreyev. 2014. "Radiation Enteropathy—pathogenesis, Treatment and Prevention." *Nature reviews. Gastroenterology & Hepatology* 11(8): 470–79.

Heller, Frank et al. 2005. "Interleukin-13 Is the Key Effector Th2 Cytokine in Ulcerative Colitis That Affects Epithelial Tight Junctions, Apoptosis, and Cell Restitution." *Gastroenterology* 129(2): 550–64.

Henderson, Paul, Johan E. Van Limbergen, Jürgen Schwarze, and David C. Wilson. 2011. "Function of the Intestinal Epithelium and Its Dysregulation in Inflammatory Bowel Disease." *Inflammatory Bowel Diseases* 17(1): 382–95.

Hermiston, M L, and J I Gordon. 1995. "In Vivo Analysis of Cadherin Function in the Mouse Intestinal Epithelium: Essential Roles in Adhesion, Maintenace of

Differentiation, and Regulation of Programmed Cell Death." *Journal of Cell Biology* 129(2): 489–506.

Herrinton, Lisa J. et al. 2012. "Incidence and Mortality of Colorectal Adenocarcinoma in Persons with Inflammatory Bowel Disease from 1998 to 2010." *Gastroenterology* 143(2): 382–89.

Hewitt, Kyle J, Rachana Agarwal, and Patrice J Morin. 2006. "The Claudin Gene Family: Expression in Normal and Neoplastic Tissues." *BMC cancer* 6: 186.

Higgins, Lisa M. et al. 1999. "Citrobacter Rodentium Infection in Mice Elicits a Mucosal Th1 Cytokine Response and Lesions Similar to Those in Murine Inflammatory Bowel Disease." *Infection and Immunity* 67(6): 3031–39.

Hill, Kristina E et al. 2004. "Neurological Dysfunction Occurs in Mice with Targeted Deletion of the Selenoprotein P Gene." *The Journal of nutrition* 134(1): 157–61.

Hill, Kristina E. et al. 2003. "Deletion of Selenoprotein P Alters Distribution of Selenium in the Mouse." *Journal of Biological Chemistry* 278(16): 13640–46.

Hill, Kristina E. et al. 2007. "The Selenium-Rich C-Terminal Domain of Mouse Selenoprotein P Is Necessary for the Supply of Selenium to Brain and Testis but Not for the Maintenance of Whole Body Selenium." *Journal of Biological Chemistry* 282(15): 10972–80.

Hooper, Lora V, and Andrew J Macpherson. 2010. "Immune Adaptations That Maintain Homeostasis with the Intestinal Microbiota." *Nature reviews. Immunology* 10(3): 159–69.

Hossain, Zakir, and Takashi Hirata. 2008. "Molecular Mechanism of Intestinal Permeability: Interaction at Tight Junctions." *Molecular bioSystems* 4(12): 1181–85.

Hua, Guoqiang et al. 2012. "Crypt Base Columnar Stem Cells in Small Intestines of Mice Are Radioresistant." *Gastroenterology* 143(5): 1266–76.

Hynds, Robert E., and Adam Giangreco. 2013. "Concise Review: The Relevance of Human Stem Cell-Derived Organoid Models for Epithelial Translational Medicine." *Stem Cells* 31(3): 417–22.

Iizuka, Masahiro, and Shiho Konno. 2011. "Wound Healing of Intestinal Epithelial Cells." *World journal of gastroenterology : WJG* 17(17): 2161–71.

Itzkowitz, Steven H, and Xianyang Yio. 2004. "Inflammation and Cancer IV . Colorectal Cancer in Inflammatory Bowel Disease : The Role of Inflammation." *American Journal of Physiology - Gastrointestinal and Liver Physiology* 287: G7–17.

Jaworska, Katrzyna et al. 2013. “A Low Selenium Level Is Associated with Lung and Laryngeal Cancers.” *PLoS ONE* 8(3): 1–6.

Jayagopal, Ashwath, Jin Long Yang, Frederick R. Haselton, and Min S. Chang. 2011. “Tight Junction-Associated Signaling Pathways Modulate Cell Proliferation in Uveal Melanoma.” *Investigative Ophthalmology and Visual Science* 52(1): 588–93.

Jess, Tine et al. 2012. “Decreasing Risk of Colorectal Cancer in Patients with Inflammatory Bowel Disease over 30 Years.” *Gastroenterology* 143(2): 375–81.e1; quiz e13–14.

Kalluri, R, and RA Weinberg. 2009. “The Basics of Epithelial-Mesenchymal Transition.” *The Journal of Clinical Investigation* 119(6): 1420–28.

Kanter, Mehmet, and Meryem Akpolat. 2008. “Vitamin C Protects against Ionizing Radiation Damage to Goblet Cells of the Ileum in Rats.” *Acta histochemica* 110(6): 481–90.

Kaper, James B, James P Nataro, and Harry L Mobley. 2004. “Pathogenic Escherichia Coli.” *Nature reviews. Microbiology* 2(2): 123–40.

Kasaikina, Marina V. et al. 2013. “Contrasting Roles of Dietary Selenium and Selenoproteins in Chemically Induced Hepatocarcinogenesis.” *Carcinogenesis* 34(5): 1089–95.

Kawaguchi, Michiya et al. 2008. “Identification of a Novel Intracellular Interaction Domain Essential for Bves Function.” *PLoS ONE* 3(5): e2261.

Khan, MA, Caixia Ma, and LA Knodler. 2006. “Toll-Like Receptor 4 Contributes to Colitis Development but Not to Host Defense during Citrobacter Rodentium Infection in Mice.” *Infection and immunity* 74(5): 2522–36.

Kim et al. 2010. “Frequent Silencing of Popeye Domain-Containing Genes, BVES and POPDC3, Is Associated with Promoter Hypermethylation in Gastric Cancer.” *Carcinogenesis* 31(9): 1685–93.

Kim et al. 2011. “NRF2 Blockade Suppresses Colon Tumor Angiogenesis by Inhibiting Hypoxia-Induced Activation of HIF-1??” *Cancer Research* 71(6): 2260–75.

Kim, Yonghyun et al. 2012. “Wnt Activation Is Implicated in Glioblastoma Radioresistance.” *Laboratory investigation; a journal of technical methods and pathology* 92(3): 466–73.

Kipp, Anna et al. 2009. “Four Selenoproteins, Protein Biosynthesis, and Wnt Signalling Are Particularly Sensitive to Limited Selenium Intake in Mouse Colon.” *Molecular Nutrition and Food Research* 53(12): 1561–72.

Kitamura, Kazuya, Yasunari Nakamoto, Shuichi Kaneko, and Naofumi Mukaida. 2004. "Pivotal Roles of Interleukin-6 in Transmural Inflammation in Murine T Cell Transfer Colitis." *Journal of leukocyte biology* 76(6): 1111–17.

Knight, Ruth F, David M Bader, and Jon R Backstrom. 2003. "Membrane Topology of Bves/Pop1A, a Cell Adhesion Molecule That Displays Dynamic Changes in Cellular Distribution during Development." *The Journal of biological chemistry* 278(35): 32872–79.

Koh, T S, and T H Benson. 1983. "Critical Re-Appraisal of Fluorometric Method for Determination of Selenium in Biological Materials." *Journal - Association of Official Analytical Chemists* 66(4): 918–26.

Koo, Bon-Kyoung et al. 2012. "Controlled Gene Expression in Primary Lgr5 Organoid Cultures." *Nature methods* 9(1): 81–83.

Korinek, V et al. 1998. "Depletion of Epithelial Stem-Cell Compartments in the Small Intestine of Mice Lacking Tcf-4." *Nature genetics* 19(4): 379–83.

Kucharzik, T et al. 2001. "Neutrophil Transmigration in Inflammatory Bowel Disease Is Associated with Differential Expression of Epithelial Intercellular Junction Proteins." *The American journal of pathology* 159(6): 2001–9.

Kühn, R et al. 1993. "Interleukin-10-Deficient Mice Develop Chronic Enterocolitis." *Cell* 75(2): 263–74.

Kurokawa, Suguru et al. 2014. "Sepp1UF Forms Are N-Terminal Selenoprotein P Truncations That Have Peroxidase Activity When Coupled with Thioredoxin Reductase-1." *Free Radical Biology and Medicine* 69: 67–76.

Van Landeghem, Laurianne et al. 2012. "Activation of Two Distinct Sox9-EGFP-Expressing Intestinal Stem Cell Populations during Crypt Regeneration after Irradiation." *American journal of physiology. Gastrointestinal and liver physiology* 302(10): G1111–32.

Lander, E S et al. 2001. "Initial Sequencing and Analysis of the Human Genome." *Nature* 409(6822): 860–921.

Larrea, MD, and Feng Hong. 2009. "RSK1 Drives p27Kip1 Phosphorylation at T198 to Promote RhoA Inhibition and Increase Cell Motility." *Proceedings of the National Academy of Sciences of the United States of America* 106(23): 9268–73.

Lebeis, Sarah L et al. 2007. "TLR Signaling Mediated by MyD88 Is Required for a Protective Innate Immune Response by Neutrophils to Citrobacter Rodentium." *Journal of immunology (Baltimore, Md. : 1950)* 179(1): 566–77.

Leibowitz, Brian J et al. 2011. “Uncoupling p53 Functions in Radiation-Induced Intestinal Damage via PUMA and p21.” *Molecular cancer research : MCR* 9(5): 616–25.

Li, and Hans Clevers. 2010. “Coexistence of Quiescent and Active Adult Stem Cells in Mammals.” *Science (New York, N.Y.)* 327(5965): 542–45.

Li, Vivian S W, and Hans Clevers. 2012. “In Vitro Expansion and Transplantation of Intestinal Crypt Stem Cells.” *Gastroenterology* 143(1): 30–34.

Lindberg, Sofia Rondin, André Olsson, Ann-Maj Persson, and Inge Olsson. 2005. “The Leukemia-Associated ETO Homologues Are Differently Expressed during Hematopoietic Differentiation.” *Experimental hematology* 33(2): 189–98.

Lippman, Scott M et al. 2009. “Effect of Selenium and Vitamin E on Risk of Prostate Cancer and Other Cancers.” *JAMA* 301: 39–51.

Loftus, Edward V, and William J Sandborn. 2002. “Epidemiology of Inflammatory Bowel Disease.” *Gastroenterology clinics of North America* 31(1): 1–20.

Lund, Pauline Kay. 2012. “Fixing the Breaks in Intestinal Stem Cells after Radiation: A Matter of DNA Damage and Death or DNA Repair and Regeneration.” *Gastroenterology* 143(5): 1144–47.

Luperchio, Steven a., and David B. Schauer. 2001. “Molecular Pathogenesis of Citrobacter Rodentium and Transmissible Murine Colonic Hyperplasia.” *Microbes and Infection* 3(4): 333–40.

Lutterbach, B et al. 1998. “ETO, a Target of t(8;21) in Acute Leukemia, Interacts with the N-CoR and mSin3 Corepressors.” *Molecular and cellular biology* 18(12): 7176–84.

Ma, Thomas Y et al. 2004. “TNF-Alpha-Induced Increase in Intestinal Epithelial Tight Junction Permeability Requires NF-Kappa B Activation.” *American journal of physiology. Gastrointestinal and liver physiology* 286(3): G367–76.

Maaser, Christian et al. 2004. “Clearance of Citrobacter Rodentium Requires B Cells but Not Secretory Immunoglobulin A (IgA) or IgM Antibodies.” *Infection and Immunity* 72(6): 3315–24.

Machen, T. E., D. Erlij, and F. B. Wooding. 1972. “Permeable Junctional Complexes. The Movement of Lanthanum across Rabbit Gallbladder and Intestine.” *Journal of Cell Biology* 54(2): 302–12.

Madsen, K L et al. 1999. “Interleukin-10 Gene-Deficient Mice Develop a Primary Intestinal Permeability Defect in Response to Enteric Microflora.” *Inflammatory bowel diseases* 5(4): 262–70.

Mahe, Maxime M et al. 2013. “Establishment of Gastrointestinal Epithelial Organoids.” *Curr Protoc Mouse Biol.* 3(December): 217–40.

Maloy, K J, and M C Kullberg. 2008. “IL-23 and Th17 Cytokines in Intestinal Homeostasis.” *Mucosal immunology* 1(5): 339–49.

Maloy, and Fiona Powrie. 2011. “Intestinal Homeostasis and Its Breakdown in Inflammatory Bowel Disease.” *Nature* 474(7351): 298–306.

Mangan, Paul R et al. 2006. “Transforming Growth Factor-Beta Induces Development of the T(H)17 Lineage.” *Nature* 441(7090): 231–34.

Margalit, Ofer et al. 2006. “BCL6 Is Regulated by p53 through a Response Element Frequently Disrupted in B-Cell Non-Hodgkin Lymphoma.” *Blood* 107(4): 1599–1607.

Marshman, Emma, Catherine Booth, and Christopher S. Potten. 2002. “The Intestinal Epithelial Stem Cell.” *BioEssays* 24(1): 91–98.

Martin, K, C S Potten, S a Roberts, and T B Kirkwood. 1998. “Altered Stem Cell Regeneration in Irradiated Intestinal Crypts of Senescent Mice.” *Journal of cell science* 111 (Pt 1): 2297–2303.

Matricon, Julien, Nicolas Barnich, and Denis Ardid. 2010. “Immunopathogenesis of Inflammatory Bowel Disease.” *Self/nonself* 1(4): 299–309.

Mazzatti, Dawn J. et al. 2005. “p53 Modulates Radiation Sensitivity Independent of p21 Transcriptional Activation.” *American Journal of Clinical Oncology* 28(1): 43–50.

Mennigen, Rudolf et al. 2009. “Probiotic Mixture VSL#3 Protects the Epithelial Barrier by Maintaining Tight Junction Protein Expression and Preventing Apoptosis in a Murine Model of Colitis.” *American journal of physiology. Gastrointestinal and liver physiology* 296(5): G1140–49.

Méplan, Catherine et al. 2009. “Relative Abundance of Selenoprotein P Isoforms in Human Plasma Depends on Genotype, Se Intake, and Cancer Status.” *Antioxidants & redox signaling* 11(11): 2631–40.

Metcalfe, Ciara, Noelyn M. Kljavin, Ryan Ybarra, and Frederic J. De Sauvage. 2014. “Lgr5+ Stem Cells Are Indispensable for Radiation-Induced Intestinal Regeneration.” *Cell Stem Cell* 14(2): 149–59.

Mills, Stacey E. 2012. *Histology for Pathologists, 4th Edition*. 4th ed. Philadelphia, Pennsylvania: Lippincott Williams & Wilkins.

Miyoshi, H et al. 1993. "The t(8;21) Translocation in Acute Myeloid Leukemia Results in Production of an AML1-MTG8 Fusion Transcript." *The EMBO journal* 12(7): 2715–21.

Moore, Amy C et al. 2008. "Myeloid Translocation Gene Family Members Associate with T-Cell Factors (TCFs) and Influence TCF-Dependent Transcription." *Molecular and cellular biology* 28(3): 977–87.

Moore, Arthur Dalley, and Anne Agur. 2009. *Clinically Oriented Anatomy, 6th Edition*. 6th ed. Philadelphia, Pennsylvania.

Mosser, David M., and Xia Zhang. 2008. "Activation of Murine Macrophages." *Current Protocols in Immunology* (SUPPL. 83): 8–15.

Neumann, Helmut et al. 2011. "Cancer Risk in IBD: How to Diagnose and How to Manage DALM and ALM." *World Journal of Gastroenterology* 17(27): 3184–91.

Neurath, M, I Fuss, and W Strober. 2000. "TNBS-Colitis." *International reviews of immunology* 19(1): 51–62.

Nguyen, Geoffrey C., and Brian Bressler. 2012. "A Tale of Two Cohorts: Are We Overestimating the Risk of Colorectal Cancer in Inflammatory Bowel Disease?" *Gastroenterology* 143(2): 288–90.

Nieuwenhuis, B. 2002. "BRCA1 and BRCA2 Heterozygosity and Repair of X-Ray-Induced DNA Damage." *International Journal of Radiation Biology* 78(4).

Nishimura, Miyuki et al. 2009. "Chemokines as Novel Therapeutic Targets for Inflammatory Bowel Disease." *Annals of the New York Academy of Sciences* 1173: 350–56.

Ojuawo, A, and L Keith. 2002. "The Serum Concentrations of Zinc, Copper and Selenium in Children with Inflammatory Bowel Disease." *The Central African journal of medicine* 48(9-10): 116–19.

Okayasu, I et al. 1990. "A Novel Method in the Induction of Reliable Experimental Acute and Chronic Ulcerative Colitis in Mice." *Gastroenterology* 98(3): 694–702.

Okayasu, I et al. 1996. "Promotion of Colorectal Neoplasia in Experimental Murine Ulcerative Colitis." *Gut* 39(1): 87–92.

Olson, Gary E., Virginia P. Winfrey, Kristina E. Hill, and Raymond F. Burk. 2008. "Megalin Mediates Selenoprotein P Uptake by Kidney Proximal Tubule Epithelial Cells." *Journal of Biological Chemistry* 283(11): 6854–60.

Osler, and David M Bader. 2004. "Bves Expression during Avian Embryogenesis." *Developmental dynamics : an official publication of the American Association of Anatomists* 229(3): 658–67.

Osler, M Chang, and D Bader. 2005. "Bves Modulates Epithelial Integrity through an Interaction at the Tight Junction." *Journal of cell science* 118(Pt 20): 4667–78.

Osler, Travis K Smith, and David M Bader. 2006. "Bves, a Member of the Popeye Domain-Containing Gene Family." *Developmental dynamics : an official publication of the American Association of Anatomists* 235(3): 586–93.

Ottewell, Penelope D et al. 2006. "Gastrin Increases Murine Intestinal Crypt Regeneration Following Injury." *Gastroenterology* 130(4): 1169–80.

Papadakis, KA, and SR Targan. 2000. "Role of Cytokines in the Pathogenesis of Inflammatory Bowel Disease." *Annual review of medicine* 51: 289–98.

Papaioannou, D et al. 2011. "Antioxidants in the Chemoprevention of Colorectal Cancer and Colorectal Adenomas in the General Population: A Systematic Review and Meta-Analysis." *Colorectal disease* 13(10): 1085–99.

Paris, F et al. 2001. "Endothelial Apoptosis as the Primary Lesion Initiating Intestinal Radiation Damage in Mice." *Science (New York, N.Y.)* 293(5528): 293–97.

Pearson, a D et al. 1982. "Intestinal Permeability in Children with Crohn's Disease and Coeliac Disease." *British medical journal (Clinical research ed.)* 285(6334): 20–21.

Pegg, A E. 1984. "Methylation of the O6 Position of Guanine in DNA Is the Most Likely Initiating Event in Carcinogenesis by Methylating Agents." *Cancer investigation* 2(3): 223–31.

Perše, Martina, and Anton Cerar. 2012. "Dextran Sodium Sulphate Colitis Mouse Model: Traps and Tricks." *Journal of biomedicine & biotechnology* 2012: 718617.

Peters, Ulrike et al. 2008. "Variation in the Selenoenzyme Genes and Risk of Advanced Distal Colorectal Adenoma." *Cancer Epidemiology Biomarkers and Prevention* 17(5): 1144–54.

Pinto, Daniel, Alex Gregorieff, Harry Begthel, and Hans Clevers. 2003. "Canonical Wnt Signals Are Essential for Homeostasis of the Intestinal Epithelium." *Genes Dev.*: 1709–13.

Poindexter, Shenika V et al. 2015. “Transcriptional Co-Repressor MTG16 Regulates Small Intestinal Crypt Proliferation and Crypt Regeneration after Radiation-Induced Injury.” *American Journal of Physiology - Gastrointestinal and Liver Physiology*.

Poritz, Lisa S. et al. 2007. “Loss of the Tight Junction Protein ZO-1 in Dextran Sulfate Sodium Induced Colitis.” *Journal of Surgical Research* 140(1): 12–19.

Porras, Monica et al. 2006. “Correlation between Cyclical Epithelial Barrier Dysfunction and Bacterial Translocation in the Relapses of Intestinal Inflammation.” *Inflammatory bowel diseases* 12(9): 843–52.

Potten. 1977. “Extreme Sensitivity of Some Intestinal Crypt Cells to X and Gamma Irradiation.” *Nature* 269(5628): 518–21.

Potten. 1990. “A Comprehensive Study of the Radiobiological Response of the Murine (BDF1) Small Intestine.” *International journal of radiation biology* 58(6): 925–73.

Potten. 2009. “The Stem Cells of Small Intestinal Crypts: Where Are They?” *Cell proliferation* 42(6): 731–50.

Potten, Catherine Booth, and D Mark Pritchard. 1997. “Stem Cell Review The Intestinal Epithelial Stem Cell : The Mucosal Governor.” : 219–43.

Potten, C S et al. 1995. “Stimulation and Inhibition of Proliferation in the Small Intestinal Crypts of the Mouse after in Vivo Administration of Growth Factors.” *Gut* 36(6): 864–73.

Potten, C S, and CA Chadwick. 1994. “Small Intestinal Growth Regulatory Factors Extracted by Simple Diffusion from Intact Irradiated Intestine and Tested in Vivo.” *Growth factors (Chur, Switzerland)* 10(1): 63–75.

Potten, and J H Hendry. 1975. “Differential Regeneration of Intestinal Proliferative Cells and Cryptogenic Cells after Irradiation.” *International journal of radiation biology and related studies in physics, chemistry, and medicine* 27(5): 413–24.

Potten, William J. Hume, Peter Reid, and John Cairns. 1978. “The Segregation of DNA in Epithelial Stem Cells.” *Cell* 15(November): 899–906.

Potten, Gary Owen, and Dawn Booth. 2002. “Intestinal Stem Cells Protect Their Genome by Selective Segregation of Template DNA Strands.” *Journal of cell science* 115(Pt 11): 2381–88.

Read R, Bellew T, Yang J-G, Hill KE, Palmer IS, Burk RF. 1990. “Selenium and Amino Acid Composition of Selenoprotein P, the Major Selenoprotein in Rat Serum.” *Journal of Biological Chemistry* 265(October 15): 17899–905.

Reese, DE, M Zavaljevski, NL Streiff, and D Bader. 1999. “Bves: A Novel Gene Expressed during Coronary Blood Vessel Development.” *Developmental biology* 209(1): 159–71.

Reya, Tannishtha, and Hans Clevers. 2005. “Wnt Signalling in Stem Cells and Cancer.” *Nature* 434(7035): 843–50.

Ripley, Anna N, Megan E Osler, Christopher V E Wright, and David Bader. 2006. “Xbves Is a Regulator of Epithelial Movement during Early Xenopus Laevis Development.” *Proceedings of the National Academy of Sciences of the United States of America* 103(3): 614–19.

Roessner, a., D. Kuester, P. Malfertheiner, and R. Schneider-Stock. 2008. “Oxidative Stress in Ulcerative Colitis-Associated Carcinogenesis.” *Pathology Research and Practice* 204(7): 511–24.

Romeo, Yves, Xiaocui Zhang, and Philippe P Roux. 2012. “Regulation and Function of the RSK Family of Protein Kinases.” *The Biochemical journal* 441(2): 553–69.

Rubin, David T et al. 2008. “Colorectal Cancer Prevention in Inflammatory Bowel Disease and the Role of 5-Aminosalicylic Acid: A Clinical Review and Update.” *Inflammatory bowel diseases* 14(2): 265–74.

Russ, Patricia K et al. 2011. “Bves Modulates Tight Junction Associated Signaling.” *PLoS ONE* 6(1): e14563.

Sampson, Natalie et al. 2011. “ROS Signaling by NOX4 Drives Fibroblast-to-Myofibroblast Differentiation in the Diseased Prostatic Stroma.” *Molecular endocrinology (Baltimore, Md.)* 25(3): 503–15.

Santos, M F et al. 1997. “Rho Proteins Play a Critical Role in Cell Migration during the Early Phase of Mucosal Restitution.” *The Journal of clinical investigation* 100(1): 216–25.

Sato, and Hans Clevers. 2013. “Growing Self-Organizing Mini-Guts from a Single Intestinal Stem Cell: Mechanism and Applications.” *Science (New York, N.Y.)* 340(6137): 1190–94.

Sato, Toshiro et al. 2009. “Single Lgr5 Stem Cells Build Crypt-Villus Structures in Vitro without a Mesenchymal Niche.” *Nature* 459(7244): 262–65.

Sato, Toshiro, Daniel E. Stange, et al. 2011. “Long-Term Expansion of Epithelial Organoids from Human Colon, Adenoma, Adenocarcinoma, and Barrett’s Epithelium.” *Gastroenterology* 141(5): 1762–72.

Sato, Toshiro, Johan H van Es, et al. 2011. “Paneth Cells Constitute the Niche for Lgr5 Stem Cells in Intestinal Crypts.” *Nature* 469(7330): 415–18.

Satoh-Takayama, Naoko et al. 2009. “The Natural Cytotoxicity Receptor NKp46 Is Dispensable for IL-22-Mediated Innate Intestinal Immune Defense against Citrobacter Rodentium.” *Journal of immunology (Baltimore, Md. : 1950)* 183(10): 6579–87.

Schäfer, Matthias, and Sabine Werner. 2008. “Cancer as an Overhealing Wound: An Old Hypothesis Revisited.” *Nature reviews. Molecular cell biology* 9(8): 628–38.

Schauer, D. B., and S. Falkow. 1993. “Attaching and Effacing Locus of a Citrobacter Freundii Biotype That Causes Transmissible Murine Colonic Hyperplasia.” *Infection and Immunity* 61(6): 2486–92.

Schembri, John, Matthias Azzopardi, and Pierre Ellul. 2014. “Small Bowel Radiation Enteritis Diagnosed by Capsule Endoscopy.” *BMJ case reports* 2014: 2013–14.

Schepers, Arnout G et al. 2012. “Lineage Tracing Reveals Lgr5+ Stem Cell Activity in Mouse Intestinal Adenomas.” *Science* 337(6095): 730–35.

Schomburg, Lutz et al. 2003. “Gene Disruption Discloses Role of Selenoprotein P in Selenium Delivery to Target Tissues.” *The Biochemical journal* 370(Pt 2): 397–402.

Seno, Hiroshi et al. 2009. “Efficient Colonic Mucosal Wound Repair Requires Trem2 Signaling.” *Proceedings of the National Academy of Sciences of the United States of America* 106(1): 256–61.

Seo, Young R, Mark R Kelley, and Martin L Smith. 2002. “Selenomethionine Regulation of p53 by a ref1-Dependent Redox Mechanism.” *Proceedings of the National Academy of Sciences of the United States of America* 99(22): 14548–53.

Shadad, Abobakr K, Frank J Sullivan, Joseph D Martin, and Laurence J Egan. 2013. “Gastrointestinal Radiation Injury: Symptoms, Risk Factors and Mechanisms.” *World journal of gastroenterology : WJG* 19(2): 185–98.

Shaker, Anisa, and Deborah C. Rubin. 2012. “Stem Cells: One Step Closer to Gut Repair.” *Nature* 485(7397): 181–82.

Shamberger, R J, and C E Willis. 1971. “Selenium Distribution and Human Cancer Mortality.” *CRC critical reviews in clinical laboratory sciences* 2(2): 211–21.

Sheehan, T. M T, and M. Gao. 1990. “Simplified Fluorometric Assay of Total Selenium in Plasma and Urine.” *Clinical Chemistry* 36(12): 2124–26.

Shen, Le. 2012. “Tight Juntions on the Pove: Molecular Mechanisms for Epithelial Barrier Regulation.” *Annals of the New York Academy of Sciences* (1258): 9–18.

Shen, Le, Liping Su, and Jerrold R. Turner. 2009. “Mechanisms and Functional Implications of Intestinal Barrier Defects.” *Digestive Diseases* 27(4): 443–49.

Shinkai, Y et al. 1992. “RAG-2-Deficient Mice Lack Mature Lymphocytes Owing to Inability to Initiate V(D)J Rearrangement.” *Cell* 68(5): 855–67.

Siegmund, Britta. 2010. “Interleukin-18 in Intestinal Inflammation: Friend and Foe?” *Immunity* 32(3): 300–302.

Simmons, Cameron P et al. 2002. “Impaired Resistance and Enhanced Pathology during Infection with a Noninvasive, Attaching-Effacing Enteric Bacterial Pathogen, Citrobacter Rodentium, in Mice Lacking IL-12 or IFN-Gamma.” *Journal of immunology (Baltimore, Md. : 1950)* 168(4): 1804–12.

Simmons, Cameron P et al. 2003. “Central Role for B Lymphocytes and CD4 + T Cells in Immunity to Infection by the Attaching and Effacing Pathogen Citrobacter Rodentium.” *Infection and Immunity*: 71(9): 5077–86.

Singh, Kshipra et al. 2011. “The Apolipoprotein E-Mimetic Peptide COG112 Inhibits NF-kappaB Signaling, Proinflammatory Cytokine Expression, and Disease Activity in Murine Models of Colitis.” *The Journal of biological chemistry* 286(5): 3839–50.

Smith et al. 2008. “Bves Directly Interacts with GEFT, and Controls Cell Shape and Movement through Regulation of Rac1/Cdc42 Activity.” *Proceedings of the National Academy of Sciences of the United States of America* 105(24): 8298–8303.

Smith, and David M Bader. 2006. “Characterization of Bves Expression during Mouse Development Using Newly Generated Immunoreagents.” *Developmental dynamics : an official publication of the American Association of Anatomists* 235(6): 1701–8.

Smith, J. Joshua et al. 2010. “Experimentally Derived Metastasis Gene Expression Profile Predicts Recurrence and Death in Patients With Colon Cancer.” *Gastroenterology* 138(3): 958–68.

Söderholm, JD, G Olaison, and KH Peterson. 2002. “Augmented Increase in Tight Junction Permeability by Luminal Stimuli in the Non-Inflamed Ileum of Crohn’s Disease.” *Gut* 50: 307–13.

Solinas, Graziella et al. 2010. “Tumor-Conditioned Macrophages Secrete Migration-Stimulating Factor: A New Marker for M2-Polarization, Influencing Tumor Cell Motility.” *Journal of immunology (Baltimore, Md. : 1950)* 185(1): 642–52.

Speckmann, Bodo et al. 2010. “Proinflammatory Cytokines down-Regulate Intestinal Selenoprotein P Biosynthesis via NOS2 Induction.” *Free Radical Biology and Medicine* 49(5): 777–85.

Steinbrecher, Astrid et al. 2010. “Effects of Selenium Status and Polymorphisms in Selenoprotein Genes on Prostate Cancer Risk in a Prospective Study of European Men.” *Cancer Epidemiology Biomarkers and Prevention* 19(11): 2958–68.

Steinbrenner, Holger, and Helmut Sies. 2013. “Selenium Homeostasis and Antioxidant Selenoproteins in Brain: Implications for Disorders in the Central Nervous System.” *Archives of Biochemistry and Biophysics* 536(2): 152–57.

Stelzner, Matthias et al. 2012. “A Nomenclature for Intestinal in Vitro Cultures.” *American journal of physiology. Gastrointestinal and liver physiology* 302(12): G1359–63.

Strober, Warren, and Ivan J Fuss. 2011. “Proinflammatory Cytokines in the Pathogenesis of Inflammatory Bowel Diseases.” *Gastroenterology* 140(6): 1756–67.

Sturm, Andreas, and Axel U Dignass. 2008. “Epithelial Restitution and Wound Healing in Inflammatory Bowel Disease.” *World journal of gastroenterology : WJG* 14(3): 348–53.

Sulli, Gabriele, R Di Micco, and FA di Fagagna. 2012. “Crosstalk between Chromatin State and DNA Damage Response in Cellular Senescence and Cancer.” *Nature Reviews Cancer* 12(10): 709–20.

Sun, Xiaolun, Bo Liu, Ryan Balfour Sartor, and Christian Jobin. 2013. “Phosphatidylinositol 3-Kinase-Γ Signaling Promotes Campylobacter Jejuni-Induced Colitis through Neutrophil Recruitment in Mice.” *Journal of immunology (Baltimore, Md. : 1950)* 190(1): 357–65.

Szatrowski, Ted P., and Carl F. Nathan. 1991. “Production of Large Amounts of Hydrogen Peroxide by Human Tumor Cells.” *Cancer Res.* 51(3): 794–98.

Thoreson, Molly, and Albert B. Reynolds. 2002. “Altered Expression of the Catenin p120 in Human Cancer: Implications for Tumor Progression.” *Differentiation* 70(9-10): 583–89.

Tian, Hua et al. 2011. “A Reserve Stem Cell Population in Small Intestine Renders Lgr5-Positive Cells Dispensable.” *Nature* 478(7368): 255–59.

Torlopp, Angela, Stephanie S Breher, Jan Schlüter, and Thomas Brand. 2006. “Comparative Analysis of mRNA and Protein Expression of Popdc1 (Bves) during Early Development in the Chick Embryo.” *Developmental dynamics : an official publication of the American Association of Anatomists* 235(3): 691–700.

Trapnell, Cole et al. 2013. “Differential Analysis of Gene Regulation at Transcript Resolution with RNA-Seq.” *Nature biotechnology* 31(1): 46–53.

Trapnell, Cole, Lior Pachter, and Steven L. Salzberg. 2009. “TopHat: Discovering Splice Junctions with RNA-Seq.” *Bioinformatics* 25(9): 1105–11.

Turner, Jerrold R. 2009. “Intestinal Mucosal Barrier Function in Health and Disease.” *Nature reviews. Immunology* 9(11): 799–809.

Ukabam, S O, J R Clamp, and B T Cooper. 1983. “Abnormal Small Intestinal Permeability to Sugars in Patients with Crohn’s Disease of the Terminal Ileum and Colon.” *Digestion* 27(2): 70–74.

Vasavada, T. K., J. R. DiAngelo, and M. K. Duncan. 2004. “Developmental Expression of Pop1/Bves.” *Journal of Histochemistry & Cytochemistry* 52(3): 371–77.

Vunta, Hema et al. 2008. “Selenium Attenuates pro-Inflammatory Gene Expression in Macrophages.” *Molecular Nutrition and Food Research* 52(11): 1316–23.

Wada, A M, D E Reese, and D M Bader. 2001. “Bves: Prototype of a New Class of Cell Adhesion Molecules Expressed during Coronary Artery Development.” *Development* 128(11): 2085–93.

Wang et al. 1998. “ETO , Fusion Partner in T (8 ; 21) Acute Myeloid Leukemia , Represses Transcription by Interaction with the Human.” *Proceedings of the National Academy of Sciences of the United States of America* 95(September): 10860–65.

Wang, Quan, Cheng Hui Fang, and Per-Olof Hasselgren. 2001. “Intestinal Permeability Is Reduced and IL-10 Levels Are Increased in Septic IL-6 Knockout Mice.” *American journal of physiology Regulatory, integrative and comparative physiology* 281(3): R1013–23.

Waterston, Robert H et al. 2002. “Initial Sequencing and Comparative Analysis of the Mouse Genome.” *Nature* 420(6915): 520–62.

Wei, Olivia L., Ashley Hilliard, Daniel Kalman, and Melanie Sherman. 2005. “Mast Cells Limit Systemic Bacterial Dissemination but Not Colitis in Response to Citrobacter Rodentium.” *Infection and Immunity* 73(4): 1978–85.

Welinder-Olsson, Christina, and Bertil Kaijser. 2005. “Enterohemorrhagic Escherichia Coli (EHEC).” *Scandinavian journal of infectious diseases* 37(6-7): 405–16.

Williams, Christopher S et al. 2011. “BVES Regulates EMT in Human Corneal and Colon Cancer Cells and Is Silenced via Promoter Methylation in Human Colorectal Carcinoma.” *Journal of Clinical Investigation* 121(10): 4056–69.

Williams, Christopher S et al. 2013. “MTG16 Contributes to Colonic Epithelial Integrity in Experimental Colitis.” *Gut* 62(10): 1446–55.

Wirtz, Stefan, Clemens Neufert, Benno Weigmann, and Markus F Neurath. 2007. “Chemically Induced Mouse Models of Intestinal Inflammation.” *Nature protocols* 2(3): 541–46.

Wirtz, Stefan, and Markus F. Neurath. 2007. “Mouse Models of Inflammatory Bowel Disease.” *Advanced Drug Delivery Reviews* 59(11): 1073–83.

Woodward, Wendy a et al. 2007. “WNT/beta-Catenin Mediates Radiation Resistance of Mouse Mammary Progenitor Cells.” *Proceedings of the National Academy of Sciences of the United States of America* 104(2): 618–23.

Wyatt, J et al. 1993. “Intestinal Permeability and the Prediction of Relapse in Crohn’s Disease.” *Lancet* 341(8858): 1437–39.

Xiao, Wusheng et al. 2013. “Selenoprotein P Regulates 1-(4-Chlorophenyl)-Benzo-2,5-Quinone-Induced Oxidative Stress and Toxicity in Human Keratinocytes.” *Free Radical Biology and Medicine* 65: 70–77.

Yamamoto, M, K Yoshizaki, T Kishimoto, and H Ito. 2000. “IL-6 Is Required for the Development of Th1 Cell-Mediated Murine Colitis.” *Journal of immunology (Baltimore, Md. : 1950)* 164(9): 4878–82.

Yang, Wan Seok et al. 2014. “Regulation of Ferroptotic Cancer Cell Death by GPX4.” *Cell* 156(1-2): 317–31.

Yap, A S. 1998. “The Morphogenetic Role of Cadherin Cell Adhesion Molecules in Human Cancer: A Thematic Review.” *Cancer investigation* 16(4): 252–61.

Ye, Dongmei, Iris Ma, and Thomas Y Ma. 2006. “Molecular Mechanism of Tumor Necrosis Factor Alpha Modulation of Intestinal Epithelial Tight Junction Barrier.” *American Journal of Physiology gastrointestinal Liver Physiology* 290: 496–504.

Young, Barbara, Geraldine O’Dowd, and Phillip Woodford. 2013. *Wheater’s Functional Histology: A Text and Colour Atlas*. 6th ed. Philadelphia, Pennsylvania: Elsevier Churchill Livingstone.

Yui, Shiro et al. 2012. “Functional Engraftment of Colon Epithelium Expanded in Vitro from a Single Adult Lgr5+ Stem Cell.” *Nature Medicine* 18(4): 618–23.

Zeisberg, M, and Eg Neilson. 2009. “Biomarkers for Epithelial-Mesenchymal Transitions.” *The Journal of Clinical Investigation* 119(6): 1429–37.

Zeissig, S et al. 2007. “Changes in Expression and Distribution of Claudin 2, 5 and 8 Lead to Discontinuous Tight Junctions and Barrier Dysfunction in Active Crohn’s Disease.” *Gut* 56(1): 61–72.

Zhang, Xia, Ricardo Goncalves, and David M. Mosser. 2008. “The Isolation and Characterization of Murine Macrophages.” *Current Protocols in Immunology* (SUPPL. 83): 1–14.

Zhang, Yuanyuan, and Xiaoli Chen. 2011. “Reducing Selenoprotein P Expression Suppresses Adipocyte Differentiation as a Result of Increased Preadipocyte Inflammation.” *American journal of physiology. Endocrinology and metabolism* 300(1): E77–85.

Zolotarevsky, Yevgeny et al. 2002. “A Membrane-Permeant Peptide That Inhibits MLC Kinase Restores Barrier Function in in Vitro Models of Intestinal Disease.” *Gastroenterology* 123(1): 163–72.